THE KINETICS OF THE DEHYDROGENATIVE BORYLATION OF TERMINAL ALKYNES AND EXPLORATION OF THE REACTIVITY OF PXP LIGATED COBALT COMPLEXES

A Dissertation

by

BRYAN JAMES FOLEY

Submitted to the Office of Graduate and Professional Studies of
Texas A&M University
in partial fulfillment of the requirements for the degree of

DOCTOR OF PHILOSOPHY

Chair of Committee,	Oleg V. Ozerov
Committee Members,	Michael Nippe
	Daniel A. Singleton
	Chad V. Mashuga
Head of Department,	Simon W. North

August 2020

Major Subject: Chemistry

ABSTRACT

Catalytic synthesis of borylated organic molecules has been of great interest given the synthetic utility of borylated material in cross-coupling reactions. However, a glaring absence from the synthetic chemist's repertoire was the catalytic synthesis of borylated alkynes. In 2013, the Ozerov group disclosed pincer iridium complexes capable of performing the dehydrogenative borylation of terminal alkynes (DHBTA). In the following years, second generation catalysts were disclosed using the 2,2'-bis(dialkylphosphino)diphenylamide (PNP) ligand.

Here we continue the development of PNP ligated iridium DHBTA catalysts and disclose a full mechanistic investigation coupling experimental results with computational investigation. Also disclosed is the first example of a readily available, air-stable iridium DHBTA precatalyst. We have discovered that the DHBTA reaction is moderately tolerant to air and moisture with sufficient pinacolborane present. The ease of handling this new precatalyst will hopefully inspire widespread use of catalytic methods for the construction of alkynylboronates.

Inspired by our success with (POCOP)Rh(Ar)(SAr') and (PNP)Rh(Ar)(SAr') in C–S bond formation reactions, (POCOP)Co(Ar)(SAr') and (PNP)Co(Ar)(SAr') were synthesized and their efficacy in C–S bond formation was investigated. The (POCOP)Co and (PNP)Co platforms were determined to be incapable of supporting catalysis. The former was prone to reductive elimination involving the pincer aryl and the latter was plagued by a swift comproportionation reaction after concerted two electron C–S

reductive elimination. The mechanism of thiolate scrambling and C–S coupling in the (PNP)Co system was investigated in detail. A series of aryl halides were added to the (PNP)Co system to capture cobalt after reductive elimination hopefully eliciting oxidative addition to the unsaturated (PNP)Co fragment; however, halogen atom abstraction predominated. The halogen atom abstraction and scrambling of ligands between cobalt centers was investigated.

Esterified phenols are attractive substrates for Suzuki-style coupling reactions given the ubiquity of phenols and the stability of the corresponding ester. To this end, the (PNP)Co system was applied to the C–O cleavage of esters. Although the active $Co^{I/III}$ comproportionation reaction prevents catalysis, this is the first documented example of cobalt mediated aryl ester C–O bond activation.

Lastly, the synthesis, characterization, and structural characterization of various cobalt silylene complexes are disclosed.

DEDICATION

To my Wife, my Nana, and my God. For all you've done for me.

ACKNOWLEDGEMENTS

I don’t think that one page can contain the amount of gratitude that I have for my Ph.D. advisor, Dr. Oleg Ozerov. Starting early in June 2015 was my attempt at securing a position in his lab while feeling as though Dr. Ozerov must be taking a gamble on me. Thankfully, he accepted me with open arms, and I can only hope that he is half as satisfied with me as a graduate student as I am with him as an advisor. I would also like to thank my committee members Dr. Michael Nippe, Dr. Daniel Singleton, and Dr. Chad Mashuga.

To Trevor Latendresse, one of my closest friends. I have greatly enjoyed our theological discussions, coffee runs, and inside jokes. I would particularly like to thank Olivia Gunther for always being there for me, and for all the sniks. To Ming-Uei, Derek, and Vinh, thank you for bringing friendship and laughter to my life. To Dr. Alex Kosanovich thank you for your consistent friendship and infections enthusiasm. I would like to thank Dr. Wei-Chun Shih and Dr. Chris Pell for their guidance and friendship. To Yihan, Sam, Brandy, Qingheng, and Patricio, I wish you the best of luck.

Thank you to my Nana, Ronald, Mom, and Grandpa for being there if I ever needed anything. A special thank you to my father and mother in-law; I couldn’t have asked for a better family to marry into and consider myself quite blessed to be a part of yours.

Lastly, thank you to my beautiful, amazing, funny, smart, incredible Wife. I would not be the person I am today without you. Thank you for inspiring me to be a better man, pushing me closer to God, and being there for me through thick and thin. You are the elbow to my macaroni and I hope that you always know we are in this together.

CONTRIBUTORS AND FUNDING SOURCES

This work was supervised by a dissertation committee consisting of Professor Oleg Ozerov, Professor Michael Nippe, and Professor Daniel Singleton of the Department of Chemistry, and Professor Chad Mashuga of the Department of Chemical Engineering.

The XRD structures for compounds **204b**, **401**, **402**, **403**, **521**, **522**, **604b**, **608a**, **804**, and (PNP)Co(Cl)$_2$ were solved by Dr. Nattamai Bhuvanesh (Department of Chemistry, TAMU). The XRD structures for compounds **404**, **405**, **406-anti** were solved by Dr. Daron Janzen (Department of Chemistry and Biochemistry, St. Catherine University). The XRD structure for compound **508** was solved by Dr. Samuel Timpa during his time as a graduate student in the Department of Chemistry at Texas A&M University. The XRD structures for compounds **515**, **516**, and **606a** were solved by Dr. Chandra Mouli Palit during his time as a graduate student in the Department of Chemistry at Texas A&M University.

A significant number of experiments in Chapter V were performed by Dr. Samuel Timpa and Dr. Chandra Mouli Palit during their time as graduate students in the Department of Chemistry at Texas A&M University. Compounds **402 - 407-anti** were prepared by Jia Zhang during either his stint as an undergraduate researcher at Texas A&M University or at his alma mater, Carleton College. Some of the initial synthesis in Chapter VI was performed by Dr. Chandra Mouli Palit during his time as a graduate student at Texas A&M University. All computational analysis was performed by Dr. Jia Zhou (Harbin Institute of Technology: Shenzhen, China).

All other work conducted for this dissertation was completed by the student independently.

This work was made possible in part by the U.S. National Science Foundation (grants CHE-1300299 and CHE-1565923 to O. V. O.) and the Welch Foundation (grant A-1717 to O. V. O.). Its contents are solely the responsibility of the authors and do not necessarily represent the official views of the U.D. National Science Foundation or the Welch Foundation.

NOMENCLATURE

$BArF_{20}$	Tetrakis(pentafluorophenyl)borate
BHT	2,6-di-*tert*-butyl-4-methylphenol
COD	1,5-Cyclooctadiene
COE	Cyclooctene
Cp	Cyclopentadienyl
DFT	Density Functional Theory
DHBTA	Dehydrogenative Borylation of Terminal Alkynes
DMAP	4-dimethylaminopyridine
DPPF	1,1'-bis(diphenylphosphino)ferrocene
Et	Ethyl
Et_2O	Diethyl Ether
HBpin	Pinacolborane, 4,4,5,5,-tetramethyl-1,3,2-dioxaborolane
HOAc	Acetic acid, ethanoic acid
^{i}Pr	Isopropyl
L	Generic Two-Electron Donor Ligand
Me	Methyl
NaOAc	Sodium Acetate
NBS	*N*–bromosuccinimide
NCS	*N*–chlorosuccinimide
NMR	Nuclear Magnetic Resonance

OA	Oxidative Addition
OAc	Acetate
OPiv	Pivalate
OTf	Triflate, trifluoromethanesulfonate
Ph	Phenyl
Piv	Pivaloyl group (*t*-BuC(O))
PTFE	Polytetrafluoroethylene
RE	Reductive Elimination
RT	Room Temperature
^{t}Bu	*Tert*-butyl
THF	Tetrahydrofuran
TMS	Trimethylsilyl
XRD	X-Ray Diffraction

TABLE OF CONTENTS

Page

ABSTRACT....ii

DEDICATION....iv

ACKNOWLEDGEMENTS....v

CONTRIBUTORS AND FUNDING SOURCES....vi

NOMENCLATURE....viii

TABLE OF CONTENTS....x

LIST OF SCHEMES....xiv

LIST OF FIGURES....xviii

LIST OF TABLES....xxviii

CHAPTER I INTRODUCTION AND LITERATURE REVIEW....1

1.1 Introduction to Cross-Coupling and General Mechanism....1
1.2 Introduction to Pincer Ligands....3
1.3 Preparation of Borylated Substrates....6
1.4 Introduction to Cobalt in Homogeneous Catalysis and Potential for Single Electron Processes....8
1.5 Introduction to the Transition Metal Mediated Cleavage of Esters....15

CHAPTER II KINETICS OF THE DEHYDROGENATIVE BORYLATION OF TERMINAL ALKYNES....20

2.1 Introduction....20
2.2 Results and Discussion....23
2.2.1 Synthesis and Reactivity of New (PNP)Ir Complexes....23
2.2.2 Preliminary Reactivity Comparison of (PNP)Ir Precatalysts....26
2.2.3 Rate Law Determination....28
2.2.4 Resting State Determination and the Role of H_2....30
2.2.5 KIE Determination and Analysis of Hammett and Eyring Plots....34
2.3 DFT Analysis....36

2.3.1 DFT Analysis of Plausible Intermediates: Boryl Migration 36
2.3.2 DFT Analysis of Plausible Intermediates: 1,2 Addition 39
2.3.3 DFT Analysis of Plausible Intermediates: Diboryl Pathway 41
2.3.4 DFT Analysis of Plausible Intermediates: Monoboryl Pathway 43
2.4 Conclusion 49
2.5 Experimental 51
2.5.1 General Considerations 51
2.5.2 Synthesis of Compounds 52
2.5.3 X-Ray Structural Determination Details for (^{Me}PNP$^{iPr/Et}$)Ir(Bpin)$_2$ (**204b)** 59
2.5.4 Experiments to Determine the Resting State of (^{Me}PNP^{iPr})IrH$_2$ **202a** During DHBTA 61
2.5.5 Experiments to Reactivities of Catalysts 65
2.5.6 Experiments to Determine the Rate Constant for (^{Me}PNP^{X})Ir Complexes 65
2.5.7 Experiments to Determine $\Delta H^{\ddagger}$ and $\Delta S^{\ddagger}$ 73
2.5.8 Experiments to Determine the Hammett Parameter (ρ) 75
2.5.9 Experiments to Determine the H/D Kinetic Isotope Effect 76
2.5.10 Experiments to Determine the Effect of H_2 on the Rate of Catalysis 79
2.5.11 DFT Calculations 81

CHAPTER III AIR STABLE DHBTA PRECURSOR 83

3.1 Introduction 83
3.2 Results and Discussion 85
3.2.1 Synthesis and Characterization of Iridium Precatalyst 85
3.2.2 (PNP)IrH(OAc) Air Stability Testing 86
3.2.3 DHBTA Performance of (PNP)Ir(H)(OAc) 86
3.3 Conclusion 90
3.4 Experimental 91
3.4.1 General Considerations 91
3.4.2 Synthesis of (PNP)IrH(OAc) 92
3.4.3 Testing Air Stability of (PNP)Ir(H)(OAc) and Borylated 4-ethynyltoluene 93
3.4.4 DHBTA Experiments Using (PNP)IrH(OAc) as a Precatalyst 96

CHAPTER IV SYNTHESIS AND REACTIVITY OF PINCER-TYPE COBALT SILYL AND SILYLENE COMPLEXES 104

4.1 Introduction 104
4.2 Results and Discussion 106
4.2.1 Cobalt Silylene Synthesis 106
4.2.2 Structural and Electronic Properties of the (PSiP)Co Series 108
4.2.3 O–H Splitting at the Co=Si Bond 111
4.3 Conclusion 114
4.4 Experimental 115
4.4.1 General Considerations 115

4.4.2 Synthesis and Characterization 116

CHAPTER V ATTEMPTS AT USING (POCOP)CO FOR C–S COUPLING 124

5.1 Introduction 124
5.2 Results and Discussion 129
5.2.1 Synthesis and Characterization of (POCOP)Co^{II} Complexes 129
5.2.2 Alternate Metalation of (POCOP) Using CoI_2. 132
5.2.3 Attempted Synthesis of (POCOP)Co(F) and (POCOP)Co(CF_3) 133
5.2.4 Synthesis and Characterization of (POCOP)Co^{III} Complexes 136
5.2.5 X-ray Structural Studies 139
5.2.6 Thermolysis and Observation of C_{ligand}–C_{Ph} Reductive Elimination From (POCOP)Co(Ph)(SPh) 141
5.2.7 Prospects for Preventing C–C Elimination with the POCOP Ligand 142
5.3 Conclusion 144
5.4 Experimental 145
5.4.1 General Considerations 145
5.4.2 Synthesis and Characterization of Cobalt Complexes 146
5.4.3 Thermolysis and Stability Studies on (POCOP)Co^{III} Complexes 155
5.4.4 Synthesis of Co Complexes Supported by ^{tBu}POCOP^{iPr} 157
5.4.5 Spectra from Attempted Synthesis of (POCOP)Co(F) 160
5.4.6 X-Ray Crystallography 162

CHAPTER VI MECHANISTIC INSIGHT INTO C–S BOND FORMATION AT (PNP)CO 168

6.1 Introduction 168
6.2 Results and Discussion 171
6.2.1 Synthesis and Characterization of (PNP)Co^{II} Complexes 171
6.2.2 Synthesis and Characterization of (PNP)Co^{III}(Ar)(X) Complexes 173
6.2.3 Synthesis and Characterization of (PNP)Co^{I} Complexes 175
6.2.4 X-ray Structural Studies 176
6.2.5 Thermolysis of (PNP)Co^{III}(Ar)(SAr) Complexes 177
6.2.6 Comproportionation Hypothesis and Reactions with Co^{I} Compounds 180
6.2.7 Reversibility of C–S RE 181
6.2.8 DFT Calculations 183
6.3 Conclusion 190
6.4 Experimental 190
6.4.1 General Considerations 190
6.4.2 Synthesis and Characterization 192
6.4.3 Probing the Mechanism of C–S Elimination From (PNP)Co 202
6.4.4 Reactions of Co^{I} Compounds 213
6.4.5 Computational Details 220
6.4.6 X-Ray Crystallography 221

CHAPTER VII ATTEMPTED OXIDATIVE ADDITION TO THE PNP COBALT FRAGMENT 226

7.1 Introduction 226
7.2 Results and Discussion 227
7.2.1 Production of and Evidence for the Existence of a T-Shaped Cobalt Fragment 227
7.2.2 Production of the Cobalt Fragment in the Presence of Aryl Halides 228
7.2.3 Ligand Exchange about (PNP)Co^{III} and Stability Testing of **607a** 232
7.2.4 Reactions between $[(PNP)Co]_2$ and Halogenated Arenes and the Fate of $•C_6H_4F$ 237
7.2.4 Single Electron Reactivity of Co^{II} Complexes Involving Thiolates 241
7.3 Conclusion 242
7.4 Experimental 242
7.4.1 General Considerations 242
7.4.2 Synthesis and Characterization 243
7.4.3 Experiments to Probe the Mechanism of Aryl Halide Activation by (PNP)Co 248
7.4.4 Stability Testing of (PNP)Co(Ph)(I) 257
7.4.5 Single Reactivity of Cobalt Complexes with Disulfides 259

CHAPTER VIII REACTIONS OF PNP LIGATED COBALT COMPLEXES WITH ALCOHOLS AND THEIR DERIVATIVES 261

8.1 Introduction 261
8.2 Results and Discussion 265
8.2.1 Synthesis of (PNP)Co(OR) Complexes for ROH Dehydrogenation and Unfortunate Lability of the PNP Ligand 265
8.2.2 Attempted Alcohol Dehydrogenation Reactions 268
8.2.2 Attempted Ester Cleavage Reactions 269
8.3 Conclusion 272
8.4 Experimental 273
8.4.1 General Considerations 273
8.4.2 Synthesis and Characterization 274
8.4.2 Reactions of Co^{II} Complexes En Route to Alcohol Dehydrogenation 279
8.4.3 Attempts at Cobalt Mediated Ester C–O Bond Cleavage 282

CHAPTER IX CONCLUSION 287

REFERENCES 290

APPENDIX A RANDOM REACTIONS 323

APPENDIX B LIST OF PUBLICATIONS RESULTING FROM PH.D. WORK 327

LIST OF SCHEMES

Page

Scheme I-1. Generic representation of oxidative addition and reductive elimination to a transition metal. 3

Scheme I-2. Oxidative addition to (PXP)M fragment (pincer truncated for DFT calculations). 5

Scheme I-3. Left: Rotation of Ph substituent required to reductively eliminate Ph–X from a 5-coordinate metal ligated by a pincer ligand. Right: The ground state structure of Pd bis aryl complexes prior to reductive elimination. 5

Scheme I-4. Top: Traditional synthesis of borylated arenes. Bottom: Transition metal catalyzed borylation of benzenes. 7

Scheme I-5. Top: Hydroboration of alkenes. Bottom: Monoborylation of alkynes. 7

Scheme I-6. Top: Hydroformylation catalyzed by dicobalt octacarbonyl. Middle: The Pauson-Khand reaction mediated by dicobalt octacarbonyl. Bottom: The Nicholas reaction catalyzed by dicobalt octacarbonyl. 9

Scheme I-7. Top: Autoxidation catalyzed by $CoCl_2$. Middle: The synthesis of substituted pyrroles catalyzed by $CoCl_2$. Bottom: Coupling of allyl halides with Grignard reagents catalyzed by $CoCl_2$. 10

Scheme I-8. Top: Radical polymerization initiated by single electron transfers from X atom abstraction by a transition metal. Middle: Radical trifluoromethylation initiated by single electron transfer from a transition metal. Bottom: Radically induced cyclization and coupling mediated by transition metals. 13

Scheme I-9. Pathways in which comproportionation between two metal centers of different oxidation states is active. Top: Comproportionation between Co^0 and Co^{II} resulting in Co^{I}. Middle: Comproportionation between Co^{I} and Co^{III} resulting in two Co^{II} complexes. Bottom: (dppf)Ni^0/Ni^{II} comproportionation events. 14

Scheme I-10. Nickel mediated cross-coupling of aryl esters with nucleophiles (nuc^-). 16

Scheme I-11. Top: Nickel catalyzed Suzuki-Miyaura cross-coupling of aryl boronic acids with aryl pivalates. Bottom: Isolated and characterized product of oxidative addition of aryl pivalates to Ni^0. 17

Scheme I-12. Pathways resulting from two types of aryl pivalate ester C–O bond cleavage. 19

Scheme II-1. Top: Conventional, stoichiometric alkynylboronate synthesis. Bottom: Iridium catalyzed DHBTA. 21

Scheme II-2. The precatalysts selected for DHBTA in this work (top) and the synthesis of new iridium compounds (bottom). 24

Scheme II-3. DHBTA reactions for alkynes in Table II-1. 28

Scheme III-1. Dehydrogenative borylation of terminal alkynes defined, and the various DHBTA precatalysts from the literature 83

Scheme III-2. Top: Synthesis of (PNP)IrH(OAc) (301). Bottom: Ageing experiments. . 84

Scheme III-3. Top: Use of 301 in DHBTA. Bottom: The resting state observed in the reactions with *p*-MeC_6H_4CCH and Me_2NCH_2CCH. 88

Scheme III-4. DHBTA in the presence of 1 eq. H_2O with a varying amount of HBpin .. 89

Scheme IV-1. Preparation of ($^{iPr}P_2Si$)Co hydrosilyl (401) and silylene complex (402) 106

Scheme IV-2. Synthesis of complexes 403-405 109

Scheme IV-3. Formation of ethoxy- and hydroxysilyl complexes from silylene 402. .. 113

Scheme V-1. Synthesis of (POCOP)Co^{II}-Hal complexes. 130

Scheme V-2. Synthesis of (POCOP)Co^{II}-X compounds. 131

Scheme V-3. Metalation of CoI_2 to (POCOP)H 133

Scheme V-4. Previously documented synthesis of 509 and 510 and current attempts as synthesizing 509. 134

Scheme V-5. Top: Reactions of 505 with haloforms. Bottom: Current attempts at synthesizing 510. 135

Scheme V-6. Synthesis of (POCOP)Co^{III} compounds 513-516 137

Scheme V-7. Top: Previously reported observations upon thermolysis of (POCOP)Rh(Ph)(SPh). Bottom: Observations for thermolysis of (POCOP)Co(Ph)(SPh). 141

Scheme V-8. Synthesis of (^{tBu}POCOP)Co^{II} complexes 521-523. 144

Scheme VI-1. C–S coupling observed for the (POCOP)Rh(Ph)(SPh) (517) and (PNP)Rh(Ph)(SPh) (601) complexes (Top), C–C coupling with the pincer carbon in (POCOP)Co(Ph)(SPh) 516 (Middle), and the subject of this work (bottom). 169

Scheme VI-2. Transmetalation reactions among (PNP)Co^{II}(X) 171

Scheme VI-3. Oxidation of (PNP)Co^{II} and synthesis of target (PNP)Co(Ar)(S-Ar) 174

Scheme VI-4. Formation of proposed (PNP)Co(PPh_3) (610) and equilibrium between $(PNP)_2Co_2$ (609) and (PNP)Co($P(Ar)_3$) (612). 176

Scheme VI-5. Top: Thermolysis of 608a and observed products. Bottom: Thermolysis of 608b and observed products. 178

Scheme VI-6. Thermolysis of a mixture of 608a and 608b. 179

Scheme VI-7. Top: Thermolysis of 608a in the presence of 605b and observed products. Bottom: Thermolysis of 608b in the presence of 6A and observed products.....180

Scheme VI-8. Reaction pathways shown to generate a 1:1 mixture of 604a and 605a. 181

Scheme VI-9. Thermolysis of $[(PNP)Co]_2$ (607) with 2-isopropylphenyl-4'-fluorophenyl sulfide (6E) and the following treatment with non-aqueous HCl.....183

Scheme VI-10. DFT calculated energies for the various transformations. Reaction free energies (at 298 K) are given over the arrows on top; reaction enthalpies in italic below. All the energies are in kcal/mol. Normalized per one mole of Co.....185

Scheme VII-1. Thermolysis of 608a under an atmosphere and the production of 701..227

Scheme VII-2. Treatment of (PDI)Co(N_2) (703) with alkyl/aryl halides and observed products.....229

Scheme VII-3. Top: Thermolysis of 608a with *p*-C_6H_4I (10 eq.) and observed products. Bottom: Thermolysis of 608a with *p*-C_6H_4Br and observed products.....230

Scheme VII-4. Relative rates of the reactions which consume 614. 232

Scheme VII-5. Potential reactions to explain formation of 607a in the thermolysis of 608a with *p*-FC_6H_4I. 233

Scheme VII-6. Thermolysis of 608a and 605b and observed diarylsulfide product. 234

Scheme VII-7. Probing the instability of 607a to heat and unsaturated Co^{I}. 235

Scheme VII-8. Top: Thermolysis of 608a with 2-allyloxyoiodobenzene and observed products. Bottom: Thermolysis of 604a with 2-allyloxyiodobenzene resulting very poor conversion. 237

Scheme VII-9. Top: Treatment of 609 with 4-fluorohalobenzenes and observed products. Bottom: Fate of fluorophenyl radical ejected from the reaction of 609 with 4-fluorohalobenzenes.....238

Scheme VII-10. Reaction of 608a with 4-fluorohalobenzene and observed products...240

Scheme VII-11. Reaction of 609 with 2-allyloxyiodobenzene and observed products. 240

Scheme VII-12. Top: Reaction of 604a with 7I and observed products. Bottom: Reaction of Co^{II} thiolates with CO and observed products. 241

Scheme VIII-1. Top: Reactions of 801 in the cleavage of vinyl and allyl acetates. Bottom: Reaction of 801 and 802 in the cleavage of aryl carboxylates yielding 803, cobalt carbonyls, and carbonyl-containing organic byproducts.....263

Scheme VIII-2. Publications by the Gosmini group. Top: Allylation of aryl halides using cobalt. Middle: Vinylation of aryl halides using cobalt. Bottom: Allylation of carbonyl compounds using cobalt. Excess reductant is used in each case. 264

Scheme VIII-3. Attempts at synthesizing (PNP)Co(OAc) (804) and (PNP)Co(OPiv) (805).....267

Scheme VIII-4. Synthesis of (PNP)Co(O^{i}Pr) (806) and (PNP)Co(OTf) (807).....268

Scheme VIII-5. Attempted alcohol dehydrogenation reactions. 269

Scheme VIII-6. Alternate synthesis of 609 and attempted synthesis from cobalt (0) powder. 270

Scheme VIII-7. Attempted C–O bond cleavage reactions mediated by (PNP)Co.....272

LIST OF FIGURES

Page

Figure I-1. Generic catalytic cycle for Group 10 metal catalyzed cross-coupling. 2

Figure I-2. Top: Generic pincer ligands. Positions X, Y, Z, E, and R indicate positions which can be modified. Bottom: Pincer ligands ordered by *trans* influence and pi acceptor ability of the central donor. (References for ligands: ^{Me}PNP^{iPr},[21] ^{py}PNP^{iPr},[22] PCP^{iPr},[23] PSi=P^{iPr},[24] PBP^{iPr} [25]) 4

Figure I-3. Literature known cobalt starting materials envisaged as precursors to pincer complexes of cobalt. Left: Co^{I} precursors. Right: Co^{II} precursors. 11

Figure I-4. Two types of C–O bond cleavage available to esters. 16

Figure II-1. POV-Ray renditions of ORTEP plots (50% probability ellipsoids) of 204b showing selected atom labeling. Hydrogen atoms are omitted. Selected bond distances (Å) and angles (deg) for 204b follow: Ir1-P1, 2.3170(15); Ir1-P2, 2.2999(16); Ir1-N1, 2.090(4); Ir1-B1, 2.043(10); Ir1-B2, 2.047(17); P1-Ir1-P2, 162.13(5); B1-Ir1-B2, 71.7(9); N1-Ir1-B1, 144.4(5); N1-Ir1-B2, 143.9(8); N1-Ir1-P1, 80.96(14); N1-Ir1-P2, 81.95(14).. 26

Figure II-2. Consumption of 4-ethynyltoluene versus time. 29

Figure II-3. Comparison of 4-ethynyltoluene DHBTA rates with four different iridium precatalysts. The values beneath each compound are k* for the DHBTA reaction catalyzed by that precatalyst where $k^* = k[H_2]^{-1}$, in L/(mol×s). 30

Figure II-4. Top: First order fit of alkyne consumption with time. Bottom: Dihydrogen concentration in solution as observed vs a 1,4-dioxane internal standard. 32

Figure II-5. Comparison of DHBTA rates of 4-ethynyltoluene and 4-(ethynyl-*d*)toluene for isolated kinetic isotope experiments catalyzed by 202a. 34

Figure II-6. Hammett plot arising from the DHBTA of a series of 4-$XC_6H_4C{\equiv}CH$ (X = CF_3, H, CH_3, OMe, NMe_2). The values for k_x here are k_{obs} for the DHBTA reaction with the designated alkyne. 35

Figure II-7. Eyring Plot arising from DHBTA of 4-ethynyltoluene with 202a at different temperatures. 36

Figure II-8. Calculated energies (free energy values underlined; enthalpies underneath in italic) for the migration of Bpin from the metal to the nitrogen atom of PNP. 37

Figure II-9. Calculated energies (free energy values underlines; enthalpies underneath in italic) for the 1,2-addition of PhCCH across the Ir-N bond and some subsequent steps 40

Figure II-10. Calculated energies for the catalytic diboryl pathway. 43

Figure II-11. Calculated energies for the catalytic monoboryl pathway. 45

Figure II-12. Global TS for the monoboryl pathway (TS219-220) corresponding to the B–H rotation. The view on the right omits the non-metal-bound atoms of the PNP ligand for clarity. 46

Figure II-13. Linearization of TS. 49

Figure II-14. The hydride region of a ^{1}H NMR (500 MHz, C_6D_6) spectrum during the borylation of 4-ethynyltoluene using 202a as a precatalyst. Two hydride resonances are observed which correspond to 205a.[47] 62

Figure II-15. $^{31}P\{^{1}H\}$ NMR (202 MHz, C_6D_6) spectrum during the borylation of 4-ethynyltoluene using 202a as a precatalyst. Only one resonance is observed. This resonance corresponds to 205a.[47] 63

Figure II-16. The hydride region of a ^{1}H NMR (500 MHz, C_6D_6) spectrum during the borylation of 4-ethynyltoluene using 202d as a precatalyst. Two hydride resonances are observed which have been assigned to ($^{F}PNP^{iPr}$)Ir(H)$_3$(Bpin) (205d) by comparison to 205a (vide supra). 64

Figure II-17. ^{19}F NMR (470 MHz, C_6D_6) spectrum during the borylation of 4-ethynyltoluene using 202d as a precatalyst. Only one resonance is observed which has been assigned to 205d. 64

Figure II-18. Influence of [HBpin] on the rate of DHBTA. 67

Figure II-19. Influence of [202a] on the rate of DHBTA 69

Figure II-20. Influence of [202b] on the rate of DHBTA 70

Figure II-21. Influence of [202c] on the rate of DHBTA. 71

Figure II-22. Influence of [202d] on the rate of DHBTA. 72

Figure II-23. ^{1}H NMR (500 MHz, C_6D_6) spectra of an *in situ* DHBTA reaction using 202a as a precatalyst (Time = 0 minutes). Top: ^{1}H NMR spectrum of the tube that would remain upright. Bottom: ^{1}H NMR spectrum of the tube that would be shaken. Neither tube was agitated at this point, and the spectra are superimposable 80

Figure II-24. ^{1}H NMR (500 MHz, C_6D_6) spectrum of in *in situ* DHBTA reaction using 202a as a precatalyst (Time = 14 minutes). Top: ^{1}H NMR spectrum of the tube that remained upright 75% of the alkyne has been converted to the alkynylboronate. Bottom: ^{1}H NMR spectrum of the tube that had been shaken. All the starting alkyne has been consumed 81

Figure III-1. $^{31}P\{^{1}H\}$ NMR (202 MHz, C_6D_6) spectra of 301 after stirring open to air for 30, 60, 110, and 180 minutes. 94

Figure III-2. ^{1}H NMR (400 MHz, C_6D_6) of samples of 301 open to air (as solids) for varying periods of time. From top to bottom: 6 days (500 MHz ^{1}H spectrum), 12 days, 24 days, and 110 days (400 MHz ^{1}H NMR spectra each) open to air in the solid state. 95

Figure III-3. ^{1}H NMR (400 MHz, C_6D_6) spectrum of a DHBTA reaction using 10^{-6} eq. 301 to borylate Me_2NCH_2CCH with 2 eq. HBpin. 97

Figure III-4. $^{31}P\{^{1}H\}$ NMR (162 MHz, C_6D_6) spectrum of 301 after complete aerobic degradation. Arrow indicates where 301 would be observed if any remained. 98

Figure III-5. ^{1}H NMR (400 MHz, C_6D_6) spectrum at 90 minute timepoint of Me_2NCH_2CCH DHBTA reaction catalyzed by aerobically degraded 301. Insert. Hydride region showing two resonances corresponding to 205a[47] 99

Figure III-6. ^{1}H NMR (500 MHz, C_6D_6) spectrum of a DHBTA reaction using 301 to borylate 4-MeC_6H_4CCH with 1 eq. H_2O and 2 eq. HBpin. Timepoint shown is 20 min after the vigorous bubbling ceased. A small amount of 4-ethyltoluene is observed as a singlet at 6.97 ppm.[47] 100

Figure III-7. ^{1}H NMR (400 MHz, C_6D_6) spectrum of a DHBTA reaction using 301 to borylate 4-MeC_6H_4CCH with 1 eq. H_2O and 4.1 eq. HBpin. Timepoint shown is 20 min after the vigorous bubbling ceased. A small amount of 4-ethyltoluene is observed as a singlet at 6.97 ppm.[47] 101

Figure III-8. ^{1}H NMR (400 MHz, C_6D_6) spectrum at 90 minute timepoint of 4-MeC_6H_4CCH DHBTA reaction catalyzed by 301 under air. Insert: Hydride region showing two resonances corresponding to 205a.[47].....103

Figure IV-1. Previously reported silylene complexes supported by pincer-type [P_2Si] ligands. 104

Figure IV-2. POV-Ray renditions of Ortep plots (50% probability ellipsoids) of hydrosilyl complex 401 and silylene complex 402 with thermal ellipsoids at the 50% probability level. Hydrogen atoms, the BArF 20 anion of 2, and cocrystallized toluene of 2 are omitted for clarity. Selected bond lengths (Å) and angles (deg) for 401: Si−Co, 2.2671(7); Co−C1, 1.750(2); Co−C2, 1.760(2); Si−Co−C1, 85.20(7); P1−Co−P2, 128.20(3). For 402: Si−Co, 2.121(2); Co−C1, 1.790(8); Co−C2, 1.770(8); Si−Co−C1, 115.1(3); P1−Co−P1*, 156.19(7). 108

Figure IV-3. Depiction of the LUMO (isovalue 0.03) of 402, calculated by M06/SDD/6-31G(d). Hydrogen atoms are omitted for clarity. 111

Figure IV-4. POV-Ray rendition of Ortep plots (50% probability ellipsoids) of complexes 403−406-anti with all hydrogen atoms (except for Co−H in 406-anti), counterions (for 405 and 406-anti), and cocrystallized solvent molecules omitted for clarity. Selected bond lengths (Å) and angles (deg) for 403: Co1−Si1, 2.2453(6); Co1−C1, 1.762(2); Co1−C2, 1.7715(19); Si1−Cl, 2.1189(8); Si−Co1−C1, 90.87(6); P1−Co1−P2, 133.65(2). For 404: Co1−Si, 2.2163(11); Co1−C1, 1.763(4); Co1−C2, 1.777(4); Si1−O3, 1.797(3); Si1−Co1−C1, 87.12(14); P1−Co1−P2, 132.49(4). For 405: Co1−Si1, 2.2229(14); Co1−C1, 1.773(5); Co1−C2, 1.761(5); Si1−N1, 1.920(4); Si1−Co1−C1, 99.71(15); P1−Co1−P2, 138.27(5). For 406-anti: Co−H, 1.43(4); Co−Si, 2.2885(9); Co−C1, 1.805(3); Co1−C2, 1.824(3); Si1−O3, 1.640(2); Si1−Co1−H1, 72.4(15); Si1−Co1−C1, 91.20(10); P1−Co1−P2, 156.46(4). 112

Figure V-1. Left: Generic Mechanism for Pd-catalyzed coupling of aryl halides with nucleophiles. Right: Previously proposed mechanism for coupling of aryl halides with nucleophiles using (POCOP)Rh. 125

Figure V-2. Proposed mechanisms for Co-catalyzed coupling reactions. Left: Suzuki-Miyaura coupling of aryl triflates; center: aryl iodide amination; right: arylation of thiols envisaged in this work. 128

Figure V-3. ^1H NMR spectrum of (POCOP)Co(Ph)(Cl) (513) showing inequivalence of the five hydrogens of the Co-bound C_6H_5 group. 139

Figure V-4. POV-Ray rendition of Ortep plot (50% probability ellipsoids) of (POCOP)Co(SPh) (508, left), (POCOP)Co(Ph)(I) (515, center), and (POCOP)Co(Ph)(SPh) (516, right). Hydrogen atoms are omitted for clarity. Selected bond distances (Å) and angles (deg) for 508: Co1-P1, 2.1816(8); Co1-P2, 2.1719(9); Co1-S1, 2.1706(8); S1-C1, 1.773(2); P1-Co1-P2,

161.86(2); C7-Co1-S1, 163.15(6); Co1-S1-C1, 119.89(7). Selected bond distances (Å) and angles (deg) for 515: Co2-P1, 2.210(2); Co2-P2, 2.204(2); Co2-I1, 2.601(2); Co2-C18, 1.907(3); Co2-C19, 1.940(3); P1-Co2-P2, 161.83(4); C18-Co2-I1, 155.19(9); C19-Co2-I1, 115.86(9); C18-Co2-C19, 88.9(1). Selected bond distances (Å) and angles (deg) for 516 follow: Co1-C25, 1.947(2); Co1-P3, 2.222(1); Co1-P1, 2.223(1); Co1-S1, 2.215(1); Co1-C1, 1.933(2); C1-Co1-C25, 89.54(8); C1-Co1-P3, 81.80(5); C1-Co1-P1, 80.24(5); C1-Co1-S1, 148.98(6); C25-Co1-S1, 119.96(6). 140

Figure V-5. ORTEP drawing (50% probability ellipsoids) of ($^{t\text{Bu}}$POCOP)Co(Cl) (521, Left) and ($^{t\text{Bu}}$POCOP)Co(Cl)(DMAP) (522, Right). Hydrogen atoms are omitted for clarity. Selected bond distances (Å) and angles (deg) for 521: Co1-C1, 1.9230(15); Co1-Cl1, 2.2157(6); Co1-P1, 2.1720(7); Co1-P2, 2.1656(6); C1-Co1-Cl1, 177.79(5); P1-Co1-P2, 163.68(2). For 522: Co1-N1, 2.074(7); Co1-P1, 2.1798(15); Co1-Cl1, 2.287(3); Co1-C1, 1.936(8) N1-Co1-Cl1, 99.7(2); P1-Co1-P1*, 159.02(11); C1-Co1-Cl1, 157.2(2); P1-Co1-Cl1, 96.02(6); P1-Co1-N1, 97.42(6).....143

Figure V-6. ^{1}H NMR (400 MHz, C_6D_6) spectrum of 513. Sample contains residual TMSCl. 151

Figure V-7. ^{1}H NMR (C_6D_6, 500 MHz) of the reaction mixture resulting from the addition of 1 eq. $CoCl_2$ and 1 eq. DMAP to ($^{t\text{Bu}}$POCOP)H.....158

Figure V-8. ^{1}H NMR (500 MHz, C_6D_6) spectrum of 521.....159

Figure V-9. ^{1}H NMR (400 MHz, C_6D_6) spectrum of 523.....160

Figure V-10. ^{1}H NMR (500 MHz, C_6D_6) spectrum of (POCOP)Co(F) reported previously. 161

Figure V-11. New attempt at synthesizing (POCOP)Co(F). Top: ^{1}H NMR (500 MHz, C_6D_6) spectrum of mixture after 3.6 eq. CsF. Bottom: ^{1}H NMR (500 MHz, C_6D_6) spectrum of mixture after addition of 68 eq. CsF. 162

Figure VI-1. Cross-coupling mechanistic cycles for Pd^0/Pd^{II} (left) and for Rh^I/Rh^{III} or Co^I/Co^{III} (right). 168

Figure VI-2. High and low spin dichotomy in POCOP and PNP pincer-supported four-coordinate complexes of Co^{II} (top) and Co^I (bottom). 173

Figure VI-3. POV-Ray renditions of ORTEP plots (50% probability ellipsoids) of 604b, 606a, and 608a. All hydrogen atoms omitted. Selected bond distances (Å) and angles (degrees) for (PNP)Co(Tol) (604b, left): N1–Co1, 1.9262(17); P1–Co1, 2.1756(7); P2–Co1, 2.1849(7); C15–Co1, 1.939(2);

N1–Co1–C15, 178.99(9); P1–Co1–P2, 172.63(3). Selected bond distances (Å) and angles (degrees) for (PNP)Co(Ph)(OAc) (606a, middle): N1–Co1, 1.9333(12); O1–Co1, 1.9896(12); O2–Co1, 2.1166(11); P1–Co1, 2.2619(7); P2–Co1, 2.2353(6); C29–Co1, 1.9403(15); C29–Co1–N1, 97.59(6); N1–Co1–O1, 165.17(5). Selected bond distances (Å) and angles (degrees) for (PNP)Co(Ph)(SPh) (608a, right): N1–Co1, 1.9497(18); P1–Co1, 2.2597(7); P2–Co1, 2.2313(7); C33–Co1, 1.933(2); S1–Co1, 2.2069(6); N1–Co1–C33, 98.54(8); N1–Co1–S1, 149.60(6). 177

Figure VI-4. Examples of three-coordinate Co complexes supported by various anionic PNP ligands. 186

Figure VI-5. Representation of the reaction coordinate for the RE of SPh_2 (6A) from (PNP)Co(Ph)(SPh) (606a) 187

Figure VI-6. DFT calculated structures of 608a (left) and the 6TS (right). 188

Figure VI-7. Plot of ln(608a integral) versus time. 203

Figure VI-8. ^{1}H NMR (500 MHz, C_6D_6) spectrum of 608b before thermolysis. 204

Figure VI-9. ^{1}H NMR (500 MHz, C_6D_6) of the thermolyzed 608b. 205

Figure VI-10. ^{19}F NMR (470 MHz, C_6D_6) of the thermolyzed 608b. 206

Figure VI-11. Variable temperature ^{19}F NMR (470 MHz, C_6D_6) observation of the mixed thermolysis of 608a with 608b (29mM and 28 mM initial concentrations respectively). Timepoints shown are at 30 minute intervals. ..208

Figure VI-12. ^{19}F (470 MHz, C_6D_6) of a pure sample of 608b spiked with 608c. 209

Figure VI-13. ^{1}H NMR (500 MHz, C_6D_6) of the mixed thermolysis of 608a with 608b after cooling to room temperature. The four expected Co(II) products are observed. 209

Figure VI-14. ^{19}F NMR (470 MHz, C_6D_6) spectrum showing the resultant mixture of thermolysis of 608b with 6A 210

Figure VI-15. ^{19}F NMR (470 MHz, C_6D_6) *in situ* spectra of thermolysis of a 1:1 mixture of 608a and 605b. 211

Figure VI-16. ^{19}F NMR (470 MHz, C_6D_6) after thermolysis of 608a in the presence of 605b showing the produced fluorinated diarylsulfide 6C. 212

Figure VI-17. ^{1}H NMR (400 MHz, C_6D_6) spectrum of the seven-day thermolysis of 604b, 605b, and 6A. Only the starting materials are observed. 213

Figure VI-18. ^{1}H NMR (500 MHz, C_6D_6) of 609 after adding PPh_3 and then tris (4-methoxyphenyl)phosphine showing closely related paramagnetically shifted ^{1}H NMR resonances. 215

Figure VI-19. ^{1}H NMR (500 MHz, C_6D_6) of 609 and 6E before heating. Sample contains residual THF and silicone grease. 217

Figure VI-20. ^{1}H NMR (500 MHz, C_6D_6) of 609 and 6E after heating at 80 °C for three days. 218

Figure VI-21. ^{1}H NMR (500 MHz, C_6D_6) of 609 and 6E after heating at 80 °C for three days and then treating with anhydrous HCl in diethyl ether. 219

Figure VI-22. GC-MS of the reaction solution resulting from treatment with HCl. GC trace (top). Mass spectrum at a retention time of 7.46 minutes (bottom).....220

Figure VII-1. (PNP)M complexes produced by the Ozerov group to generate unsaturated, T-shaped metal complexes and their corresponding activation methods. 226

Figure VII-2. ^{1}H NMR (500 MHz, C_6D_6) spectrum of 712. Sample contains residual pentane. 245

Figure VII-3. $^{31}P\{^{1}H\}$ NMR (202 MHz, C_6D_6) spectrum of 712. 245

Figure VII-4. $^{13}C\{^{1}H\}$ NMR (125 MHz, C_6D_6) spectrum of 712. 246

Figure VII-5. ^{1}H NMR (500 MHz, C_6D_6) spectrum of (PNP)Co(*p*-C_6H_4F)(I) (706). Sample contains a large amount of THF. 247

Figure VII-6. $^{31}P\{^{1}H\}$ NMR (202 MHz, C_6D_6) spectrum of (PNP)Co(*p*-C_6H_4F)(I) (706). 247

Figure VII-7. ^{19}F NMR (470 MHz, C_6D_6) spectrum of (PNP)Co(*p*-C_6H_4F)(I) (706)....248

Figure VII-8. ^{1}H NMR (400 MHz, C_6D_6) spectrum after thermolysis of 609 with *p*-C_6H_4Cl. 249

Figure VII-9. Top: Portion of GC trace of reaction mixture resulting from thermolysis of 609 with *p*-C_6H_4Cl. Bottom: Mass spectrum corresponding to GC trace at 8.68 min. m/z = 177 as expected for 7G.....250

Figure VII-10. ^{1}H NMR (500 MHz, C_6D_6) spectrum of (PNP)Co(Ph)(SPh) (608a) and *p*-FC_6H_4I (10 eq.) prior to thermolysis. Dioxane (3.35 ppm) and benzotrifluoride added as internal standards. 251

Figure VII-11. ^{1}H NMR (500 MHz, C_6D_6) Top: Aliphatic region of a mixture of 608a and *p*-FC_6H_4I before thermolysis. Bottom: Aliphatic region after thermolysis The integrated methyl resonances were selected because they were removed from overlapping resonances. 252

Figure VII-12. Expanded view of the ^{1}H NMR (500 MHz, C_6D_6) window of the thermolyzed mixture of 608a with *p*-FC_6H_4I (10 eq.) showing four identifiable (PNP)Co(X) compounds with paramagnetically shifted ^{1}H NMR resonances.....253

Figure VII-13. Expanded ^{1}H NMR (500 MHz, C_6D_6) spectral window of the thermolyzed mixture of 608a with *p*-FC_6H_4I (10 eq.) showing 604c as designated by red dots. 254

Figure VII-14. Expanded ^{1}H NMR (400 MHz, C_6D_6) spectral window of the thermolyzed mixture of 608a with *p*-FC_6H_4I and BHT (2 eq.) 605a, 604a, 604c, and 702 yielded in a 1.0:1.1:0.1:1.4 ratio. Nearly identical to the thermolysis reaction performed in the absence of BHT. 604c designated by red dots.....254

Figure VII-15. ^{1}H NMR (500 MHz, C_6D_6) spectrum of the mixture resulting from the thermolysis of 607a with 605b. 256

Figure VII-16. ^{19}F NMR (470 MHz, C_6D_6) spectrum of the mixture resulting from the thermolysis of 607a with 605a.....256

Figure VII-17. ^{1}H NMR (400MHz, C_6D_6) spectrum resulting from the thermolysis of 607a in benzene. 257

Figure VII-18. ^{1}H NMR (400 MHz, C_6D_6) resulting from the comproportionation between 607a and 609. 258

Figure VII-19. ^{1}H NMR (500 MHz, C_6D_6) spectrum showing the resultant mixture of thermolysis of 604a with 7I. 259

Figure VII-20. ^{19}F NMR (470 MHz, C_6D_6) spectrum of the products of thermolysis of 608b after addition of 1 atm CO revealing 7J and 6D in a 0.5:1.0 ratio (note two fluorines on 7J) 260

Figure VIII-1. POV-Ray rendition of Ortep plot (50% probability ellipsoids) of (PNP)Co(OAc) (804). Hydrogen atoms are omitted for clarity. Selected bond distances (Å) and angles (deg) for 804: Co1-P1, 2.2223(5); Co1-N1, 1.9144(16); Co1-O1, 2.1372(12); P1-Co1-P1*, 169.15(2); N1-Co1-O1, 149.19(4); O1-Co1-O1*, 61.61(7).....266

Figure VIII-2. ^{1}H NMR (500 MHz, C_6D_6) spectrum of 804. Sample contains non-metallated 201a 275

Figure VIII-3. ^{1}H NMR (500 MHz, C_6D_6) spectrum of 805 with free pivalic acid. 276

Figure VIII-4. ^{1}H NMR (500 MHz, C_6D_6) spectrum of 806. 277

Figure VIII-5. ^{1}H NMR (500 MHz, C_6D_6) spectrum of 807. Sample contains isopropoxytrimethylsilane. 278

Figure VIII-6. ^{19}F NMR (470 MHz, C_6D_6) spectrum of 807. Sample contains residual TMSOTf. 278

Figure VIII-7. ^{1}H NMR (400 MHz, C_6D_6) spectrum of 809. 279

Figure VIII-8. ^{1}H NMR (500 MHz, C_6D_6) spectrum of the resultant mixture from addition of >100 eq. TMSOTf to 603. 280

Figure VIII-9. ^{1}H NMR (500 MHz, C_6D_6) spectrum of an unknown paramagnet resulting from the addition of 4-fluorobenzyl alcohol to 806. 281

Figure VIII-10. Top: $^{31}P\{^{1}H\}$ NMR (202 MHz, C_6D_6) spectrum of a partially oxidized sample of 201a. Bottom: $^{31}P\{^{1}H\}$ NMR (202 MHz, C_6D_6) spectrum of the solution resulting from exposure of 806 to air. 282

Figure VIII-11. ^{1}H NMR (500 MHz, C_6D_6) spectrum of the products of thermolysis between 609 and naphthyl pivalate. 283

Figure VIII-12. ^{1}H NMR (500 MHz, C_6D_6) spectrum of the products of thermolysis between 609 and phenyl pivalate. 284

Figure VIII-13. ^{1}H NMR (400 MHz, C_6D_6) spectrum of the products of thermolysis between 609 and 4-methoxyphenyl pivalate 284

Figure VIII-14. ^{1}H NMR (400 MHz, C_6D_6) spectrum of the products of thermolysis between 609 and phenyl acetate. Unknown paramagnetic resonances do not have dots. 285

Figure VIII-15. ^{1}H NMR (400 MHz, C_6D_6) spectrum of the products of thermolysis between 609 and coumarin. 286

Figure VIII-16. $^{31}P\{^{1}H\}$ NMR (162 MHz, C_6D_6) spectrum of the products of thermolysis between 609 and coumarin. Resonances from 30-33 ppm were not identified. 286

Figure X-1. ^{1}H NMR (500 MHz, C_6D_6) spectrum of $(PNP)Co(Cl)_2$ 323

Figure X-2. POV-Ray renditions of ORTEP plots (50% probability ellipsoids) of (PNP)Co(Cl)$_2$ showing selected atom labeling. Hydrogen atoms are omitted. Selected bond distances (Å) and angles (deg) for (PNP)Co(Cl)$_2$ follow: N1-Co1, 1.8986(19); P1-Co1, 2.2760(6); Cl1-Co1, 2.2684(6); P1-Co1-P1*, 163.68(3); N1-Co1-Cl1, 126.329(17); Cl1-Co1-Cl1*, 107.34(3). . 324

Figure X-3. ^{1}H NMR (500 MHz, C_6D_6) spectrum of (SiNN)Ir(PMe$_3$)$_2$Bpin. Sample contains 1eq. of free HBpin. 325

Figure X-4. ^{31}P{^{1}H} NMR (202 MHz, C_6D_6) spectrum of (SiNN)Ir(PMe$_3$)$_2$Bpin. Sample contains residual PMe$_3$. 326

LIST OF TABLES

Page

Table I-1. Thermochemical data calculated by the Goldman group for reductive elimination of R–R' from a d^6 iridium center. 6

Table II-1. Comparison of catalyst performances with selected substrates. 27

Table II-2 k_{obs} values from ln[4-ethynyltoluene] v. time with varying [HBpin] 66

Table II-3. k_{obs} values from ln[4-ethynyltoluene] v. time with varying [202a] 68

Table II-4. k_{obs} values from ln[4-ethynyltoluene] v. time with varying [202b]. 70

Table II-5. k_{obs} values from ln[4-ethynyltoluene] v. time with varying [202c] 71

Table II-6. k_{obs} values from ln[4-ethynyltoluene] v. time with varying [202d] 72

Table II-7. Kinetic data from ln[4-ethynyltoluene] v. time at various temperatures. 73

Table II-8. k_{obs} values from ln[*p*-substituted phenylacetylene] v. time catalyzed by 202a. 75

Table II-9. k_{obs} values from ln[4-(ethynyl-*d*)toluene v. time with varying [202a] 77

Table II-10. k_{obs} values from the DHBTA of 4-ethynyltoluene at selected [202a]. 77

Table II-11. Isolated KIE values determined at two different [202a]. 77

Table II-12. k_{obs} values from ln[4-ethynyltoluene] and ln[4-(ethynyl-*d*)toluene v. time catalyzed by 202a. 78

Table III-1. Performance of 301[a] with selected substrates 88

Table IV-1. Key structural and spectroscopic parameters for silyl and silylene complexes 401-405 110

CHAPTER I

INTRODUCTION AND LITERATURE REVIEW

1.1 Introduction to Cross-Coupling and General Mechanism

Reactions catalyzed by organometallic complexes of transition metals have become increasingly common over the past century. Among the most broadly applicable of these transformations is the transition metal mediated cross-coupling to form carbon–carbon or carbon–heteroatom bonds.[1,2] These transformations have been given more and more focus since the 2010 Nobel Prize in Chemistry was awarded for palladium catalyzed cross-coupling reactions.[3] These reactions have been extended far beyond C–C bond coupling to include C–N, C–O, and C–S bond formation.[4,5,6]

These palladium style reactions typically follow a three-part mechanism involving: 1) oxidative addition of an aryl halide to the palladium zero species forming a Pd^{II} halido aryl complex 2) Transmetallation of the resultant Pd^{II} with a nucleophilic carbon or heteroatom, and then 3) reductive elimination which provides the desired product and regenerates the Pd^{0} starting material poised to undergo another catalytic cycle (Figure I-1).[2]

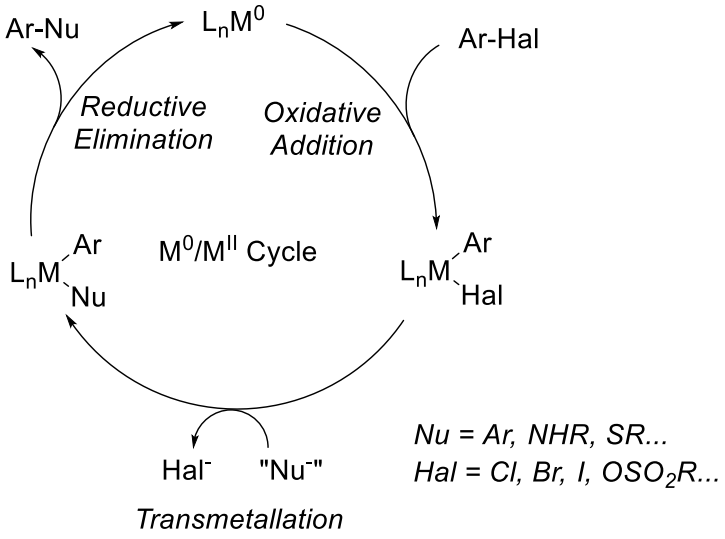

Figure I-1. Generic catalytic cycle for Group 10 metal catalyzed cross-coupling.

Almost all palladium catalyzed cross-couplings proceed via this general mechanism and this cycle has been studied in extreme detail.[1,7] The power of palladium to perform cross-coupling reactions lies in its ability to reliably undergo two e^- oxidative addition and reductive elimination reactions. The oxidative addition step involves the bond cleavage of an organic molecule which results in the formation of two new metal–ligand bonds. This process formally oxidizes the metal by two electrons; however, depending on the electronegativity of the new metal substituents, the true degree to which the metal is oxidized is uncertain.[8] The reverse of oxidative addition is reductive elimination which involves the cleavage of two palladium–ligand bonds resulting in the formation of a new bond in an organic molecule released from the metal center.[9] In this process, the formal oxidation state of the metal is decreased by two. In palladium catalyzed cross-coupling, both OA and RE are concerted and proceed via a three-membered transition state resulting in simultaneous breaking/formation of palladium–ligand bonds (Scheme I-1).[9-10]

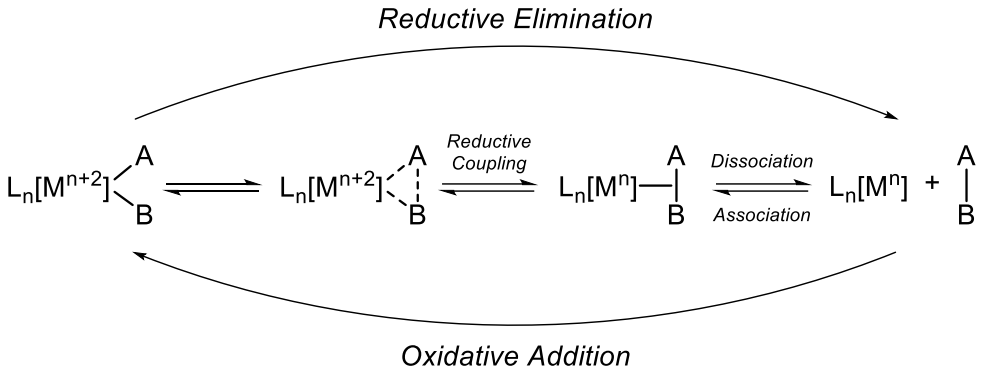

Scheme I-1. Generic representation of oxidative addition and reductive elimination to a transition metal.

A great deal of effort has been devoted to the application of this chemistry to more earth abundant, cheaper 3d transition metals including iron,[11] nickel,[12] copper,[13] and to a smaller degree, cobalt.[14]

1.2 Introduction to Pincer Ligands

Pincer ligands are tridentate meridionally binding ligands form metal complexes of high rigidity and allow for a high degree of thermal stability.[15,16] The design of pincer ligands allows for fine tuning of the electronic and steric properties of the metal center as positions X, Y, Z, E, and R in Figure I-2 (Top) can be exchanged for different atoms using slightly different synthetic methods.[15] Figure I-2 (Bottom) shows a series of pincer ligands and how they compare in relation to their donating ability to the metal as well as their *trans*- influence of the central donor. Pincer ligands are typically named by the atoms which ligate the metal. Nomenclature examples are given in Figure I-2 (Bottom). These

ligands have allowed for the isolation and characterization of complexes which are of exceptional synthetic and mechanistic interest.[17,18,19,20]

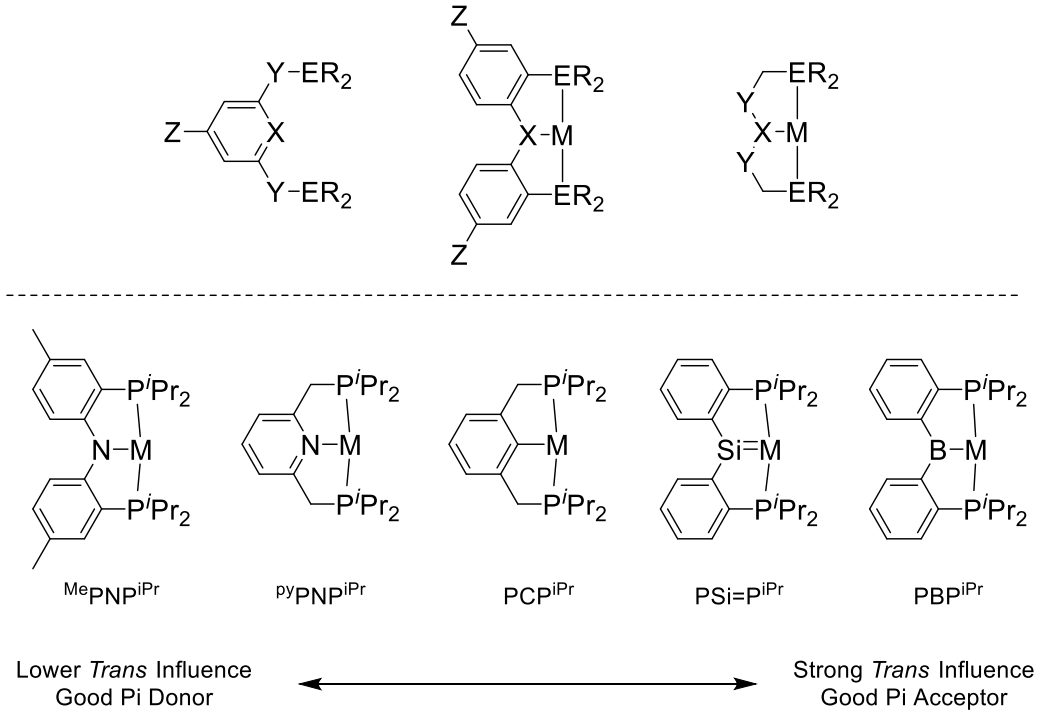

Figure I-2. Top: Generic pincer ligands. Positions X, Y, Z, E, and R indicate positions which can be modified. Bottom: Pincer ligands ordered by *trans* influence and pi acceptor ability of the central donor. (References for ligands: $^{Me}PNP^{iPr}$,[21] $^{py}PNP^{iPr}$,[22] PCP^{iPr},[23] $PSi{=}P^{iPr}$,[24] PBP^{iPr} [25])

In moving to ligands on the right of the series in Figure I-2 (Bottom), a unique caveat was discovered regarding oxidative addition to the metal center. As the central donor becomes more electron donating, it would seem that oxidative addition to the metal center would become more facile.[26] However, the more strongly donating the central donor atom of the pincer becomes, the stronger trans influence it exerts on the approaching substrate in the square plane and consequently in the 5-coordinate product.[27] As such, there exists a delicate balance between adding electron density to the metal such that the

metal can oxidatively add difficult C–X bonds yet avoid repulsing the incoming substrate or forming a high-energy product (Scheme I-2).[28]

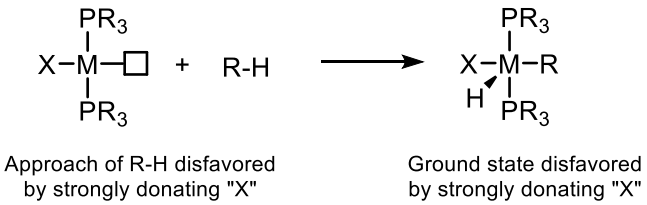

Scheme I-2. Oxidative addition to (PXP)M fragment (pincer truncated for DFT calculations).

In terms of reductive elimination, a common observation with aryl-containing 5-coordinate pincer complexes is that the aryl occupies the apical position of a square pyramid (*cis* to the central donor of the pincer). The orientation of this phenyl substituent in the ground state orthogonal or "side-on" with respect to the central donor of the pincer and the fifth ligand.[29,30] This minimizes steric repulsion between the flanking substituents and the aryl ring. In order to undergo reductive elimination, the phenyl substituent must rotate about the C–M in order to reductively eliminate with the fifth ligand (Scheme I-3).

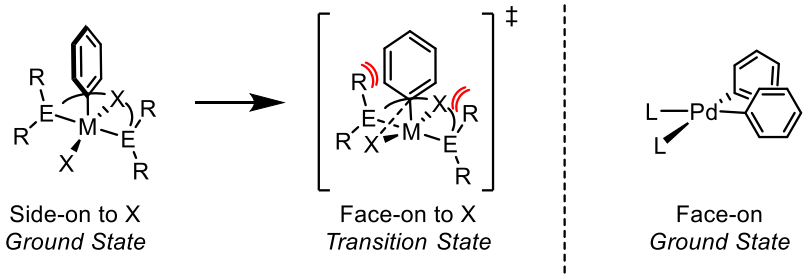

Scheme I-3. Left: Rotation of Ph substituent required to reductively eliminate Ph–X from a 5-coordinate metal ligated by a pincer ligand. Right: The ground state structure of Pd bis aryl complexes prior to reductive elimination.

The rotation of the aryl about the C–M bond is restricted by steric repulsion of the phosphine substituents. This restriction increases the barrier for reductive elimination and has been observed in several publications in our group.[31] Restricted rotation of aryls about the M–C bond may also be observed in non-pincer complexes.[32]

Table I-1. Thermochemical data calculated by the Goldman group for reductive elimination of R–R' from a d^6 iridium center.

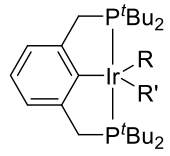 *(PCP^{tBu})Ir(R)(R')*	*R*	*R'*	*$\Delta G^{\ddagger}$ (kcal/mol)*	*ΔG (kcal/mol)*
	Ph	Ph	32.4	-25.9
	Ph	Me	27.1	-24.1
	Ph	Vinyl	20.7	-23.1
	CCPh	CCPh	7.0	-10.2

The Goldman group has studied the reductive elimination from a 5-coordinate (PCP)Ir complexes for which the barrier for reductive elimination increases with the bulk of the apical substituent (Table I-1).[33] This is in stark contrast to L_nPd^{II} complexes for which the aryl substituents are oriented "face-on" and poised for cross-coupling in the ground state.[34]

1.3 Preparation of Borylated Substrates

Borylated organic molecules are common substrates for palladium catalyzed cross-coupling reactions, appearing predominantly in Suzuki-Miyaura cross-coupling.[3] Thus, production of organic molecules containing boryl functional groups is of great interest and many different research groups have devoted effort into modification, synthesis, and advances in borylation chemistry and of new borylated materials.[19,35] Traditional synthesis

of borylated arenes involves the lithiation of aryl halides (Scheme I-4, Top).[36] The catalytic borylation of Ar–X (X = H, Hal) bonds, obviating the need for highly basic intermediates, is of particular interest and has been thoroughly studied.[36-37] Alternatives to the use of palladium have also been explored.[35b,38]

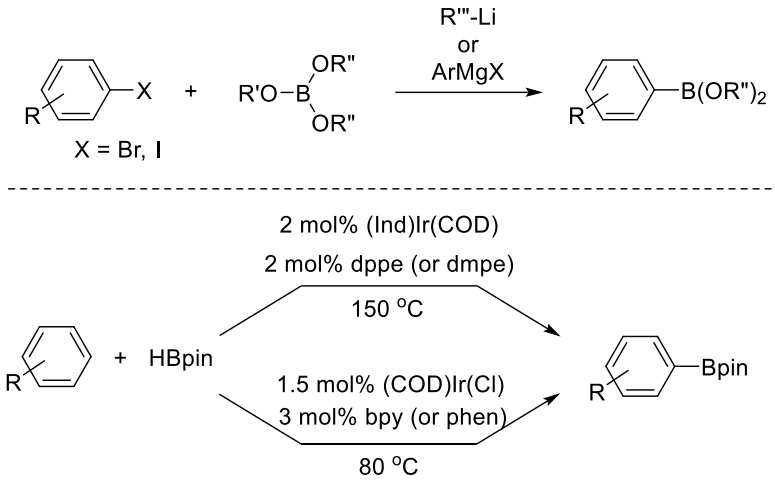

Scheme I-4. Top: Traditional synthesis of borylated arenes. Bottom: Transition metal catalyzed borylation of benzenes.

Catalytic synthesis of aliphatic and vinylic boron-containing species can be easily achieved through hydroboration of alkenes[39] (Scheme I-5, Top) or monoborylation of alkynes (Scheme I-5, Bottom);[40] respectively.

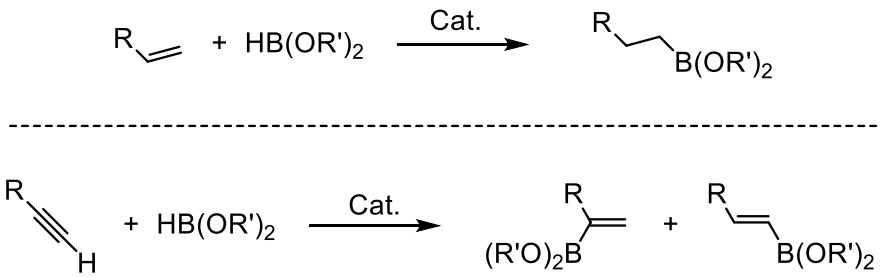

Scheme I-5. Top: Hydroboration of alkenes. Bottom: Monoborylation of alkynes.

Advances have also been made in the C–H borylation of alkanes,[41] alkenes,[42] allylic,[43] and benzylic C–H bonds.[44] Yet, a notable absence from this series is the terminal alkyne. Stoichiometric borylation of terminal alkynes has been well established and is commonly used;[45] however, our group has been particularly interested in the catalytic synthesis of alkynylboronates from alkynes and pinacolborane (See Chapters II & III).[46,47]

Given the utility of these borylated materials in not only Suzuki-Miyaura cross-coupling reactions, but also in a multitude of organic synthesis,[48] it is likely that the number of published investigations into their synthesis will continue to increase.

1.4 Introduction to Cobalt in Homogeneous Catalysis and Potential for Single Electron Processes

Cobalt has been known since the 1940's to be a transition metal active for catalysis and was initially used as a hydroformylation catalyst.[49] Hydroformylation is the net formation of aldehydes from alkenes, generically pictured in Scheme I-6 (Top). The active cobalt species for this transformation was found to be tetracarbonylhydrido cobalt. Poly-carbonyl complexes of cobalt would become much more prevalent as organometallic catalysts as dicobalt octacarbonyl was found to be very active for the Pauson-Khand reaction.[50] The Pauson-Khand reaction is a [2+2+1] between an alkyne, an alkene, and CO resulting in the formation of substituted cyclopentenones[51] (Scheme I-6, Middle). Dicobalt octacarbonyl has also been shown to perform the Nicholas reaction which is the alkylation of propargylic alcohols or their derivatives (Scheme I-6, Bottom).[52]

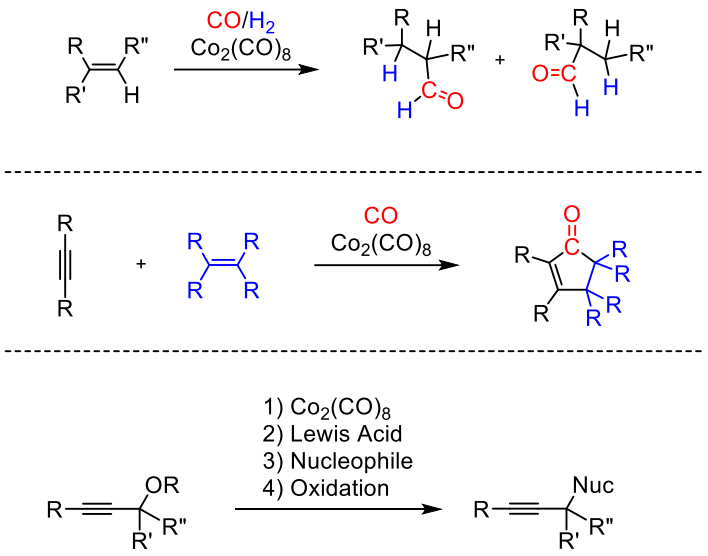

Scheme I-6. Top: Hydroformylation catalyzed by dicobalt octacarbonyl. Middle: The Pauson-Khand reaction mediated by dicobalt octacarbonyl. Bottom: The Nicholas reaction catalyzed by dicobalt octacarbonyl.

Outside of carbonyl complexes, simple cobalt salts have also found utility in catalysis. For example, cobalt (II) chloride has shown capable as a catalyst for the autoxidation of aldehydes[53] (Scheme I-7, Top), the condensation of 1,4-dipentanones to form substituted pyrroles[54] (Scheme I-7, Middle), and the cross-coupling of Grignard reagents with vinyl halides[55] (Scheme I-7, Bottom).

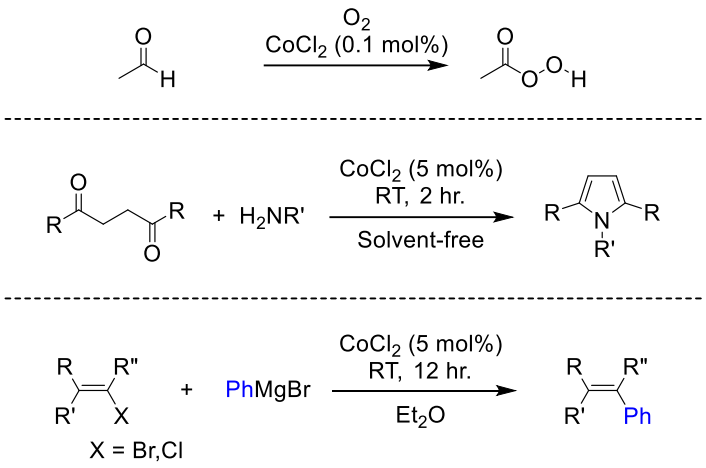

Scheme I-7. Top: Autoxidation catalyzed by $CoCl_2$. Middle: The synthesis of substituted pyrroles catalyzed by $CoCl_2$. Bottom: Coupling of allyl halides with Grignard reagents catalyzed by $CoCl_2$.

Although cobalt has a rich chemistry in organic transformations, organometallic complexes and catalytic capabilities of cobalt are largely unexplored as compared to cobalt's heavier Group 9 brethren. This is in large part due to its prevalence in forming paramagnetic cobalt complexes or participating in single electron transformations. Some work has been done using cp cobalt complexes to affect olefin insertion[56] and, in some cases, this is catalytic; however, the exploration of cobalt's ability to undergo cross-coupling reactivity is rather limited.[57]

The lower volume of cobalt complexes in the literature is a cyclic issue wherein the difficulty of working with paramagnetic cobalt materials daunts research into cobalt mediated transformations. Thus, there are fewer cobalt precursors available with which to begin the study of potential cross-coupling catalytic cycles. For example, outside of Co^{II} halide salts and the previously mentioned dicobalt octacarbonyl and tetracarbonyl hydrido cobalt, there are only a handful of cobalt materials which could be envisaged as precursors

to metal complexes. These include bis(trimethylsilylamido)cobalt,[58] dimesitylcobalt,[59] tris(triphenylphosphine)cobalt chloride,[60] bis(triphenylphosphine) bis(trimethylsilyl)amido cobalt,[61] tris(trimethylphosphine)cobalt chloride,[62] and cyclooctadienyl cyclooctadiene[63] (Figure I-3). Notably, this list excludes cobalt complexes of the cyclopentadienyl anion.[56,64]

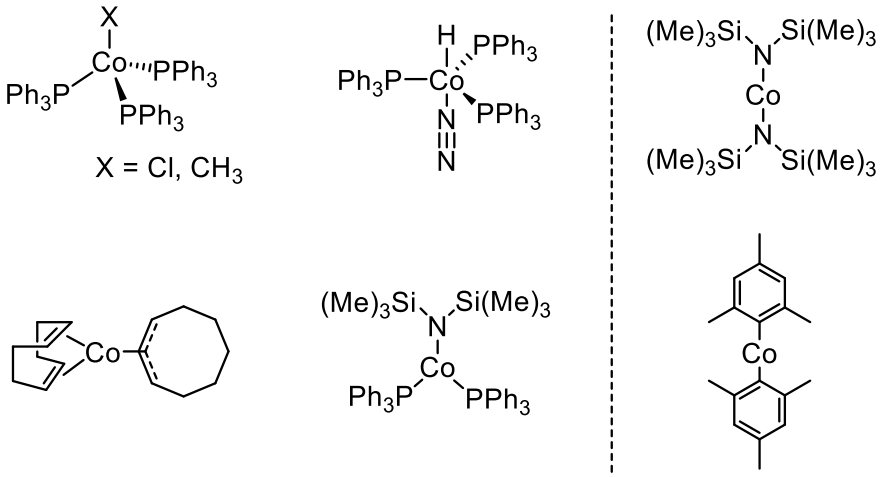

Figure I-3. Literature known cobalt starting materials envisaged as precursors to pincer complexes of cobalt. Left: Co^{I} precursors. Right: Co^{II} precursors.

Of the complexes in Figure I-3, very few are stable at room temperature and each are air sensitive. Cobalt precursors which are stable at room temperature carry ligands which are either difficult to remove or would be poisonous to catalysis. The difficulty of generating new cobalt precursors which are well defined is largely in part to the paramagnetism which obscures diagnostic NMR spectroscopic features for a given compound.

Another issue with developing successful cobalt mediated catalysis is that unlike its heavier Group 9 analogs, cobalt can readily undergo single electron transfer reactions.[65]

In some cases, single electron transformations are desirable. For example, 1) radical initiated polymerization reactions,[66] 2) radical trifluoromethylation initiation,[67] or 3) radical induced functionalizations[68] (Scheme I-8). In each case, there are specific criteria which the metal must meet in order to promote the desired reaction. In radical initiated polymerization, the metal must selectively initiate the reaction by abstraction of the generic "X" (Scheme I-8, Top). The metal must then not interact with the produced radical, nor terminate polymerization too quickly. Furthermore, the metal must not initiate the polymerization too rapidly because a surplus of R• may lead to short oligomeric species as opposed to polymerization. Similar considerations are considered for metal initiators for radical trifluoromethylation (Scheme I-8, Middle). The metal must effectively activate the "CF_3" source and then not quench the produced perfluoroalkyl radical. These reactions typically resolve with a quenching step which may be mediated by the metal. Lastly, metal-based radicals could be operative for the functionalization of organic molecules (Scheme I-8, Bottom). The example here shows radical induced cyclization reaction coupled with a radical resulting from activation of an organohalide. The metal here must not be sensitive to the alkyl radical produced by halogen atom abstraction, or the resultant radical from cyclization of the carbon chain. Single electron chemistry of transition metals has also been shown to be active in hydrogenation and hydroformylation reactions.[69]

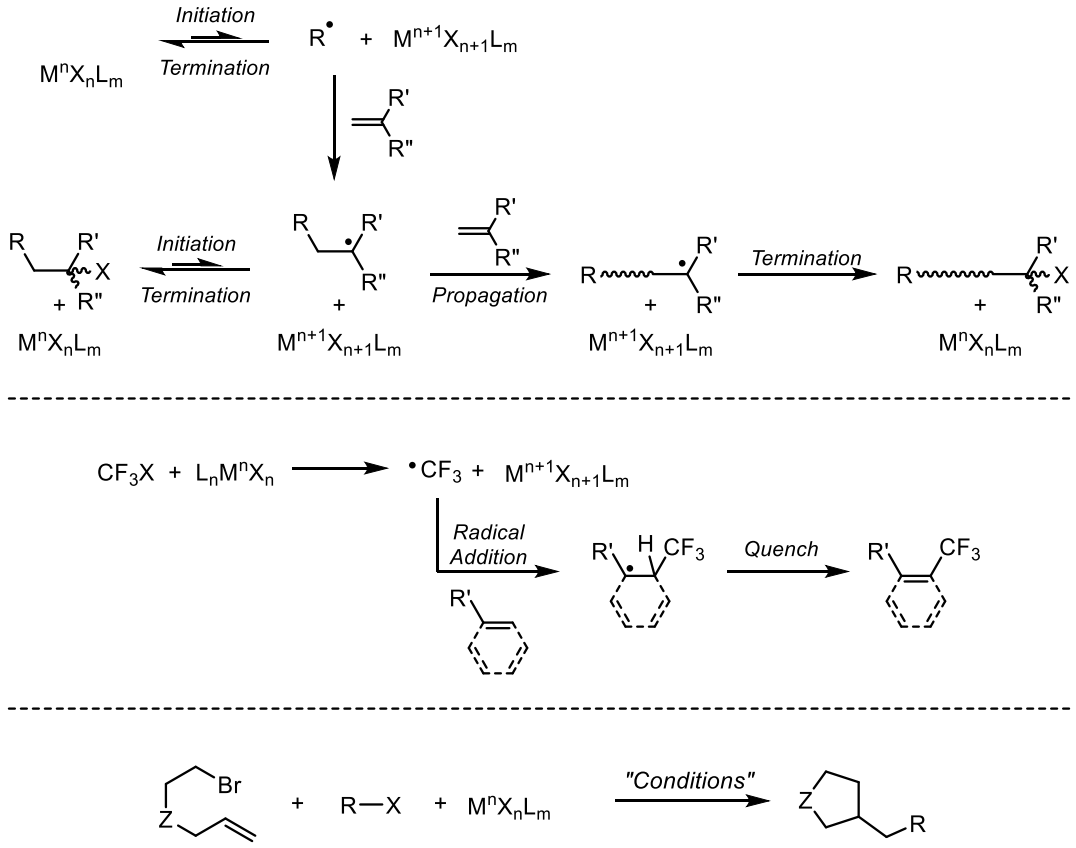

Scheme I-8. Top: Radical polymerization initiated by single electron transfers from X atom abstraction by a transition metal. Middle: Radical trifluoromethylation initiated by single electron transfer from a transition metal. Bottom: Radically induced cyclization and coupling mediated by transition metals.

Single electron reactions not only operate toward organic material but may also act upon other metals. For example, two metal complexes of different oxidation state can perform a one electron transfer to produce two products of the same oxidation state. This can be advantageous as a synthetic route (Scheme I-9, Top) or disadvantageous (Scheme I-9, Bottom).

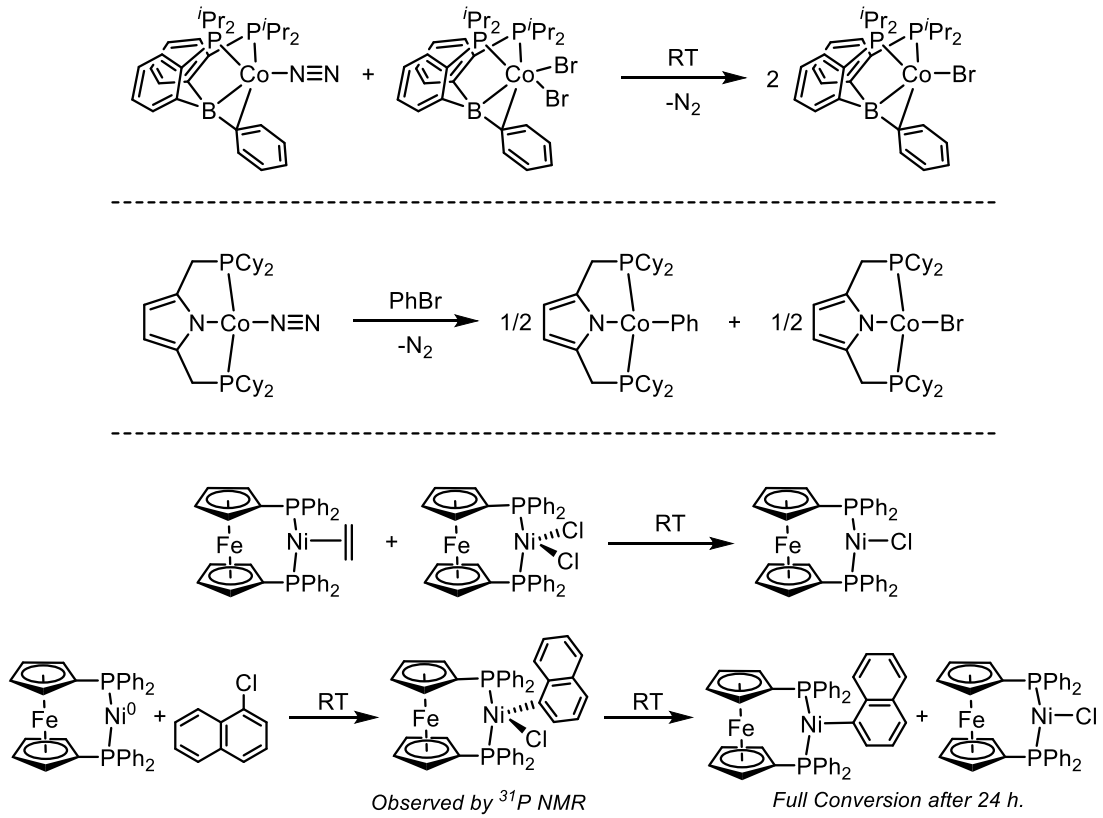

Scheme I-9. Pathways in which comproportionation between two metal centers of different oxidation states is active. Top: Comproportionation between Co^0 and Co^{II} resulting in Co^I. Middle: Comproportionation between Co^I and Co^{III} resulting in two Co^{II} complexes. Bottom: (dppf)Ni^0/Ni^{II} comproportionation events.

The Peters group takes advantage of the comproportionation between a (PBP)Co^0 and (PBP)Co^{II} complex to yield (PBP)Co^I (Scheme I-9, Top).[70] On the contrary, in designing cobalt-mediated cross-coupling catalytic cycles, these one electron processes can become detrimental. Pyrrolyl (PNP)CoN_2, when treated with an aryl bromide forms a 1:1 mixture of (PNP)Co(Ph) and (PNP)Co(Br) (Scheme I-9, Middle).[71] The authors write that this transformation highlights the single electron character prominent in their pyrrolyl

cobalt complex. Presumably this transformation occurs by oxidative addition of PhBr to (PNP)CoN_2 followed by a one-electron comproportionation.

Single electron comproportionation is not an event specific to cobalt and many comproportionation reactions between Ni^0 and Ni^{II} have been reported.[72] One specific example from the Hazari group is shown in Scheme I-9 (Bottom). In the first example,[73] the Hazari group demonstrated a comproportionation event between isolated Ni^0 and Ni^{II} forming a Ni^I complex. The second example is of particular interest to our work as this was intended to be the beginnings of an Ar–X cross-coupling catalytic cycle. However, the comproportionation event between the oxidative addition product and the leftover starting material slowly leeches catalytically competent Ni complexes out of the mixture and produces undesirable byproducts (See Chapter VI for the significance of this finding to our work).[74]

1.5 Introduction to the Transition Metal Mediated Cleavage of Esters

Transition metal-catalyzed ester C–O bond cleavage reactions are well known and have been extensively characterized in the literature.[75,76,77,78] Although some metal-catalyzed ester cleavage has been achieved with iron,[79] ruthenium,[80-81] rhodium,[80,31c] palladium,[82,83] and iridium;[84] majority of the ester cleavage literature is dominated by nickel.[85,78,86,87,88] Nickel is a readily available, inexpensive first row transition metal, and application of simple, air stable coordination complexes of nickel for selective organic transformations is appealing. To this end, the groups of Yamamoto,[75-76] Garg,[85,89,90] Chatani,[87,91] Itami,[92] Watson,[93] and others[86,94] have devoted a great deal of effort to

advancing the ester C–O cleavage-based transformations available to simple nickel complexes (Scheme I-10).

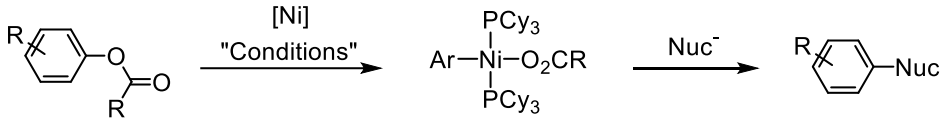

Scheme I-10. Nickel mediated cross-coupling of aryl esters with nucleophiles (nuc^-).

An early example of nickel-mediated ester cleavage of ester C–O bonds was performed by the Yamamoto group.[75] In this publication, the π-basicity of the ligands attached to nickel were altered and the proportions of Type A (acyl) v. Type B (aryl) reactions were determined (Figure I-4). By varying reaction conditions, the authors noticed that the position of the cleavage depends greatly on the phosphine attached to nickel, the type of ester that was employed, and even the source of the nickel (0) (i.e. $Ni(COD)_2$ v. $Ni(PPh_3)_4$). There was a slight propensity for alkenylated esters to undergo Type B C–O cleavages selectively because of the ability of nickel to form an η3 bis-allyl complex. Similar chemistry was performed prior to this publication as a synthetic route to η3 allyl haloacetate complexes of nickel.[95]

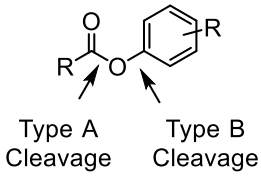

Figure I-4. Two types of C–O bond cleavage available to esters.

A year later, members of the same group performed a detailed mechanistic study of the Type A addition of ethyl benzoate to zero valent nickel complexes. Many facets of

the reaction were elucidated here, such as how various byproducts in the reaction mixture are formed, the order of the reaction with respect to various reaction components, a correlation between cleavage of the ester and basicity of the supporting phosphines, as well as the valence of the nickel complex used in the reaction. It was found that a divalent nickel complex could not perform the reaction, and that as basicity of the phosphine ligands increased, the amount of ester cleavage that occurred was increased concurrently.[76]

Advancing on this work, the Garg and Watson groups have made advances in cleaving pivalate esters using nickel tricyclohexylphosphine complexes *en route* to palladium-style cross-coupling reactions (Scheme I-11, Top).[93a]

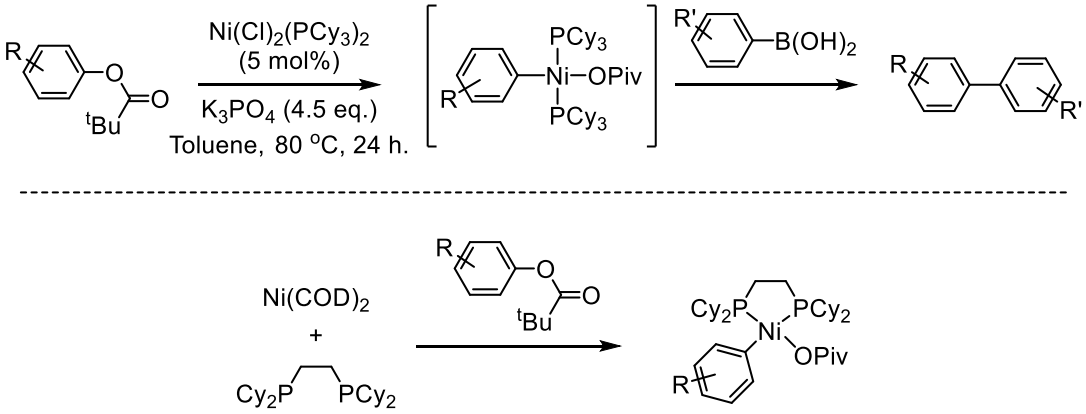

Scheme I-11. Top: Nickel catalyzed Suzuki-Miyaura cross-coupling of aryl boronic acids with aryl pivalates. Bottom: Isolated and characterized product of oxidative addition of aryl pivalates to Ni^0.

Cyclohexyl phosphines are superior to triphenylphosphines in terms of donating ability and impart nickel with more overall electron density. Phosphine ligands such as PPh3, dppe, dppf, and dppp were unable to perform the desired cross-coupling transformation, highlighting the necessity of sufficient electron density about the metal

and the difficulty of aryl pivalate activation.[85] By taking advantage of the robustness of the pivaloyl protecting group and previously discussed reaction orthogonality, Garg and coworkers were able to do sequential palladium and nickel catalysis to make complex polycyclic materials in high yields.[85] The intermediate C–O oxidative addition product was not observed by Garg in the cross-coupling of aryl pivalates. Through the use of a chelating bis-cyclohexylphosphine, the Ni^{II} product resulting from the Type B cleavage of naphthyl pivalate was isolated (Scheme I-11, Bottom).[92b]

Ester-type protecting groups can be installed in place of phenols, and then used as directing groups for arene functionalization prior to metal-catalyzed C-O cleavage. Thus, Type B ester cleavage is attractive as a means to form new bonds to a poly-functionalized arene.[85] One appealing feature of this chemistry is the orthogonality of ester cleavage with aryl halide activation which allows Suzuki-Miyaura coupling after cross-coupling of aryl esters.[85,91,96] A beneficial aspect of using aryl pivalates for initial studies is that they are known to undergo Type B ester cleavage fairly reliably. In the event of Type A cleavage a metal acyl is produced. Decarbonylation of this complex would ostensibly result in a high-energy metal *tert*-butyl complex[97] and thus prohibit a productive forward reaction.[31c,85,92a,98]

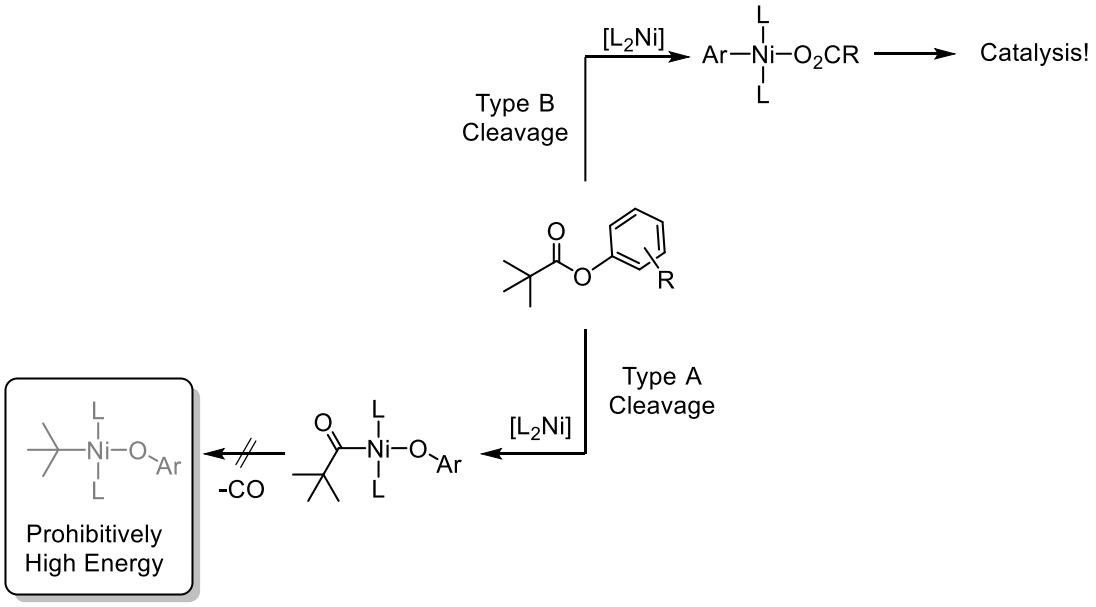

Scheme I-12. Pathways resulting from two types of aryl pivalate ester C–O bond cleavage.

Assuming analogous chemistry to our rhodium system, a cobalt (I) LXL complex should be able cleave aryl ester C–O bonds. See Chapter VIII for results from this hypothesis.

CHAPTER II

KINETICS OF THE DEHYDROGENATIVE BORYLATION OF TERMINAL ALKYNES

2.1 Introduction

Formation of C-B bonds from C-H bonds in organic molecules (C-H borylation) catalyzed by homogeneous transition metal complexes is a valuable type of C-H functionalization.[36-37,99] The discovery of C-H borylation catalysis can be traced to the turn of the century[35d,100] and the development of it into a powerful synthetic method is especially linked with the Ir-catalyzed reactions of aromatic C-H bonds.[101] Catalytic borylation of aromatic and other sp^2 and sp^3 C-H bonds has been realized with a variety of transition metals and main group complexes.[35b,38d,102,103,38a,104,38c,38b,105,106,107,42,108,44,43,109,110] The products of C–H borylation, organoboronates, are versatile building blocks in organic synthesis, permitting conversion of the C-B bond into C-C and many other carbon-element bonds.[48] In 2013, our group reported the first example of catalytic dehydrogenative borylation of C(sp)-H bonds in terminal alkynes (DHBTA) using Ir catalysts supported by a SiNN pincer ligand (Scheme II-1, Bottom).[46] The products of DHBTA, alkynylboronates, have been widely used in synthesis[111] but have been generally accessed via a conventional, non-catalytic method (Scheme II-1, Top).[45] Catalytic DHBTA greatly expands access to alkynylboronates as it is more atom-economical and functional group-tolerant. Subsequent to our 2013 report Tsuchimoto and coworkers reported DHBTA with

$Zn(OTf)_2$/pyridine, that was only applicable to the HBdan borane.[112] More recently, Bertrand's group reported DHBTA using carbene-ligated Cu catalysts that employed HBpin.[113] The following year, a $Fe(OTf)_3$ catalyzed method for alkyne borylation was published by Darcel and coworkers.[114] Last year, a (NHC)Zn DHBTA system was published by the Ingleson group.[115] We also reported DHBTA catalyzed with (POCOP)PdX complexes, however, those were only active for several turnovers.[116]

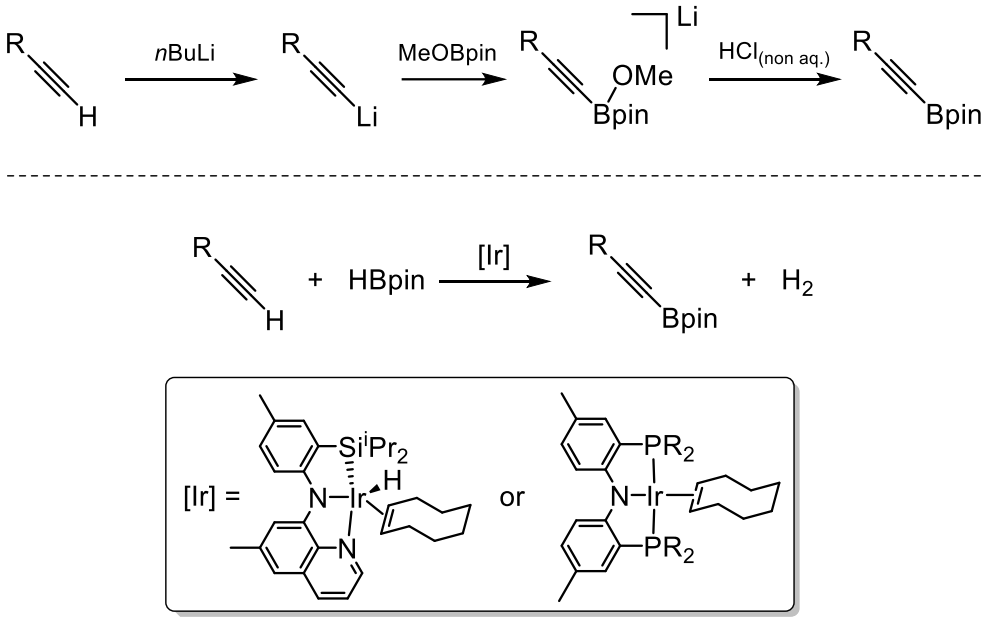

Scheme II-1. Top: Conventional, stoichiometric alkynylboronate synthesis. Bottom: Iridium catalyzed DHBTA.

Our group's exploration of DHBTA has focused on Ir. Accounting for the pincer nature of the SiNN ligand (Scheme II-1, Bottom), we systematically explored an array of pincer ligands with Ir and identified the PNP ligands (Scheme II-1, Bottom) as the most promising class.[47] The original SiNN-based system possessed high initial rates and near-perfect chemoselectivity, but was not a living system and appeared to be limited to about

a hundred TON in the best scenarios because of catalyst death. In addition, it was poorly tolerant of the propargyl-heteroatom connection in terminal alkyne substrates. The (PNP)Ir catalysts with variously substituted PNP ligands did not appear to exceed the high initial rate of the (SiNN)Ir system, and were slightly less chemoselective, with hydrogenation of a small fraction of the starting alkyne observed in some cases. However, the (PNP)Ir catalysts were much more longeval, were not deactivated by the alkyne substrate, permitted thousands of turnovers, and were tolerant of propargyl-heteroatom containing substrates.

In 2018, we reported a computational study of the mechanism of DHBTA by the (SiNN)Ir catalysts.[117] In the present work, we set out to examine the mechanism of the (PNP)Ir-based catalysts through a combination of experimental and computational efforts. The (PNP)Ir system is more amenable to detailed experimental studies because these catalysts are more robust compared to the SiNN-based ones, because of easier access to electronically and sterically modified PNP ligands, and because of the utility of ^{31}P NMR spectroscopic analysis. The discovery of the reactivity of the PNP-based systems was a result of screening of multiple pincer and bidentate ligands in our 2015 work. Although not all the amido-based pincers we examined gave rise to active Ir catalysts, it was conspicuous that only amido-centered SiNN and PNP ligands did, while PCP and POCOP-type pincer ligands did not. The computational study of the (SiNN)Ir catalysis identified a few potentially viable, low-energy mechanistic pathways that are all reliant on the migration of a Bpin ligand from Ir to the amido N of the SiNN ligand to enter the catalytic sequence. Surprisingly, the mechanistic picture of the (PNP)Ir catalysis that has emerged

from the presently reported work is different in that all the transformations take place on the Ir center. Here we present a systematic examination of the mechanistic issues that combines the experimental and the computational approach.

2.2 Results and Discussion

2.2.1 Synthesis and Reactivity of New (PNP)Ir Complexes

For the experimental studies, we prepared four Ir precatalysts with different PNP supporting ligands (Scheme II-2): the previously reported **202a** and **202c**, as well as the new complexes **202b** and **202d**.[118,17f] The **201c** ligand gave rise to the fastest catalysis in our previous study, while the **201a** ligand was judged the easiest to synthesize and to use in the experimental studies. The **201d** ligand was introduced simply for a comparison of relative rates vs. the **201a** analog (vide infra). **201b** was tested because previous work showed that both **201c** and ^{Me}PNP^{Et} ligands gave rise to faster Ir catalysts vs **201a**, and we surmised that catalysis with **201b** might be even faster. Although **201b** proved to be faster than **201a**, it is not as fast as **201c**.

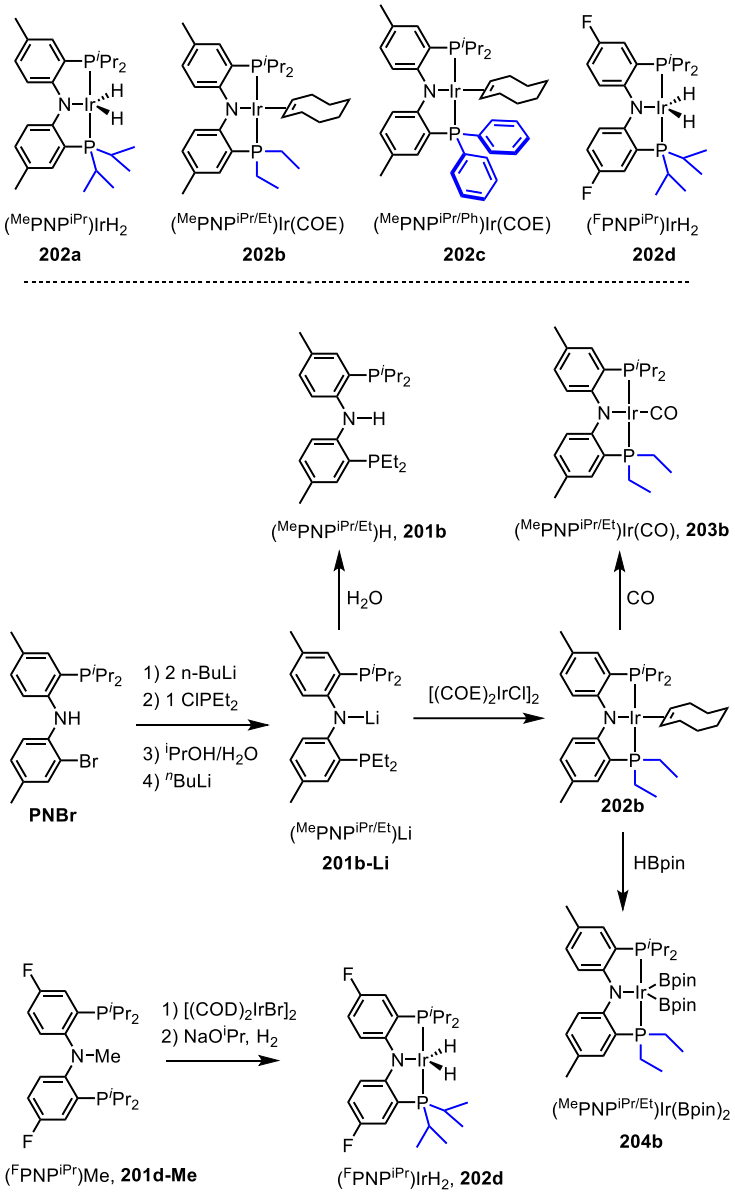

Scheme II-2. The precatalysts selected for DHBTA in this work (top) and the synthesis of new iridium compounds (bottom).

The new ligand precursors **201b-H** and **201b-Li** were prepared by methods derived from the previously reported synthesis of the **201c** analogs (Scheme II-2). The **201b-Li** so obtained was only ca. 95% pure. Nonetheless, its treatment with 0.5 equiv. of

$[(COE)_2IrCl]_2$ permitted isolation of analytically pure, orange **202b** in a 60% yield after workup and recrystallization from pentane (SchemeII-2). **202b** displayed the expected pair of doublets in the $^{31}P\{^1H\}$ spectrum at δ 28.6 and 17.4 ppm with a *trans*-phosphine coupling constant of J = 355 Hz, and the overall C_s symmetry in its ^1H and $^{13}C\{^1H\}$ NMR spectra. Treatment of an orange solution of **202b** with CO resulted in the immediate formation of spectroscopically pure ($^{Me}PNP^{iPr/Et}$)Ir(CO) (**203b**) in a pale yellow solution. The IR stretching frequency (ν_{CO} 1931 cm^{-1}) is different from the analogous ($^{Me}PNP^{iPr}$)Ir(CO) (**203a**) by only one wavenumber.[17c] Treating **202b** with 5 eq. of HBpin afforded ($^{Me}PNP^{iPr/Et}$)Ir$(BPin)_2$ (**204b**) in one of the experiments. The high lipophilicity of **204b** precluded our ability to obtain pure samples of it on a preparative scale; however, an X-ray quality crystal was grown from a saturated solution of **204b** in hexamethyldisiloxane at -35 °C (Figure II-1). This compound is best described as a Y-shaped, d^6 iridium center, very similar to the previously reported ($^{Me}PNP^{iPr}$)Ir$(Bpin)_2$ (**204a**).[47]

The synthesis of **202d** had to rely on $^{F}PN(Me)P^{iPr}$ (**201d**) as a ligand precursor,[119] since a reliable synthesis of the N–H version of this ligand has not been developed. Thermolysis (80 °C) of **201d** with 0.5 equiv. of $[(COD)IrBr]_2$, followed by the treatment of the resultant mixture with NaO^iPr under an H_2 atmosphere permitted isolation, upon workup, of **202d** in ca. 50% yield as a solid of ca. 95% purity. The initial reaction between $^{F}PN(Me)P^{iPr}$ and $[(COD)IrBr]_2$ presumably proceeds analogously to the reaction between $^{Me}PN(Me)P^{iPr}$ and $[(COD)IrCl]_2$, which was investigated in detail.[118,120] **202d** displayed overall C_{2v} symmetry in its NMR spectra and the expected similarity to **202a**.

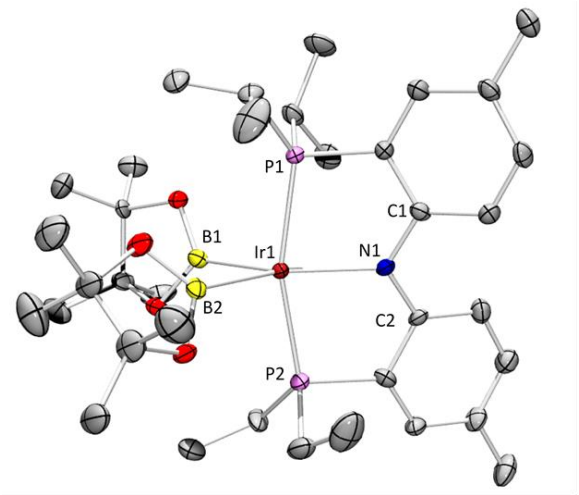

Figure II-1. POV-Ray renditions of ORTEP plots (50% probability ellipsoids) of **204b** showing selected atom labeling. Hydrogen atoms are omitted. Selected bond distances (Å) and angles (deg) for **204b** follow: Ir1-P1, 2.3170(15); Ir1-P2, 2.2999(16); Ir1-N1, 2.090(4); Ir1-B1, 2.043(10); Ir1-B2, 2.047(17); P1-Ir1-P2, 162.13(5); B1-Ir1-B2, 71.7(9); N1-Ir1-B1, 144.4(5); N1-Ir1-B2, 143.9(8); N1-Ir1-P1, 80.96(14); N1-Ir1-P2, 81.95(14).

2.2.2 Preliminary Reactivity Comparison of (PNP)Ir Precatalysts

4-Ethynyltoluene, 3-trimethylsiloxy-1-propyne, 3-dimethylamino-1-propyne, and ethoxyacetylene were selected to screen preliminary reactivity of the iridium precatalysts **202a**, **202b**, and **202c**. 3-Dimethylamino-1-propyne and ethoxyacetylene have not been previously used in DHBTA and were selected with the potential to expand the scope of the reaction. The precatalysts **202a**, **202b**, and **202c** (1% v. alkyne) were introduced to each substrate in the presence of 2 eq. of HBpin/alkyne and the progress of the reactions was monitored by ^{1}H NMR spectroscopy. Table II-1 summarizes the results of these reactions.

Compounds **202a**, **202b**, and **202c** achieved complete DHBTA of 4-ethynyltoluene as well as 3-dimethylamino-1-propyne. Our group has previously reported

that 3-trimethylsiloxy-1-propyne undergoes a hydrogenation side reaction during DHBTA which provided a unique handle for catalyst comparison. However, each **202a**, **202b**, and **202c** provided very similar ratios of DHBTA product to hydrogenated alkyne. Unfortunately, none of the complexes were able to perform DHBTA of ethoxyacetylene; instead, C–O cleavage products were observed. All in all, the new catalyst **2b** performed similar to the previously reported **202a** and **202c** in terms of selectivity and showed activity intermediate between that of **202a** and **202c**.

Entry	Alkyne	Precat.	Time	% Conv.	%Products
1	4-MeC_6H_4CCH	**2a**	10 min	30	29/1[a]
2			12 h	100	97/3[a]
3	4-MeC_6H_4CCH	**2b**	10 min	50	50/0[a]
4			12 h	100	99/1[a]
5	4-MeC_6H_4CCH	**2c**[b]	10 min	88	87/1[a]
6			12 h	100	98/2[a]
7	Me_2NCH_2CCH	**2a**	10 min	30	30
8			17 h	100	100
9	Me_2NCH_2CCH	**2b**	10 min	50	50
10			17 h	100	100
11	Me_2NCH_2CCH	**2c**	10 min	94	94
12			17 h	100	100
13	Me_3SiOCH_2CCH	**2a**	10 min	59	49/10[c]
14			19 h	100	82/18[c]
15	Me_3SiOCH_2CCH	**2b**	10 min	84	75/9[c]
16			19 h	100	89/11[c]
17	Me_3SiOCH_2CCH	**2c**	10 min	100	85/15[c]
18			19 h	100	84/16[c]
19	EtOCCH	**2a**	48 h	33	0/24[d]
20	EtOCCH	**2b**	48 h	33	0/21[d]
21	EtOCCH	**2c**[e]	48 h	11	0

Table II-1. Comparison of catalyst performances with selected substrates.

[a] DHBTA product/hydrogenated alkyne (4-ethyltoluene) [b] 0.21 mol % catalyst loading [c] DHBTA Product/hydrogenated alkyne (trimethylsiloxypropane) [d] DHBTA Product/EtOBpin [e] 0.1 mol % catalyst loading

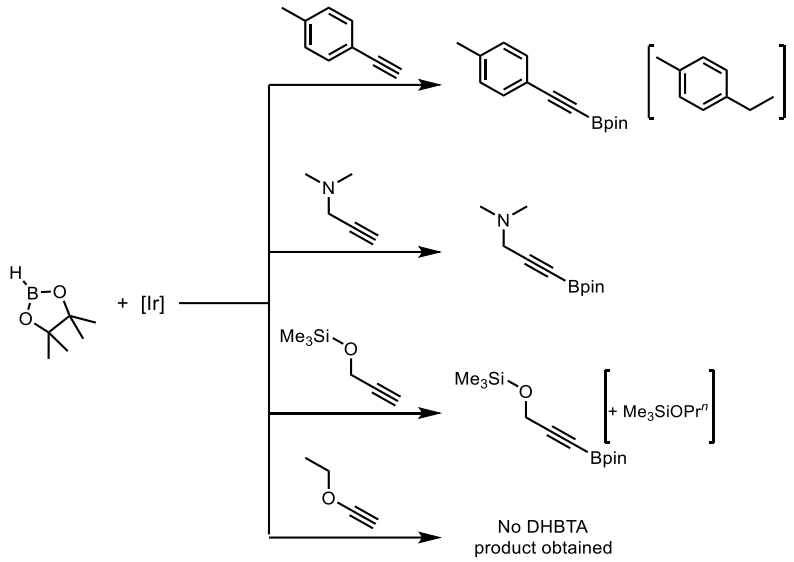

Scheme II-3. DHBTA reactions for alkynes in Table II-1.

2.2.3 Rate Law Determination

We selected 4-ethynyltoluene as the substrate for investigating the kinetics of the DHBTA reaction in detail, using four precatalysts **202a**, **202b**, **202c**, and **202d**. To probe the dependence of the rate on the concentrations of HBpin and of 4-ethynyltoluene, a series of DHBTA reactions were set up with **202a** under pseudo-first order conditions in [HBpin] in each reaction. The data from the monitoring of these reactions by ^{1}H NMR spectroscopy was most consistent with exponential decay, indicating first order dependence on [Alkyne] (Figure II-2). Considering the alternatives of zeroth or second order in [Alkyne] did not result in a satisfactory fit for the obtained data. Comparison of reactions performed under different excess [HBpin] pseudo-first order conditions did not show a perceptible dependence on [HBpin] between 0.98 and 3.0 M HBpin (see Section 2.4.6 for details).

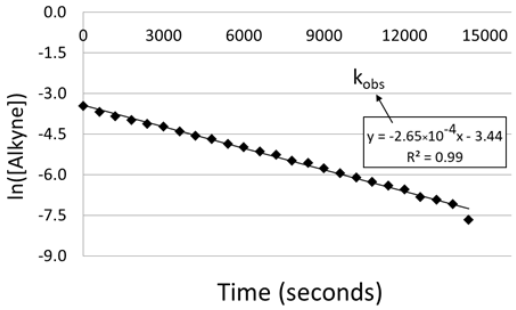

$$Rate = \frac{-d[Alk]}{dt} = k[Alk]^1\,[HBpin]^0[Cat.]^1[H_2]^{-1}$$

$$\frac{-d[Alk]}{[Alk]} = k_{obs} \times dt$$

$$where\ k_{obs} = k[Cat.][H_2]^{-1}$$

$$and\ k^* = k\,[H_2]^{-1}$$

$$\ln[Alk] = -k_{obs}\,(t)$$

Figure II-2. Consumption of 4-ethynyltoluene versus time.

Another set of analogous reactions was examined with different concentrations of **202a**. The results conformed to a linear, first-order dependence on the concentration of the Ir catalyst. Analogous investigations were carried out for the other three Ir catalysts (**202b**, **202c**, & **202d**), except that the zeroth order dependence on [HBpin] was assumed based on the **202a** studies. All four catalysts showed first-order dependence on [Alkyne] and on [Ir]. The comparison between the four catalysts is summarized in Figure II-3. The steepest slope for the reaction catalyzed by **202c** is consistent with it having been previously identified as the fastest catalyst. **202c** is about 30 times faster than **202a**, with the activity of **202d** statistically indistinguishable from **202a**.

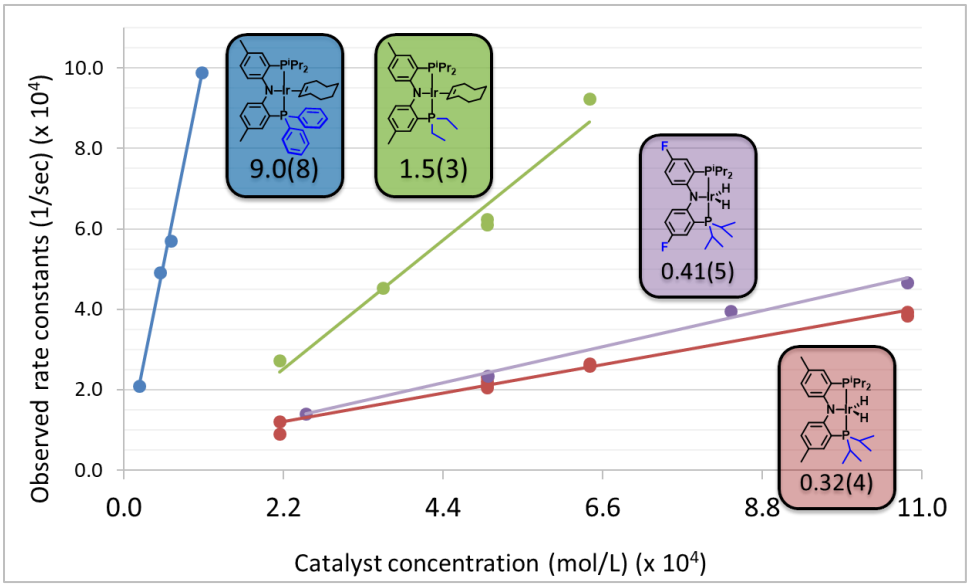

Figure II-3. Comparison of 4-ethynyltoluene DHBTA rates with four different iridium precatalysts. The values beneath each compound are k* for the DHBTA reaction catalyzed by that precatalyst where k* = $k[H_2]^{-1}$, in L/(mol×s).

2.2.4 Resting State Determination and the Role of H_2

Monitoring the DHBTA reaction by ^{1}H and ^{31}P NMR spectroscopy *in situ* under standard DHBTA conditions with $1.08x10^{-3}$ M **202a** allowed for the observation of the resting state of the (PNP)Ir fragment during catalysis. ^{1}H NMR spectroscopy revealed only two hydride resonances in a 1:2 ratio located at -5.4 and -12.5 ppm respectively, while only a single resonance at 40.8 ppm could be observed by $^{31}P\{^{1}H\}$ NMR spectroscopy. These resonances identified the previously reported ($^{Me}PNP^{iPr}$)Ir(H)$_3$(Bpin) (**205a**).[47] Similar resonances were observed for the DHBTA reaction catalyzed by **202d**, presumably corresponding to the analogous complex ($^{F}PNP^{iPr}$)Ir(H)$_3$(Bpin) (**205d**). This was further corroborated by the observation of a single ^{19}F NMR resonance, whose

chemical shift (-131 ppm) is consistent with the amido form of the PNP ligand (as opposed to an amino form with an sp^3 hybridized N).[121]

The first-order dependence on [Ir] and on [Alkyne] suggested that an interaction of an Ir intermediate and one molecule of the alkyne is part of what determines the overall rate of the reaction. Realizing that the resting state is a saturated Ir complex ($^{Me}PNP^{iPr}$)Ir(H)$_3$(Bpin) (**205a**) and also guided by the DFT results, we considered that dissociation of H_2 may need to take place prior to the interaction of the Ir complex with the alkyne. Unfavorable dissociation of H_2 from **205a** should result in an inverse dependence of the rate of the reaction on the concentration of H_2. H_2 is continuously produced as a stoichiometric product of DHBTA in a closed vessel (J. Young NMR tube), thus the total *amount* of H_2 steadily increases during the reaction. Paradoxically, this was not reflected in the kinetic runs, which displayed ostensibly well-behaved linear logarithmic decay over as many as 3-6 half-lives in dozens of experiments without substantial deceleration over time. Intrigued by this perceived discrepancy, we examined the observed concentrations of H_2 as measured by ^{1}H NMR integration vs the internal dioxane standard over the time courses of the kinetic runs. Figure II-4 shows an overlay of [H_2] with the logarithmic decay of the alkyne over the time course of one of the kinetic runs. Remarkably, the plot shows that [H_2] increases only at the earliest stages of the observation of the reaction, crests, and then slowly decreases over time. However, the overall relative variation over time is modest and appears to fall within ±10-20% of the mean value, especially if the first 2-3 datapoints are excluded. Closer examination of the local curvature of the logarithmic decay slope suggests that the apparent rate constant does

vary proportionally to 1/[H_2], and this variation is modest, within the range of the relative [H_2] variation.

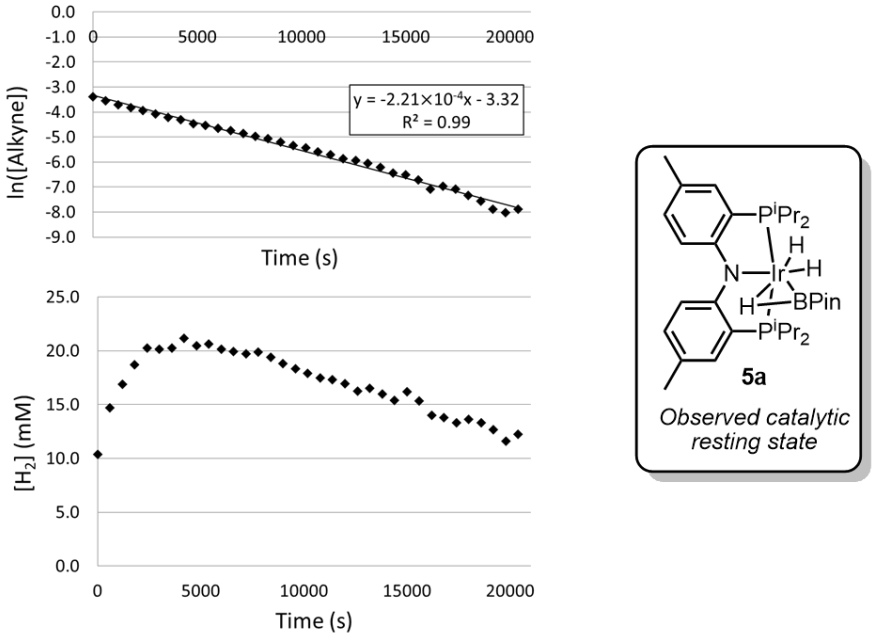

Figure II-4. Top: First order fit of alkyne consumption with time. Bottom: Dihydrogen concentration in solution as observed vs a 1,4-dioxane internal standard.

The concentration of H_2 at the last datapoint (5.7 hours) is 12.3 mM. This is 4.2 times higher than the expected equilibrium solubility of H_2 at 1 atm in benzene derived from the literature data,[122] whereas the estimated maximum pressure in our experiment is 0.46 atm. Thus, the observed H_2 concentrations and the changes observed over time cannot be governed by equilibrium solubility. Instead, we propose that the homogeneous generation of H_2 throughout the volume of the solution quickly leads to the oversaturation of the solution with H_2. A 0.7 mL solution inside a standard 5 mm NMR tube has a small cross-section interface with respect to the total volume and there is no active agitation for a tube inside an NMR spectrometer for the duration of the experiment. This leads to slow

egress of H_2 from the benzene solution into the headspace such that even after several hours, the concentration exceeds the equilibrium concentration by an order of magnitude. The period where the H_2 concentration rapidly increases from zero to the observed approximate average begins immediately after the initial sample preparation in a glovebox and is largely complete by the time of the collection of the first datapoints. The concentration of H_2 over the reaction time course then depends on the rate of H_2 production from DHBTA and the rate of escape of H_2 from the solution into the headspace. Curiously enough, these rates end up approximately equalized, resulting in what could be viewed as a homeostatic concentration of H_2. This fortuitous stability creates "quasi-pseudo-first order" conditions with respect to $[H_2]$, maintaining the legitimacy of the simplified kinetic analysis such as in Figure II-2 ($k_{obs} = k[Cat][H_2]^{-1} \approx$ const).

To confirm our hypothesis, two identically constituted DHBTA solutions in J. Young tubes were monitored by NMR spectroscopy at certain intervals. One of these samples was periodically vigorously shaken (but not stirred) manually between NMR spectra collection, whereas the other was kept stable in an upright position at all times. The "shaken" sample ($k_{obs} = 2.6(2)\times10^{-3}$) showed a six-fold increase in rate compared to the "unshaken" sample (k_{obs} $3.9(2)\times10^{-4}$) and a lower observed $[H_2]$ in solution. Ostensibly, shaking the NMR tube leads to much faster escape of H_2 from the solution into the headspace.

2.2.5 KIE Determination and Analysis of Hammett and Eyring Plots

We surmised that a kinetic isotope effect (KIE) study with C-H/C-D labeled alkyne can provide useful mechanistic information.[123] To this end, DHBTA rate measurements were performed using **202a** as the catalyst at two different catalyst loadings and 4-(ethynyl-*d*)toluene as the substrate. Those rates were then compared to the DHBTA of 4-ethynyltoluene at the same catalyst loadings (*vide supra*). Figure II-5 illustrates one such comparison. The KIE value obtained from these reactions was 1.5(1). A competition experiment in which 4-ethynyltoluene and 4-(ethynyl-*d*)toluene were loaded into the same NMR sample with **202a** resulted in a similar KIE value of 1.3(2). These modest KIE values suggested that C–H or C–D bond cleavage is not rate-determining for the overall DHBTA process.

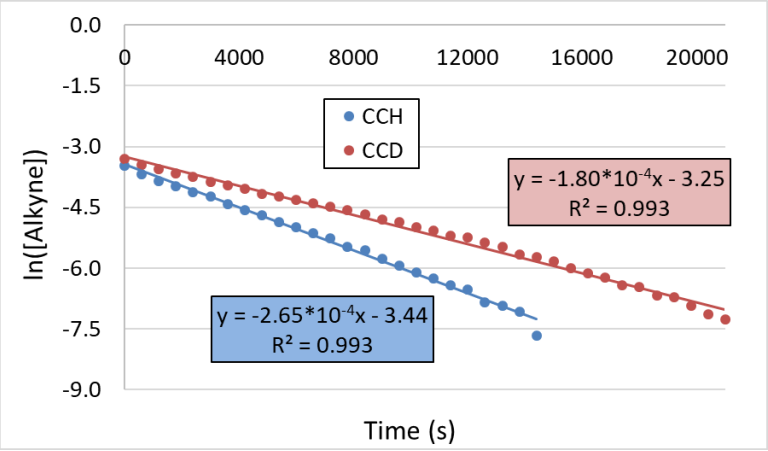

Figure II-5. Comparison of DHBTA rates of 4-ethynyltoluene and 4-(ethynyl-*d*)toluene for isolated kinetic isotope experiments catalyzed by **202a**.

Reaction rates for a series of *para*-substituted phenylacetylenes were measured using ^{1}H NMR spectroscopy during a DHBTA reaction under standard conditions catalyzed by 1% **202a**. The reactions performed here displayed first-order behavior with

respect to each of the alkynes. The resultant Hammett plot of the logarithmic rates vs the standard substituent σ-values[124] derived from this series of experiments is displayed in Figure II-6. The reaction is accelerated by an electron withdrawing *para*-substituent on phenylaceylene. The ρ value obtained for this plot is modest at 0.6(1).[125]

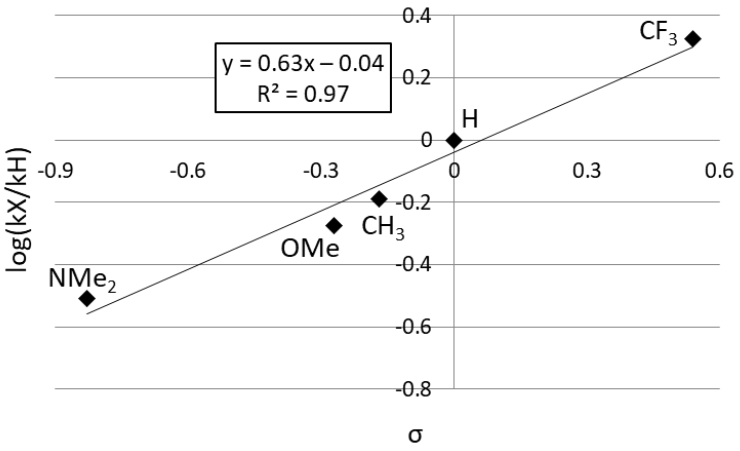

Figure II-6. Hammett plot arising from the DHBTA of a series of 4-$XC_6H_4C{\equiv}CH$ (X = CF_3, H, CH_3, OMe, NMe_2). The values for k_x here are k_{obs} for the DHBTA reaction with the designated alkyne.

Performing DHBTA of 4-ethynyltoluene at different temperatures allowed us to determine the activation parameters for the DHBTA reaction: $\Delta H^{\ddagger}$ = 16(2) kcal/mol and $\Delta S^{\ddagger}$ = -14(6) cal/(mol×K). The Eyring plot is shown in Figure II-7. For the calculation of proper rate constants, we took $[H_2]$ = 0.02 M based on the observations described above. A different constant value of $[H_2]$ would affect the $\Delta S^{\ddagger}$ but not the $\Delta H^{\ddagger}$ value. Accounting for the concentration of H_2 effectively represents an adjustment for the standard state to be at $[H_2]$ = 1 M. The modest magnitude of the entropy of activation $\Delta S^{\ddagger}$ = -14(6) cal/(mol×K) is in principle consistent with a transition state that is accessed via addition of an alkyne to the Ir catalyst but with loss of free H_2 from the ground state.

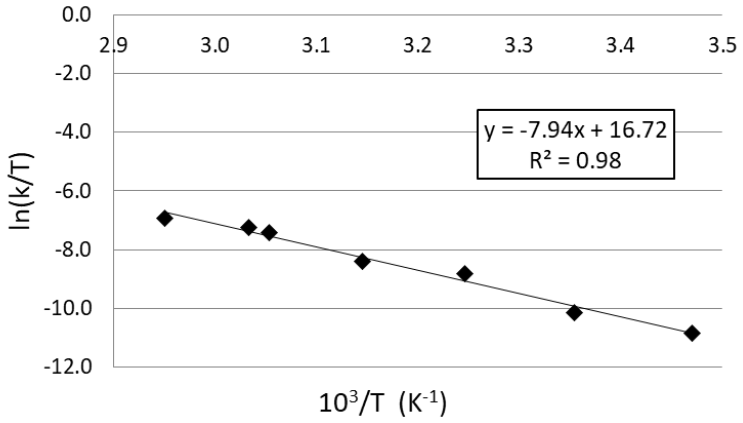

Figure II-7. Eyring Plot arising from DHBTA of 4-ethynyltoluene with **202a** at different temperatures.

2.3 DFT Analysis

2.3.1 DFT Analysis of Plausible Intermediates: Boryl Migration

DFT calculations were carried out with the Gaussian 09 program. The geometries were optimized using M06/SDD/6-311G(d,p) level of theory in the gas phase for the next two sections.

In the study of the mechanism of the (SiNN)Ir-catalyzed DHBTA, computational investigations unveiled the critical importance of the migration of the boryl ligand from Ir to the amido N. This migration opened up low-energy pathways for OA of the alkynyl C-H bond and for the subsequent C-B bond formation. In particular, computational evidence indicated that OA of the alkynyl C-H to a diboryl or a boryl/hydride Ir complex prior to boryl migration to N is prohibitively high in energy. Given that the (PNP)Ir catalysts also contain an amido-centered pincer, we set out to first explore the potential role of the Ir-to-N boryl migration. Although we previously experimentally demonstrated that (PNP)Ir(Bpin)$_2$ is not an intermediate in the catalytic cycle, we included (PNP)Ir(Bpin)$_2$

in the computational study for a more complete evaluation. We used PhCCH as the default alkyne in the DFT studies, as we did for the SiNN system

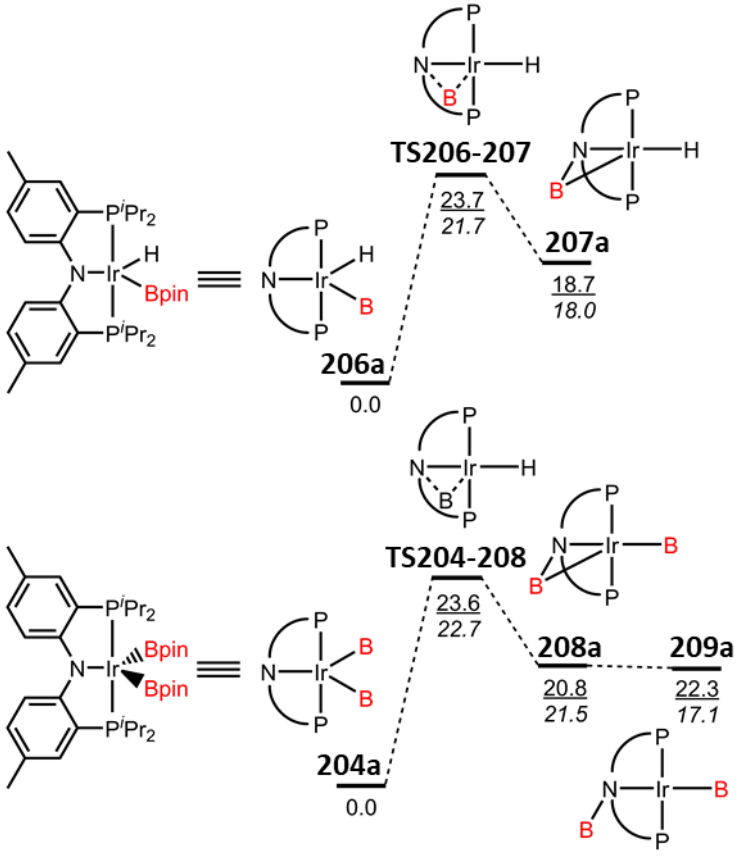

Figure II-8. Calculated energies (free energy values underlined; enthalpies underneath in italic) for the migration of Bpin from the metal to the nitrogen atom of PNP.

Migration of a Bpin substituent from Ir to N in (PNP)Ir(Bpin)$_2$ (**4a**) and (PNP)Ir(H)(Bpin) (**206a**) was calculated to be decidedly endergonic, by ca. 20.8 and 18.7 kcal/mol, respectively. The migrated boryl retains some interaction with Ir in **207a** and **208a**. It can be viewed as a BX_3 acting as a weak Z-type ligand towards Ir. For the diboryl case, the isomer (**209a**) without such interaction could also be found. The barrier for the direct boryl migration in both cases was found to be similar, 23.6 or 23.7 kcal/mol (Figure

II-8). We also considered the formation of **208a**/**209a** from **206a** and HBpin with loss of H_2, however that pathway led to even higher barrier in free energy en route to **208a/209a**. These numbers place the ground states of the N-boryl isomers **207a**-**209a** and the transition states (**TS206-207** and **TS204-208**) leading to them higher than the experimentally determined activation energies. This is true even without the consideration of the OA of the C-H bond to the species **207a**-**209a**, or any of the subsequent steps that would be necessary for the completion of the catalytic cycle. Because of these prohibitively high energies, we concluded that the Ir-to-N boryl migration in the PNP system does not provide for competitive mechanistic pathways.

The unfavorability of the boryl migration with PNP is much greater than that in the (SiNN)Ir system, where the N-boryl isomer was uphill only by a few kcal/mol.[117] The SiNN ligand possesses a highly adaptable Si-H unit as a side pincer donor. This Si-H was shown to adjust to the changes at Ir by modulating the Ir/Si-H interaction across a spectrum of silyl/hydride vs σ-Si-H interactions. Migration of a boryl from Ir to N can be viewed as N-B RE from Ir. In response, the Si-H unit in the SiNN ligand evolves from a stretched σ-complex to a decidedly silyl/hydride structure. It is possible that this Si-H adaptability is what permits an essentially ergoneutral boryl migration for (SiNN)Ir, whereas the phosphines in (PNP)Ir are not adaptable. On the other hand, it is possible that the two ligand sets simply result in two electronically very different Ir centers, with different thermodynamic propensity for N-B RE. This point of view is supported by the drastic difference in the ν_{CO} values for (PNP)IrCO (**203a**, 1930 cm^{-1}, more electron-rich Ir)[17c] and (SiNN)Ir(CO) (1977 cm^{-1}, less electron-rich Ir).[126]

2.3.2 DFT Analysis of Plausible Intermediates: 1,2 Addition

Next, the possibility of 1,2-addition of the alkynyl C-H bond across the N-Ir bond in (PNP)Ir(H)(Bpin) was considered. We previously described 1,2-addition of C-H bonds in terminal alkynes across a Pd-N bond[127] and in arenes across a Pt-N bond[17e] in cationic PNP complexes of group 10 metals. Multiple geometries of the addition products were considered, including *mer*- and *fac*- geometries of the protonated PNP (Figure II-9). Some of the isomers **210a**-**213a** were calculated to be only modestly high in energy, and transition states were found for the corresponding additions. However, the energies of the TSs are high enough that these pathways are not consistent with the experimentally observed activation energies.

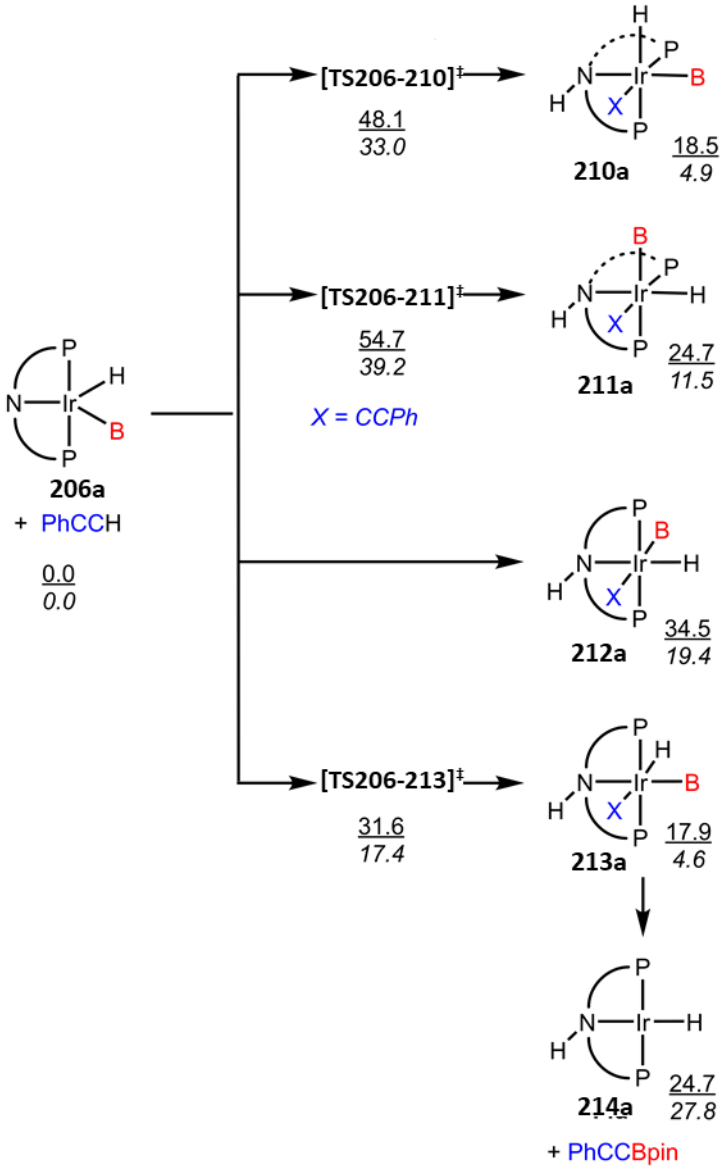

Figure II-9. Calculated energies (free energy values underlines; enthalpies underneath in italic) for the 1,2-addition of PhCCH across the Ir-N bond and some subsequent steps.

In addition, we examined the plausibility of C-B RE from **213a**, the lowest energy product of 1,2-addition (Figure II-9). The immediate product of the C-B RE (**214a**) is higher in energy than **213a**. Since the energy of the TS for this RE is expected to be even higher (calculation was not attempted), this analysis also paints the 1,2-addition-derived

pathways inconsistent with the experimentally observed rates. It should be noted that all 1,2-addition isomers **210a**-**213a** are six-coordinate, trivalent (d^6) Ir complexes. It has been previously shown in a number of cases that octahedral d^6 complexes possess relatively high barriers for concerted RE.[128] Thus, the 1,2-addition products also appear poorly suited for C-B RE for this reason.

2.3.3 DFT Analysis of Plausible Intermediates: Diboryl Pathway

In this section, DFT calculations were carried out with the Gaussian 09 program. The geometries were optimized using B3LYP/LANL2DZ/6-31G(d) level of theory in the gas phase and the energies for these geometries were then determined with the M06/SDD/6-311+G(d,p) method incorporating the benzene solvent effect via the SMD model. The next consideration was given to the OA of the alkynyl C-H bond to the Ir center of the diboryl complex **204a**. Calculations showed (Figure II-10) that the product of such OA (**215a**) is 26.8 kcal/mol higher than **204a** on the free energy surface, while the TS for this process was calculated to lie 36.3 kcal/mol higher than **204a**. This calculated value is much higher than the experimentally derived activation energy. Moreover, **TS204-215** is not even the highest point on the reaction coordinate in Figure II-10. Instead it is **TS215-216**, which corresponds to the rotation of the B-H unit subsequent to C-H OA. The analogous transition state in the monoboryl case will be discussed in more detail in the next section.

The catalytic cycle initiated by the C-H OA, B-H rotation and C-B RE to produce **206a** is complete with the steps required to add HBpin and eliminate H_2 in Figure II-10.

The overall barrier calculated for the steps corresponding to the **206a→204a** transformation in Figure II-10 is surprisingly high, at 35.4 kcal/mol for **TS217-218** relative to **206a**. Figure II-10 also makes it obvious that **204a** in the presence of H_2 is endergonic with respect to **206a** and HBpin, which means that the effective barrier for Figure 10 is even higher as **204a** should not be the ground state under the catalytic reaction conditions. These DFT results dovetail the previously reported experimental determination[47] that **204a** is not an intermediate in a catalytic cycle and neither can it rapidly access the catalytic cycle.

We have not examined experimentally or computationally whether a diboryl complex analogous to **204a** might be more relevant to the catalytic cycle for the other PNP ligands. However, the calculated barrier in Figure II-10 is large enough to suggest that a relatively modest change of phosphorus substituents in the PNP ligand should not bring the barrier into compatibility with the experimentally determined rates.

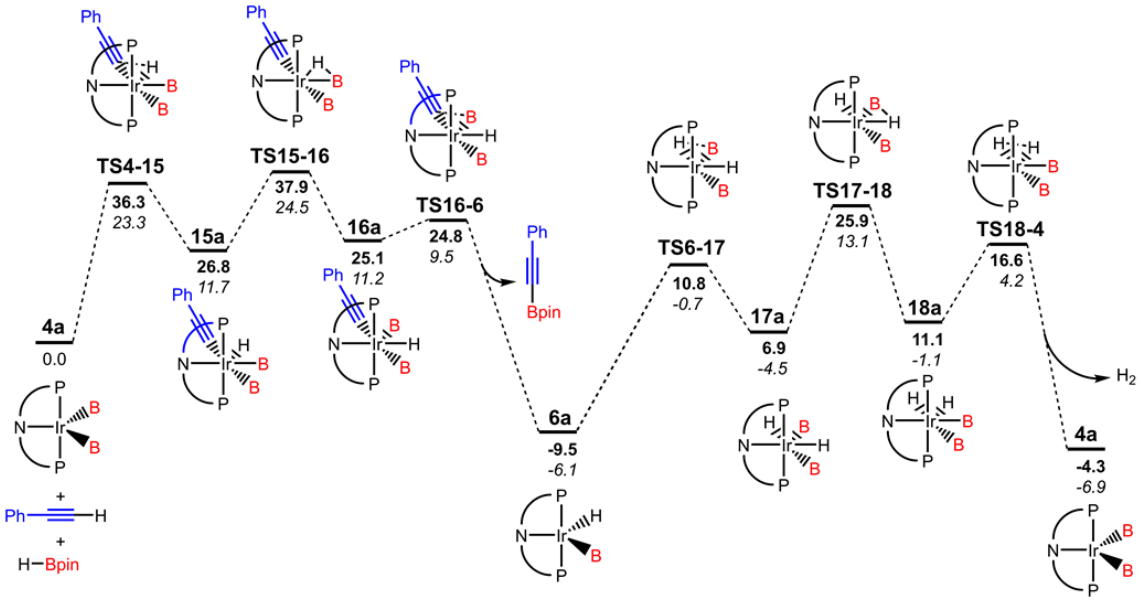

Figure II-10. Calculated energies for the catalytic diboryl pathway.

2.3.4 DFT Analysis of Plausible Intermediates: Monoboryl Pathway

Finally, we examined the "monoboryl" pathway that is initiated by OA of the alkynyl C-H bond to the Ir center in **206a** (Figure II-11). The product of this OA (**219a**) and the associated **TS206-219** are about 14-16 kcal/mol lower than the analogous energies for the OA of C-H to **204a** in Figure II-10. In order to position the alkynyl group next to B for the C-B RE step, a rotation of the B-H unit (**219a→220a**) has to take place first. This process gives rise to the highest energy **TS219-220** in the catalytic cycle. Interestingly, a global TS associated with the rotation of a B-H unit was identified in a computational study of aromatic C-H borylation with $CpFe(CO)_2BCat$ and $CpW(CO)_3BCat$ by Hall, Hartwig, and coworkers.[129] In that case, this rotation was similarly necessary in order to position the boryl ligand next to the metal-bound carbon, although the overall "piano-stool" geometry of the relevant complexes is different from

our pincer-supported system. Rotation of B-H to properly position the boryl ligand next to the metal-bound carbon was also noted in the studies of aromatic and aliphatic C-H borylation by Ir(III) boryls supported by bidentate ligands, although this was not found to be the global transition state and the geometric arrangement also differs from the (PNP)Ir case.[130]

The subsequent C-B RE is quite facile proceeding with a negligible barrier from **220a** via **TS220-202** to give the alkynylboronate product and **202a**. The overall cycle is completed via the steps effecting addition of HBpin and loss of H_2. Unlike the analogous process in the diboryl pathway in Figure II-10, the barrier for this part of the cycle within Figure II-11 is small, at only 11.6 kcal/mol in free energy (from **202a** to **TS202-205**). This is in part because loss of H_2 in Figure 11 does not require rotation of a B-H unit (**217a→218a** in Figure 10) to position two H's next to each other – in Figure II-11, they already are. In addition, it appears that addition of HBpin is thermodynamically and kinetically less endergonic to **202a** (Figure II-11) than to **206a** (Figure II-10).

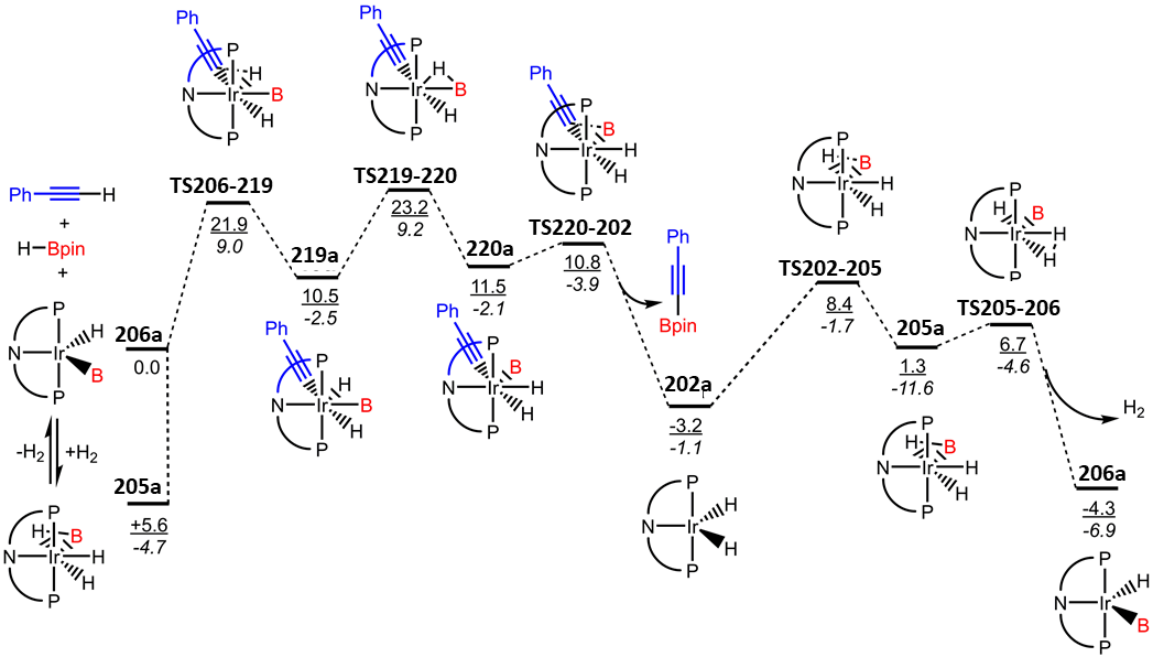

Figure II-11. Calculated energies for the catalytic monoboryl pathway.

The energies in Figure II-11 were set against zero for **6a** (+ PhCCH + HBpin) for a more consistent comparison with Figure II-10. However, experimental observations indicate that the ground state of the catalyst for the $^{i}Pr_4$ ligand is (PNP)IrH$_3$Bpin (**205a**). DFT calculations predict that the formation of **205a** from **206a** and H_2 is favorable enthalpically, but not entropically, which makes sense. Comparison of the experimentally determined activation energies ($\Delta G^{\ddagger}_{298}$ = 20(2) kcal/mol and $\Delta H^{\ddagger}$ = 16(2) kcal/mol) to the calculated TS energies relative to **205a** ($\Delta G^{\ddagger}_{298}$ = 19.2 kcal/mol and $\Delta H^{\ddagger}$ = 14.2 kcal/mol) evinces a reasonable match. Furthermore, the calculated KIE isotope values (1.3 for the B-H rotation TS and 4.4 for the OA TS) support the notion that it is the B-H rotation **TS219-220** and not the OA **TS206-219** is the global TS for the reaction.

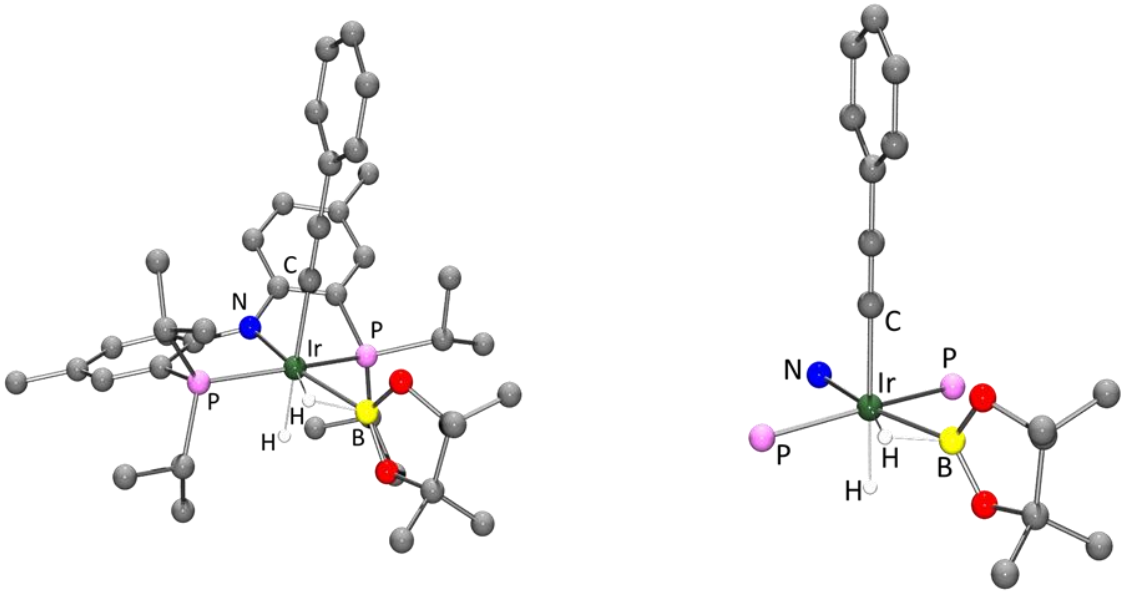

Figure II-12. Global TS for the monoboryl pathway (**TS219-220**) corresponding to the B–H rotation. The view on the right omits the non-metal-bound atoms of the PNP ligand for clarity.

The difference between the energies of the B-H rotation TS and the OA TS is modest, and it is reasonable to wonder whether our results with the particular DFT functional, alkyne and PNP ligand are representative. We examined the relative free energies for the two transition states using a series of different DFT functionals (M06, B3LYP, wB97XD, B97D3, BP86, MN15, MN15L) for the reaction of PhCCH with the (PNP)IrH_3Bpin complexes supported by the four different PNP ligands in this study (**205a**-**205d**), as well as the reactions of a series *p*-YC_6H_4CCH (Y = Me_2N, MeO, Me, H, F_3C) with **5a**. In nearly all of these permutations, the B-H rotation TS (**TS219-220** or analog) was calculated to be higher or nearly equal in free energy to the OA TS (**TS206-219** or analog), with only the reaction involving p-F_3CC_6H_4CCH with the MN15 and MN15L functionals resulting in a slightly higher OA barrier (by <1 kcal/mol).

Furthermore, the DFT results were qualitatively consistent with the experimental Hammett study. It was found that the TS free energies (relative to **206a**) for both the OA and the B–H rotation increased in the order of X as follows: F_3C < H < Me ≈ MeO < Me_2N. The same order was maintained for the TS enthalpies and was consistent for the calculations with different functionals mentioned above.

The preference for the more electron-poor alkyne in the OA step intuitively makes sense, but it is not so obvious for the B-H rotation step. It is also not obvious that for the more electron-poor alkynes the difference between the TS energies decreases (i.e., a more electron-poor alkyne decreases the energy of the B-H rotation TS to a greater degree than the OA TS). A possible explanation may be derived from the analysis of the structure of the B-H rotation TS (Figure II-12). Compared against the OA product **219** (Figure II-13), the alkynyl C in **TS219-220** ends up being positioned more linearly *trans* to the hydride (ca. 179º vs ca. 174º). This modest linearization may augment the *trans*-influence conflict between the hydride and the alkynyl. The Ir–H distance shortens slightly while the Ir–C distance lengthens upon going from **219** to **TS219-220**. The *trans*-influence of an alkynyl with a more electron-withdrawing *para*-X substituent should be weaker, thus plausibly lowering the energy of the corresponding **TS219-220** analog. The alkynyl group in **TS206-219** is also being brought into the position *trans* to the same hydride. However, in **TS206-219**, the Ir–C bond is not fully formed, the alkynyl is farther away from the metal, the C–Ir–H angle is less linear at ca. 175º, and the relative *trans*-influence considerations may not be as influential as in the **TS219-220**, where the Ir–C bond is not a partial, incipient bond. Structures **219a** and **220a** are quite similar in their details, except for the

exchange of positions of B and H. The B-H distance for the rotated H/Bpin unit (*trans* to N) in **219a** and **220a** is ca. 1.46 Å and it can be regarded as an elongated σ-BH complex.[131] In contrast, **TS219-220** displays a much shorter B-H distance of 1.345 Å, consistent with an "unelongated" σ-complex, with the B-H bond rotated approximately perpendicularly to the plane of the drawing in Figure II-13. Thus, the structure of **TS219-220** is more rigorously that of a trivalent Ir in an octahedral environment (BH occupies one coordination site), while the structures of **219a** and **220a** can be viewed as slightly shifted towards the pentagonal bipyramidal geometry expected for Ir(V) (if the boryl and the hydride were classical and each occupying its own coordination site). This perspective helps rationalize the modest changes in the *trans*-C-Ir-H angle between **219a**/**220a** and **TS219-220**.

Trans-influence considerations for the OA step may also help explain why the barrier for OA is so much higher in the diboryl case (**TS204-215**) vs the monoboryl (**TS206-219**) pathway. In the diboryl case, the alkynyl in **TS204-215** and in the OA product **215** is brought into the position *trans* to a boryl. Boryl is a stronger *trans*-influencer than a hydride, thus the *trans*-conflict is greater and the energies of the **TS204-215**, **215** and consequently the subsequent **TS215-216** are all higher. This is in part manifested in the greater Ir-C distance in **TS204-215** vs that in **TS206-219**. The relative energies (Figures II-10 and II-11) and geometries (Figure II-13) within the series **TS204-215→215→TS215-216→216** follow the trend for the series **TS206-219→219a→TS219-220→220** very closely, which suggests that the difference between the viability of the

diboryl pathway vs the monoboryl pathway is largely determined by the difference in the OA barrier.

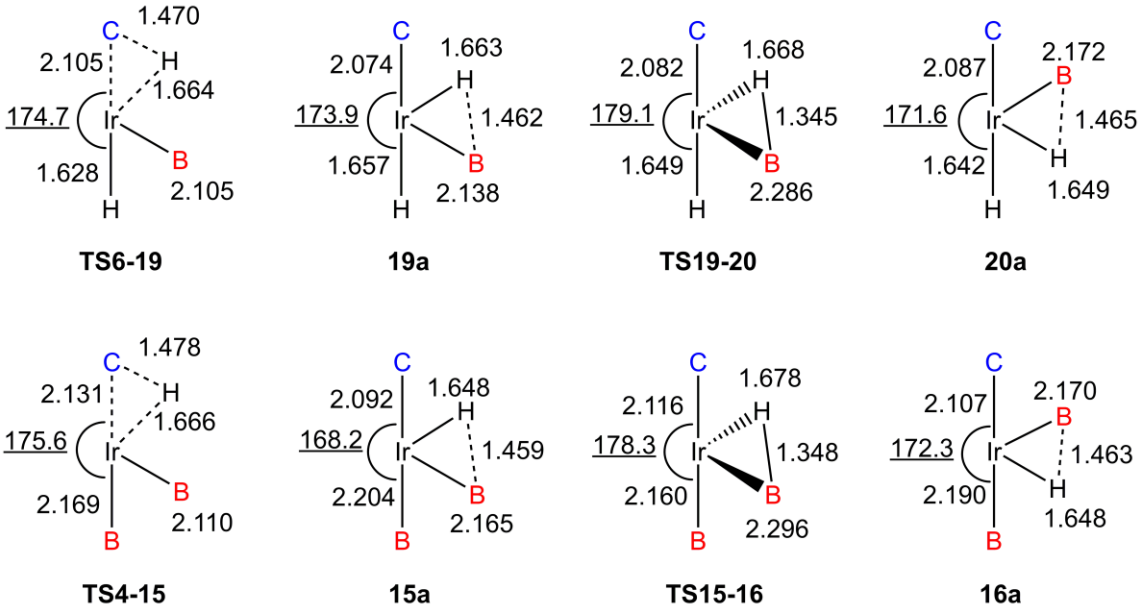

Figure II-13. Linearization of TS.

2.4 Conclusion

In summary, this study provides a comprehensive mechanistic picture of the DHBTA catalysis by (PNP)Ir complexes. The combined experimental and computational approach has proven synergistic in allowing to understand the nature of the rate-limiting sequence of events in catalysis. The global transition state corresponding to the post-OA B-H rotation was not at all an *a priori* obvious conclusion at the outset of this study. Furthermore, it did not follow obviously from the experimental data, even if it is consistent with it. It was the computational analysis that led us to identify this transition state as key to understanding the intricate mechanism of DHBTA. On the other hand, experimental findings such as the non-viability of the diboryl intermediates such as **204a** and the

identification of the (PNP)IrH_3Bpin (**205a**) resting state were important in guiding the DFT calculations. All in all, this work is a good example of how critical the feedback loop between theoretical and experimental studies is to the task of convincing delineation of organometallic mechanisms.

The results provide a significant contrast to the study of the DHBTA mechanism by the (SiNN)Ir complexes. The pivotal feature of the (SiNN)Ir mechanism, the migration of a boryl from Ir to N, turned out to be irrelevant to the mechanism by which DHBTA proceeds with (PNP)Ir. This contrast may be surprising at first realization, given that both types of catalysts are Ir complexes supported by diarylamido-centered pincer ligands. However, the two ligands turn out to be significantly different from the point of view of the feasibility of the boryl Ir-to-N migration. The SiNN ligand possesses and adaptable Si-H moiety that can modulate the electronic changes at the metal associated with the boryl migration, and the two ligands appear to have very different overall donor properties towards Ir. Furthermore, since DHBTA is now known to be catalyzed by such disparate catalysts as $Zn(OTf)_2$/pyridine, Cu(I) carbene complexes, square-planar Pd(II) complexes, in addition to the pincer-based Ir complexes, it is almost inevitable that multiple plausible DHBTA mechanisms should exist in the realm of transition metal catalysis.

Lastly, a piece of insight emerging from this work may have broader implications for the field of C-H borylation and beyond. Our DFT calculations clearly show that OA of a C-H bond *trans* to a hydride proceeds with a much lower barrier than *trans* to a boryl in an otherwise identical system (**TS206-219** vs **TS204-215**). This suggests that in systems where interconversion between boryl and hydride ligands is possible, and where

C-H activation occurs *trans* to a boryl or hydride, both possibilities may need to be examined when probing for the lowest C-H activation pathway.

2.5 Experimental

2.5.1 General Considerations

Unless otherwise specified, all manipulations were performed either inside an argon filled glove box, or by using rigorous Schlenk techniques. Pentane and diethyl ether were purified using a PureSolv MD-5 Solvent Purification System and were stored over 4Å molecular sieves in an argon-filled glove box. Fluorobenzene and hexamethyldisiloxane were purified by distillation from CaH_2 and stored over 4Å molecular sieves in an argon-filled glove box. C_6D_6 was dried over NaK, benzophenone, and 18-crown-6 then stored in an argon-filled glove box over 4Å molecular sieves prior to use. 4-ethynyltoluene, ethynylbenzene, 4-ethynylanisole, 4-ethynyl-α,α,α-trifluorotoluene, and 4-ethynyl-N,N-dimethylaniline were vacuum transferred and stored in the freezer inside of an argon-filled glove box. Deuterated 4-ethynyltoluene[132] was prepared using a modified literature procedure. The ligand ^{F}PN(Me)P^{iPr} (**201d**)[119] and iridium precatalysts (^{Me}PNP^{iPr})Ir(H)$_2$ (**202a**), (^{Me}PNP$^{iPr/Ph}$)Ir(COE) (**202c**), were prepared according to literature procedures.[47] All other chemicals were used as received from commercial vendors. Ethylene glycol was used as a temperature standard[133] for all variable temperature NMR experiments with an assumed error of 1 °C. Kinetics experiments were performed at 22 °C unless otherwise specified. All NMR spectra were acquired on a Varian Inova 300 spectrometer (^{1}H NMR, 299.951 MHz, ^{13}C NMR, 75.413 MHz, ^{31}P

NMR, 121.425 MHz), Varian Inova 400 spectrometer (^{1}H NMR, 399.535 MHz; ^{13}C NMR, 100.467 MHz; ^{11}B NMR, 128.185 MHz; ^{31}P NMR, 161.734 MHz; ^{2}H, 61.322 MHz), and Varian Inova 500 (^{1}H NMR, 499.703 MHz; ^{13}C NMR, 125.697 MHz; ^{31}P NMR, 202.265 MHz; ^{19}F NMR, 470.272) in denoted solvents. All chemical shifts are reported in δ (ppm). All ^{1}H and ^{13}C NMR spectra were referenced internally to the residual solvent signal (C_6D_6 at δ 7.16 for ^{1}H and δ 128.06 for ^{13}C NMR). ^{11}B NMR spectra were referenced externally to a solution of BF_3 etherate at δ 0. ^{31}P NMR spectra were externally referenced to an 85% phosphoric acid solution δ 0. ^{19}F NMR spectra were externally referenced to neat trifluoroacetic acid δ -78.55. Elemental analyses were performed by CALI Labs, Inc. (Highland Park, NJ).

2.5.2 Synthesis of Compounds

Synthesis of (^{Me}PNP$^{iPr/Et}$)Li (201b-Li). In an Ar-filled glove box, a 100 mL Schlenk flask was charged with **PNBr** (1.61 g, 4.10 mmol) and 50 mL diethyl ether. Once all solids dissolved, n-BuLi (3.27 mL; 2.5 M in hexanes; 8.2 mmol) was added in two portions. After three hours, chlorodiethylphosphine (0.534 g, 4.29 mmol) was added and the solution was stirred overnight. A degassed mixture of 1:1 ^{i}PrOH:H_2O (1 mL) was added to quench the reaction. This mixture stirred overnight. Volatiles were removed *in vacuo* at 70^{o} C. The residual solids were then dissolved in pentane and filtered through Celite and the volatiles were removed again resulting in a yellow oil weighing 1.52 g (~60% purity). The oil was reconstituted in 5 mL of pentane and n-BuLi (1.51 mL, 3.8 mmol) was added which precipitated yellow solids immediately. The solids were collected

on a glass frit, washed with cold pentane, and dried to produce the product as a free-flowing yellow solid of >95% purity by ^{1}H and ^{31}P NMR spectroscopy. Yield: 895 mg (54%). ^{1}H NMR (C_6D_6, 500 MHz): δ 7.20 (m, 1H, Ar-*H*), 6.98 (m, 4H, Ar-*H*), 6.89 (dd, *J* = 8.5 Hz, *J* = 1.9 Hz, 1H, Ar-*H*), 2.24 (s, 6H, Ar-*CH*$_3$), 1.94 (m, 2H, P-C*H*-Me$_2$), 1.57 (m, 2H, P-C*H*$_2$-Me), 1.32 (m, 2 H, P-C*H*$_2$-Me), 1.11 (dd, *J* = 14.0 Hz, *J* = 7.1 Hz, 6H, P-CH-(C*H*$_3$)$_2$), 0.7-1.0 (br, overlapping, 12H, P-CH-(C*H*$_3$)$_2$ & both P-CH$_2$-C*H*$_3$). ^{13}C{^{1}H} NMR (C_6D_6, 125 MHz): δ 167.1 (d, *J* = 25 Hz, Ar-N), 132.9, 132.2, 131.8, 131.5, 126.8, 125.5, 124.5, 124.2, 123.8, 23.2 (P-*C*H-Me$_2$), 20.8 (Ar-C*H*$_3$), 20.7 (Ar-C*H*$_3$), 20.1 (P-CH-*C*H$_3$), 10.38, 10.29. ^{31}P{^{1}H} NMR (C_6D_6, 202 MHz): δ -1.9, -29.0.

Synthesis of (^{Me}PNP$^{iPr/Et}$)H (201b-H) by hydrolysis of pure 201b-Li. In an Ar-filled glove box, **201b-Li** (30 mg, 0.074 mmol) was dissolved in 1 mL C_6D_6 and transferred to a 10 mL Schlenk flask. The flask was brought out of the glove box and 1 mL of degassed water was added. The solution changed from yellow to colorless in seconds. All volatiles were removed *in vacuo* at ambient temperature. The residual colorless oil was dissolved in C_6D_6 and was determined to be of >95% purity by ^{1}H and ^{31}P NMR spectroscopy. ^{1}H NMR (C_6D_6, 500 MHz): δ 8.13 (t, 1H, N-*H*), 7.36 (dd, *J* = 8.2 Hz, *J* = 4.5 Hz, 1H, Ar-*H*), 7.33 (dd, *J* = 8.3 Hz, *J* = 4.6 Hz, 1H, Ar-*H*), 7.20 (m, 1H, Ar-*H*), 7.18 (m, 1H, Ar-*H*), 6.92 (m, 1H, Ar-*H*), 6.91 (m, 1H, Ar-*H*), 2.19 (s, 3H, Ar-*CH*$_3$), 2.18 (s, 3H, Ar-*CH*$_3$), 2.02 (m, 2H, P-C*H*-Me$_2$), 1.58 (m, 4H, P-C*H*$_2$-Me), 1.11 (dd, *J* = 15.3 Hz, *J* = 7.0 Hz, 6H, P-CH-(C*H*$_3$)$_2$), 0.95-1.05 (overlapping, 12H, P-CH-(C*H*$_3$)$_2$ & both P-CH$_2$-C*H*$_3$). ^{13}C{^{1}H} NMR (C_6D_6, 125 MHz): δ 147.7 (dd, *J* = 18.9 Hz, *J* = 1.3 Hz,

Ar-N), 146.1 (dd, *J* = 18.8 Hz, *J* = 1.5 Hz, Ar-N), 134.0 (d, *J* = 1 Hz), 131.5 (d, *J* = 1 Hz), 130.7, 130.4, 130.2, 128.8, 127.6 (d, *J* = 15.2 Hz),122.9 (d, *J* = 16.4 Hz), 117.8 (d, *J* = 2.4 Hz), 117.1 (d, *J* = 2.7 Hz), 23.6 (d, *J* = 11.6 Hz, P-*C*H-CH$_3$), 20.9 (P-*C*H-*C*H$_3$), 20.6 (Ar-C*H*$_3$), 20.4 (Ar-C*H*$_3$), 19.6 (d, *J* = 11.4 Hz, P-*C*H$_2$-CH$_3$), 19.2 (d, *J* = 9.3 Hz P-CH-*C*H$_3$), 10.3 (d, *J* = 14.1 Hz, P-CH$_2$-*C*H$_3$). ^{31}P{^{1}H} NMR (C_6D_6, 202 MHz): δ -13.4 (br), -35.3 (d, *J* = 13.9 Hz).

Synthesis of (^{Me}PNP$^{iPr/Et}$)Ir(COE) (202b). A 10 mL Schlenk flask was charged with **201b-Li** (249 mg, 0.611 mmol) and 3 mL of fluorobenzene. Once all solids dissolved, [(COE)$_2$IrCl]$_2$ (258 mg, 0.594 mmol Ir) was added to the flask in one portion resulting in a red solution. After 30 min, the volatiles were removed *in vacuo*. The residue was dissolved in pentane and filtered through Celite. The volatiles were removed *in vacuo* again, and the solids were dissolved in a minimal amount of pentane and placed into a freezer at -35^o C to recrystallize. The product was yielded the next day as a red-orange powder. The supernatant was decanted and the red-orange solids were dried *in vacuo.* Yield: 248 mg (60%). ^{1}H NMR (C_6D_6, 500 MHz): δ 7.79 (dd, *J* = 8.5 Hz, *J* = 4.2 Hz, 1H, Ar-*H*), 7.75 (dd, *J* = 8.4 Hz, *J* = 4.2 Hz, 1H, Ar-*H*), 6.90 (d, *J* = 8.5 Hz, 1H, Ar-*H*), 6.88 (d, *J* = 8.5 Hz, 1H, Ar-*H*), 6.83 (d, *J* = 8.5 Hz, 1H, Ar-*H*), 6.81 (d, *J* = 8.5 Hz, 1H, Ar-*H*), 3.25 (m, 2H, COE alkenyl), 2.37 (m, 4H, overlapping P-C*H*$_2$ & two P-C*H*), 2.24 (s, 3H, Ar-C*H*$_3$), 2.20 (s, 3H, Ar-*CH*$_3$), 1.85 (m, 2H, P-C*H*$_2$), 1.70 (m, 6H, COE), 1.60 (m, 2H, COE), 1.48 (m, 2H, COE), 1.41 (m, 2H, COE), 1.27 (dd, *J* = 14.9 Hz, *J* = 7.2 Hz, 6H, P-CH-(C*H*$_3$)$_2$, 1.04 (overlapping, 12H, P-CH-(C*H*$_3$)$_2$ & both P-CH$_2$-C*H*$_3$). ^{13}C{^{1}H} NMR

(C_6D_6, 125 MHz): δ 165.1 (dd, *J* = 18.3 Hz, *J* = 3.1 Hz, Ar-N), 164.0 (dd, *J* = 17.6 Hz, *J* = 2.1 Hz, Ar-N), 131.9, 131.7 (d, *J* = 1.9 Hz), 131.5 (d, *J* = 1.8 Hz), 130.3, 126.6 (d, *J* = 1 Hz), 126.2 (d, *J* = 6.5 Hz), 126.0 (d, *J* = 48 Hz), 125.8 (d, *J* = 6.2 Hz), 122.6 (d, *J* = 45 Hz), 155.9 (d, *J* = 10.8 Hz), 115.3 (d, *J* = 9.9 Hz), 40.6 (*C*H=*C*H, COE), 32.9 (overlapping with resonance at 32.8, CH_2 COE), 32.8 (s, CH_2 COE), 27.4 (s, CH_2 COE), 24.1 (d, *J* = 22.9 Hz, P-*C*H-CH_3), 23.2 (d, *J* = 24.1 Hz, P-*C*H_2-CH_3), 20.6 (Ar-*C*H_3), 20.5 (Ar-*C*H_3), 18.9 (d, *J* = 3.8 Hz, P-CH-*C*H_3), 17.5 (P-CH-*C*H_3), 9.3 (d, *J* = 2 Hz, both P-CH_2-*C*H_3). $^{31}P\{^1H\}$ NMR (C_6D_6, 202 MHz): δ 28.6 (d, *J* = 355 Hz), 17.4 (d, *J* = 355 Hz). Elem. Anal. Calcd for $C_{32}H_{50}IrNP_2$: C, 54.68; H, 7.17. Found: C, 54.87; H, 7.02.

***In Situ* observation of (^{Me}PNP$^{iPr/Et}$)Ir(CO) (203b).** In an Ar-filled glove box, a J. Young tube was charged with **202b** (14 mg, 0.020 mmol) and 600 μL of C_6D_6. After three freeze-pump-thaw cycles, the tube was backfilled with 1 atm. CO. Immediately the solution turned from orange to pale yellow. All volatiles were removed *in vacuo*. The residue was dissolved in C_6D_6 for spectroscopic analysis. ^1H NMR (C_6D_6, 500 MHz): δ 7.74 (m, 2H, Ar-*H*), 6.92 (dd, *J* = 8.4 Hz, *J* = 2.0 Hz, 1H, Ar-*H*), 6.83 (m, 3H, Ar-*H*), 2.28 (m, 2H, P-C*H*$_2$), 2.18 (s, 6H, Ar-*CH*$_3$), 1.80 (m, 4H, P-C*H*$_2$ & both P-C*H*), 1.30 (dd, *J* = 16.9 Hz, *J* = 7.0 Hz, 6H, P-CH-(C*H*$_3$)$_2$), 1.08 (12H, overlapping doublet of triplets, *J* = 18.3 Hz, *J* = 7.6 Hz, P-CH_2-C*H*$_3$ & dd, *J* = 15.2 Hz, *J* = 6.9 Hz, P-CH-(C*H*$_3$)$_2$). $^{13}C\{^1H\}$ NMR (C_6D_6, 125 MHz): δ 186.8 (overlapping dd, apparent triplet, *J* = 8.4 Hz, Ir-*C*O), 163.6 (dd, *J* = 19.3 Hz, *J* = 3.6 Hz, Ar-N), 162.8 (dd, *J* = 20.8 Hz, *J* = 3.4 Hz, Ar-N), 132.7 (d, *J* = 1 Hz), 132.3 (d, *J* = 2 Hz), 132.2 (d, *J* = 2 Hz), 131.2 (d, *J* = 1 Hz), 126.3 (d, *J* =

7.1 Hz), 126.1 (d, *J* = 6.6 Hz), 124.1 (d, *J* = 48 Hz), 122.4 (d, *J* = 44 Hz), 116.2 (dd, *J* = 11.0 Hz, *J* = 2.9 Hz), 115.7 (dd, *J* = 11.4 Hz, *J* = 3.1 Hz), 26.6 (d, *J* = 29.7 Hz, P-*C*H-CH_3), 22.3 (d, *J* = 32.8 Hz, P-*C*H_2-CH_3), 20.4 (Ar-Me), 20.3 (Ar-Me), 19.6 (d, *J* = 4.7 Hz, P-CH-*C*H_3), 18.6 (P-CH-*C*H_3), 9.7 (P-CH_2-*C*H_3). $^{31}P\{^1H\}$ NMR (C_6D_6, 202 MHz): δ 58.0 (d, *J* = 272 Hz), 35.5 (d, *J* = 272 Hz). IR (C_6D_6) ν(CO): 1931 cm^{-1}.

Synthesis of (^{Me}PNP$^{iPr/Et}$)Ir(Bpin)$_2$ (204b). In an Ar-filled glove box, a 10 mL Schlenk flask was charged with **202b** (110 mg, 0.156 mmol), 3 mL of fluorobenzene, and pinacolborane (125 μL, 0.860 mmol). No immediate color change was observed. After stirring overnight, the volatiles were removed *in vacuo*. The residue was washed with cold hexamethyldisiloxane and dried *in vacuo* yielding **204b** as a yellow solid. Yield: 44 mg (33%). X-ray quality crystals were grown at -30 ^oC from a concentrated solution in hexamethyldisiloxane. ^1H NMR (C_6D_6, 500 MHz): δ 7.69 (dd, *J* = 8.7 Hz, *J* = 4.1 Hz, 1H, Ar-*H*), 7.67 (dd, *J* = 8.8 Hz, *J* = 4.4 Hz, 1H, Ar-*H*), 7.00 (m, 2H, Ar-*H*), 6.86 (m, 2H, Ar-*H*), 2.91 (m, 2H, P-C*H*$_2$), 2.60 (m, 2H, two P-C*H*), 2.24 (s, 3H, Ar-C*H*$_3$), 2.21 (s, 3H, Ar-C*H*$_3$), 1.99 (m, 2H, P-C*H*$_2$), 1.49 (dd, *J* = 16.2 Hz, *J* = 7.1 Hz, 6H, P-CH-(C*H*$_3$)$_2$), 1.20 (overlapping, 36H, P-CH-(C*H*$_3$)$_2$, both P-CH_2-C*H*$_3$, & C*H*$_3$ on Bpins). $^{13}C\{^1H\}$ NMR (C_6D_6, 125 MHz): δ 162.4 (dd, *J* = 16.2 Hz, *J* = 2.6 Hz, Ar-N), 161.8 (dd, *J* = 16.2 Hz, *J* = 2.6 Hz, Ar-N), 132.6, 131.3 (d, *J* = 2.2 Hz), 131.1 (d, *J* = 2.1 Hz), 130.8 (d, *J* = 1 Hz), 125.7 (d, *J* = 6.6 Hz), 125.6 (d, *J* = 5.9 Hz), 124.1 (d, *J* = 1 Hz), 123.7 (d, *J* = 1 Hz), 115.5 (d, *J* = 9.5 Hz), 114.3 (d, *J* = 10.3 Hz), 81.1 (C_{quart}, Bpin), 25.4 (CH_3, Bpin), 25.2 (CH_3, Bpin), 24.2 (br, P-*C*H-CH_3), 21.1 (br, P-*C*H-CH_3), 20.2 (Ar-Me), 20.1 (Ar-Me), 18.6 (br,

P-*C*H$_2$-CH$_3$), 17.1 (P-CH-*C*H$_3$), 9.5 (both P-CH$_2$-*C*H$_3$). ^{31}P{^{1}H} NMR (C_6D_6, 202 MHz): δ 47.6 (d, *J* = 327 Hz), 29.7 (d, *J* = 327 Hz). ^{11}B{^{1}H} NMR (C_6D_6, 128 MHz) δ 28.9 (br s). Elem. Anal. Calcd for $C_{36}H_{60}B_2IrNO_4P_2$: C, 51.07; H, 7.14. Found: C, 50.81; H, 6.95.

Variability of the product formation in reactions of 202b with HBpin. We found that the synthesis **204b** starting from **202b** (20 mg, 28 μmol) worked more reliably with 2.8 equivalents of HBpin (500 μL of a 0.13 M solution in benzene) in a 20 mL scintillation vial with 3 mL PhF. Addition of 5 equivalents of neat HBpin (30 μL, 0.20 mmol) led to an unidentified byproduct. Selected NMR data for this compound follow: (^{1}H NMR (C_6D_6, 500 MHz): δ -7.49 (br s, 1H), -13.4 (ddd, *J* = 19.6, *J* = 13.0, *J* = 6.4 Hz, 1H); ^{31}P{^{1}H} (C_6D_6, 202 MHz): δ 48.9 (d, *J* = 323 Hz), 21.2 (d, *J* = 323 Hz).

Addition of HBpin (203 μL of a 0.13 M solution in benzene, 0.026 mmol) to **202b** (18 mg, 0.026 mmol) in 250 μL of C_6D_6 in a J. Young tube resulted in the formation of a 1:1:1 mixture of **204b**, and the tentatively identified by comparison with the corresponding (^{Me}PNP^{iPr})Ir analogs (**^{Me}PNP$^{iPr/Et}$)Ir(H)$_3$(Bpin)** (**205b**) and (^{Me}PNP$^{iPr/Et}$)Ir(H)(Bpin) (**206b**). Selected NMR data are given below.

205b. (^{1}H NMR (C_6D_6, 500 MHz): δ -5.41 (br s, 1H), -12.13 (br s, 2H); ^{31}P{^{1}H} (C_6D_6, 120 MHz): δ 41.4 (d, *J* = 311 Hz), 14.5 (d, *J* = 311 Hz). Compared to (^{Me}PNP^{iPr})Ir(H)$_3$(Bpin): (^{1}H NMR (C_6D_6, 500 MHz): δ -5.35 (br s, 1H), -12.40 (br s, 2H); ^{31}P{^{1}H} (C_6D_6, 202 MHz): δ 40.8.

206b. (^{1}H NMR (C_6D_6, 500 MHz): δ -19.65 (apparent triplet, *J* = 8.0 Hz, 1H); ^{31}P{^{1}H} (C_6D_6, 120 MHz): δ 53.1 (d, *J* = 318 Hz), 32.5 (d, overlap with **204b**). Compared

to (^{Me}PNP^{iPr})Ir(H)(Bpin): (^{1}H NMR (C_6D_6, 500 MHz): δ -19.82 (t, *J* = 8.4 Hz, 1H); ^{31}P{^{1}H} (C_6D_6, 121 MHz): δ 51.8.

Synthesis of (^{F}PNP^{iPr})Ir(H)$_2$ (202d). In an Ar-filled glove box, a 50 mL culture tube was charged with **201d** (82 mg, 0.18 mmol), 10 mL of fluorobenzene, and [(COD)IrBr]$_2$ (65 mg, 0.17 mmol Ir). Stirring at ambient temperature for one hour afforded a milky, off-white solution. The tube was then brought out of the glove box and heated overnight in an 80 °C oil bath. The volatiles of the resulting green solution were removed *in vacuo* and the residue was extracted with 4 mL of fluorobenzene and transferred to a 50 mL Teflon stoppered Schlenk flask. To this flask, sodium isopropoxide (23 mg, 28 mmol) was added. No immediate color change was observed. The solution was subjected to three freeze-pump-thaw cycles and then backfilled with dihydrogen. This mixture was allowed to stir overnight yielding an orange solution. The volatiles were removed *in vacuo* and the residue was dissolved in pentane, filtered through a plug of Celite, and placed into a -35 °C freezer overnight yielding **202d** as an orange solid of ca. 95% purity by ^{1}H and ^{19}F NMR spectroscopy. Yield: 53 mg (49% yield). Note: This iridium complex performs H/D exchange with C_6D_6[134] resulting in a hydride resonance which does not integrate to the expected 2H.

^{1}H NMR (C_6D_6, 500 MHz): δ 7.50 (br s, 2H, Ar-*H*), 6.86 (dd, *J* = 7.2 Hz, *J* = 3.5 Hz, 2H, Ar-*H*), 6.76 (t, *J* = 8.3 Hz, 2H, Ar-*H*), 1.93 (br s, 4H, C*H*-(CH_3)$_2$), 1.09 (dvt, *J* = 8.3 Hz, *J* = 7.6 Hz, 12H, CH-(C*H*$_3$)$_2$), 0.86 (dvt, *J* = 7.4 Hz, *J* = 7.1 Hz, 12H, CH-(C*H*$_3$)$_2$), -25.43 (t, *J* = 9.9 Hz, 2H, Ir-(*H*)$_2$). ^{13}C{^{1}H} NMR (C_6D_6, 125 MHz): δ 162.94 (td, *J* = 10.6

Hz, *J* = 1.5 Hz), 157.01 (t, *J* = 4.3 Hz), 155.11 (t, *J* = 4.3 Hz), 119.04 (d, *J* = 21.4 Hz), 117.24 (d, *J* = 22.2 Hz), 114.56 (q, *J* = 5.7 Hz), 25.42 (t, *J* = 15.2 Hz), 19.93 (t, *J* = 3.2 Hz), 18.43 (s). $^{31}P\{^{1}H\}$ NMR (C_6D_6, 202 MHz): δ 58.33 (s). ^{19}F NMR (C_6D_6, 470 MHz): δ -129.39 (s). Elem. Anal. Calcd for $C_{24}H_{36}F_2IrNP_2$: C, 45.70; H, 5.75. Found: C, 45.62; H, 5.24.

*2.5.3 X-Ray Structural Determination Details for ($^{Me}PNP^{iPr/Et}$)Ir(Bpin)$_2$ (**204b)***

CCDC Deposition Number: 1954548. Data Collection method: A Leica MZ 75 microscope was used to identify a suitable brown block with very well-defined faces with dimensions (max, intermediate, and min) 0.16 x 0.09 x 0.029 mm^3 from a representative sample of crystals of the same habit. The crystal mounted on a nylon loop was then placed in a cold nitrogen stream (Oxford) maintained at 110 K.

A BRUKER APEX 2 X-ray (three-circle) diffractometer was employed for crystal screening, unit cell determination, and data collection. The goniometer was controlled using the APEX2 software suite, v2008-6.0.[135] The sample was optically centered with the aid of a video camera such that no translations were observed as the crystal was rotated through all positions. The detector was set at 6.0 cm from the crystal sample (APEX2, 512x512 pixel). The X-ray radiation employed was generated from a Mo sealed X-ray tube (K_α = 0.70173Å with a potential of 40 kV and a current of 40 mA).

45 data frames were taken at widths of 1°. These reflections were used to determine the unit cell using Cell_Now,[136] which indicated two component twin domains. The unit cell was verified by examination of the *h k l* overlays on several frames of data. No super-

cell or erroneous reflections were observed. After careful examination of the unit cell, an extended data collection procedure (4 sets) was initiated using omega scans.

Data reduction, structure solution, and refinement methods: Integrated intensity information for each reflection was obtained by reduction of the data frames with the program APEX3,[135] including the two domains. The integration method employed a three-dimensional profiling algorithm and all data were corrected for Lorentz and polarization factors, as well as for crystal decay effects. Finally, the data was merged and scaled to produce a suitable data set. The absorption correction program TWINABS[137] was employed to correct the data for absorption effects, as well as to separate the reflections into two files: one containing reflections from only the major component, and another containing reflections from both the twin components. The former was used for both structure solution as well as for final least squares refinement.

Systematic reflection conditions and statistical tests of the data suggested the space group *P*-1. A solution was obtained readily (Z=4; Z'=2) using XT/XS in APEX2.[135,138] Hydrogen atoms were placed in idealized positions and were set riding on the respective parent atoms. All non-hydrogen atoms were refined with anisotropic thermal parameters. Elongated thermal ellipsoids on all the $BO_2C_2(CH_3)_4$ groups suggested disorder and were modeled with two positions each (with an occupancy ratio of 0.73:0.27). Several restraints and / or constraints were added to keep the bond distances, angles, and thermal ellipsoids meaningful. Absence of additional symmetry and voids were confirmed using PLATON (ADDSYM).[139] The structure was refined (weighted least squares refinement on F^2) to

convergence.[138,140] Olex2 was employed for the final data presentation and structure plots.[140]

*2.5.4 Experiments to Determine the Resting State of (^{Me}PNP^{iPr})IrH$_2$ **202a** During DHBTA*

This section describes two experiments used to determine the resting state of the (PNP)Ir fragment during the DHBTA reaction. Figures II-8 & II-9 below show that the resting state of the iridium catalyst during the DHBTA reaction with 4-ethynyltolune is (PNP)Ir(H)$_3$Bpin which has been previously reported. This necessitates loss of H_2 from the iridium center in order to perform a catalytic turnover. Thus, [H_2] should inversely impact the rate of the reaction such that:

$$rate = \frac{-d[Alk]}{dt} = k[HBpin]^W[Alkyne]^X[Catalyst]^Y[H_2]^{-1}$$

Using (PNP)Ir(H$_2$) (202a). To a J. Young tube was added 490 µL C_6D_6, HBpin (100 µL, 0.69 mmol), **202a** (75 µL of a 0.01 M stock solution, 7.5 x 10^{-4} mmol), and 4-ethynyltoluene (35 µL of a 1 M stock solution (with 0.35 M dioxane), 0.035 mmol). The total volume of the reaction was 700 µL. The reaction was monitored by ^{1}H and ^{31}P NMR spectroscopy.

Using (F-PNP)Ir(H$_2$) (202d). To a J. Young tube was added 510 µL C_6D_6, HBpin (100 µL, 0.69 mmol), solution **202d** (50 µLof a 0.12 M stock solution, 5.9 x 10^{-4} mmol), and 4-ethynyltoluene (35 µL of a 1 M stock solution (with 0.35 M dioxane), 0.035 mmol).

The total volume of the reaction was 700 µL. The reaction was monitored by ^{1}H, and ^{19}F NMR spectroscopy.

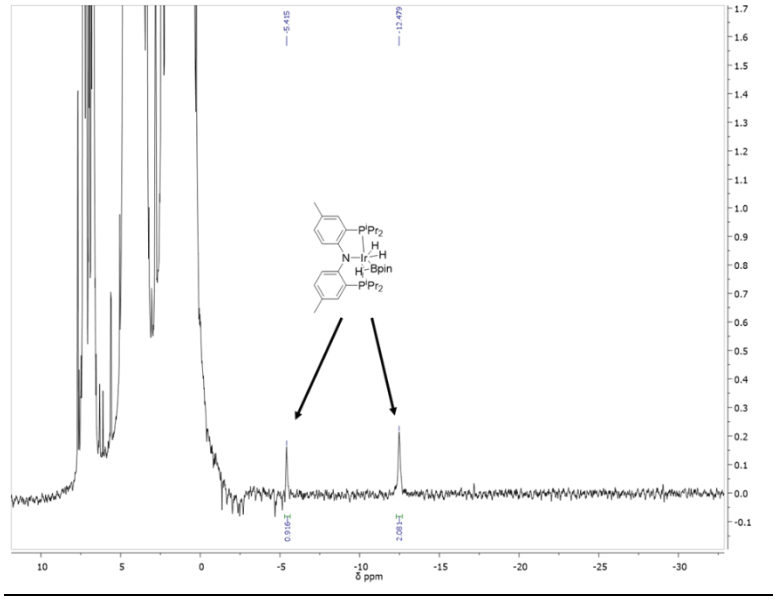

Figure II-14. The hydride region of a ^{1}H NMR (500 MHz, C_6D_6) spectrum during the borylation of 4-ethynyltoluene using **202a** as a precatalyst. Two hydride resonances are observed which correspond to **205a**.[47]

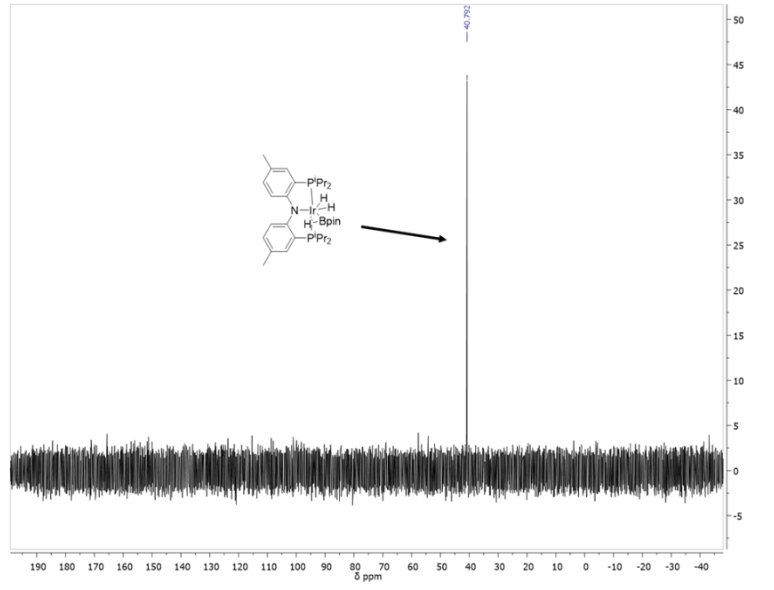

Figure II-15. $^{31}P\{^{1}H\}$ NMR (202 MHz, C_6D_6) spectrum during the borylation of 4-ethynyltoluene using **202a** as a precatalyst. Only one resonance is observed. This resonance corresponds to **205a**.[47]

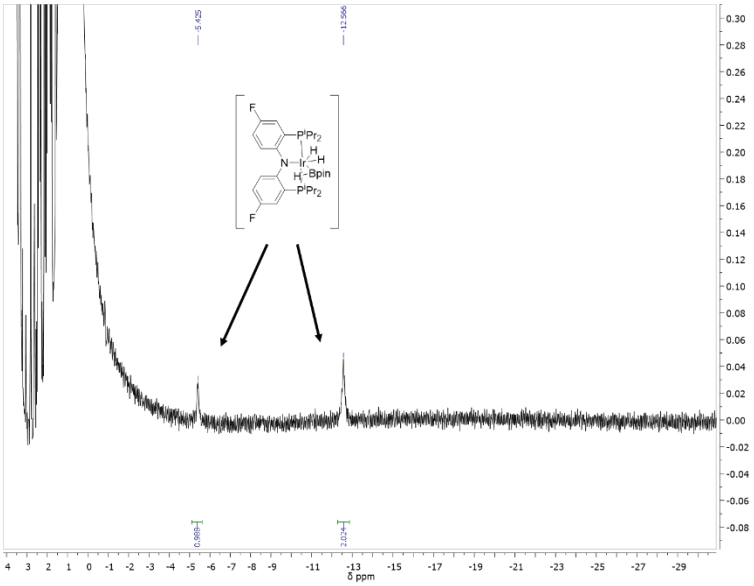

Figure II-16. The hydride region of a ^{1}H NMR (500 MHz, C_6D_6) spectrum during the borylation of 4-ethynyltoluene using **202d** as a precatalyst. Two hydride resonances are observed which have been assigned to ($^{F}PNP^{iPr}$)Ir(H)$_3$(Bpin) (**205d**) by comparison to **205a** (vide supra).

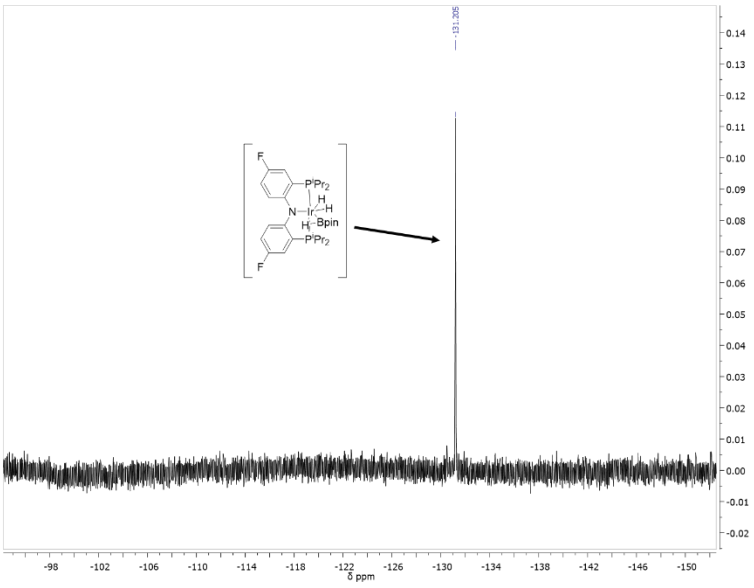

Figure II-17. ^{19}F NMR (470 MHz, C_6D_6) spectrum during the borylation of 4-ethynyltoluene using **202d** as a precatalyst. Only one resonance is observed which has been assigned to **205d**.

2.5.5 Experiments to Reactivities of Catalysts

General procedure for reactivity comparison. To a J. Young tube was added HBpin (430 μL of a 0.16 M stock solution, 0.070 mmol), Ir catalyst (35 μL of a 0.01 M stock solution, 3.5 x 10^{-4} mmol), and alkyne (35 μL of a 1 M stock solution (with 0.35 M dioxane), 0.035 mmol alkyne). The total volume of the solution was 500 μL. The reaction progress was monitored by ^{1}H NMR spectroscopy. The results from these experiments are displayed in Table II-1. Note, this procedure was deviated from for **202c** as designated in the footnotes in Table II-1.

$Me_2NCH_2C{\equiv}C$-Bpin. ^{1}H NMR (C_6D_6, 500 MHz): δ 3.07 (s, 2H), 2.11 (s, 6H), 0.99 (s, 12H). $^{13}C\{^{1}H\}$ NMR (C_6D_6, 125 MHz): δ 99.0 (br, NCH_2C), 83.9 (C_{quart}, Bpin), 48.6 (N-(CH_3)$_2$), 44.0 (CH_2), 24.7 (CH_3, Bpin). $^{11}B\{^{1}H\}$ NMR (C_6D_6, 128 MHz) δ 23.9. ESI^+ (Low Resolution, Unit Mass): Calcd. for $C_{11}H_{20}BNO_2$ $(M+H)^+$: 210.16. Found: 210.04.

Borylated 3-trimethylsiloxy-1-propyne[47] and borylated 4-ethynyltoluene[46] were identified according to literature precedent.

2.5.6 Experiments to Determine the Rate Constant for ($^{Me}PNP^{X}$)Ir Complexes

$$rate = \frac{-d[Alk]}{dt} = k[HBpin]^W[Alkyne]^X[Catalyst]^Y[H_2]^{-1}$$

A variable, k_{obs}, was defined to determine the k value for the DHBTA reaction using various precatalysts.

$$k_{obs} = k[HBpin]^{W}[Catalyst]^{Y}[H_2]^{-1}$$

Such that:

$$d[ln(alkyne)] = -k_{obs} * dt$$

In multiple reactions, the slope (k_{obs}) of the linear regression of ln[alkyne] v. time was recorded (Table II-2). The linearity of these graphs was indicative of first order dependence on [alkyne] (Figure II-2). The resultant graph below shows that varying [HBpin] under a pseudo-first order concentration of HBpin does not change the rate of the reaction revealing a zeroth order dependence of the reaction on HBpin. It was assumed that the order of the reaction with respect to HBpin remained zero throughout all reaction variations presented in this work.

Table II-2 k_{obs} values from ln[4-ethynyltoluene] v. time with varying [HBpin]

[HBpin] (mol/L)	k_{obs} (x 10^4) (s^{-1})
1.0	2.1(6)
1.0	2.3(2)
1.5	2.1(5)
2.0	2.1(4)
3.0	2.0(1)

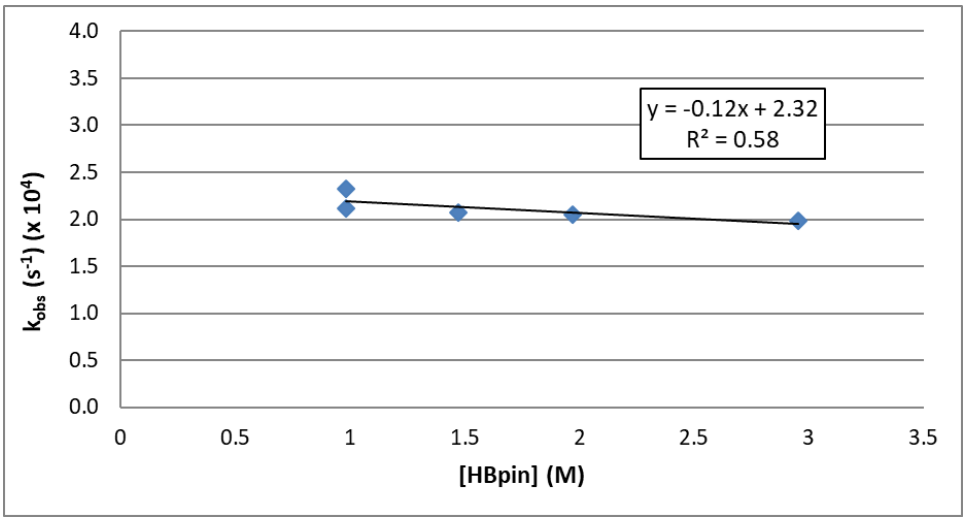

Figure II-18. Influence of [HBpin] on the rate of DHBTA.

No rate dependence on the [HBpin] was observed between 1.0 and 3.01 M HBpin (Figure II-18). The errors for the k_{obs} values were defined as double the standard deviation of the slope provided by the LINEST function in Microsoft Excel.

Knowing that the order of the reaction in HBpin is zero simplifies k_{obs} such that:

$$k_{obs} = k[Cat]^{Y}[H_2]^{-1}$$

In multiple reactions, the slope (k_{obs}) of the linear regression of ln[alkyne] v. time was recorded with variable catalyst concentrations. The value of k_{obs} was plotted against the catalyst concentration yielding k* as the slope value where:

$$k^{*} = k[H_2]^{-1}$$

The linear dependence of the k* plot reveals that the reaction is first order in the iridium complexes under pseudo-first order conditions with respect to HBpin.

General procedure for determining the dependence of the rate on the Ir precatalysts. To a J. Young tube was added HBpin (100 μL, 0.69 mmol), 4-ethynyltoluene (35 μL of a 1 M stock solution (with 0.35 M dioxane), 0.035 mmol alkyne), a variable amount of the iridium precatalyst, and enough C_6D_6 such that the total volume of the solution was 700 μL. The reaction progress was monitored by ^1H NMR spectroscopy. For each of the precatalysts: **202a**, **202b**, **202c**, and **202d**, the slope (k_{obs}) of the linear regression of ln[alkyne] v. time was recorded (Tables II-3, II-4, II-5, and II-6 respectively) and graphed v. the corresponding precatalyst concentration (Figures II-19, II-20, II-21, and II-22 respectively).

Table II-3. k_{obs} values from ln[4-ethynyltoluene] v. time with varying [**202a**]

[**202a**] (mol/L)	k_{obs} (x 10^4) (s^{-1})
2.1 x 10^{-4}	0.90(5)
2.1 x 10^{-4}	1.2(1)
5.0 x 10^{-4}	2.20(8)
5.0 x 10^{-4}	2.1(5)
5.0 x 10^{-4}	2.3(2)
5.0 x 10^{-4}	2.1(6)
6.4 x 10^{-4}	2.65(9)
6.4 x 10^{-4}	2.6(4)
1.1 x 10^{-3}	3.9(1)
1.1 x 10^{-3}	3.8(4)

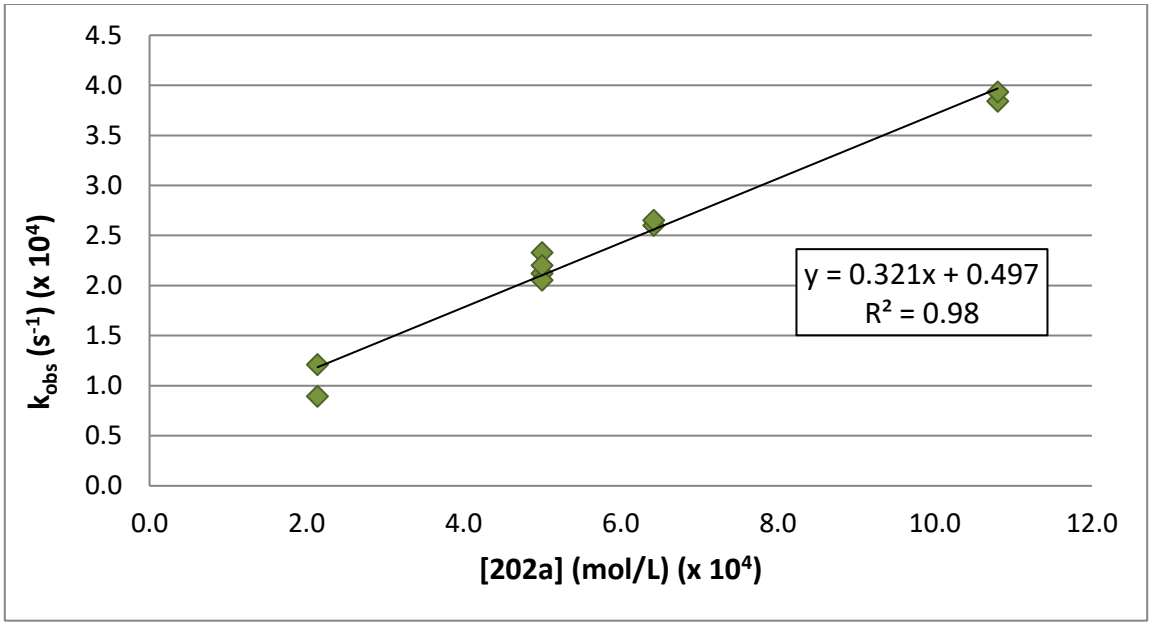

Figure II-19. Influence of [**202a**] on the rate of DHBTA

For the DHBTA of 4-ethynyltoluene with **202a**, k* = 0.32(4) L/(mol x sec). The errors for the k_{obs} values were defined as double the standard deviation of the slope provided by the LINEST function in Microsoft Excel.

Table II-4. k_{obs} values from ln[4-ethynyltoluene] v. time with varying [**202b**].

[**202b**] (mol/L)	k_{obs} (x 10^4) (s^{-1})
2.1 x 10^{-4}	2.7(1)
3.6 x 10^{-4}	4.5(6)
5.0 x 10^{-4}	6.2(4)
5.0 x 10^{-4}	6.1(4)
6.4 x 10^{-4}	9(1)

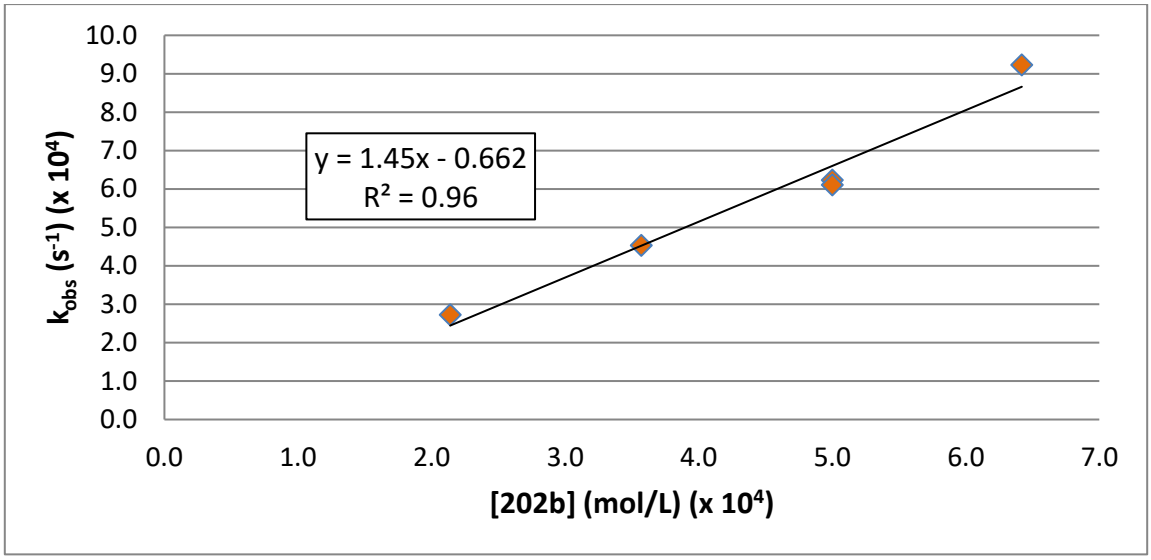

Figure II-20. Influence of [**202b**] on the rate of DHBTA

For the DHBTA of 4-ethynyltoluene with **202b**, k* = 1.5(3) L/(mol x sec). The errors for the k_{obs} values were defined as double the standard deviation of the slope provided by the LINEST function in Microsoft Excel.

Table II-5. k_{obs} values from ln[4-ethynyltoluene] v. time with varying [**202c**]

[**202c**] (mol/L)	k_{obs} (x 10^4) (s^{-1})
2.1 x 10^{-5}	2.1 ± 0.1
5.0 x 10^{-5}	4.9 ± 0.1
6.4 x 10^{-5}	5.7 ± 0.4
1.1 x 10^{-4}	9.9 ± 0.7

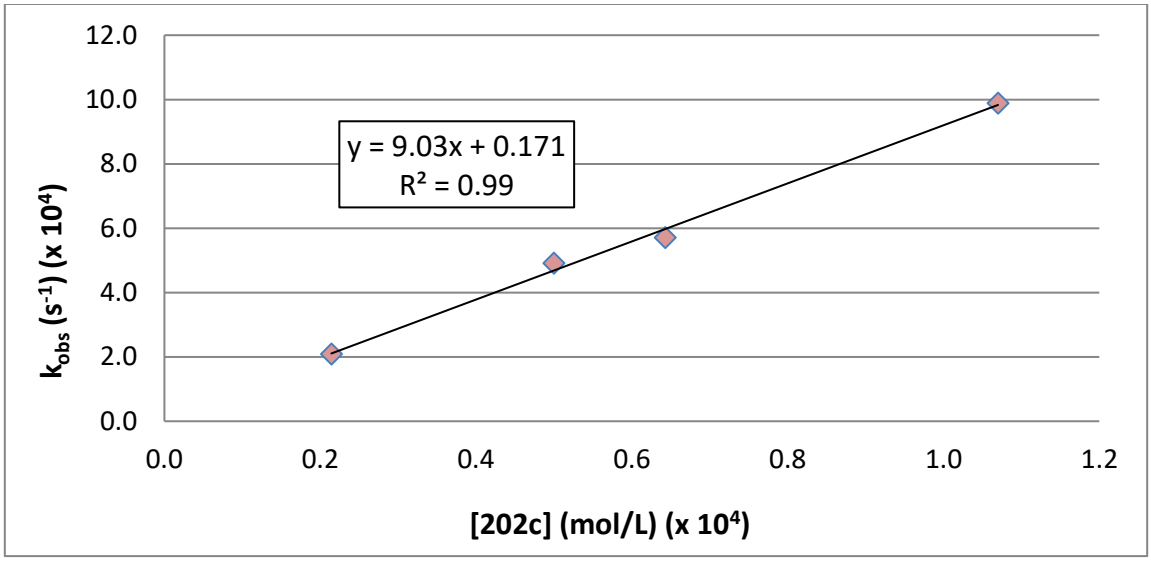

Figure II-21. Influence of **[202c]** on the rate of DHBTA.

For the DHBTA of 4-ethynyltoluene with **202c**, k* = 9.0(8) L/(mol x sec). The errors for the k_{obs} values were defined as double the standard deviation of the slope provided by the LINEST function in Microsoft Excel.

Table II-6. k_{obs} values from ln[4-ethynyltoluene] v. time with varying [**202d**]

[**202d**] (mol/L)	k_{obs} (x 10^4) (s^{-1})
2.5 x 10^{-4}	1.40(3)
5.0 x 10^{-4}	2.34(8)
8.4 x 10^{-4}	4.0(2)
1.1 x 10^{-3}	4.7(2)

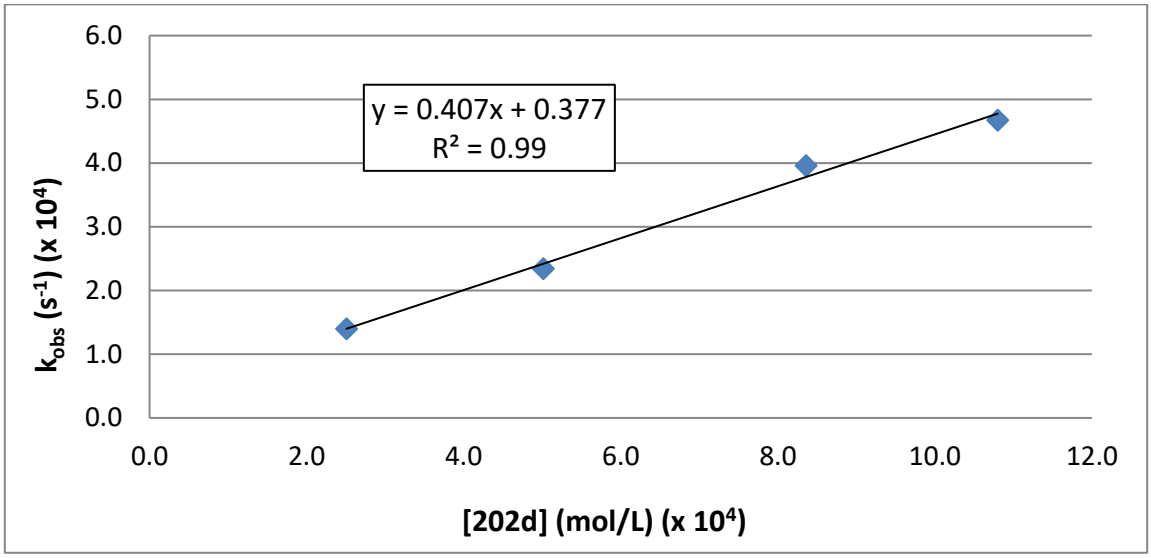

Figure II-22. Influence of [**202d**] on the rate of DHBTA.

For the DHBTA of 4-ethynyltoluene with **202d**, k* = 0.41(5) L/(mol x sec). The errors for the k_{obs} values were defined as double the standard deviation of the slope provided by the LINEST function in Microsoft Excel.

2.5.7 Experiments to Determine $\Delta H^{\ddagger}$ and $\Delta S^{\ddagger}$

Plotting ln(k/T) against 1/T using the Eyring equation:

$$\ln\left(\frac{k}{T}\right) = \left(\frac{-\Delta H^{\ddagger}}{R}\right)\left(\frac{1}{T}\right) + \ln\left(\frac{k_B}{h}\right) + \left(\frac{\Delta S^{\ddagger}}{R}\right)$$

yields a linear relationship. Both the enthalpy ($\Delta H^{\ddagger}$) and entropy ($\Delta S^{\ddagger}$) for the reaction can be extracted from the slope and Y-intercept respectively. The true rate constant, k, can be obtained by dividing each k_{obs} by the respective initial catalyst loading and multiplying by the average [H_2] (≈ 0.02 mol/L).

General procedure for performing DHBTA reactions to construct an Eyring Plot. To a J. Young tube was added HBpin (100 μL, 0.69 mmol), 4-ethynyltoluene (35 μL of a 1 M stock solution (with 0.35 M dioxane), 0.035 mmol alkyne), **202a** (15 μL if a 0.01 M stock solution, 1.5 x 10^{-4} mmol), and C_6D_6 (550 μL). The J. Young tube was placed into a preheated NMR spectrometer at variable elevated temperatures. The reaction progress was monitored by ^{1}H NMR spectroscopy and the slope (k_{obs}) of the linear regression of ln[alkyne] v. time was recorded (Table II-7).

Table II-7. Kinetic data from ln[4-ethynyltoluene] v. time at various temperatures.

T (°C)	T (K)	k_{obs} (x 10^4) (s^{-1})	k (x 10^2) (s^{-1})	ln(k/T)	1/T (x 10^3) (K^{-1})
65.8	338.9	35(3)	33(3)	-6.9	2.95
56.6	329.7	25(3)	23(3)	-7.2	3.03
54.3	327.5	21(2)	19(2)	-7.4	3.05
44.7	317.9	7.8(5)	7.2(5)	-8.4	3.15
34.9	308.1	4.9(2)	4.6(2)	-8.8	3.25
25.0	298.2	1.26(6)	1.18(6)	-10.1	3.35
15.0	288.2	0.61(4)	0.57(4)	-10.8	3.47

The errors for the k_{obs} values were defined as double the standard deviation of the slope provided by the LINEST function in Microsoft Excel for each of the above experiments. For Eyring Plot, the error of the slope provided by LINEST was doubled and multiplied by the ideal gas constant to provide the error in $\Delta H^{\ddagger}$. The error in the Y-intercept of the Eyring Plot was doubled and used with the Y-intercept, to calculate the error in $\Delta S^{\ddagger}$. The addition and subtraction of double the standard deviation from the Y-intercept value yielded a total error of ± 6 cal/(mol×K) with respect to the calculated entropy values.

$$slope = \left(\frac{-\Delta H^{\ddagger}}{R}\right)$$

$$-\Delta H^{\ddagger} = 16(2)\frac{kcal}{mol}$$

$$Y\ intercept = \ln\left(\frac{k_B}{h}\right) + \left(\frac{\Delta S^{\ddagger}}{R}\right)$$

$$\Delta S^{\ddagger} = -14(6)\frac{cal}{mol\ x\ K}$$

For the DHBTA of 4-ethynyltoluene with **202a**, the enthalpy of activation is 16(2) kcal/mol, and the entropy of activation is -14(6) cal/(mol x K).

2.5.8 Experiments to Determine the Hammett Parameter (ρ)

Plotting:

$$\ln [Alk]_t = -k_{obs}(t) + ln[Alk]_0$$

for the DHBTA of a series of *p*-substituted phenylacetylenes catalyzed by **202a**, potting the logarithm of the normalized observed rate constants $\log(k_{obs\_x}/k_{obs\_H})$ against literature reported sigma values[124] using:

$$\log\left(\frac{k_{obsX}}{k_{obsH}}\right) = \rho\sigma$$

yields a linear relationship. The value of the slope provides information regarding the dependence on the electron donating/withdrawing ability of the *para*-substituent.

General procedure for performing DHBTA reactions to construct a Hammett Plot. To a J. Young tube was added HBpin (100 μL, 0.69 mmol), alkyne (35 μL of a 1 M stock solution (with 0.35 M dioxane), 0.035 mmol alkyne), **202a** (35 μL of a 0.01 M stock solution, 0.035 mmol) and C_6D_6 (530 μL). The reaction progress was monitored by ^{1}H NMR spectroscopy and the slope (k_{obs}) of the linear regression of ln[alkyne] v. time was recorded (Table II-8).

Table II-8. k_{obs} values from ln[*p*-substituted phenylacetylene] v. time catalyzed by **202a**.

p-substituent	Sigma value[124]	k_{obs} (x 10^4) 1/(sec x M)	k_x/k_H
CF_3	0.54	7(1)	2.1(3)
H	0	3.4(3)	1.0(1)
CH_3	-0.17	2.20(8)	0.64(6)
OCH_3	-0.27	1.81(4)	0.53(5)
$N(CH_3)_2$	-0.83	1.05(1)	0.31(3)

The errors for the k_{obs} values were defined as double the standard deviation of the slope provided by the LINEST function in Microsoft Excel.

For the DHBTA of *p*-substituted phenylacetylenes with **202a**, the ρ value is 0.6(1).

2.5.9 Experiments to Determine the H/D Kinetic Isotope Effect

For isolated KIE value: Plotting:

$$\ln [Alk]_t = -k_{obs}(t) + ln[Alk]_0$$

reveals values of k_{obs} as the value of the slope. Dividing the observed rate constants of the DHBTA of 4-ethynyl toluene by the rate constant of the DHBTA of 4-(Ethynyl-*d*)toluene yields the isolated kinetic isotope effect.

$$KIE = \frac{k_H}{k_D}$$

To a J. Young tube was added 530 μL C_6D_6, HBpin (100 μL, 0.69 mmol), **202a** (35 μL of a 0.01 M stock solution, 3.5 x 10^{-4} mmol), and 4-(Ethynyl-*d*)toluene (35 μL of a 1 M stock solution (with 0.35 M dioxane), 0.035 mmol). The total volume of the solution was 700 μL. The reaction progress was monitored by ^{1}H NMR spectroscopy and the slope (k_{obs}) of the linear regression of ln[alkyne] v. time was recorded (Table II-9).

In a separate, more concentrated experiment, a J. Young tube was charged with the following: 520 μL C_6D_6, HBpin (100 μL, 0.69 mmol), **202a** (45 μL of a 0.01 M stock solution, 4.5 x 10^{-4} mmol), and 4-(Ethynyl-*d*)toluene (35 μL of a 1 M stock solution (with 0.35 M dioxane), 0.035 mmol). The total volume of the solution was 700 μL. The reaction progress was monitored by ^{1}H NMR spectroscopy the slope (k_{obs}) of the linear regression of ln[alkyne] v. time was recorded (Table II-9).

Table II-9. k_{obs} values from ln[4-(ethynyl-*d*)toluene v. time with varying [**202a**]

[**202a**] (mol/L)	k_{obs} (x 10^4) (s^{-1})
5.0 x 10^{-4}	1.48(2)
6.4 x 10^{-4}	1.80(5)

The k_{obs} values for the borylation of 4-(ethynyl-*d*)toluene using **202a** were compared to the values for the borylation of 4-ethynyltoluene at the same catalyst loading (Table II-10). The ratio of these two k_{obs} values provides the KIE value for the reaction (Table II-11).

Table II-10. k_{obs} values from the DHBTA of 4-ethynyltoluene at selected [**202a**].

[**202a**] (mol/L)	k_{obs} (x 10^4) (s^{-1})
5.0 x 10^{-4}	2.20(8)
6.4 x 10^{-4}	2.65(9)

$$KIE_{isol.} = \frac{k_H}{k_D} = \frac{2.20(8)}{1.48(2)} = 1.48(6)$$

$$KIE_{isol.} = \frac{k_H}{k_D} = \frac{2.65(9)}{1.80(5)} = 1.47(6)$$

Table II-11. Isolated KIE values determined at two different [**202a**].

[**202a**] (mol/L)	H/D KIE Value
5.0 x 10^{-4}	1.48(6)
6.4 x 10^{-4}	1.47(6)

For a competition KIE value. To a J. Young tube was added 450 μL of a 1:1 solution of C_6D_6:C_6H_6, deuterated cyclohexane (50 μL of a 0.093 M solution in C_6H_6), HBpin (100 μL, 0.69 mmol), solution **202a** (15 μL of a 0.01 M stock solution, 1.5 x 10^{-4} mmol), and mixture of 4-ethynyltoluene (1.05 M) and 4-(ethynyl-*d*)toluene (1.01 M) (85

μL, 0.088 mmol total alkyne). The total volume of the solution was 700 μL. The reaction progress was monitored by alternating ^{1}H and ^{2}H NMR spectroscopy and the slope (k_{obs}) of the linear regression of ln[alkyne] v. time was recorded (Table II-12).

Table II-12. k_{obs} values from ln[4-ethynyltoluene] and ln[4-(ethynyl-*d*)toluene v. time catalyzed by **202a**.

	k_{obs} (x 10^4) (s^{-1})
Protio-	0.99(3)
Deuterio-	0.8(1)

The errors for the k_{obs} values were defined as double the standard deviation of the slope provided by the LINEST function in Microsoft Excel.

$$KIE_{comp.} = \frac{k_H}{k_D} = \frac{0.99(3)}{0.8(1)} = 1.3(2)$$

The spectra for the competition kinetic isotope experiment, when processed in Mestrenova, have some disturbances in the baseline beginning with the ninth time point. We reprocessed these spectra using the CRAFT program within VnmrJ. When processed in this fashion, the kinetic isotope effect value is 1.5(3). Using the integrations from Mestrenova with the amplitudes provided by CRAFT, we can arrive at a value of 1.5(1); however, neither of these values are statistically different from the competition KIE value we report here of 1.3(2).

2.5.10 Experiments to Determine the Effect of H_2 on the Rate of Catalysis

Agitated DHBTA experiment. To a J. Young tube was added 490 µL C_6D_6, HBpin (100 µL, 0.69 mmol), solution **202a** (75 µL of a 0.01 M stock solution, 7.5 x 10^{-4} mmol), and solution 4-ethynyltoluene (35 µL of a 1 M stock solution (also 0.35 M dioxane), 0.035 mmol). The total volume of the reaction was 700 µL. The tube was manually shaken between NMR acquisition, and the reaction was monitored by ^{1}H NMR spectroscopy.

Static DHBTA experiment. To a J. Young tube was added 490 µL C_6D_6, HBpin (100 µL, 0.69 mmol), solution **202a** (75 µL of a 0.01 M stock solution, 7.5 x 10^{-4} mmol), and solution 4-ethynyltoluene (35 µL of a 1 M stock solution (also 0.35 M dioxane), 0.035 mmol). The total volume of the reaction was 700 µL. The tube was kept upright between NMR acquisition, and the reaction was monitored by ^{1}H NMR spectroscopy.

The ^{1}H NMR spectra below show that each of these two DHBTA reactions began at the same rate. However, manual shaking of one of the tubes greatly accelerated the rate of alkyne borylation. The tube which was left undisturbed had a k_{obs} = 3.9(2)x10^{-4} (s^{-1}) whereas the shaken tube showed a six-fold rate increase where k_{obs} = 2.6(2)x10^{-3} (s^{-1}) and contained considerably less dissolved H_2.

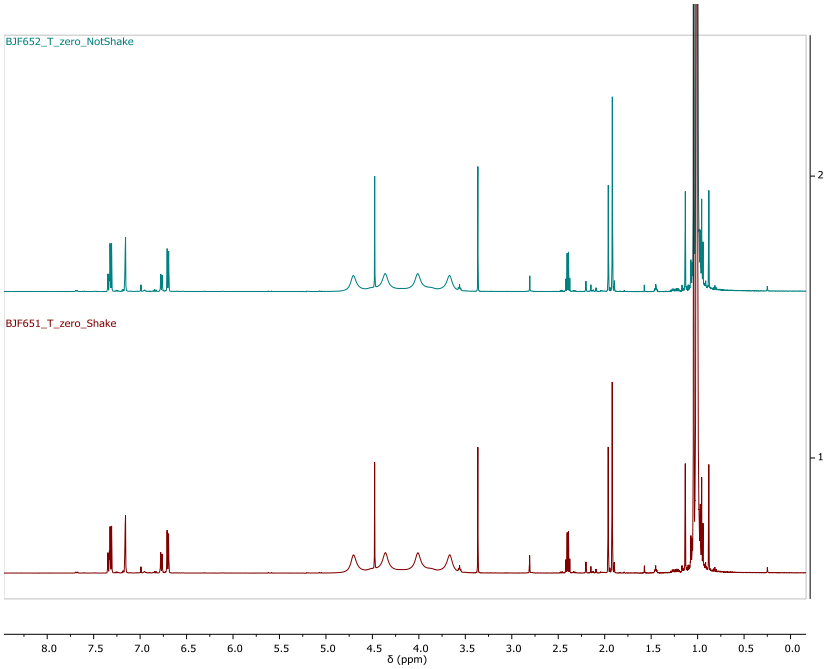

Figure II-23. ^{1}H NMR (500 MHz, C_6D_6) spectra of an *in situ* DHBTA reaction using **202a** as a precatalyst (Time = 0 minutes). Top: ^{1}H NMR spectrum of the tube that would remain upright. Bottom: ^{1}H NMR spectrum of the tube that would be shaken. Neither tube was agitated at this point, and the spectra are superimposable

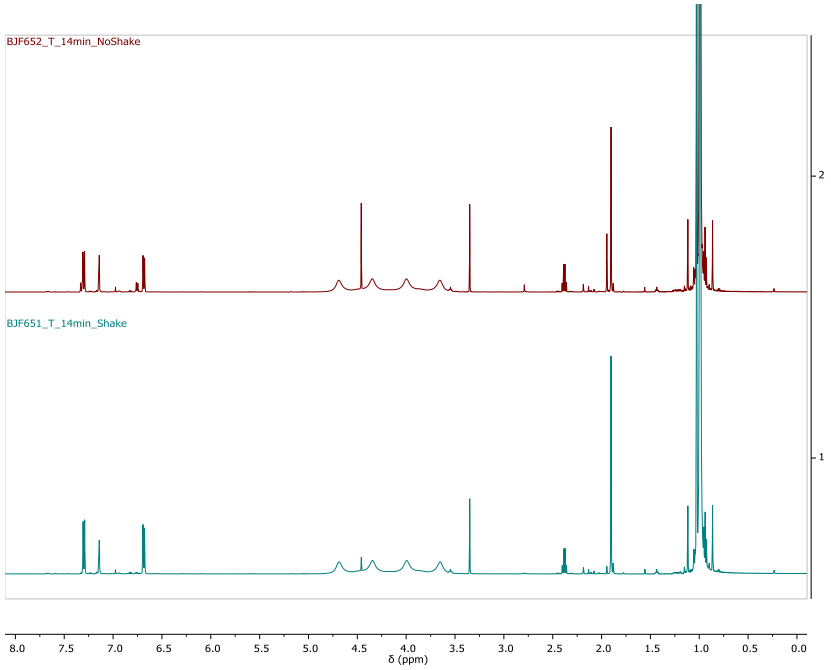

Figure II-24. ^{1}H NMR (500 MHz, C_6D_6) spectrum of in *in situ* DHBTA reaction using **202a** as a precatalyst (Time = 14 minutes). Top: ^{1}H NMR spectrum of the tube that remained upright 75% of the alkyne has been converted to the alkynylboronate. Bottom: ^{1}H NMR spectrum of the tube that had been shaken. All the starting alkyne has been consumed

2.5.11 DFT Calculations

Calculations were carried out using the Gaussian 09 program. The calculations depicted in Figures 8 and 9 were carried out using M06 with SDD pseudopotentials and basis set for Ir atom and 6-311G(d,p) basis set for the other atoms in gas phase for both the geometry optimization and energy calculation.

For the calculations depicted in Figures II-10 and II-11, the geometries were optimized using B3LYP with LANL2DZ pseudopotentials and basis set for Ir atom and 6-31G(d) basis set for the other atoms in the gas phase. The single-point energies and solvent effects were computed with the M06 functional using the SDD pseudopotentials

and basis set for Ir atom and the 6-311+G(d,p) basis set for the other atoms based on the gas-phase optimized structures. The solvation energies were evaluated by a self-consistent reaction field (SCRF) using the SMD implicit solvent model.

CHAPTER III

AIR STABLE DHBTA PRECURSOR

3.1 Introduction

C-H borylation is a powerful method of functionalization of various C-H bonds.[36-37,99] The products of C-H borylation are typically organoboronates or other derivatives of organoboronic acids. Organoboronates are valuable synthetic intermediates that permit construction of new carbon-carbon and carbon-heteroatom bonds.[48] Some of the most impressive successes in C-H borylation are associated with Ir-catalyzed C-H borylation of aromatic C(sp^2)-H bonds.[35d,100-101]

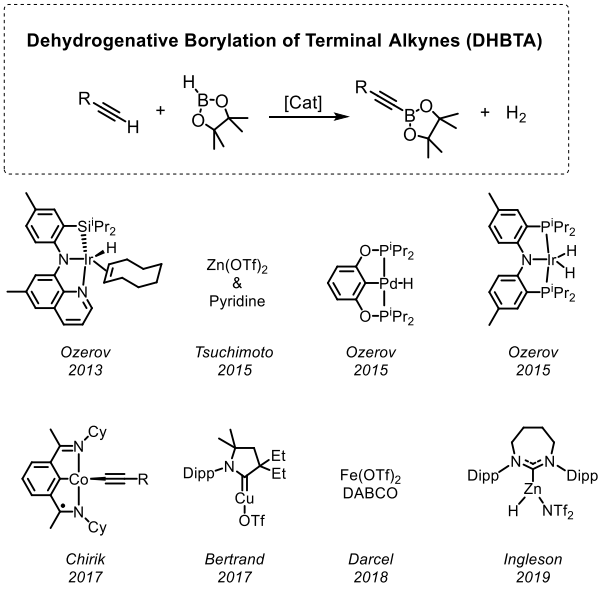

Scheme III-1. Dehydrogenative borylation of terminal alkynes defined, and the various DHBTA precatalysts from the literature

Our group has been interested in the dehydrogenative borylation of terminal alkynes (DHBTA, Scheme III-1). The products of DHBTA are alkynylboronates, which

can be used in a variety of synthetic transformations.[111] We originally reported that an Ir catalyst supported by a SiNN-type pincer ligand was highly chemoselective and gave rise only to DHBTA products with about 100 TON with a variety of alkynes, but largely excluding those with propargyl-heteroatom connections.[46] We later explored a variety of other pincers as supporting ligands for Ir in DHBTA and discovered that the diarylamido-based PNP ligands perform very well in that role.[47] Several different PNP ligands have been studied.[47] It was shown that these are highly longeval catalysts, capable of thousands of TON with a variety of alkynes that now included propargyl-substituted ones. Other groups reported DHBTA catalysts based on Zn,[112,115] Cu,[113] and Fe,[114] and we reported a Pd-based DHBTA catalyst (Scheme III-1).[116] Chirik et al also reported a Co catalyst that produces alkynylboronates from terminal alkynes *en route* to 1,1-diborated alkene products.[141] These are interesting examples, especially in the sense of the remarkable diversity of the nature of possible DHBTA catalysts, but they do not rival the (PNP)Ir system[47] in terms of activity, longevity, or alkyne substrate scope.

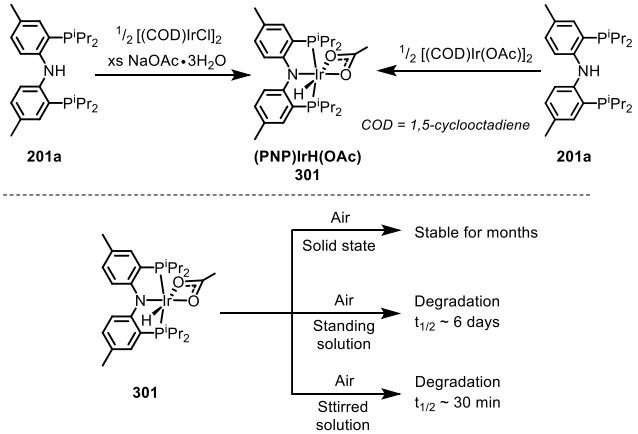

Scheme III-2. Top: Synthesis of (PNP)IrH(OAc) (**301**). Bottom: Ageing experiments.

The downside of the (PNP)Ir-catalyzed DHBTA is that all the pre-catalysts used thus far have been air-sensitive compounds and the DHBTA reactions were carried out under inert atmosphere and in dry, deoxygenated solvents.[47] However, we surmised that it should be possible to design a (PNP)Ir precatalyst that would possess some air stability while being capable of effective initiation of DHBTA. We also surmised that even if the Ir precursor is converted to some new Ir–O containing "decomposition" products upon interaction with air and/or moisture, they might be converted back to the active species in the DHBTA mixture by the action of the excess of HBpin present. In this, we were influenced by the existing work on the reactions of Ir pincer complexes with O_2.[142] Lastly, we wondered whether the presence of water might not be inhibitory to DHBTA but rather simply serve as an undesirable but catalytically benign sink for some of the HBpin reagent. The present work reports our findings that these conjectures had merit and it that an effective, air- and moisture-tolerant DHBTA catalyst is indeed possible.

3.2 Results and Discussion

3.2.1 Synthesis and Characterization of Iridium Precatalyst

We hypothesized that a saturated, 18-electron (PNP)Ir complex might possess useful stability towards air and moisture. We zeroed in on (PNP)IrH(OAc) (**301**) as a promising candidate that should be easily converted into DHBTA-relevant species upon reaction with excess HBpin in a catalytic DHBTA mixture. Combining **201a**, $[(COD)IrCl]_2$, and $NaOAc•3H_2O$ in a vial with fluorobenzene and stirring for 4 h resulted in a red-orange solution. Recrystallization from pentane afforded **301** cleanly as a dusty

orange powder in 84% yield (Scheme III-2). The same product was also obtained by treatment of a toluene solution of **201a** with a slight deficiency of $[(COD)Ir(OAc)]_n$. **301** displayed NMR spectroscopic features consistent with a C_s symmetric PNP complex. The ^1H NMR hydride chemical shift near -34 ppm is indicative of a hydride *trans*- to a weakly *trans*-influencing oxygen donor of a κ^2 acetate.

3.2.2 (PNP)IrH(OAc) Air Stability Testing

The resistance of **301** to aerobic decomposition was tested in the solid state and in solution. A series of open vials containing solid samples of **301** were kept in a cabinet in the laboratory under air. Periodically, a sample was removed and brought back into an argon-filled glovebox where the solids were dissolved in anhydrous, deoxygenated C_6D_6 for NMR spectroscopic analysis. Even after 110 days, no degradation of the iridium complex could be detected (Figure III-2). Exposing a standing benzene solution of **301** in an NMR tube to air for five days resulted in the decomposition of only ~45% of the complex (NMR evidence). However, stirring a solution of **301** open to air results in complete decomposition in 3 hours (Figure III-1). Thus, **301** is fully resistant to air as a solid on the scale of at least months but is degraded in solution at a rate concomitant with the degree of agitation.

3.2.3 DHBTA Performance of (PNP)Ir(H)(OAc)

The effectiveness of **301** as a DHBTA precatalyst was tested in the catalysis of the reaction of $4\text{-}MeC_6H_4CCH$ with HBpin. The rate at which **301** performs was found to be

indistinguishable from the rate of DHBTA with **202a** as the precatalyst (Scheme III-3). Moreover, observation of the hydride region of the ^{1}H NMR during a DHBTA reaction initiated by **301** revealed the presence of only two hydride resonances (δ -5.35 ppm and -12.40 ppm, 1:2 ratio) corresponding to **205a** (Scheme III-3, Figures III-5 & III-8). This indicates that under standard DHBTA conditions, the same resting state is reached starting from **202a** or **301**. **301** was further used as a precatalyst for the DHBTA of 3-dimethylamino-1-propyne, 3-trimethylsiloxy-1-propyne, and 1-decyne. Clean borylation of 3-dimethylamino-1-propyne and 1-decyne were achieved. The apparent rates of these were very similar to those catalyzed by **202a**. In borylating 3-trimethylsiloxy-1-propyne and *p*-$MeC_6H_4C{\equiv}CH$, the ratio of the DHBTA product to hydrogenated side product was very similar to the ratio observed with **202a** as a precatalyst.[47]

Interestingly, a solution of fully aerobically degraded **301** was also capable of performing DHBTA under standard conditions (Figures III-4 & III-5). This implies that the mixture of oxygenated iridium species can be revived by HBpin and reenter the catalytic cycle. In a separate experiment meant to push the limits of catalytic turnover, 200 picomoles of **301** was added to a 200 μmol sample of 3-dimethylamino-1-propyne and HBpin. After ca. 3 months at 80 °C, >100,000 turnovers were recorded in an ongoing reaction (Figure III-3)!

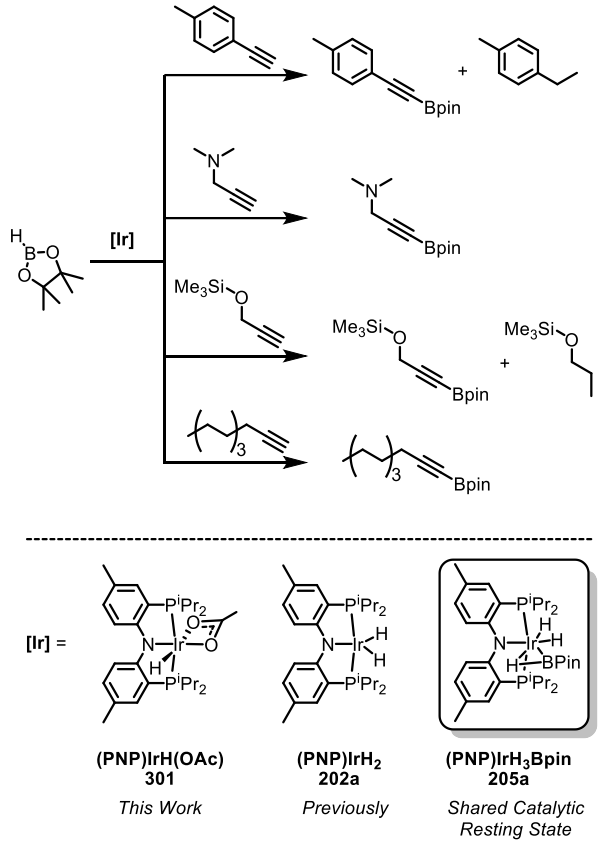

Scheme III-3. Top: Use of **301** in DHBTA. Bottom: The resting state observed in the reactions with *p*-MeC_6H_4CCH and Me_2NCH_2CCH.

Table III-1. Performance of **301**[a] with selected substrates

Entry	Alkyne	Time	% Conv.	%Products
1	4-MeC_6H_4CCH	10 min	46	41/3[b]
2		30 min	61	56/5
3		20 h	100	92/8
4	Me_2NCH_2CCH	10 min	24	24
5		50 min	57	57
6		20 h	100	100
7	Me_3SiOCH_2CCH	10 min	43	38/5[c]
8		55 min	72	64/8
9		19 h	100	86/14
10	*n*-$C_8H_{17}CCH$	10 min	14	14
11		60 min	30	30
12		19 h	80	80
13		72 h	100	100

[a]0.29 µmol (0.84 mol%) catalyst loading. [b]DHBTA product/hydrogenated alkyne (4-ethyltoluene). [c]DHBTA product/hydrogenated alkyne (trimethylsiloxypropane).

To test the sensitivity of DHBTA to water, two DHBTA reactions were conducted under dry argon. Each was carried out with one equivalent of water per alkyne, but the first contained two equivalents of HBpin and the second contained four (also vs alkyne). The first reaction resulted in the consumption of only half of the alkyne yet all the HBpin had been consumed. The second afforded complete conversion of the alkyne to 4-$MeC_6H_4C{\equiv}CBpin$ and 4-ethyltoluene (Figures III-6 & III-7). These results strongly suggest that a reaction with water consumes some of the HBpin reagent to make $(Bpin)_2O$ but is not otherwise detrimental to the DHBTA catalysis.[143] We further determined that 4-$MeC_6H_4C{\equiv}CBpin$ is reasonably stable towards aerobic degradation as after 22 h of exposure to air both as a solid and in a standing solution, less than 10% of the product had degraded as observed by ^1H NMR spectroscopy.

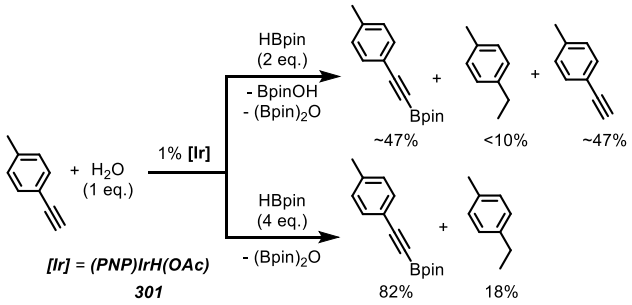

Scheme III-4. DHBTA in the presence of 1 eq. H_2O with a varying amount of HBpin

Next, we performed a preparative scale DHBTA experiment in toluene solvent (HPLC grade) that had not been dried after purchase. The toluene solution of HBpin and 4-ethynyltoluene was sparged with nitrogen prior to the addition of **301** and nitrogen continued to be bubbled through during the reaction. After 90 min, the volatiles were

removed and the flask was taken into an Ar-filled glovebox. ^{1}H NMR spectroscopic analysis revealed the presence of $(Bpin)_2O$ in addition to the desired 4-Me-$C_6H_4C{\equiv}CBpin$. Recrystallization from pentane yielded 4-$MeC_6H_4C{\equiv}CBpin$ of >97% purity in a 84% yield. This experiment confirmed that the presence of some water is not fatal to DHBTA and that dinitrogen is not detrimental to the reaction.[144,145]

To evaluate whether an inert atmosphere is at all necessary for DHBTA, we carried out an experiment that was fully constituted in air. A vial was loaded with HBpin, 4-$MeC_6H_4C{\equiv}CH$, and 0.75 mol% **301** in C_6D_6 (which was used as received), and then sealed. It was periodically agitated by hand and vented to relieve excess pressure over the course of 90 min. After 90 min, the reaction was analyzed by NMR spectrometry, and complete conversion of 4-$MeC_6H_4C{\equiv}CH$ to 4-$MeC_6H_4C{\equiv}CBpin$ and 4-ethyltoluene in 93:7 ratio was noted (Figure III-8).

3.3 Conclusion

In summary, it has been demonstrated that PNP-supported Ir catalysis of DHBTA is generally tolerant of the presence of water and air in the reaction mixture, provided a sufficient excess of HBpin is present to consume H_2O and O_2 stoichiometrically. The catalysis is also compatible with dinitrogen. **301** is an effective and convenient DHBTA precatalyst that is stable to air in the solid state for months and in solution for up to hours or days, depending on the degree of mixing. Moreover, its degradation under air appears to be reversible by action of the excess of HBpin in the catalytic mixture.

3.4 Experimental

3.4.1 General Considerations

Unless otherwise specified, all manipulations were performed either inside an argon-filled glove box, or by using Schlenk techniques. Pentane and THF were dried using a PureSolv MD-5 Solvent Purification System and were stored over 4Å molecular sieves in an argon-filled glove box. C_6D_6 was dried over NaK, benzophenone, and 18-crown-6 then stored in an argon-filled glove box over 4Å molecular sieves prior to use. Fluorobenzene was dried by refluxing over CaH_2 and stored in an argon-filled glovebox over 4Å molecular sieves prior to use. 4-$MeC_6H_4C{\equiv}CH$, $Me_3SiOCH_2C{\equiv}CH$, and $Me_2NCH_2C{\equiv}CH$ were vacuum transferred and stored in the freezer inside of an argon-filled glovebox. **201a**[21] and iridium precursors $[(COD)Ir(OAc)]_n$[146] and $[(COD)IrCl]_2$[147] were synthesized according to literature precedent. All other chemicals were used as received from commercial vendors. Argon was used from standard gas cylinders with 99.998% purity. Nitrogen gas was supplied from a boiloff cistern. All NMR spectra were acquired on a Bruker 400 spectrometer (^{1}H NMR, 400.09 MHz; ^{13}C NMR, 100.60 MHz; ^{31}P NMR, 161.96 MHz), and Varian Inova 500 (^{1}H NMR, 499.703 MHz; ^{13}C NMR, 125.697 MHz; ^{31}P NMR, 202.265 MHz) in denoted solvents. All chemical shifts are reported in δ (ppm). All ^{1}H and ^{13}C NMR spectra were referenced internally to the residual solvent signal (C_6D_6 at δ 7.16 for ^{1}H and δ 128.06 for ^{13}C NMR). ^{31}P NMR spectra were externally referenced to an 85% phosphoric acid solution δ 0. Elemental analyses were performed by CALI Labs, Inc. (Highland Park, NJ).

3.4.2 Synthesis of (PNP)IrH(OAc)

(PNP)IrH(OAc) (301). Method A. In an Ar-filled glove box, a 20 mL scintillation vial was charged with **201a** (97 mg, 0.23 mmol), $[(COD)IrCl]_2$ (75 mg, 0.22 mmol Ir), and $NaOAc•3H_2O$ (63 mg, 0.46 mmol). Fluorobenzene was added and the solution was allowed to stir for four hours. The volatiles were removed *in vacuo* and ca. 10 mL pentane was added to the residue. Tan-orange solids precipitated and the suspension was placed into a -35 °C freezer in the glove box overnight. The supernatant was decanted and the solids were dried *in vacuo* yielding the product as a dusty orange solid of >99% purity. Yield: 128 mg (83%) **Method B.** In an Ar-filed glove box, a 25 mL Schlenk flask was charged with $[(COD)Ir(OAc)]_n$ (363 mg, 1.0 mmol) and **201a** (468 mg, 1.1 mmol). Toluene was added and the resulting solution was stirred overnight. The volatiles were removed *in vacuo* while heating in a 30 °C oil bath. A 3:2 mixture of pentane to fluorobenzene was used to dissolve the residue and recrystallization in a -35 °C freezer overnight resulted in formation of the product as a dusty brown-orange powder. Yield: 0.276 g (40%). ^{1}H NMR (C_6D_6, 400 MHz): δ 7.74 (dt, J = 8.6 Hz, J = 2.2 Hz, 2H), 6.97 (br d, J = 2.2 Hz, 2H), 6.65 (dd, J = 8.7 Hz, J = 2.2 Hz 2H), 2.61 (m, 2H), 2.29 (m, 2H), 2.21 (s, 6H, tolyl methyls), 1.75 (s, 3H, OAc–CH_3), 1.35 (dvt, J = 7.6 Hz, J = 7.6 Hz, 6H, P–CH–(CH_3)$_2$), 1.23 (overlapping dvt, J = 7.6 Hz, J = 6.9 Hz, 12H, P–CH–(CH_3)$_2$), 1.11 (dvt, J = 7.3 Hz, J = 7.3 Hz, 6H, P–CH–(CH_3)$_2$), -33.16 (t, J = 13.1 Hz, 1H, Ir–H). ^{13}C{^{1}H} NMR (C_6D_6, 100 MHz): δ 185.51 (s, C=O), 163.24 (t, J = 9.3 Hz), 131.40 (s), 131.07 (s), 125.08 (t, J = 3.5 Hz,), 122.12 (t, J = 23.7 Hz), 116.53 (t, J = 4.8 Hz), 25.85 (t, J = 16.3 Hz, P–CH–(CH$_3$)$_2$), 25.56 (t, J = 13.4 Hz, P–CH–(CH$_3$)$_2$), 23.89 (s, OAc–CH$_3$), 20.47 (s,

backbone tolyl methyls), 18.91 (s, P–CH–(CH_3)$_2$), 18.47 (s, P–CH–(CH_3)$_2$), 18.23 (s, P–CH–(CH_3)$_2$), 17.61 (s, P–CH–(CH_3)$_2$). $^{31}P\{^1H\}$ NMR (C_6D_6, 202 MHz): δ 35.6. Elem. Anal. Calcd. for $C_{28}H_{44}IrNO_2P_2$: C, 49.40; H, 6.51. Found: C, 49.10; H, 6.17.

3.4.3 Testing Air Stability of (PNP)Ir(H)(OAc) and Borylated 4-ethynyltoluene

Testing solution-state stability of 301 against aerobic oxidation. A 700 µL benzene solution of **301** (80 mg, 0.12 mmol) in a J. Young tube under argon was exposed to air for 15 minutes, after which a $^{31}P\{^1H\}$ NMR spectrum was acquired. This tube was then reopened and sat upright in the fume hood for five days, at which point a second $^{31}P\{^1H\}$ NMR spectrum was acquired. After five days, approximately 54% of the phosphorus compounds existed as **301** giving an approximate $T_{1/2}$ in standing solution for aerobic oxidation of **301** of six days.

Testing solution-state stability of 301 against aerobic oxidation with stirring. A 2 mL benzene solution of **301** (40.2 mg, 0.059 mmol) with a magnetic stir bar in an 8 mL vial under argon was exposed to air with rapid stirring. Aliquots were removed at various timepoints and analyzed by $^{31}P\{^1H\}$ NMR spectroscopy. **301** was completely degraded after 3 hours of stirring open to air.

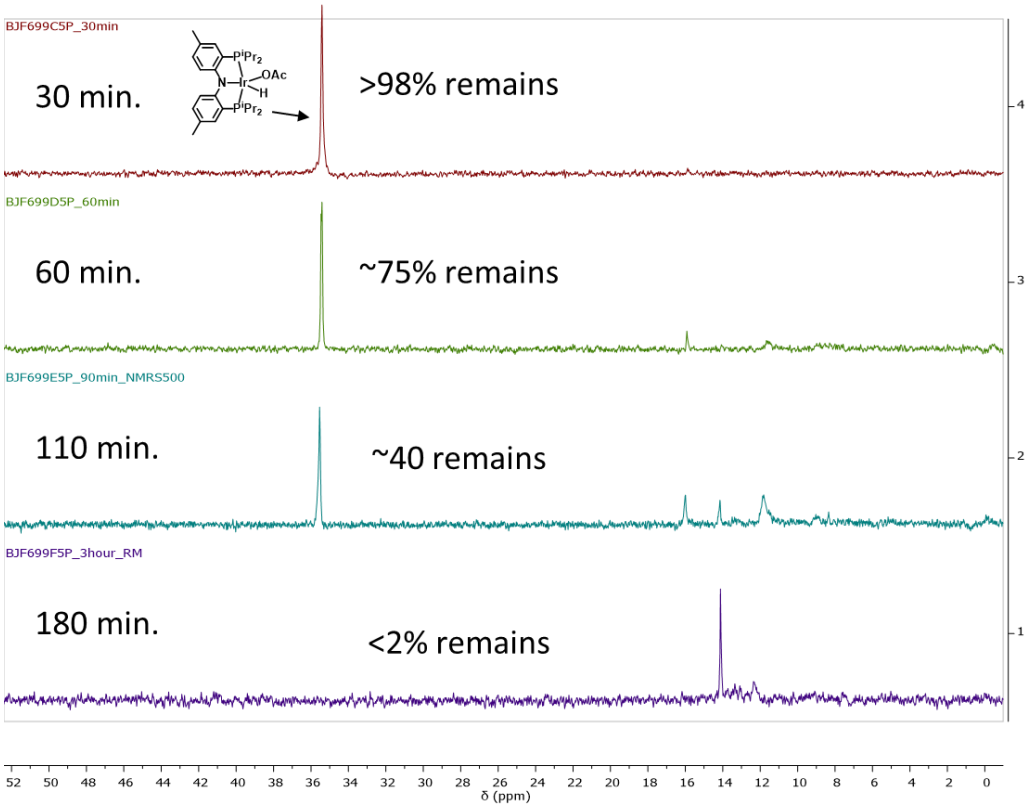

Figure III-1. $^{31}P\{^{1}H\}$ NMR (202 MHz, C_6D_6) spectra of **301** after stirring open to air for 30, 60, 110, and 180 minutes.

Testing solid-state stability of 301 against aerobic oxidation. A 90 mg sample of **301** was divided into six 2 mL vials and sat on a shelf in the laboratory open to air. A vial was removed from the shelf periodically (6 days, 12 days, 18 days, 24 days, & 110 days) and brought into the glovebox where the solids were dissolved in anhydrous C_6D_6 for NMR spectroscopic analysis. The proton and phosphorus spectra for the samples of **301** that had been exposed to air appear unchanged versus the spectra obtained from a freshly recrystallized sample of **301**.

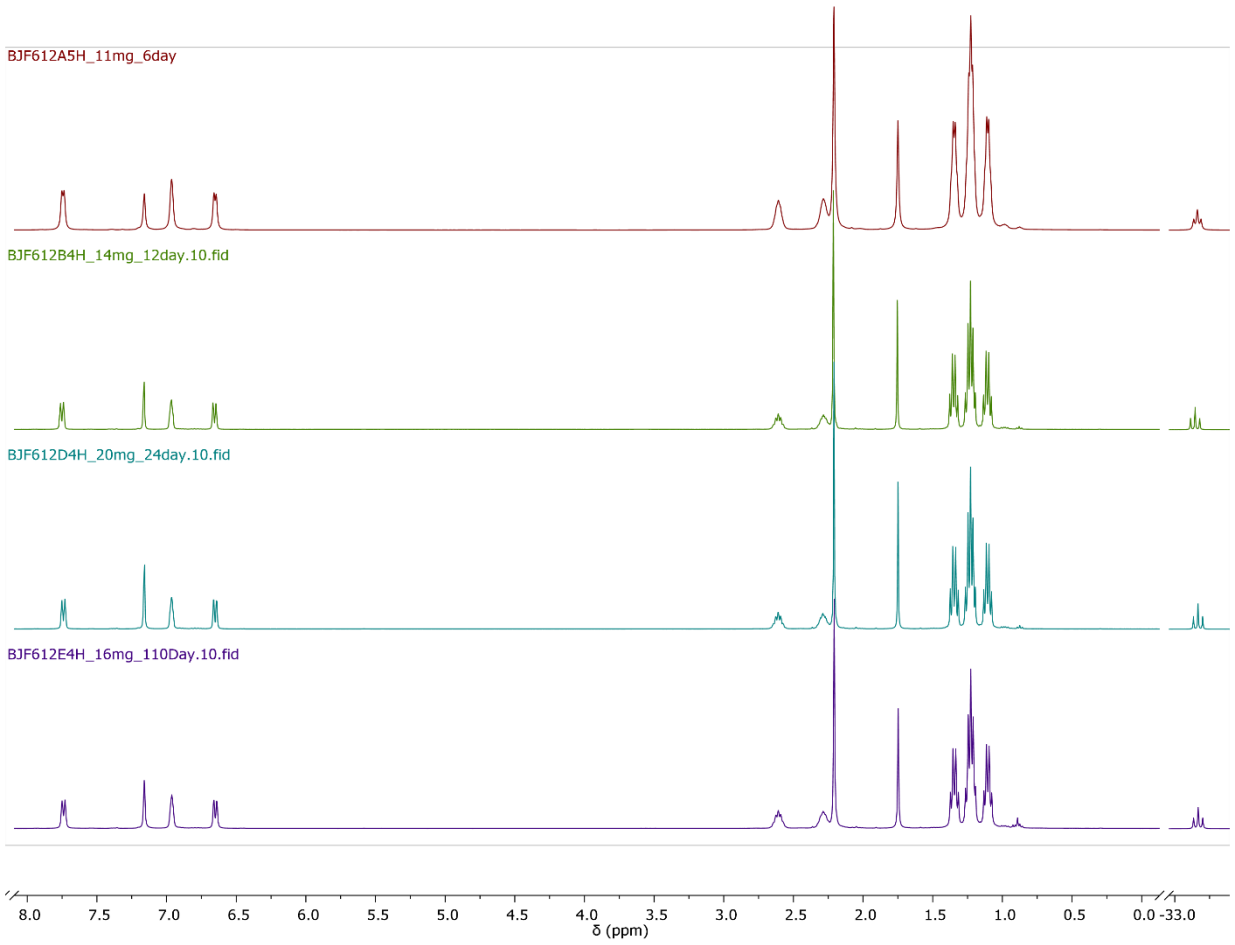

Figure III-2. ^{1}H NMR (400 MHz, C_6D_6) of samples of **301** open to air (as solids) for varying periods of time. From top to bottom: 6 days (500 MHz ^{1}H spectrum), 12 days, 24 days, and 110 days (400 MHz ^{1}H NMR spectra each) open to air in the solid state.

Testing solution-state stability of 4-MeC_6H_4C≡CBpin against aerobic oxidation. A solution of 4-MeC_6H_4C≡CBpin in a J. Young tube was brought out of the glovebox and a ^{1}H and ^{11}B{^{1}H} NMR were acquired. The tube was opened to air for two minutes. Another set of ^{1}H and ^{11}B{^{1}H} NMR spectra were acquired. Minimal degradation of the alkynylboronate was observed. The tube was left uncapped in a fume hood overnight

in an upright position. The resulting solution was found to be of >97% purity 4-$MeC_6H_4C{\equiv}CBpin$ by ^1H and $^{11}B\{^1H\}$ NMR spectroscopy.

Testing solid-state stability of 4-$MeC_6H_4C{\equiv}CBpin$ against aerobic oxidation. 4-$MeC_6H_4C{\equiv}CBpin$ (15 mg) was weighed into a 2 mL vial and sat on a shelf in the laboratory open to air overnight. The sample was dissolved in C_6D_6 (not dried or deoxygenated) for NMR spectroscopic analysis. The resulting solution was found to be of >94% purity 4-$MeC_6H_4C{\equiv}CBpin$ by ^1H and $^{11}B\{^1H\}$ NMR spectroscopy.

3.4.4 DHBTA Experiments Using (PNP)IrH(OAc) as a Precatalyst

General procedure for alkyne substrate scope for DHBTA. In an Ar-filled glovebox, a J. Young tube was charged with HBpin (430 µL of 0.16 M stock, 70 µmol), alkyne (35 µL of 1 M stock solution, 35 µmol), and **301** (35 µL of 0.0084 M stock solution, 0.29 µmol). The tube was then sealed an NMR acquisition began. See Table III-1 for timepoints and percent conversions.

NMR Data for $Me_2NCH_2C{\equiv}C$-Bpin. ^1H NMR (C_6D_6, 500 MHz): δ 3.07 (s, 2H), 2.11 (s, 6H), 0.99 (s, 12H). $^{13}C\{^1H\}$ NMR (C_6D_6, 125 MHz): δ 99.0 (br, $NCH_2\mathit{C}$), 83.9 (C_{quart}, Bpin), 48.6 (N-($\mathit{C}H_3)_2$), 44.0 ($\mathit{C}H_2$), 24.7 (CH_3, Bpin). $^{11}B\{^1H\}$ NMR (C_6D_6, 128 MHz) δ 23.9. ESI^+ (Low Resolution, Unit Mass): Calcd. for $C_{11}H_{20}BNO_2$ $(M+H)^+$: 210.16. Found: 210.04.

Borylated 3-trimethylsiloxy-1-propyne[47] and borylated 4-ethynyltoluene[46] were identified according to literature precedent.

Testing of the catalytic longevity of 301. In an Ar-filled glovebox, a J. Young tube was charged with HBpin (60 µL, 0.41 mmol), $Me_2NCH_2C{\equiv}CH$ (200 µL of a 1 M stock solution, 0.2 mmol) and **301** (190 µL of a 1.1 x 10^{-6} M stock solution, 2.0 x 10^{-7} mmol). This tube was placed in an 80 °C oil bath. The progress of this reaction was monitored by ^{1}H and $^{11}B\{^{1}H\}$ NMR spectroscopy. Conversion up to 13.8% is shown, corresponding to 138,000 turnovers.

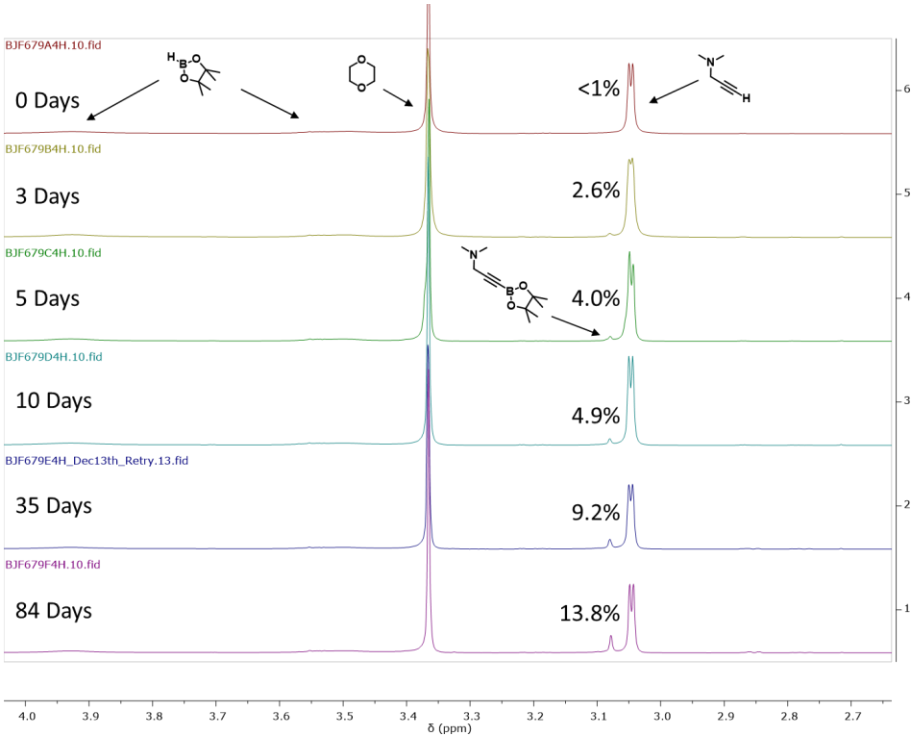

Figure III-3. ^{1}H NMR (400 MHz, C_6D_6) spectrum of a DHBTA reaction using 10^{-6} eq. **301** to borylate Me_2NCH_2CCH with 2 eq. HBpin.

DHBTA of $Me_2NCH_2C{\equiv}CH$ with completely air-degraded (PNP)IrH(OAc). A benzene solution of **301** (14.3 mg, 0.021 mmol) was stirred open to air in a fume hood for one week resulting in the total decomposition of **301** and evaporation of the volatiles. The black residue in the vial was brought back into an Ar-filled glovebox and reconstituted in 2 mL C_6D_6 yielding a stock solution of ca. 0.01 M Ir. A portion of this stock solution (35 µL, 0.35 µmol) was added to a J. Young tube along with $Me_2NCH_2C{\equiv}CH$ (35 µL of a 1 M stock solution, 35 µmol) and HBpin (430 µL of a 0.16 M stock solution, 69 µmol). ^1H NMR observation revealed the formation of $Me_2NCH_2C{\equiv}CBpin$ as well as H_2 indicating that the iridium complex is DHBTA active. Indeed, **205a** was observed in the catalytic mixture.

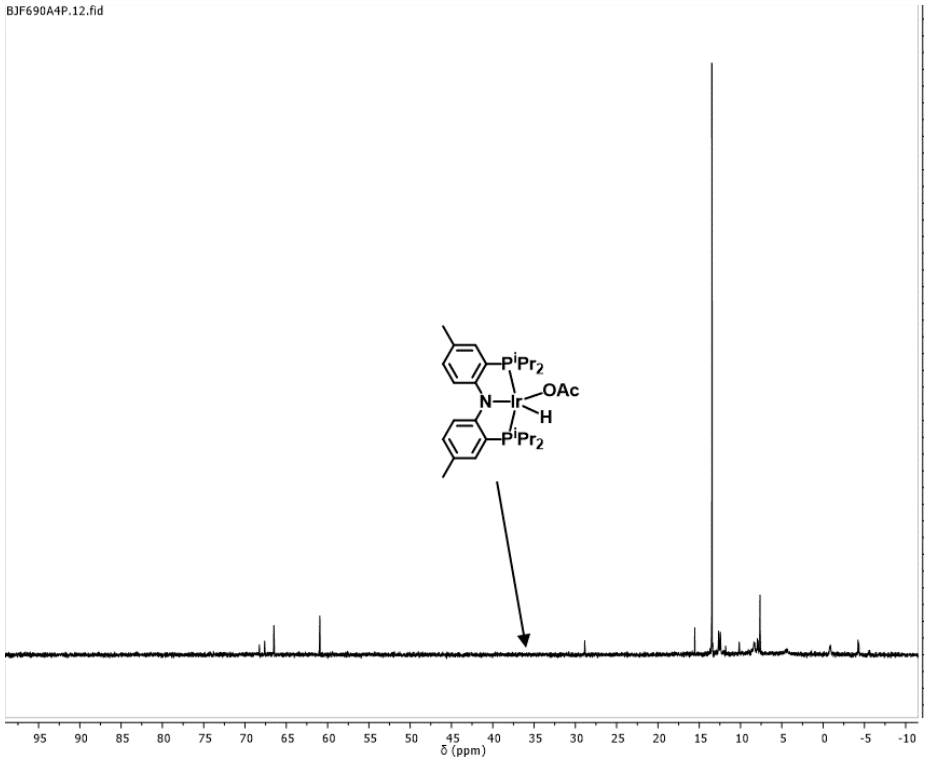

Figure III-4. $^{31}P\{^1H\}$ NMR (162 MHz, C_6D_6) spectrum of **301** after complete aerobic degradation. Arrow indicates where **301** would be observed if any remained.

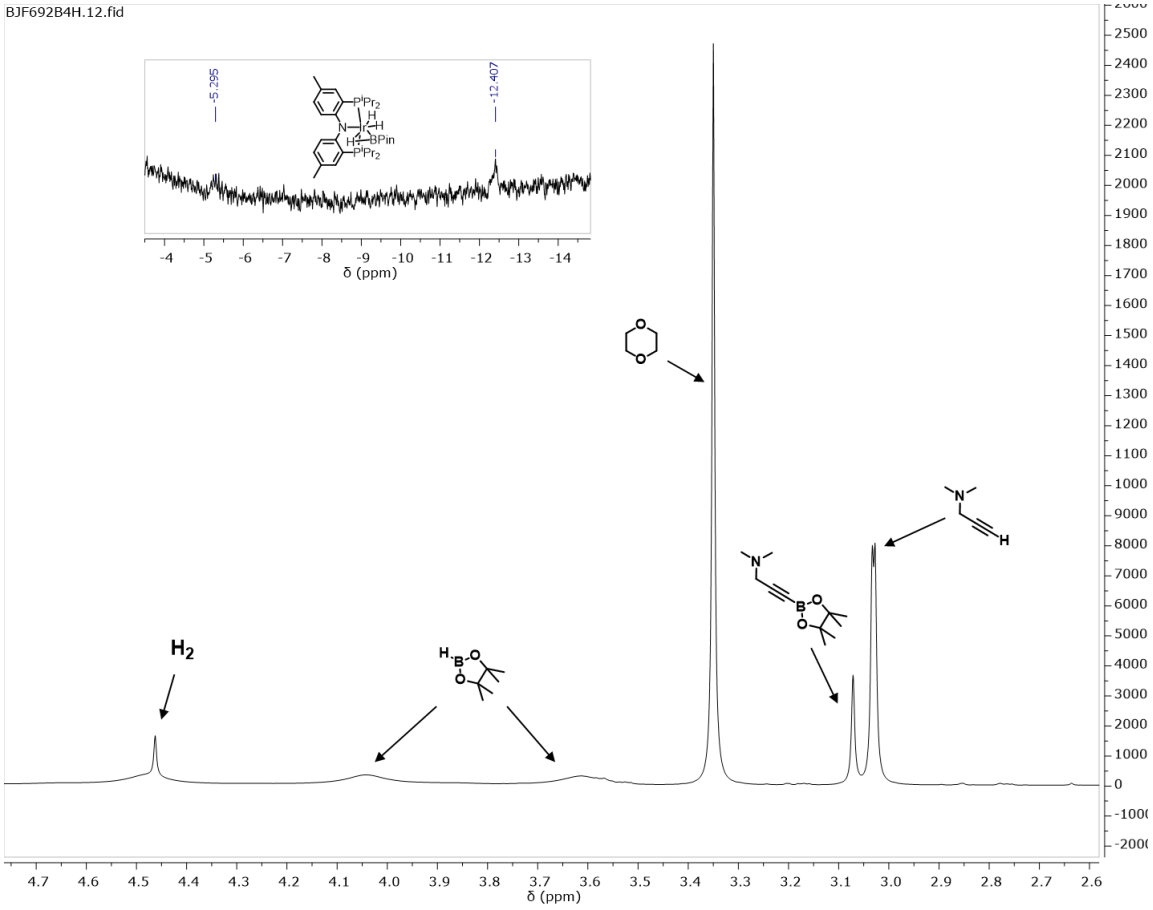

Figure III-5. ^{1}H NMR (400 MHz, C_6D_6) spectrum at 90 minute timepoint of Me_2NCH_2CCH DHBTA reaction catalyzed by aerobically degraded **301**. Insert. Hydride region showing two resonances corresponding to **205a**[47]

DHBTA of 4-MeC$_6$H$_4$C≡CH in the presence of 1 eq. water and 2 eq. HBpin.

In an Ar-filled glovebox, a J. Young tube was charged with C_6D_6 (320 µL), HBpin (30 µL, 210 µmol), **301** (100 µL of 0.01 M stock solution, 1.0 µmol) and 4-MeC$_6$H$_4$C≡CH (100 µL of 1 M stock solution, 100 µmol), and H_2O (50 µL of 2.2 M stock solution in THF, 110 µmol). Upon addition of the solution of H_2O, the solution began vigorously bubbling. The tube was not closed until the vigorous bubbling subsided. After sealing the

tube, a ^{1}H NMR spectrum was acquired. After 20 minutes, another ^{1}H NMR spectrum was acquired and no change was observed. All the HBpin had been consumed and ~50% of the alkyne was converted into 4-MeC_6H_4C≡CBpin. The tube was returned to the glove box and addition of HBpin (45 µL, 315 µmol) to the tube resulted in more vigorous bubbling.

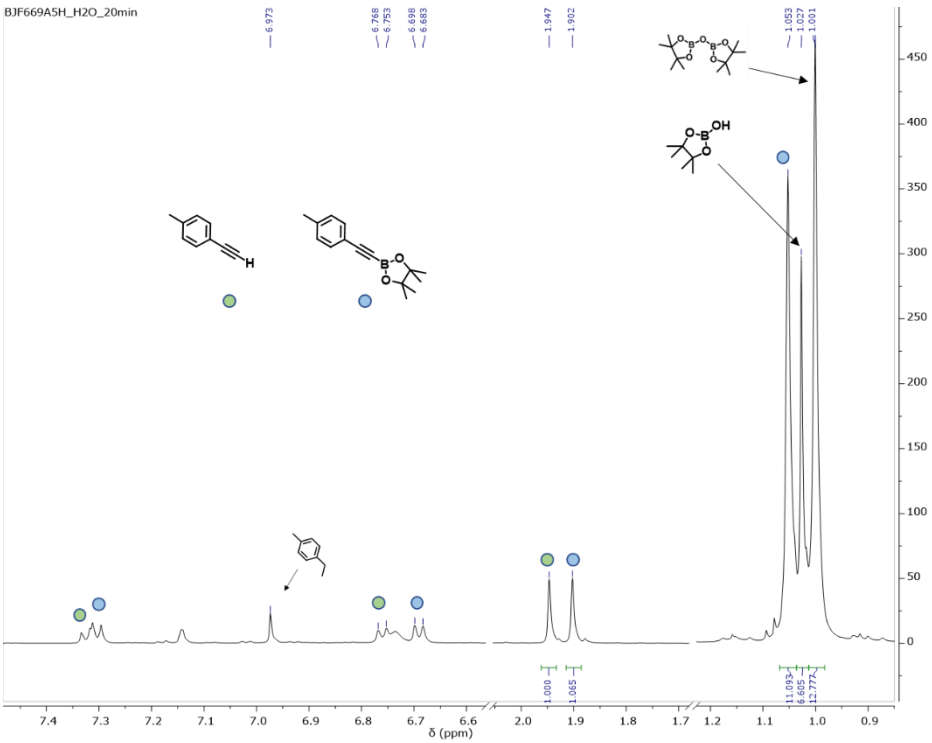

Figure III-6. ^{1}H NMR (500 MHz, C_6D_6) spectrum of a DHBTA reaction using **301** to borylate 4-MeC_6H_4CCH with 1 eq. H_2O and 2 eq. HBpin. Timepoint shown is 20 min after the vigorous bubbling ceased. A small amount of 4-ethyltoluene is observed as a singlet at 6.97 ppm.[47]

DHBTA of 4-MeC_6H_4C≡CH in the presence of 1 eq. water and 4.1 eq. HBpin.

In an Ar-filled glovebox, a J. Young tube was charged with C_6D_6 (290 µL), HBpin (60 µL, 0.41 mmol), **(PNP)IrH(OAc)** (100 µL of 0.084 M stock solution, 0.84 µmol), 4-MeC_6H_4C≡CH (100 µL of 1 M stock solution, 0.10 mmol), and H_2O (50 µL of 2.2 M

stock solution in THF, 0.11 mmol). Upon addition of H_2O, the solution began vigorously bubbling. The tube was not closed until the vigorous bubbling had subsided. After sealing the tube, a ^{1}H NMR spectrum was acquired. The following day, another ^{1}H NMR spectrum was acquired and no change was observed. All the HBpin had been consumed and the major organic products were 4-MeC_6H_4C≡CBpin and 4-ethyltoluene in an 82:18 ratio.

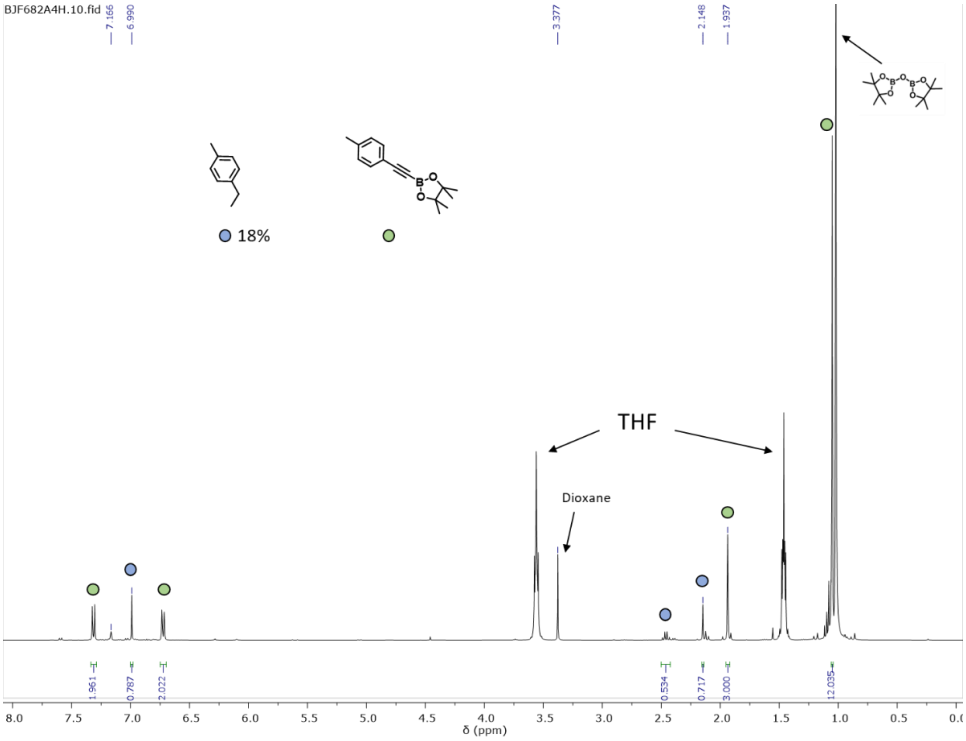

Figure III-7. ^{1}H NMR (400 MHz, C_6D_6) spectrum of a DHBTA reaction using **301** to borylate 4-MeC_6H_4CCH with 1 eq. H_2O and 4.1 eq. HBpin. Timepoint shown is 20 min after the vigorous bubbling ceased. A small amount of 4-ethyltoluene is observed as a singlet at 6.97 ppm.[47]

Preparative scale DHBTA of 4-MeC_6H_4C≡CH under nitrogen in as-received toluene solvent. In a fume hood, a 25 mL, round bottom flask was charged with a magnetic stir bar and 20 mL of HPLC grade toluene that had not been dried prior to use. A needle from a nitrogen line was inserted into the flask and the toluene was sparged for

40 min. 4-MeC_6H_4C≡CH (not dried, 500 µL, 3.9 mmol) and pinacolborane (from an Ar-filled glovebox; 1.25 mL, 8.6 mmol) were added to the flask and the mixture was sparged for an additional 20 minutes. **301** was added as a C_6D_6 solution (500 µL of 0.061 M stock solution, 0.030 mmol) and the flask was stirred at ambient temperature under continual sparging for 90 minutes. The volatiles were then removed *in vacuo* providing a chalky residue. ^{1}H, ^{13}C{^{1}H}, and ^{11}B{^{1}H} NMR spectroscopy revealed the presence of $Bpin_2O$ (14%). Recrystallization from anhydrous pentane in the glove box provided 4-Me-C_6H_4-C≡C-Bpin of >98% purity (803 mg, 84%).

Executing the DHBTA of 4-MeC_6H_4C≡CH under air in as-received C_6D_6 solvent. In a fume hood, a 2 mL vial was charged with HBpin (from an Ar-filled glovebox, 75 µL, 0.52 mmol), 4-MeC_6H_4C≡CH (35 µL, 0.28 mmol), **301** (1.3 mg, 1.9 µmol), and 600 µL C_6D_6. The loading was done in air, and C_6D_6 and 4-MeC_6H_4C≡CH were used as received, without any purification. The vial was capped and swirled by hand. The solution bubbled and the cap was removed periodically to relieve any built-up pressure. After 90 minutes, the solution was transferred to a J. Young tube for NMR analysis. ^{1}H NMR spectroscopic analysis revealed the complete conversion of 4-MeC_6H_4C≡CH to 4-MeC_6H_4C≡CBpin and 7% 4-ethyltoluene.[47]

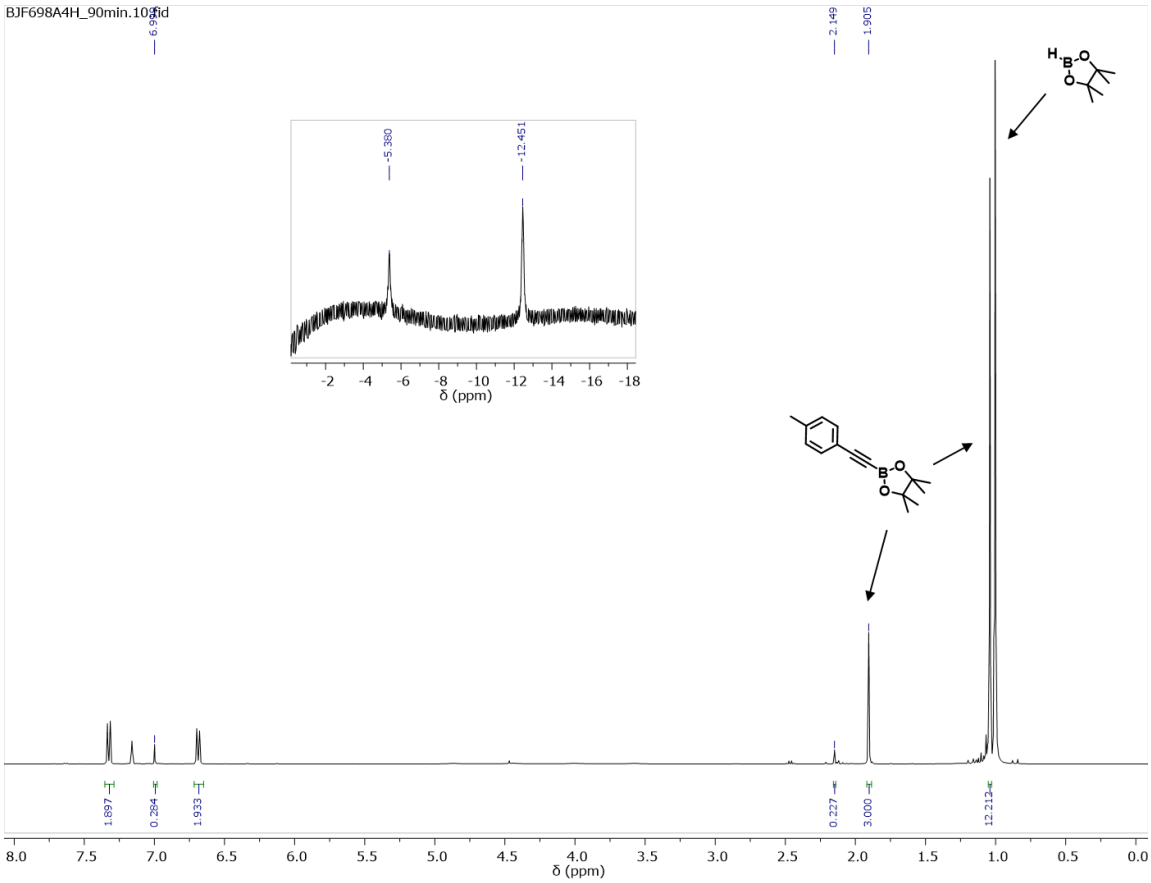

Figure III-8. ^{1}H NMR (400 MHz, C_6D_6) spectrum at 90 minute timepoint of 4-MeC_6H_4CCH DHBTA reaction catalyzed by **301** under air. Insert: Hydride region showing two resonances corresponding to **205a**.[47]

CHAPTER IV

SYNTHESIS AND REACTIVITY OF PINCER-TYPE COBALT SILYL AND SILYLENE COMPLEXES*

4.1 Introduction

Metal silylenes ($M{=}SiR_2$) have been shown to exhibit a variety of modes of reactivity, often quite distinct from their metal carbene congeners.[148] Though silylenes have been implicated as important intermediates in hydrosilylation catalysis,[149] their utilization in general has been limited by their high reactivity. Base-free silylene complexes featuring first-row transition metals are particularly unusual. Examples have been reported for titanium,[150] chromium,[151] manganese,[152] iron,[153] and nickel.[154] However, cobalt represents a notable absence from this series.

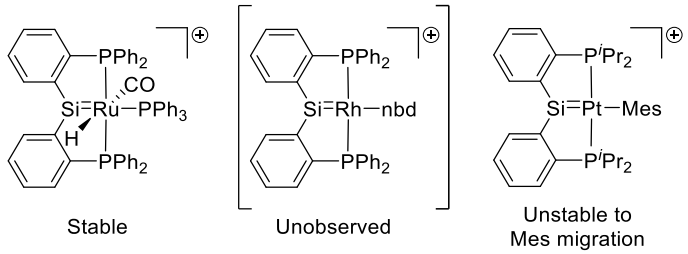

Figure IV-1. Previously reported silylene complexes supported by pincer-type [P_2Si] ligands.

* Reprinted in part with permission from "Synthesis and Reactivity of Pincer-Type Cobalt Silyl and Silylene Complexes" by Zhang, J.; Foley, B. J.; Bhuvanesh, N.; Zhou, J.; Janzen, D. E.; Whited, M. T.; Ozerov, O. V. *Organometallics* **2018**, *37*, 3956-3962. Copyright 2018 American Chemical Society.

Our research groups have recently developed the coordination chemistry of a pincer-type [P_2Si] ligand with an eye toward utilizing the chelate to approach silylene complexes for application in new stoichiometric and catalytic reactions (Figure IV-1).[24,155] The chemistry of [P_2Si] complexes with a central silyl donor was originally explored by the Turculet, Iwasawa, and Milstein groups.[156] In one recent study, we showed that a cationic ruthenium(II) silylene supported by a [P_2Si] ligand was quite stable, yet reactivity prospects were limited by the coordinatively saturated metal center.[155c] When related rhodium species were examined, the intermediacy of rhodium silylene cations was implicated in the formation of triflatosilyl rhodium diene complexes.[155a] In another study, we found that unsaturated cationic (P_2Si=)Pt silylene complexes are accessible yet prone to rearrangement via X-type ligand migration to the highly Lewis-acidic silylene unit, affording a T-shaped mesitylsilyl platinum cation from the complex shown in Figure IV-1.[24] In an effort to attenuate such reactivity and maximize prospects for metal/silylene cooperativity, we have shifted our attention to group 9 metals. We envisioned that silylene complexes of monovalent group 9 metal centers may be more robust due to stronger M→Si π-backbonding and because the complex is designed not to carry X-type ligands on the metal. Here we report coordination of [P_2Si] to cobalt, allowing synthesis, characterization, and preliminary reactivity studies of the first base-free cobalt silylene complex.

4.2 Results and Discussion

4.2.1 Cobalt Silylene Synthesis

Reaction of the ($^{i\text{Pr}}$P$_2$Si)H$_2$ proligand[24] with Co$_2$(CO)$_8$ afforded the diamagnetic hydrosilyl complex ($^{i\text{Pr}}$P$_2$Si$^{\text{H}}$)Co(CO)$_2$ (**401**) with evolution of CO and H$_2$ (Scheme IV-1).[157] Complex **401** exhibits several spectroscopic features consistent with its formulation shown in Scheme IV-1, including prominent infrared bands for the Si–H (ν_{SiH} = 2048 cm^{-1}) and C≡O (ν_{CO} = 1958, 1908 cm^{-1}) stretching modes, with the Si–H stretch observed at similar energy to a related hydrosilyl ruthenium complex.[155c] The ^{1}H NMR (δ 6.15 ppm (s, $^1J_{SiH}$ = 182 Hz)) and ^{29}Si NMR (δ 54.8 ppm) resonances for the Si–H moiety in **1** are consistent with the expectations for a hydrosilyl complex of this type.[158] Complex **401** has been further characterized by X-ray crystallography, revealing a trigonal-bipyramidal geometry (τ parameter[159] of 0.84) with the silyl and one of the CO ligands in the axial positions (Figure IV-2).

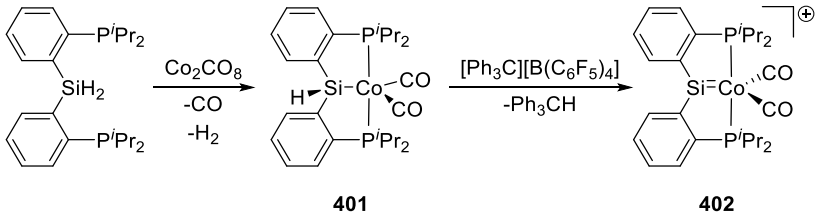

Scheme IV-1. Preparation of ($^{i\text{Pr}}$P$_2$Si)Co hydrosilyl (**401**) and silylene complex (**402**)

Hydride abstraction from **401** with trityl tetrakis(pentafluorophenyl)borate (Ph$_3$C•BAr$^{\text{F}}{}_{20}$) was accomplished in high yield in fluorobenzene, affording the first example of a base-free cobalt silylene complex (**402**, [($^{i\text{Pr}}$P$_2$Si=)Co(CO)$_2$][BAr$^{\text{F}}{}_{20}$])

(Scheme IV-1). The clearest spectroscopic evidence for the formation of **402** comes from its ^{29}Si chemical shift (δ 285 ppm), a significant downfield shift from the precursor consistent with what has been observed for related base-free metal silylenes (δ 200–370 ppm).[148b] The weaker donating nature of the formally neutral, π-accepting silylene ligand in **402** vs the anionic silyl in **401** leads to a ca. 70 cm^{-1} blue-shift in the C≡O stretching frequencies (ν_{CO} = 2028, 1983 cm^{-1}) relative to **401**.

The molecular structure of **402** was determined by X-ray crystallography (Figure IV-2), revealing a five-coordinate geometry about Co. Although the τ = 0.30 for this structure, it is nonetheless best analyzed as trigonal bipyramidal, with the axial phosphines deviating slightly from linearity (∠PCoP = 156°) because of the chelate constraint. The structure possesses a rigorous crystallographic C_s symmetry (in the $Cmc2_1$ space group), which is unusual for structures of pincer complexes based on the bis(*o*-phosphinoaryl)element motif. This observed solid-state symmetry is related to the presence of a trigonal-planar silicon center with coplanar aromatic rings. The coplanarity of these rings with the central element is rare, even for sp^2-hybridized, planar central atoms,[17f,160,161] and is presumably a consequence of the stabilization of the electron-deficient Si center via conjugation with the aromatic rings and the larger size of silicon versus C, N, and B. The possibility silicon conjugation with the aromatic rings in **402** is supported by a 0.05 Å shorter Si–C_{Ar} bond relative to **401**, though the sp^2 hybridization in **2** also likely plays some role in this shortening. Only rotation of isopropyl groups about the P–C bond appears to be needed to attain the time-averaged C_{2v} symmetry observed by NMR in solutions of **402**. The Co–Si bond length in **402** (2.121(2) Å) is among the shortest

reported, similar to those for amidinate-supported, base-stabilized CpCo(I) silylene complexes reported by Stalke and co-workers (2.114 Å)[162] and Driess and co-workers (2.125 Å and 2.120 Å)[163] yet longer than the Co–Si distance in a phosphine supported Co=Si=Co silicide reported by Tilley and co-workers.[164] Although no direct analogy is available for cobalt, the Si–Co bond shortening (ca. 7%) upon hydride abstraction from **401** is similar to what has been observed between Cp*Ru hydrosilyl and cationic silylene complexes.[165]

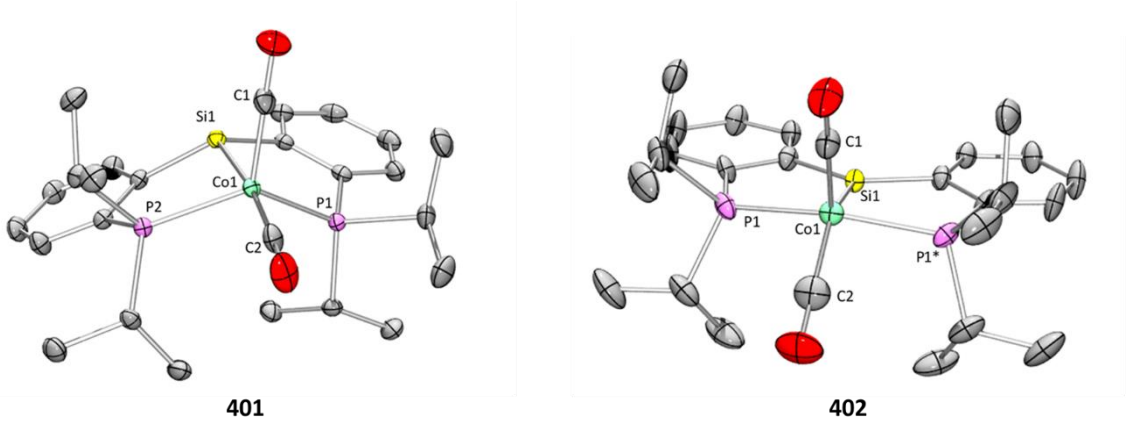

Figure IV-2. POV-Ray renditions of Ortep plots (50% probability ellipsoids) of hydrosilyl complex **401** and silylene complex **402** with thermal ellipsoids at the 50% probability level. Hydrogen atoms, the BArF 20 anion of 2, and cocrystallized toluene of 2 are omitted for clarity. Selected bond lengths (Å) and angles (deg) for **401**: Si−Co, 2.2671(7); Co−C1, 1.750(2); Co−C2, 1.760(2); Si−Co−C1, 85.20(7); P1−Co−P2, 128.20(3). For **402**: Si−Co, 2.121(2); Co−C1, 1.790(8); Co−C2, 1.770(8); Si−Co−C1, 115.1(3); P1−Co−P1*, 156.19(7).

4.2.2 Structural and Electronic Properties of the (PSiP)Co Series

To build on our understanding of silylene complex **402**, we prepared a series of $(P_2Si^X)Co(CO)_2^{n+}$ complexes, with X representing anionic or neutral Lewis bases. The

chlorosilyl complex ($^{iPr}P_2Si^{Cl}$)Co(CO)$_2$ (**403**) was synthesized by heating hydrosilyl complex **401** in chloroform at 80 °C for 20 h. The related triflatosilyl complex **404** could be prepared by hydride abstraction from **401** using trityl triflate. Finally, the cationic, pyridine-stabilized silylene complex **405** was synthesized by addition of pyridine to silylene **402** (Scheme IV-2). Complexes **403**–**405** were isolated as single crystals and analyzed by X-ray crystallography (Figure IV-4). The Si center in **403**–**405** is pyramidalized (Table IV-1) to a similar degree, as it is in **401**, and the Co–Si bond lengths are also similar in these four compounds, consistent with a single Co–Si bond.

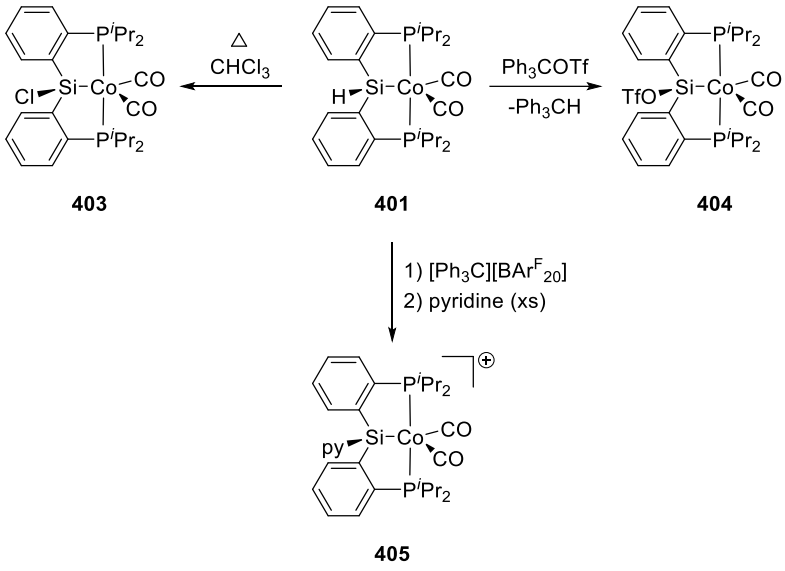

Scheme IV-2. Synthesis of complexes **403**-**405**

Complexes **401**–**405** compositionally differ by the nature of the donor attached to the silylene center (where **402** is donor-free). The relative influence of the nature of this donor is apparent from the comparison of the ν_{CO} values (Table IV-1). Introduction of stronger donors (triflate, pyridine, chloride, hydride) leads to the decrease in the CO

stretching frequencies over a range of ca. 70 cm^{-1}, consistent with strong Co→Si π-backbonding in **402** that is progressively attenuated with stronger donors on Si.

Table IV-1. Key structural and spectroscopic parameters for silyl and silylene complexes **401**-**405**

	401	**402**	**403**	**404**	**405**
∑∠Si[a]	333.6°	360.0°	334.9°	341.7°	340.4°
$d_{Co–Si}$ (Å) *[calcd]*	2.2671(7) *[2.276]*	2.121(2) *[2.114]*	2.2453(6) *[2.262]*	2.216(1)	2.223(1)
δ ^{29}Si *[calcd]*	54.8 *[74]*	284.6 *[341]*	93.7 *[120]*	108.8	114.0
ν_{CO} (cm^{-1})	1958 1908	2028 1983	1970 1921	1987 1938	1990 1939

[a] ∑∠Si = sum of bond angles around silicon, excluding H (**401**), Cl (**403**), OTf (**404**), or N_{pyr} (**405**).

Since **402** is the first complex of its type on cobalt and a rare example of a stable group 9 silylene, we endeavored to understand the nature of Co–Si bonding and the electronics at silicon using computational methods (see details in Section 4.4.1). The molecular structures calculated for **401**, **402** (with the counterion included), and **403** agreed reasonably well with the X-ray data. The calculated ^{29}Si NMR chemical shifts were somewhat higher than the experimental values (Table IV-1), but in a consistent fashion and confirming the strong downfield shift for **402**. It is common for silylene complexes obtained by abstraction of an α-X anion from a silyl precursor to be highly electrophilic at Si.[148b] In the extreme, these structures can be viewed as metal-substituted silylium cations. Examination of the calculated LUMO of **402** (Figure IV-3) shows that it is indeed centered primarily on Si, with delocalization into the aromatic rings and some contribution from Co. On the other hand, the Wiberg index[166] for the Co=Si bond in **402** was calculated

to be 0.98, notably higher than the 0.74 value obtained for the $[(P_2Si=)Pt–mesityl]^+$ complex.[24] Thus our hypothesis that a monovalent Co should be more capable of π-bonding with the Si center is borne out at least to a modest extent.

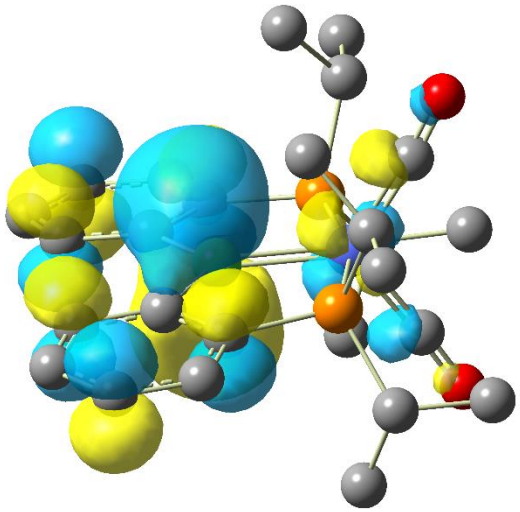

Figure IV-3. Depiction of the LUMO (isovalue 0.03) of **402**, calculated by M06/SDD/6-31G(d). Hydrogen atoms are omitted for clarity.

4.2.3 O–H Splitting at the Co=Si Bond

The theoretical and experimental studies presented above, combined with many studies on related metal silylene complexes, suggest that the silicon center in **402** should be very electrophilic. A side product was also frequently observed during the reactions **402**, which we attributed to reaction of the acidic silylene cation with trace water. Thus, we report here preliminary reactivity of **402** with ethanol and water in order to understand the interactions of silylene **402** with O–H bonds.

Exposure of **402** to ethanol results in a mixture of two hydride-containing products (^{31}P NMR: δ 96.9 ppm (major) and 99.0 ppm (minor); ^{1}H NMR δ −9.43 (t, $^3J_{PH}$ = 33.7 Hz,

major) and −12.38 (t, $^{3}J_{PH}$ = 38.5 Hz, minor)). Heating the mixture at 50 °C for 1 h leads to complete conversion to the previously minor isomer, which was identified by X-ray crystallography as an ethoxysilyl cobalt hydride, [($^{iPr}P_2Si^{OEt}$)CoH(CO)$_2$][BAr$^{F}_{20}$] (**406-anti**) with the ethoxy and hydride oriented *anti* to one another (dihedral angle of 178(2)°) (Figure IV-4). The silyl donor in **406-anti** is pyramidalized, in a manner similar to hydrosilyl complex **401**. The cobalt hydride, which was located in the difference map, bends significantly toward silicon (∠Si–Co–H = 72.3(15)°, d_{SiH} = 2.30(4) Å), consistent with the expected high Lewis acidity of the silyl donor and indicating a weak Si/Co–H interaction (Secondary Interaction between a Silicon and a Hydrogen Atom, SISHA).[167]

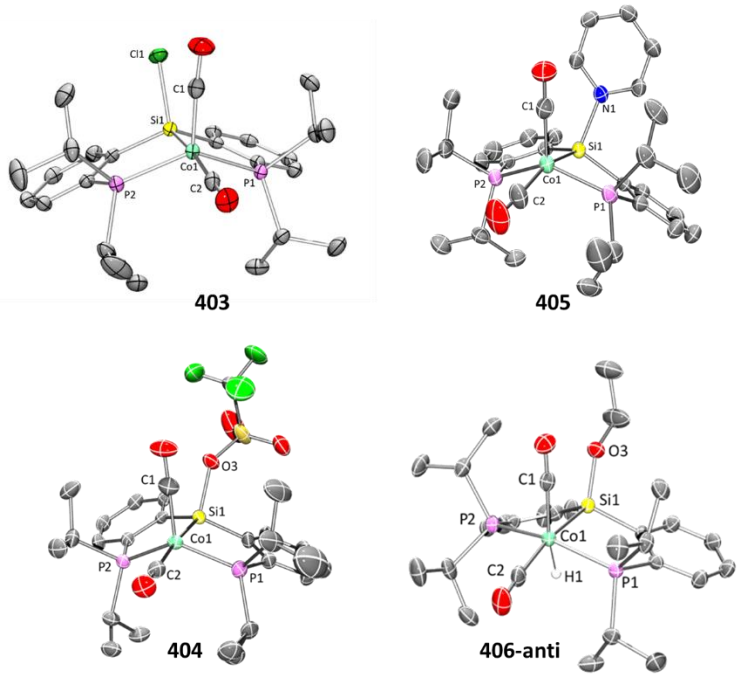

Figure IV-4. POV-Ray rendition of Ortep plots (50% probability ellipsoids) of complexes **403**−**406-anti** with all hydrogen atoms (except for Co−H in **406-anti**), counterions (for **405** and **406-anti**), and cocrystallized solvent molecules omitted for clarity. Selected bond lengths (Å) and angles (deg) for **403**: Co1−Si1, 2.2453(6); Co1−C1, 1.762(2); Co1−C2, 1.7715(19); Si1−Cl, 2.1189(8); Si−Co1−C1, 90.87(6); P1−Co1−P2, 133.65(2). For **404**: Co1−Si, 2.2163(11); Co1−C1, 1.763(4); Co1−C2, 1.777(4); Si1−O3, 1.797(3);

Si1−Co1−C1, 87.12(14); P1−Co1−P2, 132.49(4). For **405**: Co1−Si1, 2.2229(14); Co1−C1, 1.773(5); Co1−C2, 1.761(5); Si1−N1, 1.920(4); Si1−Co1−C1, 99.71(15); P1−Co1−P2, 138.27(5). For **406-anti**: Co−H, 1.43(4); Co−Si, 2.2885(9); Co−C1, 1.805(3); Co1−C2, 1.824(3); Si1−O3, 1.640(2); Si1−Co1−H1, 72.4(15); Si1−Co1−C1, 91.20(10); P1−Co1−P2, 156.46(4).

Based on the observations described above, the reaction of **402** with ethanol appears first to afford a complex with ethoxy and hydride oriented *syn* (**406-syn**) as a kinetic product, which isomerizes to the fully characterized *anti* isomer **406-anti** upon heating. Such a reaction course is consistent with the fact that the Lewis-acidic silylene would be expected to react first by coordination of ethanol to silicon, followed by fast proton transfer from ethanol to the cobalt center. Isomerization to **406-anti** occurs readily with only one equivalent of ethanol and thus does not require exogenous ethanol. The expected high acidity of the Co(III) hydride cation with π-accepting carbonyl co-ligands[168] suggests that isomerization may occur by proton transfer, perhaps mediated by solvent, though we cannot rule out Si/H reductive elimination followed by oxidative addition to give the *anti* isomer.

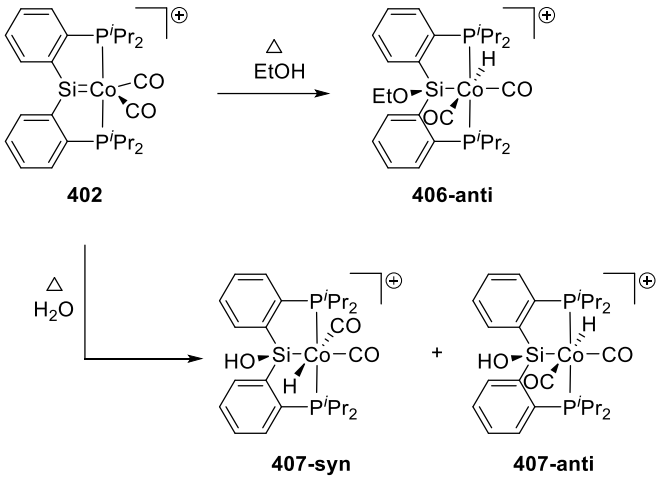

402 **406-anti** **407-syn** **407-anti**

Scheme IV-3. Formation of ethoxy- and hydroxysilyl complexes from silylene **402**.

Reaction of silylene **402** with water (≥1 equiv) proceeds with more complexity, initially forming a mixture of three as-yet unidentified hydride-containing intermediates and converging upon heating to a mixture represented by a single, broad ^{31}P NMR signal (δ 99.8 ppm). Further examination by ^{1}H NMR showed the presence of two overlapping Co–*H* signals in a 3:1 ratio. These signals are associated with two singlets (δ 2.86 (major) and 2.34 (minor) ppm) assigned as Si–O*H*, and the presence of silanol functionality is supported by a broad infrared peak at 3618 cm^{-1}.[169] Taking all the spectroscopic data into account, we assign the ultimate products from reacting **402** with water as *syn* and *anti* hydroxysilyl cobalt hydride complexes (Scheme IV-3). It is not clear at this time whether the *syn* or *anti* isomer is formed as the major product, though analogy with the corresponding ethanol reaction suggests that the *anti* isomer may be favored. The initial course of the reaction of silylene **402** with water is not clear at this point. It is somewhat surprising, based on findings with platinum,[24] that a silanol (Si–OH) forms rather than a disiloxane (Si–O–Si). Although siloxane intermediates may be present in the reaction, the evidence suggests that under our conditions they are not the thermodynamic products, and they cannot be favored by utilizing less than 1 equiv of water.

4.3 Conclusion

In conclusion, we have presented syntheses of a series of pincer-type (P_2Si)Co silyl and silylene complexes. The cationic base-free silylene **402** is the first of its type on cobalt. It is isolable and crystallizable, and it reacts readily with pyridine, ethanol, and water. Reaction with ethanol and water leads to heterolytic cleavage of the O–H bond to form a

cationic Co(III) hydride complex with alkoxy- or hydroxy-substituted silyl donor. These reactions suggest that further Co/Si cooperative reactivity may be realized for **402** and related pincer-supported silylenes. Such reactivity will be the subject of future studies.

4.4 Experimental

4.4.1 General Considerations

All manipulations were carried out in an argon- or nitrogen-filled glove box. Routine solvents were purchased from Sigma-Aldrich and were deoxygenated and dried using a Glass Contour Solvent Purification System or PureSolv MD-5 Solvent Purification System and were stored over 4Å molecular sieves in an inert-atmosphere glove box. Ethanol was purchased in dry and degassed form from Sigma-Aldrich and used as received. Fluorobenzene was dried via reflux over CaH_2, vacuum-transferred, and stored over 4Å molecular sieves. NMR solvents (Cambridge Isotope Labs) were degassed and vacuum-transferred from sodium/benzophenone (benzene-d_6 and toluene-d_8) or refluxed over and vacuum-transferred from CaH_2 (dichloromethane-d_2 and bromobenzene-d_5), then stored in an argon-filled glove box over 4Å molecular sieves prior to use. All other chemicals were used as received from commercial vendors. The ($^{i\text{Pr}}$P$_2$Si)H$_2$ ligand,[24] $Ph_3C{\cdot}BAr^F{}_{20}$,[170] and $Ph_3C{\bullet}OTf$[171] were prepared according to literature procedures. Other reagents were purchased from commercial vendors and used without further purification.

Characterization methods. NMR spectra were recorded at ambient temperature on a Bruker Avance III HD 400 (^{1}H, 400.13 MHz; ^{13}C, 100.61 MHz; ^{19}F, 376.50 MHz; ^{29}Si, 79.50 MHz; ^{31}P, 161.98 MHz) or Varian Inova 500 (^{1}H, 499.68 MHz; ^{13}C,

125.47 MHz; ^{19}F, 470.11 MHz; ^{29}Si, 99.32 MHz; ^{31}P, 202.29 MHz) NMR spectrometer. ^{1}H and ^{13}C NMR chemical shifts were referenced to residual solvent; ^{19}F, ^{29}Si, and ^{31}P NMR chemical shifts are reported relative to external standards of neat trifluoroacetic acid (−78.55 ppm), tetramethylsilane (0 ppm), and 85% H_3PO_4 (0 ppm), respectively. All chemical shifts are reported in δ (ppm). Infrared spectra were obtained on an Agilent CARY 630 ATR-FTIR, Mattson 4020 Galaxy Series, or Thermo Scientific Nicolet iS5 FTIR spectrometer. Elemental analyses were performed by CALI Labs, Inc. (Highland Park, NJ) or Midwest Microlab, LLC.

Computational details. All computations were carried out with the Gaussian09 program.[172] All of the geometries were fully optimized by M06[173] functional. The Stuttgart basis set and the associated effective core potential (ECP) was used for Co atoms, and an all-electron 6-31G(d) basis set was used for the other atoms. Based on the optimized structures, B3LYP/SDD/6-311+G(2d,p) level of theory was then used for the NMR calculation using the GIAO method relative to TMS.

4.4.2 Synthesis and Characterization

($^{i\mathrm{Pr}}$P$_2$Si$^{\mathrm{H}}$)Co(CO)$_2$ (401). A 20 mL scintillation vial was charged with $Co_2(CO)_8$ (50 mg, 0.15 mmol) and 8 mL toluene. To this was added a solution of the ($^{i\mathrm{Pr}}P_2Si)H_2$ ligand (0.81 mL, 0.36 M in toluene, 0.29 mmol) with stirring, causing a color change from dark brown to bright yellow with bubbling as CO and H_2 were evolved. The reaction was allowed to proceed with stirring for 1 h and the volatiles were removed *in vacuo*. The orange residue was dissolved in minimal pentane, filtered, and crystallized at –35 °C to

give pure **401** as a crop of yellow/orange crystals suitable for X-ray diffraction. Yield: 92 mg (59%). ^{1}H NMR (C_6D_6, 500 MHz): δ 7.91 (d, J = 7.2 Hz, 2H), 7.23 (dd, J_1 = 7.7 Hz, J_2 = 3.0 Hz), 7.18 (td, J_1 = 7.2 Hz, J_2 = 2.0 Hz, 2H), 7.07 (t, J = 7.5 Hz, 2H), 6.15 (s, $^{1}J_{SiH}$ = 182 Hz, 1H, Si–*H*), 2.24 (m, 4H), 1.26 (dvt, J_1 = 8.8 Hz, J_2 = 7.0 Hz, 6H), 0.92 (dvt, J_1 = 8.1 Hz, J_2 = 6.8 Hz, 6H), 0.87–0.80 (overlapping dvt, 12H). ^{13}C{^{1}H} NMR (C_6D_6, 120 MHz): δ 220.4 (br s, Co–*C*O), 207.2 (br s, Co–*C*O), 154.1 (quin, J = 30 Hz), 145.2 (dd, J_1 = 22 Hz, J_2 = 20 Hz), 133.3 (t, J = 11 Hz), 129.7, 128.4 (br s, overlap with C_6D_6), 128.0 (overlap with C_6D_6), 31.7 (t, J = 15 Hz, P–*C*H–$(CH_3)_2$), 29.6 (t, J = 8.6 Hz, P–*C*H–$(CH_3)_2$), 19.0 (t, J = 2.4 Hz, *C*H_3), 18.84 (s, overlapping), 18.82 (t, J = 2.2 Hz, overlapping), 18.53 (t, J = 1.3 Hz). ^{31}P{^{1}H} NMR (C_6D_6, 202 MHz): δ 93.8 (br s). ^{29}Si{^{1}H} (C_6H_5F, 79 MHz): δ 54.8 (t, J_{SiP} = 22 Hz). IR (ATR, cm^{-1}): 2048 (SiH), 1958 (CO), 1908 (CO). Anal. calcd. for $C_{26}H_{37}CoO_2P_2Si$: C, 58.86; H, 7.03. Found: C, 59.16; H, 7.25.

[(^{iPr}P$_2$Si=)Co(CO)$_2$][BAr$^{F}_{20}$] (402). ($^{iPr}P_2Si^{H}$)Co(CO)$_2$ (**401**) (31 mg, 0.058 mmol) and trityl tetrakis(pentafluorophenyl)borate (Ph_3C•BAr^{F}_{20}) (55 mg, 0.060 mmol) were separately dissolved in fluorobenzene (2 mL each), and the Ph_3C•BAr^{F}_{20} solution was added dropwise to the solution of **401** with stirring, causing an immediate color change from yellow to red. Pentane (10 mL) was added to precipitate the desired product. The supernatant was removed and the resulting red/orange powder was washed with pentane (3 × 3 mL). Residual pentane was removed *in vacuo* to afford [(^{iPr}P$_2$Si=)Co(CO)$_2$][BAr$^{F}_{20}$] **(402)**. Crude yield: 68 mg (94%). The solid could be further purified by crystallization from a toluene:fluorobenzene (3:1) solution at –35 °C. Recrystallized yield (as toluene solvate): 37 mg (49%). ^{1}H NMR (C_6D_5Br, 500 MHz): δ

7.96 (m, 2H), 7.47 (m, 4H), 2.46 (m, 4H), 0.88-0.75 (m, 24H). $^{13}C\{^{1}H\}$ NMR (C_6H_5F, 120 MHz): For cation portion only. δ 202.0 (br s, Co–*C*O), 149.0 (t, *J* = 22 Hz), 148.0 (t, *J* = 25 Hz), 132.9 (t, *J* = 9 Hz), 132.5 (s), 132.3 (s), 130.4 (s), 28.0 (t, *J* = 12.9 Hz, P–*C*H–$(CH_3)_2$), 17.2 (s, *C*H_3), 16.3 (s, *C*H_3). ^{19}F NMR (C_6D_5Br, 470 MHz): δ –133.1 (br s, 2F), –163.5 (t, *J* = 21 Hz, 1F), –167.3 (br s, 2F). $^{29}Si\{^{1}H\}$ NMR (C_6H_5F, 99 MHz): δ 284.6 (br s). $^{31}P\{^{1}H\}$ NMR (C_6D_5Br, 202 MHz): δ 105.1. IR (ATR, cm^{-1}): 2028 (CO), 1983 (CO). Anal. calcd. for $C_{50}H_{36}BCoF_{20}O_2P_2Si$: C, 49.69; H, 3.00. Found: C, 51.00; H, 2.99. *NOTE:* Microanalysis showed high values for C due to the presence of co-crystallized toluene evident in NMR spectra and the crystal structure of **402**.

($^{i\mathrm{Pr}}$P$_2$Si$^{\mathrm{Cl}}$)Co(CO)$_2$ (403). A 20 mL scintillation vial was charged with ($^{i\mathrm{Pr}}P_2Si^{H}$)Co(CO)$_2$ (**401**) (65 mg, 0.12 mmol), 5 mL C_6D_6, and $CDCl_3$ (ca. 300 μL). The mixture was heated in the sealed vial at 85 °C for 20 h, leading to a gradual change in solution color from yellow to green. Volatiles were removed *in vacuo* and the resulting pale-green powder was washed with cold pentane (3 × 3 mL). The solid was then dried *in vacuo* to afford pure **403**. Yield: 62 mg (90%). Single crystals suitable for X-ray diffraction were grown from a 3:1 pentane:toluene solution at –35 °C. ^{1}H NMR (C_6D_6, 500 MHz): δ 8.16 (d, *J* = 7.3 Hz, 2H), 7.22 (m, 4H), 7.08 (t, *J* = 7.3 Hz, 2H), 2.29 (m, 4H), 1.26 (dvt, J_1 = 8.6 Hz, J_2 = 6.8 Hz, 6H), 0.96 (dvt, J_1 = 8.2 Hz, J_2 = 6.9 Hz, 6H), 0.88-0.74 (overlapping dvt, 12H). $^{13}C\{^{1}H\}$ NMR (C_6D_6, 120 MHz): δ 219.4 (Co–*C*O), 205.9 (Co–*C*O), 156.0 (m), 144.2 (m), 133.1 (t, *J* = 11 Hz), 130.5 (s), 128.9 (t, *J* = 2 Hz), 32.0 (t, *J* = 15 Hz, P–*C*H–$(CH_3)_2$), 29.8 (t, *J* = 10 Hz, P–*C*H–$(CH_3)_2$), 19.4 (t, *J* = 2 Hz, *C*H_3), 19.0 (s, *C*H_3), 18.97 (t, *J* = 2 Hz, *C*H_3), 18.8 (br s, *C*H_3). $^{29}Si\{^{1}H\}$ (C_6D_6, 99 MHz): δ 93.7 (t, J_{SiP}

= 30 Hz). $^{31}P\{^{1}H\}$ NMR (C_6D_6, 202 MHz): δ 95.2 (br s). IR (ATR, cm^{-1}): 1970 (CO), 1921 (CO). Anal. calcd. for $C_{36}H_{36}ClCoO_2P_2Si$: C, 55.27; H, 6.42. Found: C, 55.74; H, 6.45.

($^{iPr}P_2Si^{OTf}$)Co(CO)$_2$ (404). ($^{iPr}P_2Si^{H}$)Co(CO)$_2$ (**401**) (50 mg, 0.094 mmol) and trityl trifluoromethanesulfonate (Ph_3C•OTf; 37 mg, 0.094 mmol) were separately dissolved in dichloromethane (2 mL each), and the Ph_3C•OTf solution was added dropwise to the stirring solution of **401**. The reaction mixture was stirred for 5 min and all volatiles were removed *in vacuo*. The resulting oil was washed with cold pentane (3 mL) to remove most of the triphenylmethane byproduct (desired product **404** also has some pentane solubility, so some **404** was lost in this step). The resulting powder was dissolved in minimal pentane and crystallized at −35 °C, affording yellow crystals of analytically pure **404**. Recrystallized yield: 24 mg (38%). ^{1}H NMR (C_6D_6, 400 MHz): δ 8.55 (dt, J_1 = 7.5 Hz, J_2 = 1.1 Hz, 2H), 7.26 (tdd, J_1 = 7.4 Hz, J_2 = 2.5 Hz, J_3= 1.0 Hz, 2H), 7.20 (m, 2H), 7.07 (m, 2H), 2.25 (m, 4H), 1.24 (dvt, J_1 = 9.5 Hz, J_2 = 6.9 Hz, 6H), 0.93 (dvt, J_1 = 9.1 Hz, J_2 = 6.9 Hz, 6H), 0.83 – 0.66 (m, 12H). $^{13}C\{^{1}H\}$ NMR (C_6D_6, 100.6 MHz): δ 218.1 (br s, Co–*C*O), 204.3, (br s, Co–*C*O), 151.4 (t, J = 27 Hz), 145.6 (t, J = 22 Hz), 133.6 (t, J = 11 Hz), 131.0, 129.8 (t, J = 2.7 Hz), 119.4 (q, J = 318 Hz, –*C*F_3), 31.5 (t, J = 15 Hz), 30.3 (t, J = 10 Hz), 19.33, 18.91, 18.79, 18.23. $^{19}F\{^{1}H\}$ NMR (C_6D_6, 376.3 MHz): δ –77.3. $^{29}Si\{^{1}H\}$ NMR (C_6D_6, 79.5 MHz): δ 108.8 (t, J = 34 Hz). $^{31}P\{^{1}H\}$ NMR (C_6D_6, 161.9 MHz): δ 96.0. IR (CH_2Cl_2, cm^{-1}): 1987 (CO), 1938 (CO). Anal. calcd. for $C_{27}H_{36}CoF_3O_5P_2SSi$: C, 47.79; H, 5.35. Found: C, 47.73; H, 5.20.

[(^{iPr}P$_2$Si^{Py})Co(CO)$_2$][BAr$^F{}_{20}$] (405). (^{iPr}P$_2$Si^H)Co(CO)$_2$ (**401**) (60 mg, 0.11 mmol) and trityl tetrakis(pentafluorophenyl)borate (Ph$_3$C•BAr$^F{}_{20}$; 104 mg, 0.11 mmol) were separately dissolved in fluorobenzene (2 mL each), and the Ph$_3$C•BAr$^F{}_{20}$ solution was added dropwise to the stirring fluorobenzene solution of **401**, causing an immediate color change form yellow to red. After 5 min, excess pyridine (ca. 15 μL) was added to the reaction mixture via pipette, causing a color change from red to yellow. Pentane (10 mL) was added with stirring to precipitate the desired product, which was isolated by filtration and washed with pentane (3 × 3 mL) and dried *in vacuo*, affording pure **405**. Yield: 131 mg (89%). ^{1}H NMR (CD_2Cl_2, 400 MHz): δ 8.23 (tt, J_1 = 7.7 Hz, J_2 = 1.5 Hz, 1H, pyr *para* C–*H*), 7.99–7.89 (m, 4H), 7.86–7.77 (m, 2H), 7.74–7.61 (m, 6H), 2.91 (m, 2H), 2.59 (m, 2H), 1.38 (dvt, J_1 = 9.9 Hz, J_2 = 6.8 Hz, 6H), 1.15 (dvt, J_1 = 7.4 Hz, J_2 = 6.3 Hz, 6H), 0.91 (overlapping dvt, 12H). ^{13}C{^{1}H} NMR (CD_2Cl_2, 100.6 MHz): <u>For cation portion only</u>. δ 215.7 (Co–*C*O), 204.8 (Co–*C*O), 148.9–147.7 (m), 146.7, 145.4, 133.2 (t, J = 10 Hz), 132.6, 132.0 , 130.6, 127.6, 31.8 (t, J = 11 Hz), 31.4 (t, J = 15 Hz), 19.8, 19.3, 19.2, 19.0. ^{19}F{^{1}H} NMR (CD_2Cl_2, 376.3 MHz): δ −133.0 (br), –163.5 (t, J = 20.4 Hz), –167.4 (t, J = 19.6 Hz). ^{29}Si{^{1}H} NMR (CD_2Cl_2, 79.5 MHz): δ 114.0 (t, $^3J_{SiP}$ = 34 Hz). ^{31}P{^{1}H} NMR (CD_2Cl_2, 161.9 MHz): δ 97.5. IR (CH_2Cl_2, cm^{-1}): 1990 (CO), 1939 (CO). Anal. calcd. for $C_{55}H_{41}BCoF_{20}NO_2P_2Si$: C, 51.30; H, 3.21. Found: C, 51.09; H, 3.21.

[(^{iPr}P$_2$Si^{OEt})Co(H)(CO)$_2$][BAr$^F{}_{20}$] (406). (^{iPr}P$_2$Si^H)Co(CO)$_2$ (**1**) (40 mg, 0.075 mmol) and trityl tetrakis(pentafluorophenyl)borate (Ph$_3$C•BAr$^F{}_{20}$; 69.6 mg, 0.075 mmol) were separately dissolved in fluorobenzene (2 mL each), and the Ph$_3$C•BAr$^F{}_{20}$ solution was added dropwise to the stirring fluorobenzene solution of **401**. After 5 min, excess

ethanol (ca. 15 μL) was added to the reaction mixture via pipette and the mixture was heated at 55 °C for 1 h. Pentane (10 mL) was added to precipitate the desired product, which was isolated by filtration as a pale yellow powder, washed with pentane (3 × 3 mL), and dried *in vacuo* to give pure **406**. Yield: 87 mg (92%). Single crystals suitable for X-ray diffraction were grown from a 3:1 diethyl ether:fluorobenzene solution at −35 °C. ^{1}H NMR (CD_2Cl_2, 400 MHz): δ 8.14 (d, *J* = 7.4 Hz, 2H), 7.79 (m, 2H), 7.73 (t, *J* = 7.3 Hz, 2H), 7.66 (t, *J* = 6.7 Hz, 2H), 3.56 (q, *J* = 7.0 Hz, 2H, –OC*H*$_2$CH$_3$), 2.91 (m, 2H), 2.79 (m, 2H), 1.44 (dvt, J_1 = 10.6 Hz, J_2 = 7.4 Hz, 6H), 1.25 (dvt, J_1 = 8.8 Hz, J_2 = 7.4 Hz, 6H), 1.16 (dvt, J_1 = 10.4 Hz, J_2 = 7.0 Hz, 6H), 1.09 (dvt, J_1 = 10.4 Hz, J_2 = 7.1 Hz, 6H), 1.05 (t, *J* = 6.9 Hz, 3H, –OCH$_2$C*H*$_3$), −12.25 (t, *J* = 38.6 Hz, 1H, Co–*H*). ^{13}C{^{1}H} NMR (CD_2Cl_2, 100.6 MHz): <u>For cation portion only</u> (NOTE: Co–*C*O not visible). δ 150.5 (t, *J* = 20 Hz), 139.86 (t, *J* = 27 Hz), 133.4 (t, *J* = 10 Hz), 132.7, 131.5 (t, *J* = 3.9 Hz), 130.0 (t, *J* = 2.9 Hz), 61.5, 31.6 (t, *J* = 16 Hz), 30.8 (t, *J* = 11 Hz), 19.2, 18.8, 18.7, 18.2, 18.1. ^{29}Si{^{1}H} NMR (CD_2Cl_2, 79.5 MHz): δ 62.4 (t, $^{3}J_{SiP}$ = 9.1 Hz). ^{31}P{^{1}H} NMR (CD_2Cl_2, 161.9 MHz): δ 99.2. IR (CH_2Cl_2, cm^{-1}): 2067 (CO), 2041 (CO). *Note:* Samples of **406** routinely failed microanalysis, even after recrystallization. However, multinuclear NMR spectroscopy indicates high purity (>97%) for this material.

[(*i*^{Pr}P$_2$Si^{OH})Co(H)(CO)$_2$][BAr$^{F}_{20}$] (407-syn and 407-anti, mixture of isomers**).** (*i*^{Pr}P$_2$Si^{H})Co(CO)$_2$ (**401**) (40 mg, 0.075 mmol) and trityl tetrakis(pentafluorophenyl)borate (Ph$_3$C•BAr$^{F}_{20}$; 69.6 mg, 0.075 mmol) were separately dissolved in fluorobenzene (2 mL each), and the Ph$_3$C•BAr$^{F}_{20}$ solution was added dropwise to the stirring fluorobenzene solution of **1**. After 5 min, excess water (ca. 15 μL) was added via pipette and the mixture

was heated at 80 °C overnight. Pentane (10 mL) was added to precipitate the desired product, which was isolated by filtration, washed with pentane (3 × 3 mL), and dried *in vacuo* to afford **407** as a pale-yellow powder consisting of an approximately 3:1 mixture of two isomers. Analysis of the mixture by ^{1}H NMR showed mostly overlapping peaks for the major and minor isomers, so only diagnostic peaks are reported for the minor isomer. ^{1}H NMR of major isomer (CD_2Cl_2, 400 MHz): δ 8.17 (d, J = 7.4 Hz, 2H), 7.83–7.57 (m, 6H), 2.97–2.84 (m, 2H, PC*H*$(CH_3)_2$), 2.86 (s, 1H, Si–O*H*), 2.88–2.76 (m, 2H, PC*H*$(CH_3)_2$), 1.42 (m, 6H, PCH(C*H*$_3)_2$), 1.28 (m, 6H, PCH(C*H*$_3)_2$), 1.19 (m, 6H, PCH(C*H*$_3)_2$), 1.06 (m, 6H, PCH(C*H*$_3)_2$), −12.16 (t, $^{2}J_{PH}$ = 38.7 Hz, 1H, Co–*H*). Distinct ^{1}H NMR peaks for minor isomer: 2.80–2.68 (m, PC*H*$(CH_3)_2$), 2.55–2.42 (m, PC*H*$(CH_3)_2$), 2.34 (s, 1H, Si–O*H*), −12.11 (t, $^{2}J_{PH}$ = 35.8 Hz, 1H, Co–*H*). ^{29}Si{^{1}H} NMR for mixture of isomers (CD_2Cl_2, 161.9 MHz): δ 62.4 (t, $^{3}J_{SiP}$ = 9.6 Hz). ^{31}P{^{1}H} NMR for mixture of isomers (CD_2Cl_2, 161.9 MHz): δ 99.8 (br). IR for mixture of isomers (CH_2Cl_2, cm^{-1}): 3618 (br, OH of silanol), 2068 (CO), 2038 (CO).

X-ray crystallography. Single-crystal X-ray diffraction data for compounds **401**–**403** were collected on a Bruker APEX 2 diffractometer using Mo Kα radiation (λ = 0.71073 Å), cooled to 110 K using a cold nitrogen stream (Oxford). Integrated intensity information for each reflection was obtained by reduction of the data frames with the program APEX2.[135] The integration method employed a three-dimensional profiling algorithm and all data were corrected for *Lp* and decay. Finally, the data were merged and scaled to produce a suitable data set. The absorption correction program SADABS[174] was

employed to correct the data for absorption effects. Absence of additional symmetry and voids were confirmed using PLATON (ADDSYM).[139]

Single-crystal X-ray diffraction data for compounds **404**–**406** were collected on a Rigaku XtaLAB mini diffractometer using Mo Kα radiation (λ = 0.71073 Å), cooled to 173 K using a cold air stream provided by an Oxford Cryosystems desktop cooler (Oxford Cryosystems Ltd, Oxford). The crystals were mounted on a MiTeGen micromount (MiTeGen, LLC, Ithaca, NY) using STP oil. The frames were integrated using CrystalClear-SM Expert 3.1 b27[175] to give the *hkl* files corrected for *Lp* and decay. Data were corrected for absorption effects using a multiscan method (REQAB).[140] Absence of additional symmetry and voids were confirmed using PLATON (ADDSYM).[139]

All structures were solved using SHELXS-2013 and refined using SHELXL-2013 with the Olex2 software package.[140] All non-hydrogen atoms were refined with anisotropic thermal parameters. Cobalt and silicon hydrides were located in the Fourier difference maps and refined isotropically; all other hydrogen atoms were inferred geometrically from neighboring sites and refined with riding thermal parameters. ORTEP drawings were prepared using ORTEP-3 for Windows V2013.1[176] and POV-Ray for Windows v3.6.[177] Crystallographic data for the complexes have been deposited at the Cambridge Crystallographic Data Centre (Nos. 1845823–1845828).

Special crystallographic refinement details. Triflatosilyl complex **404** contained two approximately equivalent molecules in the asymmetric unit, one of which exhibited a triflate that was disordered over two positions. In order to allow suitable refinement, the two triflates were subjected to EADP restraints.

CHAPTER V

ATTEMPTS AT USING (POCOP)CO FOR C–S COUPLING[†]

5.1 Introduction

Transition metal-mediated coupling reactions of aryl halides have become an irreplaceable part of a chemist's repertoire because of their ever-increasing scope and applicability. The majority of these coupling reactions use palladium[1,7] in chemistry that was honored by the 2010 Nobel Prize.[3] Expansion of this chemistry to include other metals, especially the cheaper and more abundant 3d elements such as Ni,[178] Cu,[13b,179] and Fe,[180] has been receiving an increased amount of attention.[181] Classical aryl halide coupling reactions rely on two-electron, concerted processes taking place at a single metal center: oxidative addition (OA) to break the Ar−Hal bond and reductive elimination (RE) to make the Ar−Z bond in the product (Figure V-1).[2] Two-electron processes such as these present a well-known challenge in the chemistry of 3d metals.[182]

[†] Reprinted in part with permission from "Synthesis of (POCOP)Co(Ph)(X) Pincer Complexes and Observation of Aryl-Aryl Reductive Elimination Involving the Pincer Aryl" by Foley, B. J.; Palit, C. M.; Timpa, S. D.; Ozerov, O. V. *Organometallics* **2018**, *37*, 3803-3812. Copyright 2018 American Chemical Society.

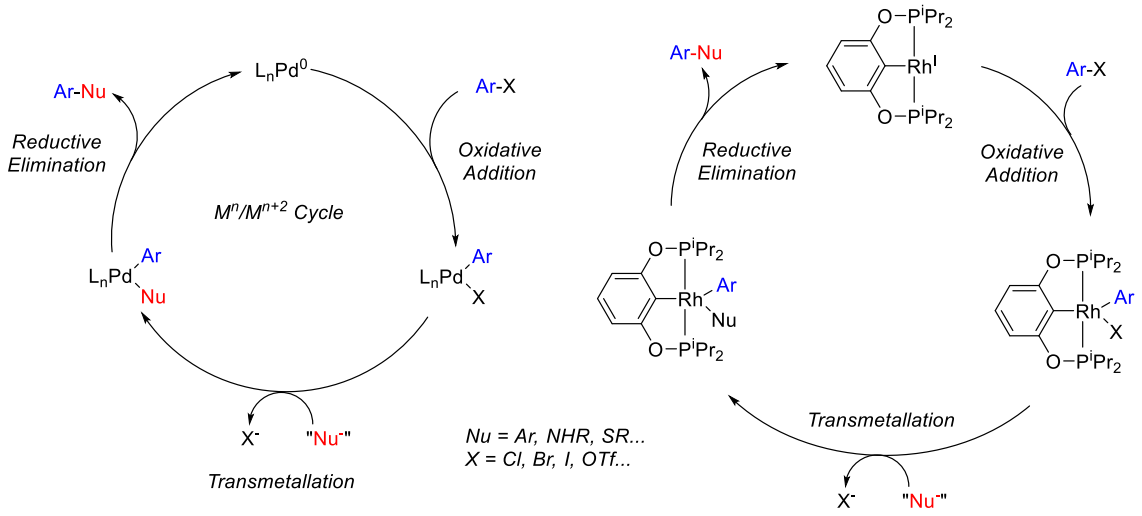

Figure V-1. Left: Generic Mechanism for Pd-catalyzed coupling of aryl halides with nucleophiles. Right: Previously proposed mechanism for coupling of aryl halides with nucleophiles using (POCOP)Rh.

We have reported on the ability of (POCOP)Rh complexes and other pincer complexes of Rh to catalyze coupling reactions of aryl halides.[18,183] In addition, we extensively documented the elementary reactions of OA and RE taking place at pincer-supported Rh.[30,31b,31c,184] In these reactions, the three-coordinate, monovalent (pincer)Rh fragment acts as a functional mimic of an LPd^0 species in the Pd-catalyzed cycles (Figure V-1). The Rh reactions thus involve cycling between Rh(I) and Rh(III) oxidation states (d^8/d^6) in contrast to Pd(0) and Pd(II) (d^{10}/d^8). An analogous cycle can also be imagined for cobalt in which it cycles between Co(I) and Co(III) through OA and RE steps. We became interested in examining whether the requisite OA and RE reactions might indeed be feasible for the (pincer)Co system.

Examples of aryl halide coupling[185] catalysis with simple cobalt(II) halide precursors have been reported.[14] Oshima et al. disclosed alkylation of aryl bromides with

primary alkyl Grignard reagents catalyzed by $CoCl_2$ with NHC supporting ligands.[186] Cheng et al. described arylation of thiols using CoI_2/ DPPE with a stoichiometric Zn additive.[187] Amatore and Gosmini reported reductive cross-coupling of two aryl halides using $CoBr_2/PPh_3$ with added stoichiometric Mn.[188] The latter two groups proposed a Co(I)/Co(III) catalytic cycle; however, mechanistic details were not investigated, and direct evidence that favored this pathway was not reported. Duan et al. described coupling of aryl fluorides with aryl Grignards catalyzed by $CoCl_2$ in the presence of near stoichiometric $Ti(OEt)_4$, proposing a Ti-assisted C−F OA to Co in an undefined oxidation state.[189]

In 2014, Fout and co-workers published a study of Cocatalyzed amination of aryl halides with $LiN(SiMe_3)_2$ and, less successfully, with other amine derivatives.[61] In this case, the key intermediate $(Ph_3P)_2CoN(SiMe_3)_2$ was isolated and identified. It was shown to effect catalysis and to react with iodobenzene in a stoichiometric reaction to produce $Ph–N(SiMe_3)_2$. This provided some experimental support for the Co(I)/Co(III) mechanism proposed by Fout and co-workers (Figure V-2). Nonetheless, the Co(III) intermediates were not observed, and consequently, the RE from Co(III) was not directly documented. A rare example of well-defined C−C RE from Co(III) involving two sp^3-hybridized carbons was reported by Xu and Bernskoetter in 2011, who demonstrated that elimination of ethane from $(Me_3P)_3CoMe_2I$ required initial dissociation of a PMe_3 ligand.[190] The results of Fout and Bernskoetter dovetail our findings with Rh in the sense that concerted RE from a d^6 Co(III) or Rh(III) center requires a five- and not six-coordinate complex, while OA to the d^8 Co(I) or Rh(I) requires a three-coordinate complex. This dynamic is

also well understood for a number of d^6/d^8 systems in general.[9] With Co, however, there is also the likelihood of the involvement of different spin states (S = 0 or S = 1) for the Co(I) and Co(III) complexes. For example, Fout's $(Ph_3P)_2CoN(SiMe_3)_2$ possesses a triplet configuration as does the analogous T-shaped (^{Si}PNP)Co complex (where ^{Si}PNP is [(^{t}Bu$_2$PSCH$_2$Me$_2$Si)$_2$N], Fryzuk's[191] pincer) investigated by Caulton et al.[192] Five-coordinate Co(III) complexes relevant as products of OA of aryl halides to Co(I) and their derivatives meant to undergo aryl−X RE have not been closely studied, to the best of our knowledge. However, Li et al. described *o*-imine-directed OA of aryl−fluoride bonds to Co(I) to give six-coordinate Co(III)−aryls, which subsequently underwent apparent C−C reductive elimination upon carbonylation.[193]

In 2016, the Chirik group reported catalysis of a version of a Suzuki−Miyaura cross-coupling between aryl triflates and arylboronates.[194] This reaction was catalyzed by a Co complex supported by a neutral pyridine/bis(phosphine) PN*P pincer ligand. What appeared to be unusual about this system is that it ostensibly required OA of aryl triflate to a four-coordinate, square planar (PN*P)Co−aryl complex (Figure V-2). The stoichiometric reaction between PhOTf and (PN*P)Co−Ar was indeed observed, but curiously, the analogous reactions with PhCl, PhBr, and PhI did not proceed similarly, yielding only partial conversion to the expected C−C coupling product. It is possible that the modest and varied catalytic success in this work (0−20 TON spread with a series of substrates) is reflective of the fact that OA to four-coordinate Co is accessible only with the most favorable substitution patterns, although it is also possible the behavior of Co in this system differs from what would be expected from its heavier, precious metal brethren.

The Chirik group also disclosed a series of studies of the various borylations of C−H bonds catalyzed by similar PN*P-supported Co catalysts.[35b,103,195] In those reports, OA to four-coordinate Co intermediates also appears to be necessary; however, OA of C−H, B−H, or B−B bonds can in general be viewed as kinetically more facile than OA of aryl halides. Fout et al. have described catalytic hydrogenation, hydroboration, and hydrosilylation using Co catalysts supported by an anionic CCC pincer and ostensibly operating via Co^{I} /Co^{III} cycles.[196]

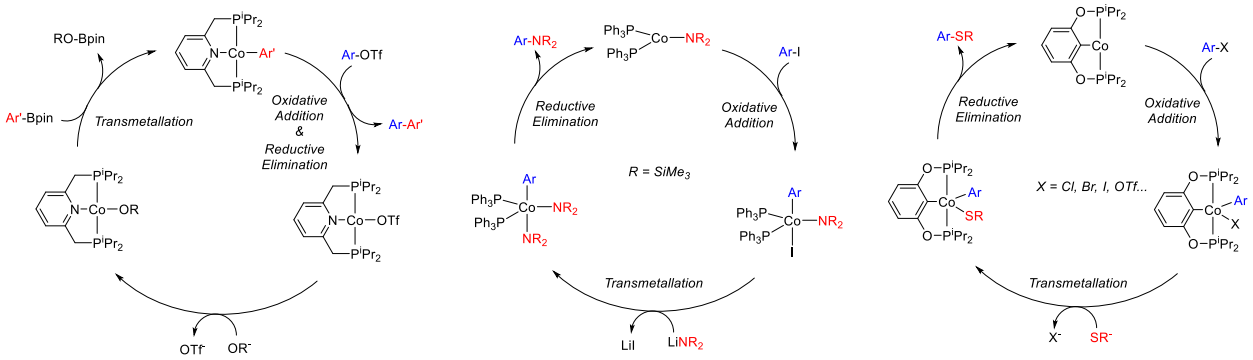

Figure V-2. Proposed mechanisms for Co-catalyzed coupling reactions. Left: Suzuki-Miyaura coupling of aryl triflates; center: aryl iodide amination; right: arylation of thiols envisaged in this work.

With this background in mind, we envisaged that an anionic pincer support such as POCOP would provide access to three coordinate Co(I) and five-coordinate Co(III) complexes (Figure V-2), as it did in the case of Rh. In this report, we focused on accessing the Co(III) intermediates in the expected catalytic cycle and on evaluating the potential for RE. In particular, we chose to pursue C−S RE, based on the recent success in catalyzing such coupling with Rh and on the general grounds of the C−S reaction being one of the easier aryl−heteroarom RE reactions.[197]

5.2 Results and Discussion

5.2.1 Synthesis and Characterization of (POCOP)Co^{II} Complexes

The introduction of the POCOP ligand into the coordination sphere of Co was accomplished by reaction of (POCOP)H with anhydrous $CoCl_2$ in the presence of dimethylaminopyridine (DMAP), producing (POCOP)Co(Cl) (**501**) as a bright yellow solid in a 29% yield upon workup (Scheme V-1). This reaction produced a large amount of a blue byproduct. This solid was collected, and single crystals suitable for X-ray diffraction were grown from a concentrated acetonitrile solution. The structure was determined to be [(DMAP)H][(DMAP)$CoCl_3$] with a unit cell matching that previously reported.[198] **501** is most closely related to (POCOP$^{t\text{Bu}}$)CoI reported by Goldberg, Heinekey, and coworkers.[199] A few differently substituted (POCOP)Co(CO)n (n = 1 or 2) complexes were very recently disclosed by Guan et al.[157] The ^{1}H nuclear magnetic resonance (NMR) spectrum of **501** displayed four broad, strongly contact-shifted signals with integral ratios of 24:4:2:1, consistent with formation of a paramagnetic Co^{II} complex. The signals with relative intensities of 24 (two overlapping resonances of 12 H each) and 4 correspond to the methyl and methine protons of the isopropyl groups, respectively; the resonances with intensities of 2 and 1 correspond to the aromatic protons of the aryl backbone. An Evans method measurement of the magnetic moment in solution yielded 2.2(1) μB, consistent with a single unpaired electron, as would be expected for an approximately square-planar, low-spin Co(II) complex. Strongly contact-shifted but resolved ^{1}H NMR resonances are consistent with a low-spin, square-planar complex of Co(II), in contrast to the (pseudo)tetrahedral Co(II) complexes with the S = 3/2 ground

state. It appears that the preference for low spin versus high spin for four-coordinate Co(II) pincer complexes may vary depending on the strength of field of the substituents about the Co center. For example, Fryzuk reported that (^{Si}PNP^{Ph})CoCl was pseudotetrahedral, possessed an S = 3/2 ground state, and was NMR-silent, but replacement of the chloride with a more donating, stronger-field methyl resulted in a low-spin, square planar (^{Si}PNP^{Ph})CoMe, for which ^{1}H NMR spectra could be observed, integrated, and interpreted.[200] The presence of a central aryl donor along with two phosphinites in the POCOP ligand appears to be enough to ensure a low-spin configuration. In addition, the stronger preference of POCOP for a square-planar over tetrahedral geometry should further stabilize the low-spin geometry. Indeed, Co(II) complexes of similar aryl/bis(phosphine) type 5,5-pincers[201] have also been reported to be low-spin, square-planar compounds.[202]

501 readily served as a starting material for the synthesis of derivative (POCOP)CoX complexes. Treatment of solutions of **501** with Me_3Si-X (X = Br, I, or OTf) resulted in rapid and clean formation of (POCOP)Co(Br) (**502**), (POCOP)Co(I) (**503**), and (POCOP)Co(OTf) (**504**) (Scheme V-1).

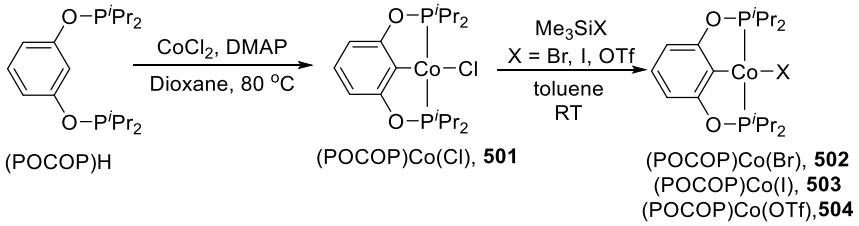

Scheme V-1. Synthesis of (POCOP)Co^{II}-Hal complexes.

Reaction of **501** with NaO^{t}Bu, MeLi, and PhLi resulted in the formation of (POCOP)Co(O^{t}Bu) (**505**), (POCOP)Co(Me) (**506**), and (POCOP)Co(Ph) (**507**), respectively. The synthesis of (POCOP)Co-SPh (**508**) was readily accomplished in 77% isolated yield by treatment of **501** with thiophenol, surprisingly not requiring addition of a base (Scheme V-2). All the Co^{II} complexes (**501**−**508**) displayed clearly analogous patterns in their ^{1}H NMR spectra, corresponding to the same 12:12:4:2:1 set of resonances noted for **501**. These data are indicative of all these compounds being low-spin Co(II) complexes possessing C_{2v} symmetry on the NMR time scale in solution.

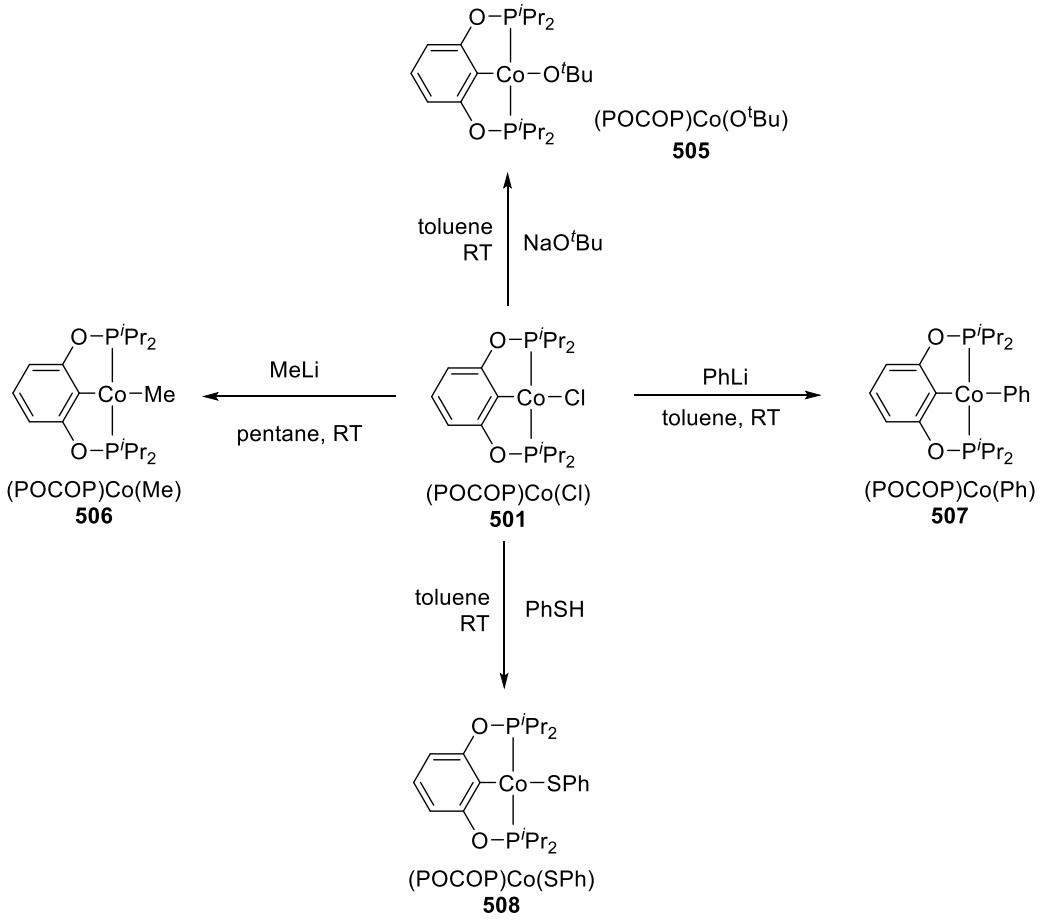

Scheme V-2. Synthesis of (POCOP)Co^{II}-X compounds.

5.2.2 Alternate Metalation of (POCOP) Using CoI_2.[‡]

Given the low yield of the metalation of (POCOP)H with $CoCl_2$, other CoI_2 was treated with the POCOP ligand to evaluate its metalation potential. Addition of CoI_2 in THF to (POCOP)H in the absence of light resulted in a white "fog" in the vial and ^{1}H NMR spectroscopy revealed the formation of (POCOP)Co(I) ostensibly by ejection of HI; however, this may leave as cobalt-containing ion pair as in the metalation of (POCOP)H with DMAP and $CoCl_2$.

To prevent release of HI in the glovebox, bases were added to attenuate HI production. Addition of DMAP or NEt_3 to (POCOP)H prior to addition of CoI_2 (in the absence of light) resulted in the smooth formation of (POCOP)Co(I) with no observed "fog." Heating the reaction performed with DMAP yielded no change versus stirring at room temperature. In each case, ^{1}H NMR spectroscopy revealed the formation of (POCOP)Co(I). This result indicates that introduction of (POCOP) to the coordination sphere of cobalt is possible at room temperature in the glovebox without the need for pre-lithiation of the ligand[199] (Scheme V-3).

Preliminary results also show that (POCOP)H can be metallated to $CoCl_2$ by refluxing (POCOP)H with $CoCl_2$ in THF overnight forming **501** without the need for a base.

[‡] This section is an addition to the original manuscript.

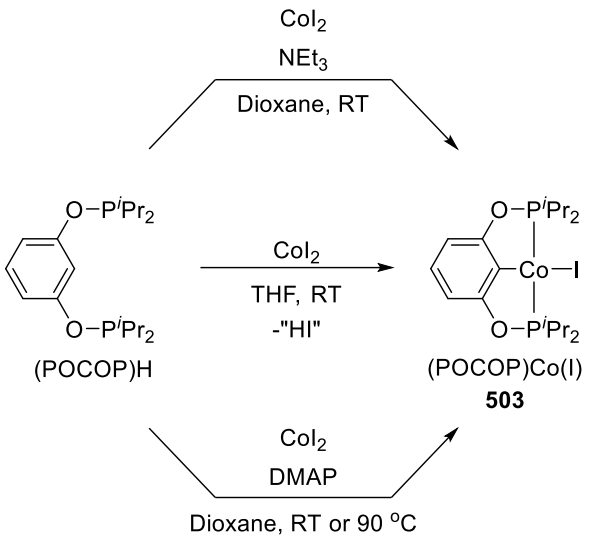

Scheme V-3. Metalation of CoI_2 to (POCOP)H

5.2.3 Attempted Synthesis of (POCOP)Co(F) and (POCOP)Co(CF_3)[§]

A previous group member recorded the synthesis of (POCOP)Co(F) (**509**) by addition of 3 eq. CsF to **504** in PhF and has supported their results with elemental analysis. However, this reaction was found to be irreproducible by two other group members. Addition of 3.6 eq. of CsF to **504** in PhF overnight yielded no reaction. Instead, if 13 eq. CsF were added to **504** in PhF only minimal conversion to **509** was observed ~9% (Scheme V-4). Addition of an additional 68 equivalents of CsF to this reaction yielded the complete consumption of **504** overnight; however, a second set of resonances resembling **509** were formed. These resonances may correspond to (POCOP)Co(F)•CsF (**511**), yet the addition of a second equivalent of **504** did not yield the desired product. These results

[§] This section is an addition to the original manuscript.

were reproduced with anhydrous CsF from two different sources, one from CsF stored in a vial in an Ar-filled glovebox of an unknown origin, the other freshly purchased from Beantown Chemical (Lot no. 50002520). The discrepancy between this work and previous work may originate from the differing level of hydration of the CsF. Of note also is that the addition of 3 eq. CsF to **503** in PhF provided only minimal conversion to **509** after 3 days at RT.

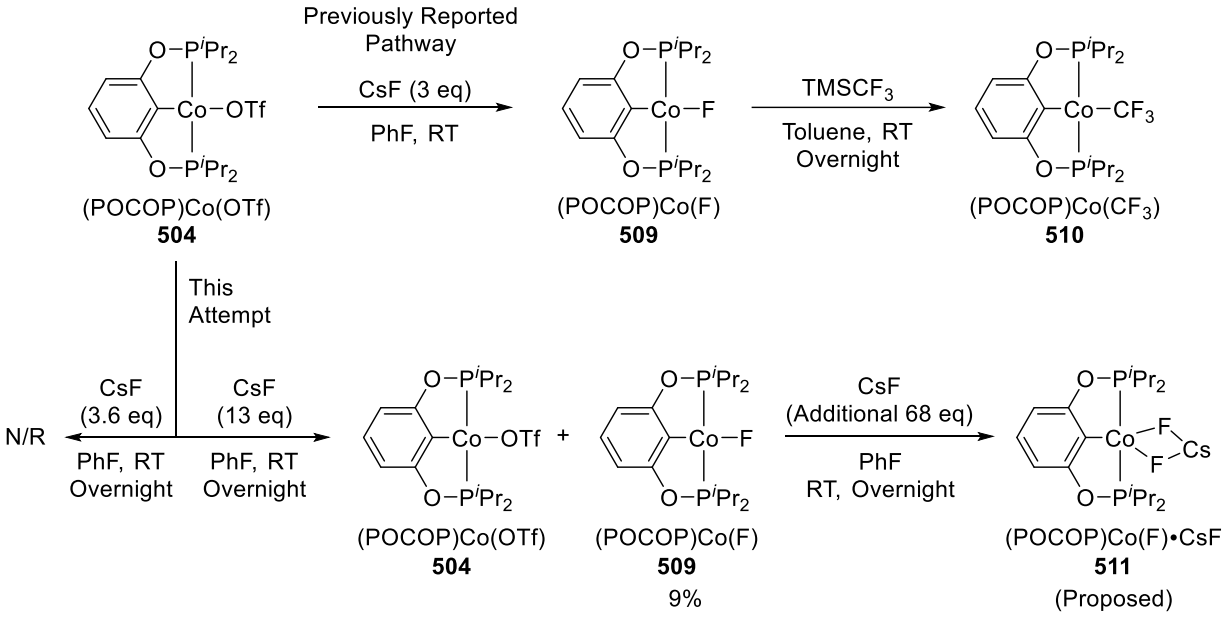

Scheme V-4. Previously documented synthesis of **509** and **510** and current attempts as synthesizing **509**.

Without **509** in hand, we attempted to synthesize **510** via transmetalation of **505** with $TMSCF_3$; however, after 24 hours, TMSF and HCF_3 were observed in the ^{19}F NMR spectrum. The TMSF may originate from Na^+ mediated degradation of the **510** followed by reaction of TMSX with NaF. If this is indeed the method of decomposition, it suggests that the **510** is exceptionally sensitive to trace salt contaminants.

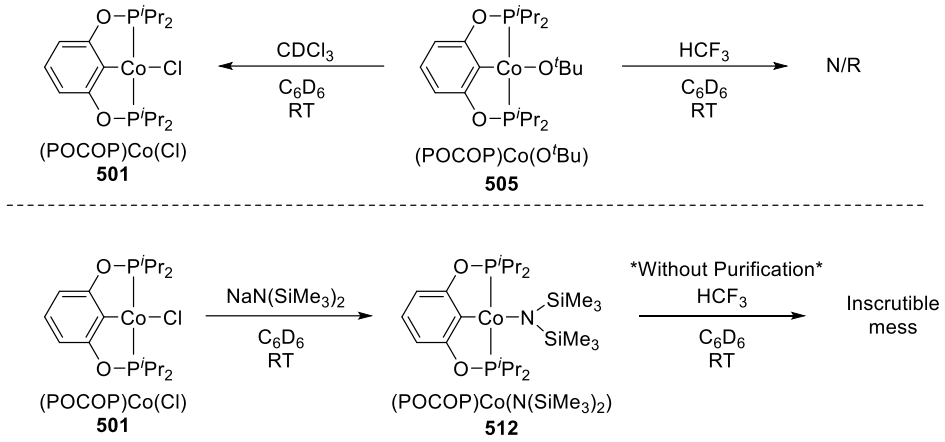

Scheme V-5. Top: Reactions of 505 with haloforms. Bottom: Current attempts at synthesizing **510**.

Looking at the formation of L_nCuCF_3 in the literature[203] inspired us to investigate the reaction between **505** and HCF_3. Unfortunately, this afforded no reaction (Scheme V-5, Top). Although, of note is that **505** is sensitive to the presence of chlorinated solvents, completely regenerating **501** in 12 hours after exposure to chloroform. Inferring from this that the *tert*-butoxy- substituent was not a potent enough endogenous base to activate fluoroform, we set our sights on the synthesis of a (POCOP)Co(NR_2) complex.

Treatment of **501** with $NaN(SiMe_3)_2$ in a J. Young NMR tube resulted in the clean formation of a new complex with paramagnetically shifted ^{1}H NMR resonances. The clean 4:24:18:2:1 ratio in the ^{1}H NMR spectrum supported the assignment of (POCOP)Co($N(SiMe_3)_2$ (**512**, Scheme V-5, Bottom). After addition of HCF_3 to this tube (with no purification), ^{19}F NMR spectroscopy revealed the formation of multiple new fluorine compounds including Me_3SiF, supporting the notion that **510** is sensitive to trace alkali-metal salt contaminants. This also explains the formation of Me_3SiF, as the silyl

amide (or silyl amine byproduct) could rapidly react with NaF and cleave the N–Si bond. Isolation of pure **512** and treatment with HCF_3 may yield a more favorable result and obviate the need for a three-step synthesis to arrive at **510**.

5.2.4 Synthesis and Characterization of (POCOP)Co^{III} Complexes

Oxidation of (POCOP)CoPh (**507**) with NCS at room temperature (RT) for 12 h in pentane resulted in a mixture of **501** and a new compound identified as (POCOP)Co(Ph)(Cl) (**513**), along with some biphenyl (Scheme V-6). Compound **513** in these mixtures decayed over time into biphenyl and **501**. Pure samples of **513** could be isolated in minute yields by recrystallization from these reaction mixtures; however, solutions of **513** obtained in this fashion inevitably degraded into **501** and biphenyl, as well. In contrast, oxidation of **507** with 0.55 equiv of $PhI(OAc)_2$ overnight in toluene led to clean isolation of (POCOP)Co(Ph)(OAc) (**514**) in 80% yield without any detectable amounts of paramagnetic impurities or biphenyl. **514** was found to be stable at RT in a solution in C_6D_6, and no detectable decomposition was observed after heating the same solution at 80 °C for 90 min. **514** offered an alternative synthetic route to Co^{III} aryl halide complexes. Metathetic reactions of **514** with Me_3SiCl and Me_3SiI in C_6D_6 cleanly yielded (POCOP)Co(Ph)(Cl) (**513**) and (POCOP)Co(Ph)(I) (**515**), after 18 h and 10 min, respectively (Scheme V-6).In Section 6.2.2, the synthesis of (PNP)Co(Ph)(I) (**605a**) can be performed from the reaction between (PNP)Co(Ph) (**602a**) and I_2. However, this does not work for the POCOP case as a significant amount of (POCOP)Co(I) (**503**) was observed in this case.

515 readily reacted with sodium thiophenolate to furnish (POCOP)Co(Ph)(SPh) (**516**). Interestingly, **513** synthesized by this route was much less prone to decomposition (<5% after 2 days at RT in C_6D_6) than the material obtained from **507** and NCS. No decomposition was evident by NMR upon aging solutions of **515** for 5 days at RT. It is possible that decomposition of **513** is catalyzed by traces of NCS or some other NCS-derived impurities, possibly in combination with residual Co^{II} complexes.

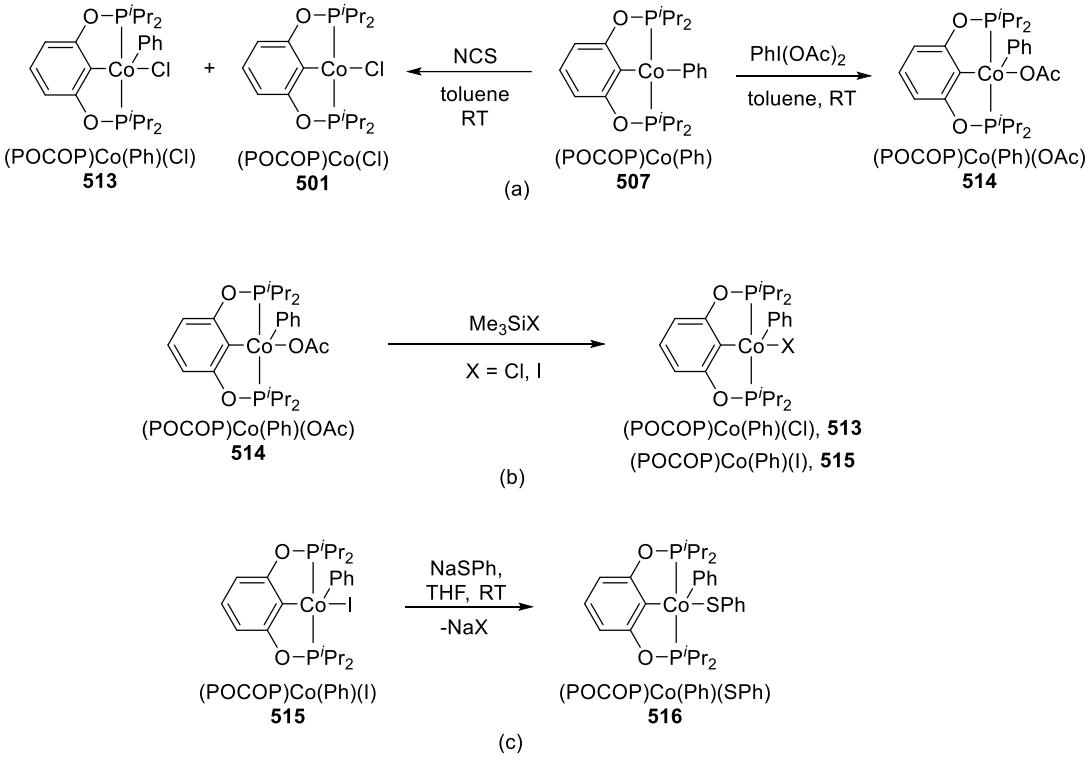

Scheme V-6. Synthesis of (POCOP)Co^{III} compounds **513-516**

Co^{III} complexes of the type (POCOP)Co(Ph)(X) [where X = Cl, OAc, I, and SPh (**513**–**516**, respectively)] all show well resolved NMR spectra with resonances in the diamagnetic region. One interesting feature shared by the ^{1}H NMR spectra of **513**–**516** is

the observation of five separate resonances for the protons on the phenyl ligand spread between ~5 and ~8 ppm in chemical shift (Figure V-3). The ortho and meta protons of the C_6H_5 group appear as broad humps, whereas the proton of the para position appears as a sharp triplet. These features indicate restricted rotation of the Ph ligand about the Co−Ph bond. Such restricted rotation was also observed for analogous (POCOP)Rh systems in our previous reports for Rh-catalyzed C−S and C−N coupling,[18,183] as well as other complexes of the type (pincer)Rh(Ar)(X) where the aryl group is cis to the central pincer donor.[31b,31c,204] We previously discussed how this orientation of the metal−aryl group (edge-on toward the X) and its restricted rotation are a detriment to the reductive elimination reactions with Rh[183b] and, presumably, Co, as well. The low-spin nature of these Co(III) complexes is ostensibly due to the presence of strong-field aryl ligands in the coordination sphere of Co. A comparison can be drawn with the report of Lippard et al. on five-coordinate Co(III) complexes of the type (NNNN)CoX, where NNNN is a dianionic, tetradentate tropocoronand ligand.[205] In their case, X = Cl corresponded to a paramagnetic Co(III) center whereas X = alkyl corresponded to a diamagnetic Co(III). Five-coordinate, low-spin Co(III) compounds with acyl and alkenyl donors were also reported by Klein et al.[206]

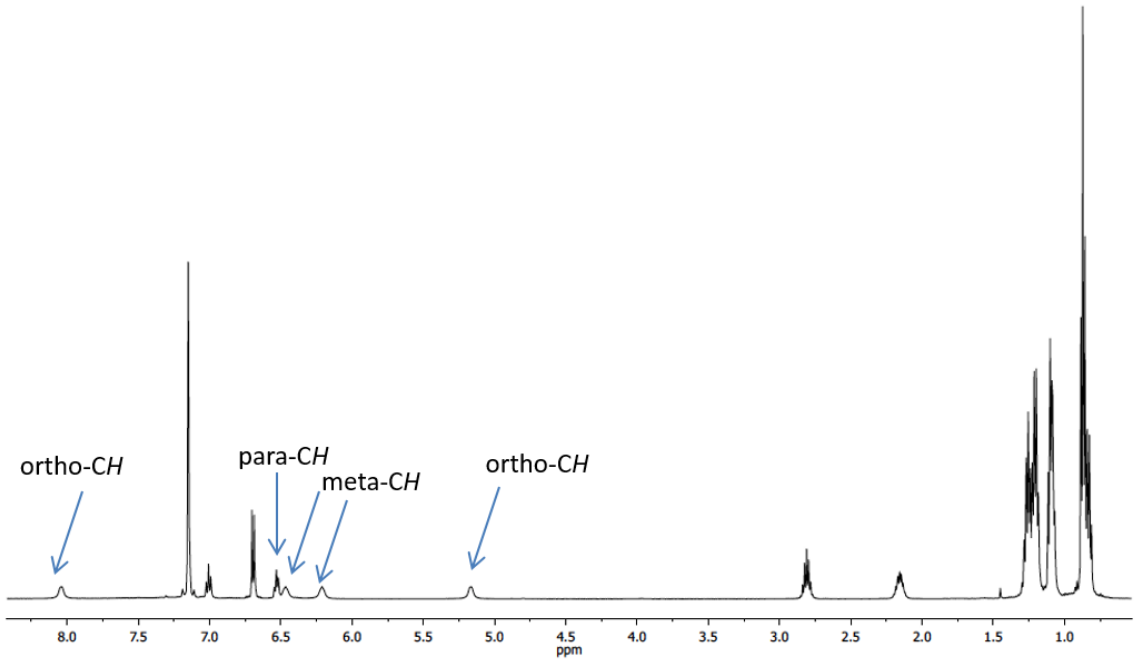

Figure V-3. ^{1}H NMR spectrum of (POCOP)Co(Ph)(Cl) (**513**) showing inequivalence of the five hydrogens of the Co-bound C_6H_5 group.

5.2.5 X-ray Structural Studies

The solid-state structures of **508**, **515**, and **516** complexes were determined via X-ray diffraction studies of crystals grown from pentane solutions at −35 °C. (POCOP)Co(SPh) (**508**) was observed to crystallize in the monoclinic system in the $P2_{1/c}$ space group, yielding yellow crystals. The ligands attain a slightly distorted square-planar geometry around the Co center, with the P1−Co1−P2 and C7−Co1−S1 angles being <180° at 161.86(2)° and 163.15(6)°, respectively (Figure V-4). (POCOP)Co^{III} compounds **515** and **516** crystallized attaining the $P2_{1/n}$ and $P2_{1/c}$ space groups, respectively. The geometry around the Co centers is distorted square pyramidal with the Ph ligand occupying the apical position placing the strongly *trans* influence ligands (Ph and central C_{aryl} of

POCOP) *cis* to each other with the I and S atoms distorted slightly out of plane from their ideal positions in a square pyramidal structure.[29] Comparison of the structures of **515** and **516** with the analogous Rh structures published previously by our group[18,183a] reveals very similar geometrical arrangements of donor atoms about Co^{III} and about Rh^{III}, only with shorter Co−ligand distances.

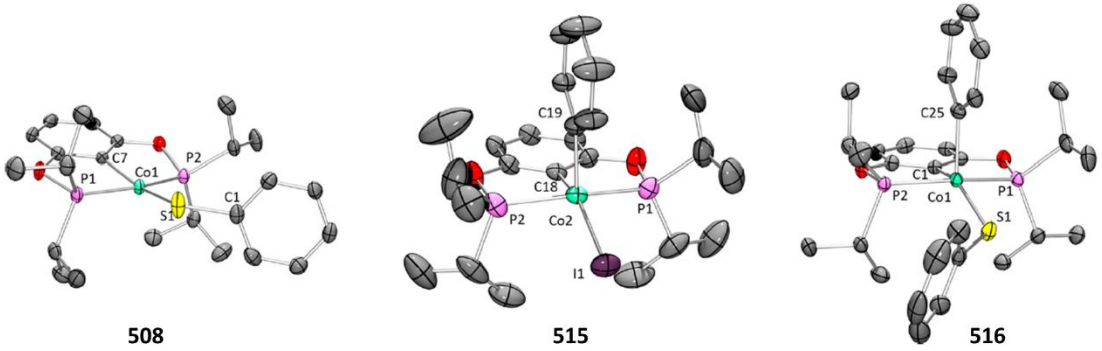

Figure V-4. POV-Ray rendition of Ortep plot (50% probability ellipsoids) of (POCOP)Co(SPh) (**508**, left), (POCOP)Co(Ph)(I) (**515**, center), and (POCOP)Co(Ph)(SPh) (**516**, right). Hydrogen atoms are omitted for clarity. Selected bond distances (Å) and angles (deg) for **508**: Co1-P1, 2.1816(8); Co1-P2, 2.1719(9); Co1-S1, 2.1706(8); S1-C1, 1.773(2); P1-Co1-P2, 161.86(2); C7-Co1-S1, 163.15(6); Co1-S1-C1, 119.89(7). Selected bond distances (Å) and angles (deg) for **515**: Co2-P1, 2.210(2); Co2-P2, 2.204(2); Co2-I1, 2.601(2); Co2-C18, 1.907(3); Co2-C19, 1.940(3); P1-Co2-P2, 161.83(4); C18-Co2-I1, 155.19(9); C19-Co2-I1, 115.86(9); C18-Co2-C19, 88.9(1). Selected bond distances (Å) and angles (deg) for **516** follow: Co1-C25, 1.947(2); Co1-P3, 2.222(1); Co1-P1, 2.223(1); Co1-S1, 2.215(1); Co1-C1, 1.933(2); C1-Co1-C25, 89.54(8); C1-Co1-P3, 81.80(5); C1-Co1-P1, 80.24(5); C1-Co1-S1, 148.98(6); C25-Co1-S1, 119.96(6).

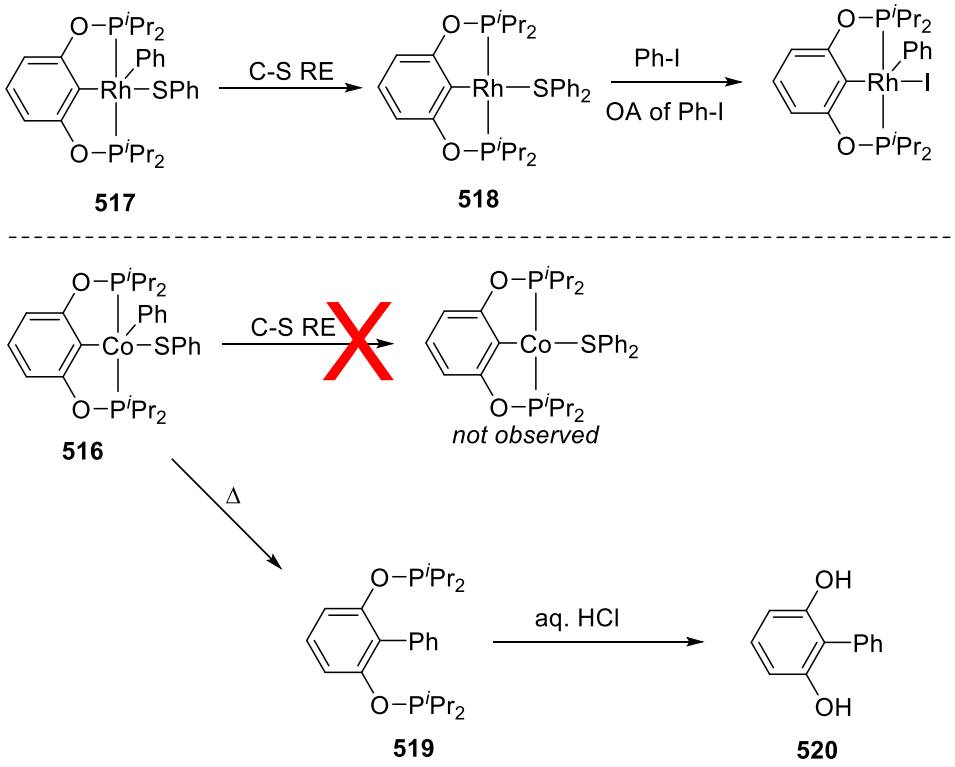

Scheme V-7. Top: Previously reported observations upon thermolysis of (POCOP)Rh(Ph)(SPh). Bottom: Observations for thermolysis of (POCOP)Co(Ph)(SPh).

5.2.6 Thermolysis and Observation of C_{ligand}–C_{Ph} Reductive Elimination From (POCOP)Co(Ph)(SPh)

In the analogous (POCOP)Rh system,[18] thermolysis of (POCOP)Rh(Ph)(SPh) (**517**) at 65 °C for 32 h yielded a 48:1 mixture of (POCOP)Rh(SPh_2) (**518**) and (POCOP)Rh(Ph)(SPh) (**517**) (Scheme V-7). Thermolysis of **516** in C_6D_6 at 80 °C however, proceeded to give **519** in 1 h (Scheme V-7) as the predominant product that could be observed by NMR spectroscopy (80% conversion with respect to an internal standard, ^{31}P NMR δ 148.7). The rest of the NMR-observable species is a mixture of **507** (10%) and other unidentified paramagnetic products. Formation of free **519** implies

ejection of the "CoSPh" fragment, but we were not able to determine the fate of Co in this transformation.

519 was identified on the basis of comparison of its ^{1}H, ^{13}C, and ^{31}P spectra with those of the free (POCOP)H ligand and the various (POCOP)Co compounds. The ^{1}H NMR spectra of **519** are clearly those of a diamagnetic compound and do not show virtual coupling features that are present in diamagnetic transition metal POCOP complexes with trans-disposed phosphines. The ^{31}P NMR chemical shift of the **519** resonance is quite close that of that (POCOP)H. Hydrolysis of **519** with aqueous HCl followed by extraction with dichloromethane and filtration through silica gave the known 2-phenylresorcinol[207] (**520**) in near-quantitative yield, confirming the proposed nature of **519**.

5.2.7 Prospects for Preventing C–C Elimination with the POCOP Ligand[**]

In order for the apical phenyl of the square pyramid to eliminate with the central aryl of the pincer, the ligand must flex to accommodate an overlap of atomic orbitals. Our group has established some precedent with Rh that installing *tert*-butyl substituents on the 3 and 5 position of the POCOP backbone can enforce a more rigid geometry about the metal.[208] Thus, installing a 3,5-di-*tert*-butylated POCOP ligand ($^{t\text{Bu}}$POCOP) on Co may allow for successful C–S elimination. Treating ($^{t\text{Bu}}$POCOP)H with 2 eq. $CoCl_2$ and 2 eq. DMAP resulted in the formation of ($^{t\text{Bu}}$POCOP)Co(Cl) (**521**) whereas treatment of the

[**] This section is an addition to the original manuscript.

same ligand with 1 eq. $CoCl_2$ and 1 eq. DMAP resulted in a mixture of products from which ($^{t\text{Bu}}$POCOP)Co(Cl)(DMAP) (**522**) was recrystallized (Figure V-5, Scheme V-8).

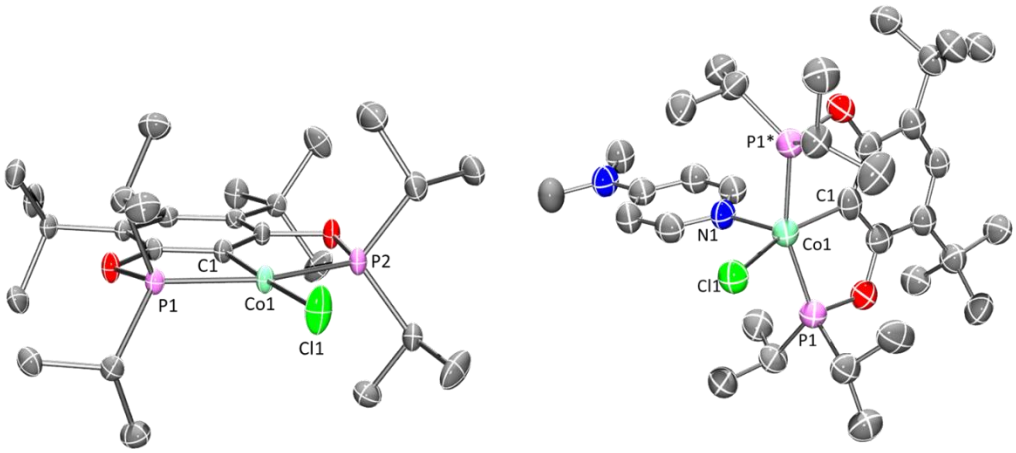

521 **522**

Figure V-5. ORTEP drawing (50% probability ellipsoids) of ($^{t\text{Bu}}$POCOP)Co(Cl) (**521**, Left) and ($^{t\text{Bu}}$POCOP)Co(Cl)(DMAP) (**522**, Right). Hydrogen atoms are omitted for clarity. Selected bond distances (Å) and angles (deg) for **521**: Co1-C1, 1.9230(15); Co1-Cl1, 2.2157(6); Co1-P1, 2.1720(7); Co1-P2, 2.1656(6); C1-Co1-Cl1, 177.79(5); P1-Co1-P2, 163.68(2). For **522**: Co1-N1, 2.074(7); Co1-P1, 2.1798(15); Co1-Cl1, 2.287(3); Co1-C1, 1.936(8) N1-Co1-Cl1, 99.7(2); P1-Co1-P1*, 159.02(11); C1-Co1-Cl1, 157.2(2); P1-Co1-Cl1, 96.02(6); P1-Co1-N1, 97.42(6).

In a similar fashion as **501**, addition of 1 eq. PhLi to ($^{t\text{Bu}}$POCOP)Co(Cl)resulted in the spectroscopic observation of ($^{t\text{Bu}}$POCOP)Co(Ph) (**523**) (Scheme V-8); however this compound was not isolated. Formation of the Co(Ar)(SR) complex with the $^{t\text{Bu}}$POCOP ligand may engender the metal with enough rigidity to prevent C–C elimination allow for C–S elimination.

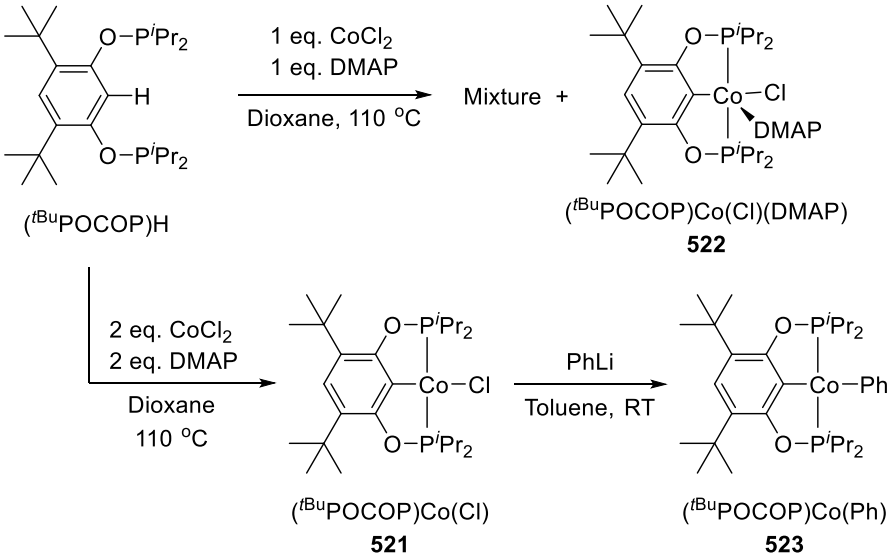

Scheme V-8. Synthesis of ($^{t\text{Bu}}$POCOP)Co$^{\text{II}}$ complexes **521-523**.

5.3 Conclusion

The POCOP supporting ligand allowed preparation of a series of Co(II) and Co(III) complexes. In particular, we were successful in preparing five-coordinate Co(III) complexes envisioned as intermediates in the catalytic cycle for catalytic coupling of aryl halides with thiols. They were found to be structurally similar to the catalytically competent Rh analogues. In contrast to the Rh behavior,[18] thermolysis of Co(III) aryl/ thiolato complex **516** did not result in the desired carbon−sulfur reductive elimination. Instead, **516** underwent an apparent intramolecular carbon−carbon RE, coupling the aryl of the POCOP pincer with the Ph group on Co. Such intramolecular C−C RE was not observed in the analogous Rh system. However, calculations on the related (POCOP)Rh(Ar)(NHR) complexes previously showed[183b] that the intramolecular C−C RE is kinetically easily accessible yet does not lead to a favorable product in the case of a

unimolecular Rh system. On the other hand, we did previously observe intramolecular C−C RE from (POCOP)Rh(CH=CH_2)(I) with the formation of a dimeric Rh^I product.[208]

It appears likely that C−C RE in the present Co system is likewise kinetically accessible, and ostensibly, ejection of Co from the pincer framework happens more readily than with Rh. All in all, our observations suggest that the POCOP ligand is not well suited for supporting catalysis of aryl halide coupling in the Co(I)/Co(III) cycle because of preferential intramolecular C−C RE from Co(III) aryl complexes. This may well be a detriment to the use of carbon-centered pincers in general for this purpose, and our further explorations will focus on pincer ligands with different central donor atoms.

5.4 Experimental

5.4.1 General Considerations

Unless otherwise specified, all manipulations were performed under an argon atmosphere using standard Schlenk line or glovebox techniques. Toluene, ether, tetrahydrofuran (THF), pentane, and isooctane were dried and deoxygenated (by purging) using an Innovative Technologies MD-5 solvent purification system and stored over molecular sieves in an Ar-filled glovebox. C_6D_6 and hexanes were dried over and distilled from a NaK/Ph_2CO/18-crown-6 mixture and stored over molecular sieves in an Ar-filled glovebox. (POCOP)H[209] and ($^{t\text{Bu}}$POCOP)H[19] were synthesized according to published procedures. NaSPh was prepared by reacting PhSH with 1 equiv. of NaH in THF followed by removal of volatiles and washing of the residue with Et_2O. All other chemicals were used as received from commercial vendors. NMR spectra were recorded on a Varian

NMRS 500 spectrometer (^{1}H NMR, 499.686 MHz; ^{13}C NMR, 125.659 MHz; ^{31}P NMR, 202.298 MHz; ^{19}F NMR, 470.111 MHz), a Bruker 400 spectrometer (^{1}H NMR, 400.2 MHz), and a Varian Inova 300 spectrometer (^{1}H NMR, 299.951 MHz; ^{13}C NMR, 75.413 MHz; ^{31}P NMR, 121.425 MHz). All ^{1}H and ^{13}C NMR spectra were referenced internally to the residual solvent signal (C_6D_6 at δ 7.16 for ^{1}H NMR and δ 128.06 for ^{13}C NMR). ^{31}P NMR spectra were referenced externally using 85% H_3PO_4 at δ 0. ^{19}F NMR spectra were referenced externally using neat CF_3CO_2H at δ −78.55. Elemental analyses were performed by CALI Laboratories, Inc. (Parsippany, NJ).

5.4.2 Synthesis and Characterization of Cobalt Complexes

(POCOP)CoCl (**501**). (POCOP)H (2.054 g, 5.99 mmol) was combined with $CoCl_2$ (1.68 g, 12.9 mmol) and DMAP (1.54 g, 12.6 mmol) in a Teflon-capped flask and partially dissolved in dioxane. The flask was heated at 90 °C for 20 h, producing a green solution. The solution was passed through a pad of Celite, and volatiles were removed by vacuum. The product was extracted with pentane, passed through a pad of Celite, and dried under vacuum to give a bright yellow-green solid. The product was recrystallized from pentane at −35 °C to give a yellow crystalline solid (750 mg, 29%). The compound displayed broad signals outside of the standard diamagnetic range in its ^{1}H NMR spectrum, indicative of a paramagnetic complex: ^{1}H NMR (500 MHz, C_6D_6) δ 43.72 (bs, 4H), 12.11 (bs, 24H), −14.71 (bs, 2H), −53.02 (bs, 1H). Anal. Calcd for $C_{18}H_{31}ClCoO_2P_2$: C, 49.61; H, 7.17. Found: C, 49.54; H, 7.08. The magnetic moment for **501** was determined to be 2.2(1) μB by the Evans method. Note: This compound can be synthesized using 1

eq. of $CoCl_2$ and 1 eq. of DMAP; however, this leads to a sticky, difficult-to-handle paste. The use of 2 eq. of $CoCl_2$ and 2 eq. DMAP yields the product as dry, easy to handle yellow needles.

(POCOP)CoBr (**502**). **501** (28 mg, 0.064 mmol) was added to a J. Young tube and dissolved in C_6D_6. Me_3SiBr (10 μL, 0.076 mmol) was added to the sample, resulting in a color change to slightly yellow-green. The reaction was complete after 10 min at RT as indicated by complete conversion to a new paramagnetic product and the presence of Me_3SiCl in the ^1H NMR spectrum. The volatiles were removed by vacuum to give a yellow powder. The product was recrystallized from a saturated pentane solution at −35 °C to give an orange crystalline solid (22 mg, 72%): ^1H NMR (500 MHz, C_6D_6) δ 45.16 (bs, 4H), 12.75 (bs, 12H), 12.00 (bs, 12H), −17.91 (bs, 2H), −41.58 (bs, 1H). Anal. Calcd. for $C_{18}H_{31}BrCoO_2P_2$: C, 45.02; H, 6.51. Found: C, 44.95; H, 6.63.

(POCOP)CoI (**503**). Method 1. **501** (30 mg, 0.069 mmol) was added to a J. Young tube and dissolved in C_6D_6. Me_3SiI (11 μL, 0.078 mmol) was added to the sample, resulting in a color change to yellow-green. The color was slightly darker than that observed with (POCOP)CoBr. The reaction was complete after 10 min at RT as indicated by complete conversion to a new paramagnetic product and the presence of Me_3SiCl in the ^1H NMR spectrum. The volatiles were removed by vacuum to give a yellow powder. The product was recrystallized from a saturated pentane solution at −35 °C to give a dark orange crystalline solid (15 mg, 43%).

Method 2. In an Ar-filled glove box with all laboratory lights off, a 50 mL culture tube was charged with (POCOP)H (544 mg, 1.6 mmol), CoI_2 (510 mg, 1.6 mmol), and

triethylamine (185 mg, 1.8 mmol), and THF (20 mL). The solution turned green and was stirred overnight. The following day, the contents of the tube were filtered through a pad of Celite and the volatiles were removed in vacuo. The residue was extracted with pentane and placed in a -35 °C freezer to recrystallize affording the product after two days (309 mg, 37% unoptimized): ^{1}H NMR (500 MHz, C_6D_6) δ 40.35 (bs, 4H), 12.81 (bs, 12H), 12.01 (bs, 12H), −20.18 (bs, 2H), −27.73 (bs, 1H).

(POCOP)CoOTf (**504**). **501** (712 mg, 1.64 mmol) was added to a Schlenk flask and dissolved in C_6D_6. The solution was treated with Me_3SiOTf (592 μL, 3.27 mmol). This led to no noticeable color change; however, the ^{1}H NMR spectrum of this reaction showed conversion to a new product along with the signal for Me_3SiCl. The volatiles were removed from the reaction mixture by vacuum to give a yellow-orange solid (850 mg, 94%): ^{1}H NMR (500 MHz, C_6D_6) δ 39.06 (bs, 4H, $CHMe_2$), 11.26 (bs, 12H, $CHMe_2$), 9.99 (bs, 12H, $CHMe_2$), −24.72 (bs, 1H, Ar-H), −26.33 (bs, 2H, Ar-H); ^{19}F NMR (470 MHz, C_6D_6) δ −92.6. Anal. Calcd for $C_{19}H_{31}CoF_3O_5P_2S$: C, 41.54; H, 5.69. Found: C, 41.37; H, 5.58. Note: The ^{19}F NMR resonance for this compound is sensitive to excess triflate. The ^{19}F resonance of -92.6 ppm was obtained after subsequent recrystallizations; however, shifts as downfield as -82.7 ppm have been observed for this compound.

(POCOP)CoO^{t}Bu (**505**). **501** (185 mg, 0.42 mmol) was added to a Schlenk flask and dissolved in toluene. NaO^{t}Bu (41 mg, 0.43 mmol) was added to the solution, resulting in an immediate color change to orange. The reaction mixture was stirred at RT for 1 h. The volatiles were removed under vacuum. The product was extracted with pentane, passed through a pad of Celite, and dried under vacuum. The product was recrystallized

from a concentrated toluene solution layered with pentane at −35 °C to give a brown solid (127 mg, 63%): ^{1}H NMR (500 MHz, C_6D_6) δ 14.98 (bs, 4H), 4.34 (bs, 26H), −9.93 (bs, 9H), −80.23 (bs, 1H). Anal. Calcd for $C_{22}H_{40}CoO_3P_2$: C, 55.81; H, 8.52. Found: C, 55.71; H, 8.36.

(POCOP)Co(Me) (**506**). **501** (170 mg, 0.391 mmol) was added to a Schlenk flask and dissolved in pentane. The solution was treated with MeLi (293 μL, 1.6 M in OEt_2, 0.25 mmol), leading to an immediate color change from light yellow to dark green. After being stirred for 30 min at RT, the solution was passed through a pad of Celite, and the volatiles were removed by vacuum to give a green solid. The solid was recrystallized from toluene layered with pentane at −35 °C to give a dark green crystalline solid (120 mg, 74%). The compound displayed broad signals outside of the standard diamagnetic range in the ^{1}H NMR spectrum, indicative of a paramagnetic complex: ^{1}H NMR (300 MHz, C6D6) δ 53.26 (bs, 4H), 13.14 (bs, 12H), 11.71 (bs, 12H), −9.08 (bs, 5H), −45.83 (bs, 1H). Anal. Calcd for $C_{19}H_{34}CoO_2P_2$: C, 54.94; H, 8.25. Found: C, 54.85; H, 8.50.

(POCOP)Co(Ph) (**507**). **501** (91 mg, 0.21 mmol) was added to a Schlenk flask and dissolved in pentane. The solution was treated with PhLi (140 μL, 1.8 M in $^nBu_2O$, 0.25 mmol), leading to an immediate color change from light yellow to dark green. After being stirred for 30 min at RT, the solution was passed through a pad of Celite, and the volatiles were removed by vacuum to give a green solid. The solid was recrystallized from toluene layered with pentane at −35 °C to give a dark green crystalline solid (81 mg, 81%). The compound displayed broad signals outside of the standard diamagnetic range in the ^{1}H NMR spectrum, indicative of a paramagnetic complex: ^{1}H NMR (500 MHz, C_6D_6) δ

36.21 (bs, 4H), 13.87 (bs, 1H), 12.04 (bs, 12H), 7.54 (bs, 12H), −7.38 (bs, 1H), −15.84 (bs, 2H), −20.15 (bs, 2H), −40.56 (bs, 2H). Anal. Calcd for $C_{24}H_{36}CoO_2P_2$: C, 60.38; H, 7.60. Found: C, 60.22; H, 7.69.

(POCOP)Co(SPh) (**508**). **501** (100 mg, 0.229 mmol) was added to a Schlenk flask and dissolved in ∼10 mL of toluene. To this was added PhSH (24.6 μL, 26.5 mg, 0.240 mmol) using a syringe. The reaction mixture was stirred at RT for 4 h. The volatiles were removed under vacuum. The product was extracted with pentane, passed through a pad of Celite, and dried under vacuum. The product was recrystallized from a concentrated pentane solution at −35 °C to give yellow crystals (90 mg, 77%): ^{1}H NMR (500 MHz, C_6D_6) δ 35.78 (br, 4H), 8.58 (br, 24H), 6.20 (br, 2H), 4.08 (br, 1H), −2.84 (br, 2H), −20.89 (br, 2H), −67.93 (br, 1H). Anal. Calcd for $C_{24}H_{36}CoO_2P_2S$: C, 56.58; H, 7.12. Found: C, 56.48; H, 7.04.

Spectroscopic observation of (POCOP)Co(N(SiMe$_3$)$_2$) (**512**). **501** (87 mg, 0.20 mmol) was dissolved in C_6D_6 in a J. Young tube. To this solution was added Sodium bis(trimethylsilyl)amide (36 mg, 0.19 mmol). ^{1}H NMR spectroscopy revealed a new complex which displayed broad signals outside of the standard diamagnetic range in the ^{1}H NMR spectrum, indicative of a paramagnetic complex. ^{1}H NMR (400 MHz, C_6D_6) δ 42.95 (br, 4H), 12.15 (br, 24H), -5.07 (br, 18H), -18.65 (br, 2H), -43.38 (br, 1H).

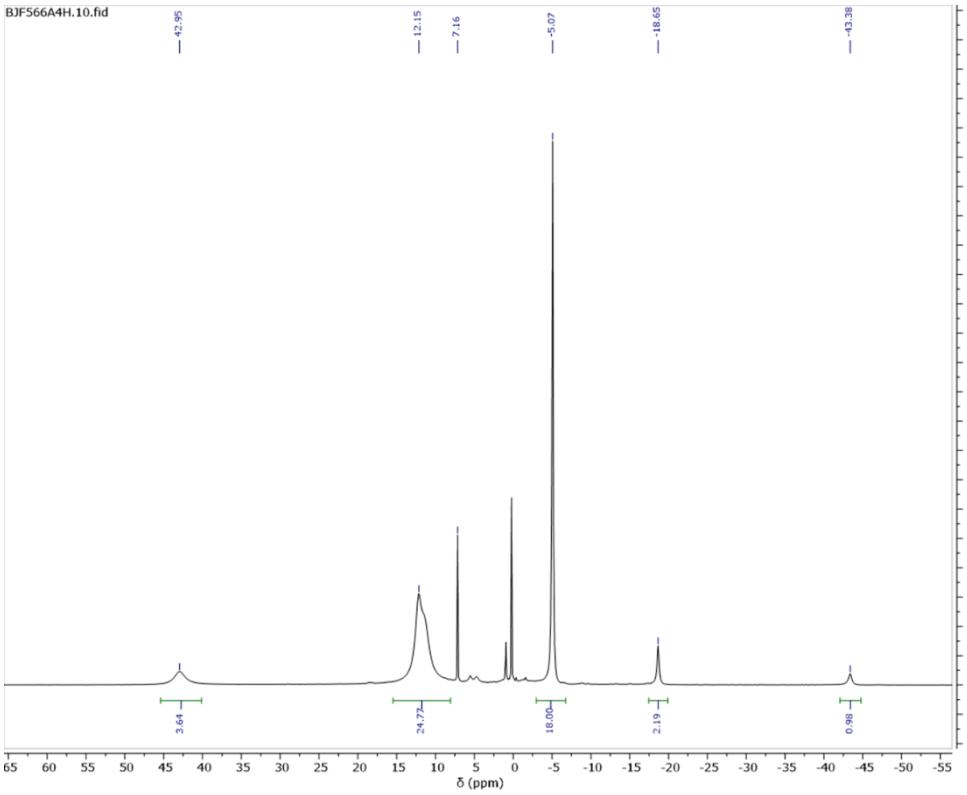

Figure V-6. ^{1}H NMR (400 MHz, C_6D_6) spectrum of **513**. Sample contains residual TMSCl.

(POCOP)Co(Ph)(Cl) (**513**). Method 1. **507** (194 mg, 0.41 mmol) was added to a Schlenk flask and dissolved in pentane. The solution was treated with NCS (58 mg, 0.44 mmol) and stirred at RT for 12 h, producing a green-yellow solution. A blue insoluble solid crashed out of the pentane solution and was removed by filtration. The volatiles were removed under vacuum to give a green-yellow solid. The ^{1}H NMR spectrum of this solid shows paramagnetic signals corresponding to **501** as well as diamagnetic signals corresponding to **513**. The solid was dissolved in pentane and crystallized at −35 °C. The recrystallization produced a green crystalline solid and yellow crystalline solid. The yellow solid was determined to be **501**, and the green solid was determined to be

(POCOP)Co(Ph)(Cl) (**513**). Dissolution of the green solid in C_6D_6 showed clean **513** in the ^{1}H NMR spectrum. After several hours at RT, the same sample showed formation of **501** and biphenyl in addition to **513** in the ^{1}H NMR spectrum.

Method 2. (POCOP)Co(Ph)(OAc) (**514**) (12 mg, 0.022 mmol) was dissolved in ~800 μL of C_6D_6 in a J. Young NMR tube with a PTFE screw cap. To this was added Me_3SiCl (3.40 μL, 2.91 mg, 0.27 mmol) using a syringe. The mixed solution was left to stir at RT for 18 h, and complete conversion to **513** was observed using NMR spectroscopy. The volatiles were removed, and pure **513** was observed as a green solid. The green solid was dissolved in a minimal amount of pentane and placed in the freezer at −35 °C overnight, after which dark green crystals were obtained: ^{1}H NMR (500 MHz, C_6D_6) δ 8.04 (bs, 1H, Ph-*H*), 7.01 (t, *J* = 8.5 Hz, 1H, Ar-*H*), 6.69 (d, *J* = 8.0 Hz, 2H, Ar-*H*), 6.53 (t, *J* = 7.0 Hz, 1H, Ph-*H*), 6.47 (bs, 1H, Ph-*H*), 6.21 (bs, 1H, Ph-*H*), 5.17 (bs, 1H, Ph-*H*), 2.81 (m, 2H, C*H*Me2), 2.16 (m, 2H, C*H*Me2), 1.21 (dvt, *J* = 7.7 Hz, *J* = 7.1 Hz, 6H, CH*Me*$_2$), 1.09 (overlapping dvt, 12H, CH*Me*$_2$), 0.83 (dvt, *J* = 8.1 Hz, *J* = 7.5 Hz, 6H, CH*Me*$_2$); ^{13}C{^{1}H} NMR (125 MHz, C_6D_6) δ 171.0 (t, *J* = 8 Hz, *C*-Co), 140.9 (br), 137.5 (br), 128.9 (br), 127.6 (br), 125.0 (br), 123.7 (s), 106.8 (t, *J* = 5.4 Hz, *C*–O), 29.9 (t, *J* = 9.2 Hz, *C*HMe$_2$), 27.9 (t, *J* = 11.7 Hz, *C*HMe$_2$), 18.6 (s, CH*Me*$_2$), 17.5 (s, CH*Me*$_2$), 16.0 (s, CH*Me*$_2$), 15.7 (s, CH*Me*$_2$); ^{31}P{^{1}H} NMR (202 MHz, C_6D_6) δ 176.7 (bs).

(POCOP)Co(Ph)(OAc) (**514**). **507** (300 mg, 0.629 mmol) was added to Schlenk flask and dissolved in toluene to give a dark green solution. $PhI(OAc)_2$ (101 mg, 0.314 mmol) was added to the reaction mixture. The solution quickly became light yellow in color. After being stirred overnight at RT, the solution became red in color. The volatiles

were removed in vacuo. The product was extracted with pentane and passed through a pad of Celite. The volatiles were removed to give a red-orange solid. The solid was dissolved in a minimum amount of pentane and left overnight at −35 °C to yield a red crystalline solid (270 mg, 80%): ^{1}H NMR (500 MHz, C_6D_6) δ 8.07 (d, *J* = 9.5 Hz, 1H, Ph), 6.99 (t, *J* = 6.5 Hz, 1H, Ar), 6.96 (t, *J* = 6.5 Hz, 1H, Ph), 6.81 (t, *J* = 6.5 Hz, 1H, Ph), 6.68 (d, *J* = 6.0 Hz, 2H, Ar), 6.63 (t, *J* = 9.5 Hz, 1H, Ph), 5.79 (d, *J* = 9.5 Hz, 1H, Ph), 2.58 (bm, 2H, C*H*Me$_2$), 1.94 (m, 2H, C*H*Me$_2$), 1.75 (s, 3H, CO_2*Me*), 1.29 (dvt, *J* = 6.9 Hz, *J* = 6.7 Hz, 6H, CH*Me*$_2$), 1.17 (dvt, *J* = 7.2 Hz, *J* = 7.1 Hz, 6H, CH*Me*$_2$), 1.02 (dvt, *J* = 6.8 Hz, *J* = 6.5 Hz, 6H, CH*Me*$_2$), 0.88 (dvt, *J* = 8.6 Hz, *J* = 7.6 Hz, 6H, CH*Me*$_2$); ^{13}C{^{1}H} NMR (125 MHz, C_6D_6) δ 182.6 (s, *C*O_2Me), 168.5 (t, *J* = 8.4 Hz, *C*-Co), 141.8 (s), 141.2 (s), 134.9 (s), 129.1 (s), 127.6 (s), 125.4 (s), 123.4(s), 106.3 (t, *J* = 5.0 Hz, *C*-O), 28.6 (t, *J* = 6.7 Hz, *C*HMe$_2$), 28.2 (t, *J* = 11 Hz, *C*HMe$_2$), 23.7 (s, CO_2*Me*), 17.8 (s, CH*Me*$_2$), 17.2 (s, CH*Me*$_2$), 16.4 (s, CH*Me*$_2$), 15.8 (s, CH*Me*$_2$); ^{31}P{^{1}H} NMR (202 MHz, C_6D_6) δ 179.3 (bs).

(POCOP)Co(Ph)(I) (**515**). (POCOP)Co(Ph)(OAc) (**514**) (54 mg, 0.099 mmol) was dissolved in ∼800 μL of C_6D_6 in a J. Young NMR tube with a PTFE screw cap. To this was added Me_3SiI (16 μL, 22 mg, 0.110 mmol) using a syringe. Complete conversion to **515** was observed using NMR spectroscopy after 10 min. The contents of the NMR tube were transferred to a 25 mL Schlenk flask; the volatiles were removed, and pure **515** was obtained as a green solid (40 mg retrieved from the flask, 67% yield): ^{1}H NMR (300 MHz, C_6D_6) δ 7.43 (bs, 1H, Ph-*H*), 7.05 (t, *J* = 8.5 Hz, 1H, Ar-*H*), 6.67 (d, *J* = 8.0 Hz, 2H, Ar-*H*), 6.42−6.35 (overlapping m, 2H, Ph-*H*), 6.09 (bs, 1H, Ph-*H*), 5.16 (bs, 1H, Ph-*H*), 3.22 (m, 2H, C*H*Me$_2$), 2.31 (m, 2H, C*H*Me$_2$), 1.34 (dvt, *J* = 8.0 Hz, *J* = 7.4 Hz, 6H,

CH*Me*$_2$), 1.13 (dvt, *J* = 6.7 Hz, *J* = 5.7 Hz, 6H, CH*Me*$_2$), 0.91 (dvt, *J* = 8.5 Hz, *J* = 7.3 Hz, 6H, CH*Me*$_2$), 0.83 (dvt, *J* = 8.3 Hz, *J* = 7.4 Hz, 6H CH*Me*$_2$); $^{13}C\{^1H\}$ NMR (125 MHz, C_6D_6) δ 170.2 (t, *J* = 8 Hz, *C*-Co), 140.5 (s), 138.2 (s), 131.1 (br), 129.0 (s), 124.3 (s), 124.0 (s), 106.9 (t, *J* = 5.4 Hz, *C*-O), 31.8 (t, *J* = 9.2 Hz, *C*HMe$_2$), 28.5 (t, *J* = 11.7 Hz, *C*HMe2), 18.8 (s, CH*Me*$_2$), 17.6 (s, CH*Me*$_2$), 17.0 (s, CH*Me*$_2$), 16.6 (s, CH*Me*$_2$); $^{31}P\{^1H\}$ NMR (120 MHz, C_6D_6) δ 184.5 (bs). Anal. Calcd for $C_{24}H_{36}CoIO_2P_2$: C, 47.70; H, 6.00. Found: C, 47.62; H, 5.81. No significant decomposition of **515**, in a solution in ∼800 μL of C_6D_6 in a J. Young NMR tube with a PTFE screw cap, to **503** was detected by NMR spectroscopy over a period of 5 days

(POCOP)Co(Ph)(SPh) (**516**). (POCOP)Co(Ph)(I) (**515**) (40 mg, 0.067 mmol) was dissolved in ∼5 mL of THF in a Schlenk flask, and the solution was cooled to −35 °C. To this was added sodium thiophenolate (10 mg, 0.069 mmol) while the mixture was being stirred. The reaction mixture was left to stir at RT for 1 h. The volatiles were pumped off, and the products were extracted by pentane and filtered through a pad of Celite on a glass frit. The volatiles were removed under vacuum, producing a brownish yellow powder. This material was extracted with ∼3 mL of cold $(Me_3Si)_2O$, and the resultant solution was placed in the freezer for recrystallization at −35 °C. Overnight recrystallization yielded **516** as a brown powder (30 mg, 84%): ^1H NMR (500 MHz, C_6D_6) δ 8.30 (bs, 1H, Ph-*H*), 7.77−7.72 (m, 2H, Ar-*H*), 7.07−6.91 (overlapping m, 4H, Ar-*H*), 6.74 (d, *J* = 9 Hz, 2H, Ar-*H*), 6.61 (t, *J* = 5.8 Hz, 2H, Ar-*H*), 6.34 (bs, 1H, Ph-*H*), 5.38 (bs, 1H, Ph-*H*), 2.42 (m, 2H, C*H*Me$_2$), 2.32 (m, 2H, C*H*Me$_2$), 1.17− 1.02 (overlapping dvt, 18H, CH*Me*$_2$), 0.72 (dvt, *J* = 7.6 Hz, *J* = 7.4 Hz, 6H, CH*Me*$_2$); $^{13}C\{^1H\}$ NMR (75 MHz,

C_6D_6) δ 169.0 (t, *J* = 9 Hz, *C*-Co), 141.7 (s), 137.2 (s), 133.5 (s), 124.6 (br), 123.6 (s), 106.2 (t, *J* = 5.5 Hz, *C*-O), 29.8 (t, *J* = 8.5 Hz, *C*HMe$_2$), 29.1 (t, *J* = 11.7 Hz, *C*HMe$_2$), 19.6 (t, *J* = 1.6 Hz, CH*Me*$_2$), 17.1 (t, *J* = 2.2 Hz, CH*Me*$_2$), 16.5 (s, CH*Me*$_2$), 16.2 (s, CH*Me*$_2$); $^{31}P\{^1H\}$ NMR (120 MHz, C_6D_6) δ 183.3 (bs). Anal. Calcd. for $C_{30}H_{41}CoO_2P_2S$: C, 61.43; H, 7.05. Found: C, 61.61; H, 6.91.

5.4.3 Thermolysis and Stability Studies on (POCOP)Co^{III} Complexes

Decomposition of (POCOP)Co(Ph)(Cl) (513) at RT. **513** (8.1 mg, 0.016 mmol) was dissolved in ~600 μL of C_6D_6 in a PTFE-capped J. Young NMR tube. 1,4-Dioxane (2 μL, 2 mg, 0.02 mmol) was added using a syringe to serve as an internal standard. The NMR tube was left at RT for several days, and the decomposition of **513** was monitored by ^{1}H NMR spectroscopy. After 4 days, the composition of the reaction mixture as observed by ^{1}H NMR was **513** (70% of the initial concentration), **501** [28% of the initial concentration of **513**], and **507** [<2 % of the initial concentration of **513**]. Biphenyl [14% of the initial concentration of **513**] was also observed.

Decomposition of (POCOP)Co(Ph)(Cl) (513) at RT with BHT as a radical inhibitor. 513 (8.1 mg, 0.016 mmol) was dissolved in ~600 μL of C_6D_6 in a PTFE-capped J. Young NMR tube. 1,4-Dioxane (2 μL, 2 mg, 0.02 mmol) was added using a syringe to serve as an internal standard. BHT (3.5 mg, 0.016 mmol) was also added to this mixture. The NMR tube was left at RT for several days, and the decomposition of **513** was monitored by ^{1}H NMR spectroscopy. After 4 days, the composition of the reaction mixture as observed by ^{1}H NMR was **513** (75% of the initial concentration), **501** [24% of the initial

concentration of **513**], and **507** [<1% of the initial concentration of **513**]. Biphenyl [12% of the initial concentration of **513**] was also observed.

Thermolysis of (POCOP)Co(Ph)(SPh) (516) with an internal standard. 516 (4 mg, 7 μmol) was dissolved in ~600 μL of C_6D_6 in a PTFE-capped J. Young NMR tube. 1,4-Dioxane (2 μL, 2 mg, 0.02 mmol) was added using a syringe to serve as an internal standard. The NMR tube was then placed in an oil bath at 80 °C for 30 min. Upon analysis of the sample by ^{1}H and ^{31}P NMR spectroscopy, 80% conversion to **519** was observed: ^{1}H NMR (C_6D_6) δ 7.52−7.42 (m, 3H, Ar-*H*), 7.36−7.24 (overlapping m, 5H, Ar-*H*), 7.22−7.05 (m overlapping with solvent, 4H, Ar-*H*), 7.22−7.05 (overlapping m, 2H, Ar-*H*), 1.55 (m, 4 H, C*H*Me$_2$), 0.99−0.81 (m, 24H, CH*Me*$_2$); $^{31}P\{^{1}H\}$ NMR (C_6D_6) δ 148.7.

Scaled-up thermolysis of (POCOP)Co(Ph)(SPh) (516) with an internal standard and subsequent hydrolysis and analysis of the obtained products. 516 (34 mg, 58 μmol) was dissolved in ~600 μL of C_6D_6 in a PTFE-capped J. Young NMR tube. 1,4-Dioxane (2 μL, 2 mg, 0.02 mmol) was added using a syringe to serve as an internal standard. The NMR tube was then placed in an oil bath at 80 °C for 30 min. Upon analysis of the sample by ^{1}H and ^{31}P NMR spectroscopy, 80% conversion to **519** was observed, with the rest of the **516** converting to **507** and other unidentified decomposition products. The volatiles were removed in vacuo, and the solids were redissolved in ~2 mL of CH_2Cl_2. The solution was washed with 3 × 5 mL of concentrated HCl followed by 3 × 5 mL of distilled water. The organic layer was extracted and passed through silica, and the volatiles were removed in vacuo to yield a pale yellow solid. The solid was washed with 2 × 2 mL of hexanes and dried in vacuo to give a solid **520** (7 mg, 66%). ^{1}H and ^{13}C NMR data for

520 matched those of 2-phenylresorcinol: ^{1}H NMR (C_6D_6, 500 MHz) δ 7.58 (t, *J* = 7.5 Hz, 2H, Ar-*H*), 7.49 (t, *J* = 7.5 Hz, 1H, Ar-*H*), 7.43 (d, *J* = 7.0 Hz, 2H, Ar-*H*), 7.15 (t, *J* = 7.5 Hz, 1H, Ar-*H*), 6.59 (d, *J* = 8.0 Hz, 2H, Ar-*H*), 4.83 (s, 2H, O-*H*); ^{13}C{^{1}H} NMR (C_6D_6, 126 MHz) δ 153.6, 131.0, 130.8, 130.4, 129.7, 129.4, 115.5, 107.8.

5.4.4 Synthesis of Co Complexes Supported by ^{tBu}POCOP^{iPr}

Attempted metalation using 1 eq. $CoCl_2$ and 1 eq. DMAP. In an Ar-filled glove, a 50 mL culture tube was charged with $^{t\text{Bu}}$POCOP$^{i\text{Pr}}$ (756 mg, 1.7 mmol), $CoCl_2$ (215 mg, 1.7 mmol), and DMAP (216 mg, 1.8 mmol). Dioxane (20 mL) was added to these solids and the tube was heated in a 90 °C oil bath overnight. The solution was filtered through a pad of Celite, dried *in vacuo*, and the residue was extracted with pentane and placed in a -35 °C freezer in the glove box. The solution produced very large crystals overnight. Among these crystals was ($^{t\text{Bu}}$POCOP)Co(Cl)(DMAP) (**522**) which was characterized by X-ray diffractometry. However, ^{1}H NMR resonances corresponding to **522** were not located. The ^{1}H NMR spectrum for the obtained solids shows a variety of diamagnetic material including free ligand and a second set of shifted isopropyl methyl resonances which have not been identified.

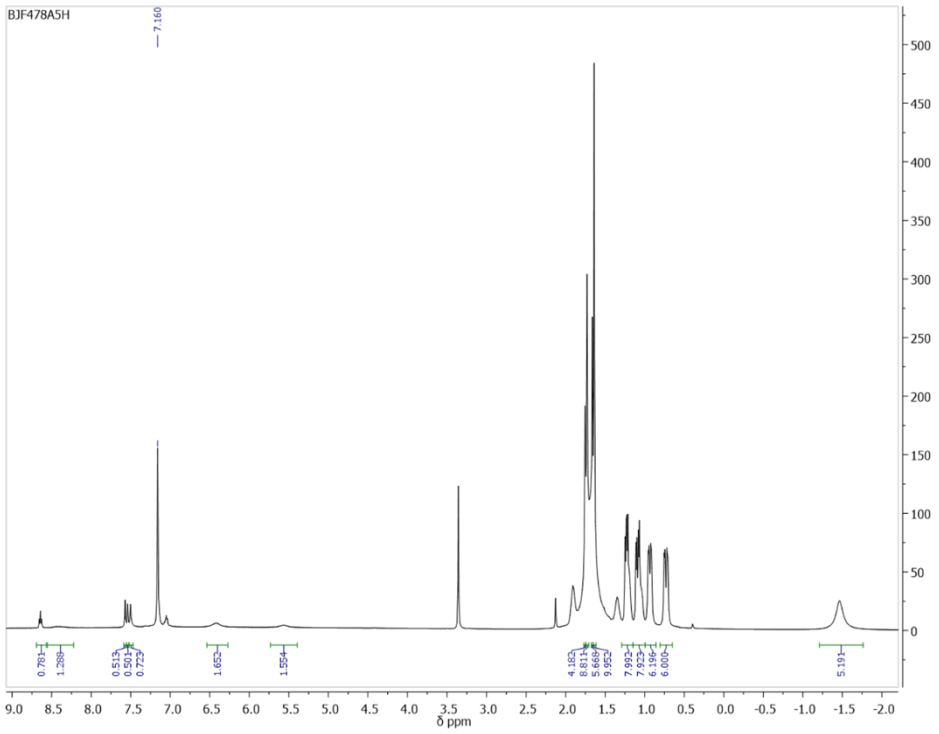

Figure V-7. ^{1}H NMR (C_6D_6, 500 MHz) of the reaction mixture resulting from the addition of 1 eq. $CoCl_2$ and 1 eq. DMAP to ($^{t\text{Bu}}$POCOP)H.

($^{t\text{Bu}}$POCOP)CoCl (521). In an Ar-filled glove, a 50 mL culture tube was charged with ($^{t\text{Bu}}$POCOP)H (654 mg, 1.4 mmol), $CoCl_2$ (399 mg, 3.1 mmol), and 12 mL dioxane. The tube was swirled by hand to help mix the suspension of $CoCl_2$ with the ligand. DMAP (394 mg, 3.2 mmol) was then added resulting in the formation of a blue precipitate and a yellow supernatant (Note: this may mean the reaction proceeds at RT, the yellow supernatant in the synthesis of **501** is indicative that **501** is being formed). The culture tube was heated in an 80 °C oil bath overnight. The contents of the tube were filtered through a pad of Celite and the volatiles were removed *in vacuo*. The residue was extracted with pentane and a small amount of PhF was added to help with dissolution. The suspension was filtered through a plug of Celite and the volatiles were removed *in vacuo*. The residue

was dissolved in 20 mL pentane leaving behind a small amount of blue precipitate. This supernatant was filtered again through a plug of Celite and placed into a -35 °C freezer within the glovebox affording **521** as a crystalline solid suitable for X-ray diffraction analysis (430 mg, 54%). ^{1}H NMR (500 MHz, C_6D_6) δ 46.26 (4H), 12.51 & 11.57 (overlap, 24H), 1.45 (18H), -60.71 (1H).

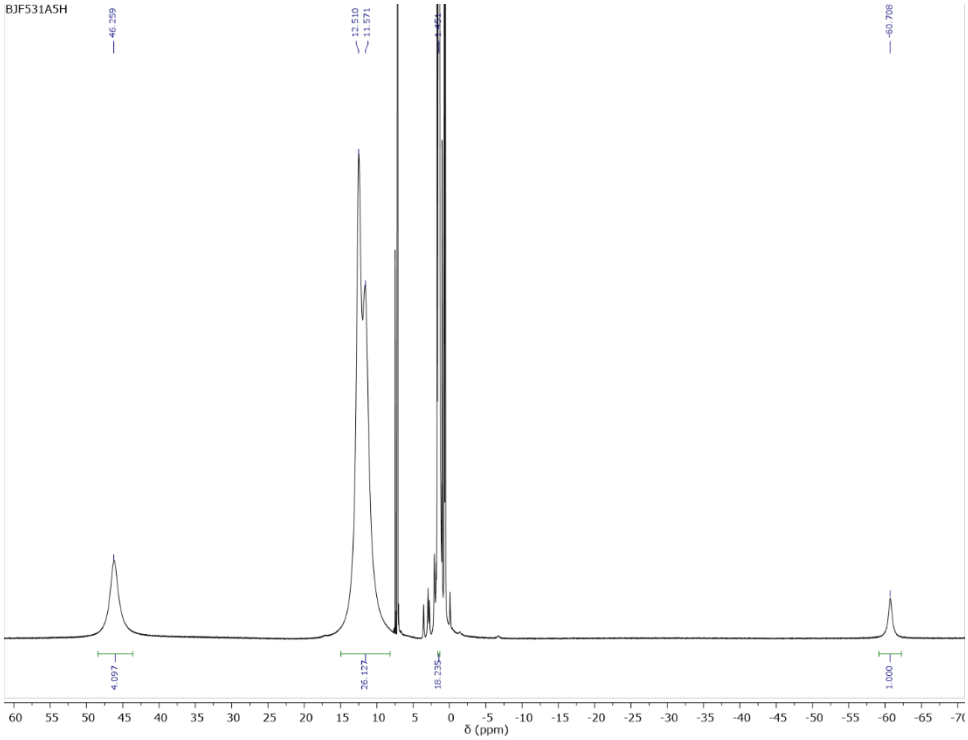

Figure V-8. ^{1}H NMR (500 MHz, C_6D_6) spectrum of **521**.

Spectroscopic observation of (^{tBu}POCOP)CoPh (523). In an Ar-filled glove, a 20 mL scintillation vial was charged with **521** (430 mg, 0.79 mmol) and dissolved in 12 mL toluene. To this stirring solution was added PhLi (445 µL of a 1.8 M stock solution, 0.80 mmol) in two portions. This solution was allowed to stir overnight. The solution was filtered through a pad of Celite and the volatiles were removed *in vacuo* in a 50 °C water

bath. The residue was dissolved in pentane and placed in a -35 °C freezer in the glovebox for multiple days resulting in the formation of only a few solids. No further isolation was attempted. ^{1}H NMR spectroscopic analysis of these solids showed the expected pattern for **523**. ^{1}H NMR (400 MHz, C_6D_6) δ 42.22 (4H), 13.12 (12H), 12.08 (1H), 7.99 (12H), 2.20 (18H), -13.66 (1H), -21.07 (2H), -49.93 (2H).

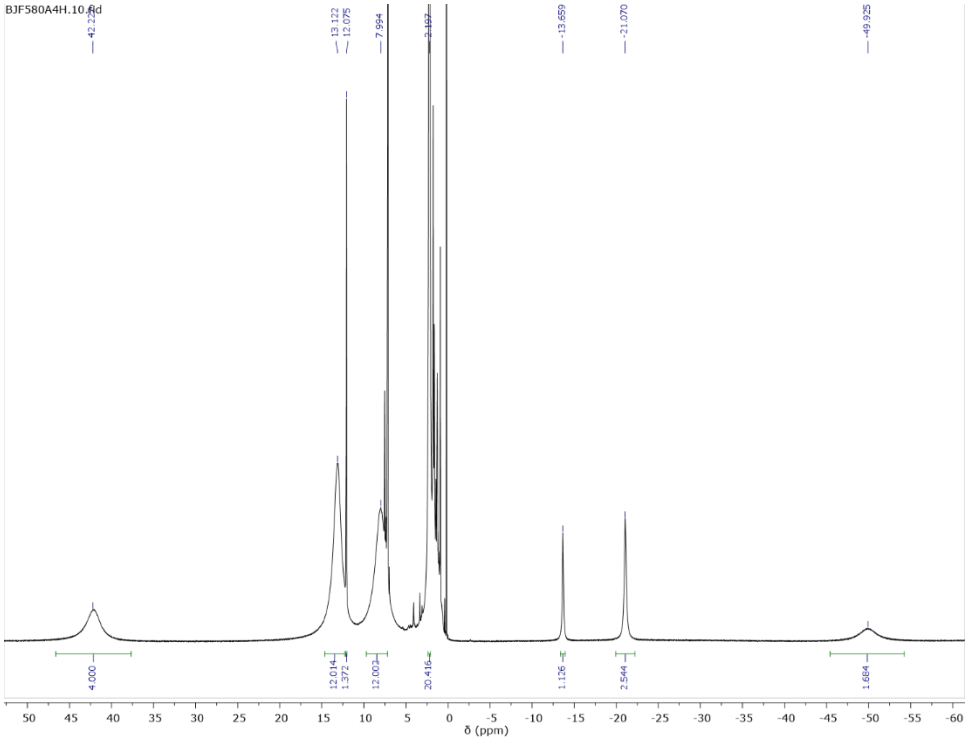

Figure V-9. ^{1}H NMR (400 MHz, C_6D_6) spectrum of **523**.

5.4.5 Spectra from Attempted Synthesis of (POCOP)Co(F)

Attempt at synthesizing (POCOP)Co(F) (509) with 3.6 eq. CsF. In an Ar-filled glove box, a scintillation vial was charged with **504** (162 mg, 0.29 mmol), CsF (160 mg, 1.0 mmol), and 10 mL PhF. The contents of the vial were stirred overnight. The volatiles were removed *in vacuo* and the residue was extracted with pentane. The extract was

filtered through a pad of Celite and placed in a -35 °C freezer overnight. The resulting crystals, as analyzed by ^{1}H NMR spectroscopy, were pure **504**.

Attempt at synthesizing (POCOP)Co(F) (509) with CsF in large excess. In an Ar-filled glove box, a scintillation vial was charged with **504** (50 mg, 0.091 mmol), CsF (185 mg, 1.2 mmol), and 10 mL PhF. The contents of the vial were stirred overnight. The volatiles were removed *in vacuo* and the residue was extracted with C_6D_6 for ^{1}H NMR analysis (ca. 10% conversion was observed, Figure V-11 Top). The NMR sample was poured back into the original vial and more CsF (940 mg, 6.2 mmol) was added along with 10 mL PhF. After stirring overnight, the volatiles were removed and the residue was extracted with pentane, filtered through Celite, and dried *in vacuo*. ^{1}H NMR analysis of this residue revealed a new set of paramagnetically shifted resonances that were not recognized (Figure V-11 Bottom).

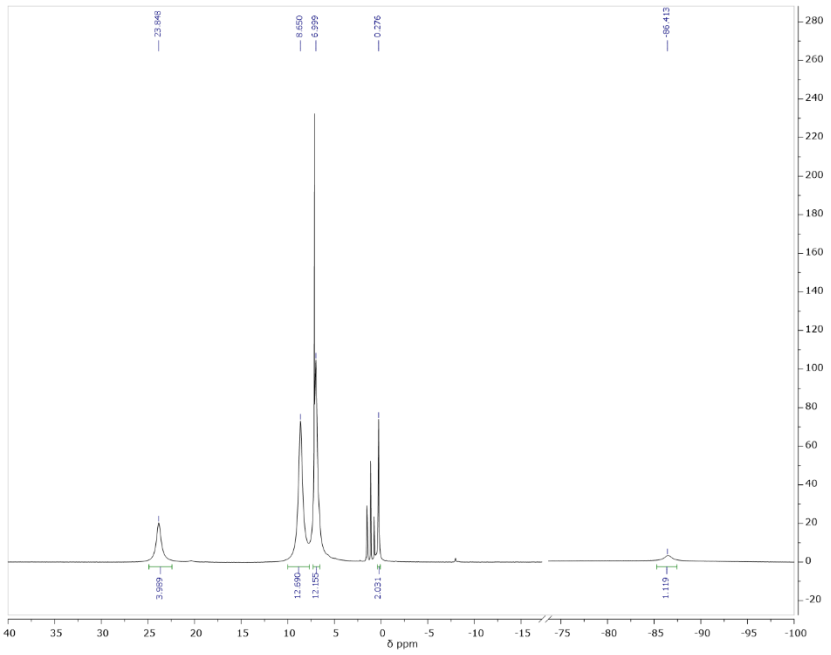

Figure V-10. ^{1}H NMR (500 MHz, C_6D_6) spectrum of (POCOP)Co(F) reported previously.

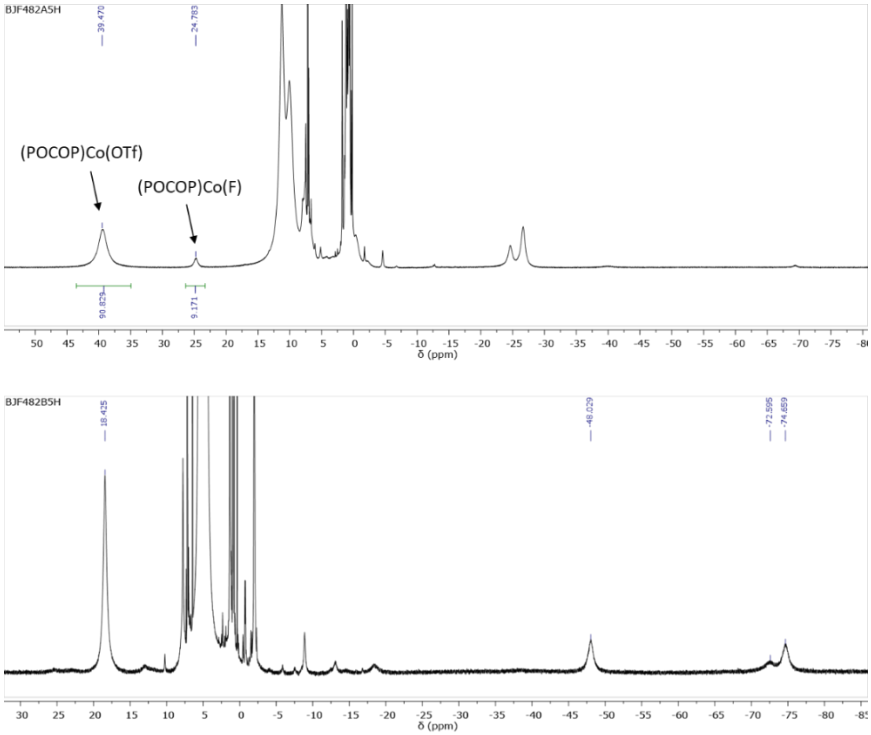

Figure V-11. New attempt at synthesizing (POCOP)Co(F). Top: ^{1}H NMR (500 MHz, C_6D_6) spectrum of mixture after 3.6 eq. CsF. Bottom: ^{1}H NMR (500 MHz, C_6D_6) spectrum of mixture after addition of 68 eq. CsF.

5.4.6 X-Ray Crystallography

X-Ray data collection, solution, and refinement for (POCOP)Co(SPh) (508). A single orange crystal of suitable size and quality (0.06 × 0.08 × 0.10 mm) was selected from a representative sample of crystals of the same habit using an optical microscope, mounted onto a nylon loop and placed in a cold stream of nitrogen (110 K). Low-temperature X-ray data were obtained on a Bruker APEXII CCD based diffractometer (Mo sealed X-ray tube, K_α = 0.71073 Å). All diffractometer manipulations, including data collection, integration and scaling were carried out using the Bruker APEXII software.[135] An absorption correction was applied using SADABS.[174] The space group was determined

on the basis of systematic absences and intensity statistics and the structure was solved by direct methods and refined by full-matrix least squares on F^2. The structure was solved in the monoclinic $P_{21/c}$ space group using XS[138] (incorporated in X-Seed). This symmetry was confirmed by PLATON.[139] All non-hydrogen atoms were refined with anisotropic thermal parameters. Hydrogen atoms were placed in idealized positions and refined using riding model. The structure was refined (weighted least squares refinement on F^2) to convergence.

X-Ray data collection, solution, and refinement for (POCOP)Co(Ph)(I) (515). A green, multi-faceted crystal of suitable size and quality (0.09 x 0.06 x 0.04 mm) was selected using an optical microscope and mounted onto a nylon loop. Low temperature (150 K) X-ray data were obtained on a Bruker APEXII CCD based diffractometer (Mo sealed X-ray tube, K_α = 0.71073 Å). All diffractometer manipulations, including data collection, integration and scaling were carried out using the Bruker APEXII software.[135] An absorption correction was applied using SADABS.[174] The structure was initially solved in the monoclinic $P_{21/n}$ space group using XS[138] (incorporated in SHELXTL). The solution was refined by full-matrix least squares on F^2. No additional symmetry was found using ADDSYMM incorporated into the PLATON program.[139] All non-hydrogen atoms were refined with anisotropic thermal parameters. All hydrogen atoms on the main residue were placed in idealized positions and refined using a riding model. The structure was refined (weighted least squares refinement on F^2) and the final least-squares refinement converged to R_1 = 0.0404 ($I > 2\sigma(I)$, 5597 data) and wR_2 = 0.1062 (F^2, 6849 data, 278 parameters).

X-Ray data collection, solution, and refinement for (POCOP)Co(Ph)(SPh) (516). A dark red, multi-faceted crystal of suitable size and quality (0.08 x 0.06 x 0.04 mm) was selected using an optical microscope and mounted onto a nylon loop. Low temperature (150 K) X-ray data were obtained on a Bruker APEXII CCD based diffractometer (Mo sealed X-ray tube, K_α = 0.71073 Å). All diffractometer manipulations, including data collection, integration and scaling were carried out using the Bruker APEXII software.[135] An absorption correction was applied using SADABS.[174] The structure was initially solved in the monoclinic $P_{21/c}$ space group using XS[138] (incorporated in SHELXTL). The solution was refined by full-matrix least squares on F^2. No additional symmetry was found using ADDSYMM incorporated into the PLATON program.[139] All non-hydrogen atoms were refined with anisotropic thermal parameters. The structure was refined (weighted least squares refinement on F^2) and the final least-squares refinement converged to R_1 = 0.0348 ($I > 2\sigma(I)$, 5592 data) and wR_2 = 0.0929 (F^2, 7005 data, 333 parameters).

X-Ray data collection, solution, and refinement for (^{tBu}POCOP)Co(Cl) (521). A Leica MZ 7$_5$ microscope was used to identify a suitable red block with very well defined faces with dimensions (max, intermediate, and min) 0.473 x 0.434 x 0.304 mm^3 from a representative sample of crystals of the same habit. The crystal mounted on a nylon loop was then placed in a cold nitrogen stream (Oxford) maintained at 110 K.

A BRUKER APEX 2 Duo X-ray (three-circle) diffractometer was employed for crystal screening, unit cell determination, and data collection. The goniometer was controlled using the APEX3 software suite, v2017.3-0.[135] The sample was optically centered with the aid of a video camera such that no translations were observed as the

crystal was rotated through all positions. The detector was set at 6.0 cm from the crystal sample (APEX2, 512x512 pixel). The X-ray radiation employed was generated from a Mo sealed X-ray tube (K_α = 0.71073Å with a potential of 40 kV and a current of 40 mA).

45 data frames were taken at widths of 1.0°. These reflections were used in the auto-indexing procedure to determine the unit cell. A suitable cell was found and refined by nonlinear least squares and Bravais lattice procedures. The unit cell was verified by examination of the *h k l* overlays on several frames of data. No super-cell or erroneous reflections were observed.

After careful examination of the unit cell, an extended data collection procedure (4 sets) was initiated using omega scans.

Integrated intensity information for each reflection was obtained by reduction of the data frames with the program APEX3.[135] The integration method employed a three dimensional profiling algorithm and all data were corrected for Lorentz and polarization factors, as well as for crystal decay effects. Finally, the data was merged and scaled to produce a suitable data set. The absorption correction program SADABS[174] was employed to correct the data for absorption effects.

Systematic reflection conditions and statistical tests of the data suggested the space group $P2_1/n$. A solution was obtained readily using XT/XS in APEX2.[135,138] Hydrogen atoms were placed in idealized positions and were set riding on the respective parent atoms. All non-hydrogen atoms were refined with anisotropic thermal parameters. Absence of additional symmetry and voids were confirmed using PLATON (ADDSYM).[139] The structure was refined (weighted least squares refinement on F^2) to

convergence.[138],[140] Olex2 was employed for the final data presentation and structure plots.[140]

X-Ray data collection, solution, and refinement for (^{tBu}POCOP)Co(Cl)(DMAP) (522). A Leica MZ 75 microscope was used to identify a suitable small red needle with very well defined faces with dimensions (max, intermediate, and min) 0.025 x 0.015 x 0.013 mm^3 from a representative sample of crystals of the same habit. The crystal mounted on a nylon loop was then placed in a cold nitrogen stream (Oxford) maintained at 100 K.

A BRUKER Venture X-ray (kappa geometry) diffractometer was employed for crystal screening, unit cell determination, and data collection. The goniometer was controlled using the APEX3 software suite.[135] The sample was optically centered with the aid of a video camera such that no translations were observed as the crystal was rotated through all positions. The X-ray radiation employed was generated from a Cu-Iμs X-ray tube (K_α = 1.5418Å with a potential of 50 kV and a current of 1.0mA).

45 data frames were taken at widths of 1°. These reflections were used to determine the unit cell. The unit cell was verified by examination of the *h k l* overlays on several frames of data. No super-cell or erroneous reflections were observed.

After careful examination of the unit cell, an extended data collection procedure (20 sets) was initiated using omega and phi scans.

Integrated intensity information for each reflection was obtained by reduction of the data frames with the program APEX3.[135] The integration method employed a three dimensional profiling algorithm and all data were corrected for Lorentz and polarization

factors, as well as for crystal decay effects. Finally the data was merged and scaled to produce a suitable data set. The absorption correction program SADABS[174] was employed to correct the data for absorption effects.

Systematic reflection conditions and statistical tests of the data suggested the space group *Pnma*. A solution was obtained readily (Z=4; Z'=0.5) using XT/XS in APEX3.[135,138] A molecule of toluene was found solvated; disordered between two positions related by symmetry with half occupancy each. Hydrogen atoms were placed in idealized positions and were set riding on the respective parent atoms. All non-hydrogen atoms were refined with anisotropic thermal parameters. Absence of additional symmetry or void were confirmed using PLATON (ADDSYM).[139] The structure was refined (weighted least squares refinement on F^2) to convergence.[138,140] Olex2 was employed for the final data presentation and structure plots.[140]

CHAPTER VI

MECHANISTIC INSIGHT INTO C–S BOND FORMATION AT (PNP)CO

6.1 Introduction

Carbon-heteroatom cross-coupling has become an immensely powerful synthetic tool in recent years.[210] The existing art on cross-coupling reactions is historically dominated by palladium,[1] with additional prominence by another group 10 metal Ni,[178c,211] as well as a group 11 metal Cu.[13] There has recently been a renewed push to find alternatives to homogeneous precious metal catalysts from among cheaper, more Earth-abundant metals.[182a,212]

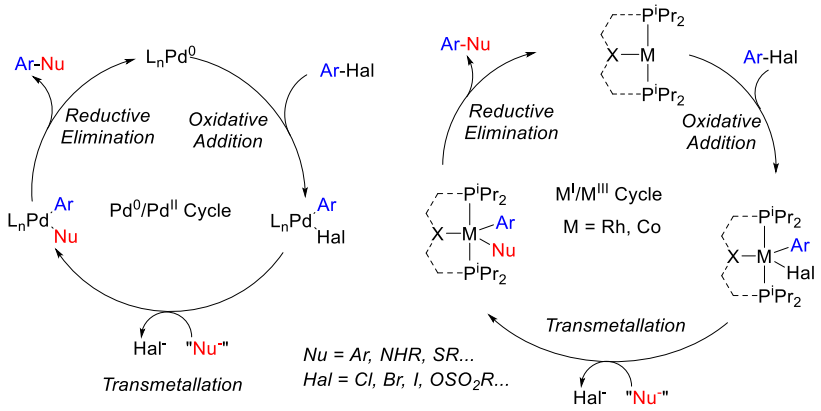

Figure VI-1. Cross-coupling mechanistic cycles for Pd^0/Pd^{II} (left) and for Rh^I/Rh^{III} or Co^I/Co^{III} (right).

Cross-coupling reactions of aryl (pseudo)halides with nucleophiles typically rely on the oxidative addition (OA) – transmetallation (TM) – reductive elimination (RE) cycles such as depicted in Figure VI-1. The OA and RE steps are two-electron processes that are well established for Pd. Our group has been interested in the potential of the

analogous OA-TM-RE cycle to enable cross-coupling catalysis by group 9 metals. Pd (and Ni) go through the M^0/M^{II} oxidation states corresponding to the d^{10}/d^8 configurations. For group 9 metals, we have targeted the M^I/M^{III} oxidation states (d^8/d^6). In particular, we were able to establish that a T-shaped Rh^I center supported by an anionic pincer ligand possesses a rather striking similarity in its reactivity to the LPd^0 fragment.[30,31b,183,208] This approach with Rh proved especially fruitful in catalytic C-S coupling.[18]

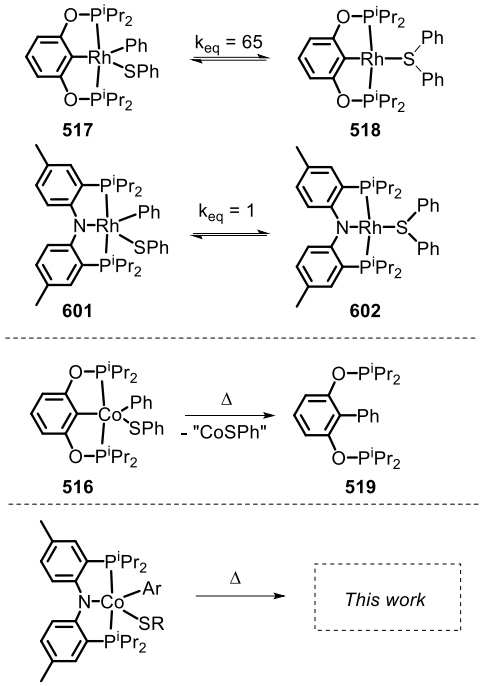

Scheme VI-1. C–S coupling observed for the (POCOP)Rh(Ph)(SPh) (**517**) and (PNP)Rh(Ph)(SPh) (**601**) complexes (Top), C–C coupling with the pincer carbon in (POCOP)Co(Ph)(SPh) **516** (Middle), and the subject of this work (bottom).

It is easy to envisage the steps of the analogous pincer-supported $Co^{I/III}$ cycle (Figure VI-1). However, in the chemistry of 3d metals, competition from one-electron pathways to the desired two-electron steps is something that must be closely considered.[182b] In principle, there is a substantial body of literature describing Co-based

cross-coupling catalysis.[14] and Co^{I}/Co^{III} cycles are often proposed.[187-188,213] However, firm mechanistic information remains rather limited. Fout and coworkers analyzed a Co-catalyzed aryl halide amination system in 2014[61] where the Co^{I}/Co^{III} cycle was strongly implicated but the individual steps of OA and RE were not observed. Chirik et al. reported on the C-C coupling of aryl triflates in 2016, where it appears that the Co^{I}/Co^{III} cycle should operate but the details were not uncovered.[194] Bernskoetter's group reported a well-defined example of C-C RE from Co^{III} in 2011,[190] but this involved coupling of two CH_3 groups, only indirectly related to aryl halide reactions. However, outside of aryl halide coupling reactions, there have in recent years appeared examples of homogeneous catalysis by pincer-supported Co complexes where two-electron OA/RE steps are either well understood or strongly suggested.[35b,65,103,190,195a,196a-c,196e,214]

In 2018, we reported on the reactivity of (POCOP)Co(Ph)(SPh) (**516**).[31a] In contrast to (POCOP)Rh(Ph)(SPh) (**517**) or (PNP)Rh(Ph)(SPh) (**601**), it did not undergo C–S RE but instead a RE of the phenyl with the pincer aryl (Scheme VI-1). Because of this, the POCOP system did not allow for the investigation of the C-S RE. We surmised that the analogous RE with the amido of a PNP pincer should be less likely and set off to examine the reactivity of (PNP)Co(Ar)(SAr) complexes. The present report details our efforts in the synthesis of five-coordinate Co^{III}-aryl/thiolate complexes supported by the PNP ligand, their propensity to undergo concerted C-S RE, and the subsequent comproportionation reactivity that again diverges from the Rh system.

6.2 Results and Discussion

6.2.1 Synthesis and Characterization of (PNP)Co^{II} Complexes

Treatment of the previously reported square planar, low spin, S = ½ (PNP)Co(Cl) (**603**)[215] with selected aryl nucleophiles resulted in the formation of the corresponding Co^{II} aryl complexes (Scheme VI-2). Clean transmetalation of **603** was also accomplished using sodium thiophenolate reagents to give Co(II) thiolate complexes **605a-605c** (Scheme VI-2). Complexes **604a-604c** were green to dark teal in color. They exhibited paramagnetically shifted ^{1}H NMR resonances contained in the +40 to -30 ppm range, except for the resonances at around -90 ppm in complexes **604a-604c** which we tentatively assign as *ortho*-hydrogens of the Co-bound aryl rings. No ^{31}P NMR resonances were detected for these complexes.

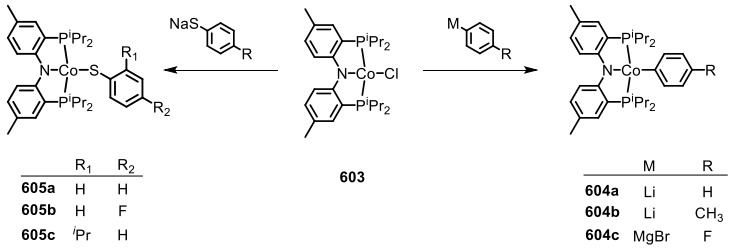

	R$_1$	R$_2$
605a	H	H
605b	H	F
605c	^{i}Pr	H

	M	R
604a	Li	H
604b	Li	CH_3
604c	MgBr	F

Scheme VI-2. Transmetalation reactions among (PNP)Co^{II}(X)

Examination of the literature shows that four-coordinate Co(II) complexes of anionic pincer ligands are known with both a low-spin S= ½ configuration (square-planar geometry) and a high-spin S = $^{3}/_{2}$ configuration (pseudotetrahedral geometry). Low-spin, square-planar Co(II) complexes give rise to paramagnetically shifted ^{1}H NMR resonances that are broad compared to diamagnetic compounds, but are typically interpretable in terms of their relative integration and chemical (in)equivalence. High-spin Co(II)

compounds tend to produce ^{1}H NMR spectra that are broadened beyond useful interpretation. Complexes **604a-c** and **605a-c** in the present work and the (POCOP)CoX complexes (Figure VI-2) recently reported by us[31a] and Heinekey et al.[216] are all low-spin compounds. The same is true for the (PNP1)CoX complexes of the pyrrolyl-based PNP ligand by Tonzetich et al.[217] and Nishibayashi et al.[218] In contrast, Co(II) halide complexes of the Fryzuk-type PNP2 and Gade's carbazole-based PNP3 ligands are high-spin.[200,219,220] On the other hand, (PNP2)Co(CH_2Ph) and (PNP3)CoH are low spin.[200,220] It is clear that the presence of even one strong-field ligand such as hydride or aryl/alkyl ensures the low-spin configuration, but it is interesting that the various Co^{II} complexes in Figure VI-2 contain low and high-spin complexes with essentially the same set of donors. (e.g., high-spin (PNP2)CoCl vs low-spin (PNP)CoCl (**603**) or (PNP1)CoBr) We surmise that the geometric constraint of the ligand plays a role in enforcing the corresponding geometry and thus spin state, with the less flexible PNP and PNP1 favoring square planar, low-spin Co^{II}.

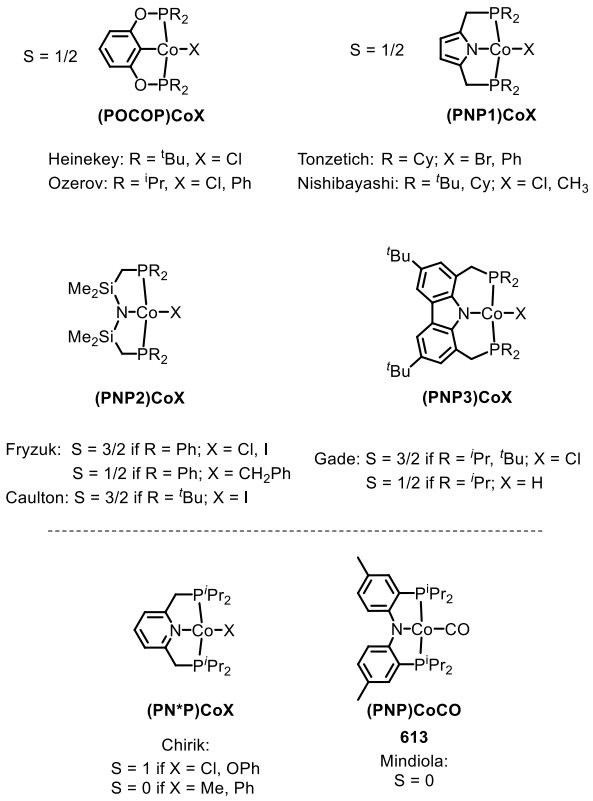

Figure VI-2. High and low spin dichotomy in POCOP and PNP pincer-supported four-coordinate complexes of Co^{II} (top) and Co^{I} (bottom).

6.2.2 Synthesis and Characterization of (PNP)Co^{III}(Ar)(X) Complexes

As is the case in our (POCOP)Co system,[31a] reacting (PNP)Co(Aryl) complexes (**604a** and **604b**) with 0.5 eq. of $PhI(OAc)_2$ led to the clean formation of (PNP)Co(Aryl)(OAc) (**606a** and **606b)**, isolated in good yield as tan solid after workup (Scheme VI-3). Treatment of **606a** or **606b**with Me_3SiI furnished (PNP)Co(Aryl)(I) complexes **607a** and **607b**. **607a** and **607b** can also be prepared via reaction of **604a** and **604b** with 0.5 equiv. of I_2. Transmetalation from **607a** or **607b** using sodium thiophenolate or 4-fluorothiophenolate proceeded smoothly providing (PNP)Co(Aryl)(S-Aryl)

complexes **608a-c** as dark blue solids in good yields after recrystallization (Scheme VI-3).

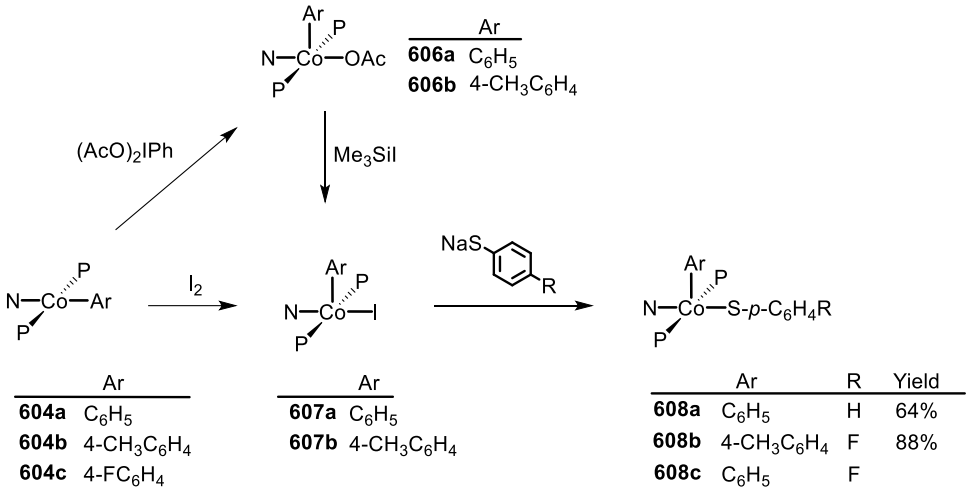

Scheme VI-3. Oxidation of (PNP)Co^{II} and synthesis of target (PNP)Co(Ar)(S-Ar)

The (PNP)Co(Ar)(X) compounds gave rise to ^{1}H, ^{31}P, and ^{13}C NMR spectra expected for these diamagnetic complexes. The resonances arising from the Co-bound aryl group exhibited inequivalence between the two ortho- and between the two meta-hydrogens, characteristic of restricted rotation of the metal-bound aryl oriented *cis* to the central donor of a pincer ligand with two side –PPr$^{i}_{2}$ arms.[31] In the cases of the aryl/-thiolate complexes **608a**-**608c**, these aromatic resonances were broad humps, whereas in the aryl/-halide **607a**-**607b** and aryl/-acetato complexes **606a**-**606b**, sharp resonances with well-resolved fine structure were observed.

6.2.3 Synthesis and Characterization of (PNP)Co^{I} Complexes

Treatment of **611**[61] with **201a** liberated triphenyl phosphine and $HN(SiMe_3)_2$. A wide ^1H NMR spectral window revealed a new set of paramagnetically shifted ^1H NMR resonances which we have assigned to **610** (Scheme VI-4). **610** appears to be in equilibrium with diamagnetic **609** (previously reported by Mindiola et al.)[215] on the timescale of experimental handling, as freshly made (PNP)Co(PPh_3) (**610**) was observed to produce **609** when left overnight in a -35 °C freezer, while addition of 12 equiv. of PPh_3 to **609** led to the observation of **610** (Scheme VI-4). Addition of 12 eq. of tris(4-methoxyphenyl)phosphine to this mixture gave rise to a second set of distinct but very similar paramagnetically shifted ^1H NMR resonances we interpret as belonging to **612**. This observation supports the notion that **610** is a PPh_3-bound Co complex.

Based on the paramagnetically shifted ^1H NMR spectra, we assume that both **610** and **612** possess an S = 1 ground state. As with four-coordinate Co(II), there are examples of both high-spin and low-spin pincer complexes of Co(I) (S = 1 or 0) (Figure VI-2, bottom). With the pyridine-centered PN*P ligand, complexes substituted with stronger field Me or Ph are low-spin, while Cl or OAr as the fourth donor are high-spin.[194,195b] With the PNP ligand, CO in place of PPh_3 in **610** was reported to give a low-spin carbonyl complex (PNP)Co(CO) (**613**). Thus, it appears that the presence of at least one strong-field ligand (CO, or hydride/alkyl/aryl) is needed to ensure an S = 0 ground state.

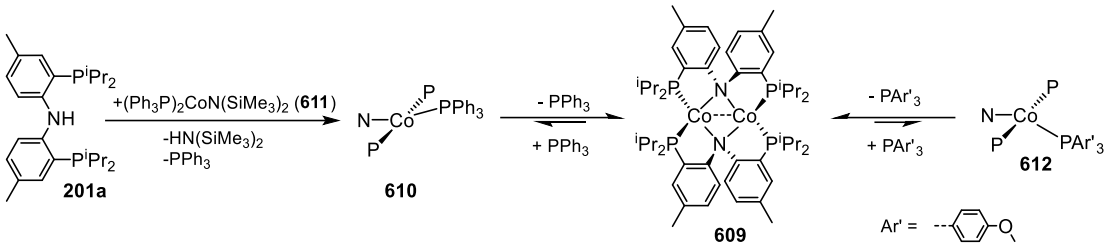

Scheme VI-4. Formation of proposed (PNP)Co(PPh_3) (**610**) and equilibrium between $(PNP)_2Co_2$ (**609**) and (PNP)Co($P(Ar)_3$) (**612**).

6.2.4 X-ray Structural Studies

Single crystals of **604b**, **606a**, and **608a** suitable for X-ray diffraction were grown from hydrocarbon solvents at -35 °C (Figure VI-3). The geometry about the cobalt center in the solid-state structure of **604b** is slightly distorted square planar. The Co-bound tolyl ring in **604b** is approximately perpendicular to the Co/P/N/P plane.

606a is a pseudo-octahedral complex with a κ^2 acetate coordination. The two oxygens of the acetate are bound *trans* to two donors of markedly different *trans*-influence (amido N vs phenyl C), which is reflected in the large difference between the two Co-O bond distances (ca. 0.13 Å). The geometry about Co in **608a** is intermediate between square-pyramidal with the phenyl *trans* to the empty site and Y-shaped (with the thiolate at the base of the Y). The preference of low-spin five-coordinate d^6 complexes for square-pyramidal and Y-shaped geometries have been discussed elsewhere.[29] The angles, bond

lengths, and orientation of the thioaryl ligand about the cobalt center for **608a** are similar to those that we reported for **516**.

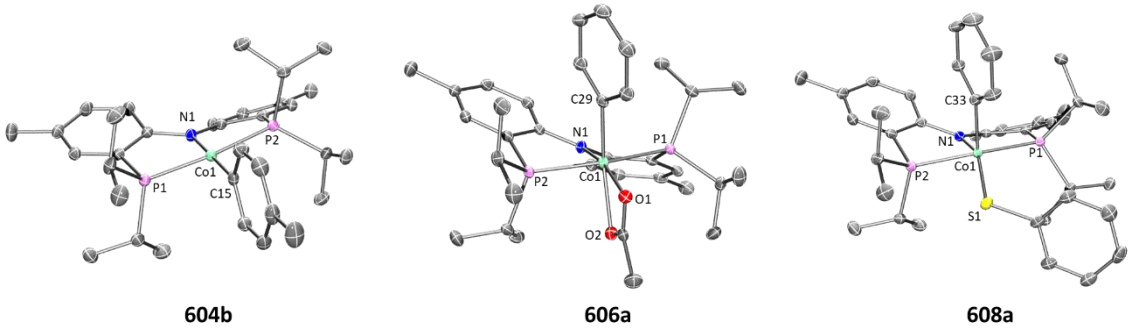

Figure VI-3. POV-Ray renditions of ORTEP plots (50% probability ellipsoids) of **604b**, **606a**, and **608a**. All hydrogen atoms omitted. Selected bond distances (Å) and angles (degrees) for (PNP)Co(Tol) (**604b**, left): N1–Co1, 1.9262(17); P1–Co1, 2.1756(7); P2–Co1, 2.1849(7); C15–Co1, 1.939(2); N1–Co1–C15, 178.99(9); P1–Co1–P2, 172.63(3). Selected bond distances (Å) and angles (degrees) for (PNP)Co(Ph)(OAc) (**606a**, middle): N1–Co1, 1.9333(12); O1–Co1, 1.9896(12); O2–Co1, 2.1166(11); P1–Co1, 2.2619(7); P2–Co1, 2.2353(6); C29–Co1, 1.9403(15); C29–Co1–N1, 97.59(6); N1–Co1–O1, 165.17(5). Selected bond distances (Å) and angles (degrees) for (PNP)Co(Ph)(SPh) (**608a**, right): N1–Co1, 1.9497(18); P1–Co1, 2.2597(7); P2–Co1, 2.2313(7); C33–Co1, 1.933(2); S1–Co1, 2.2069(6); N1–Co1–C33, 98.54(8); N1–Co1–S1, 149.60(6).

6.2.5 Thermolysis of (PNP)Co^{III}(Ar)(SAr) Complexes

Thermolysis of **608a** in benzene led to the formation of **604a**, **605a**, and **6A** in a 1:1:1 ratio (Scheme VI-5, Top). Further investigation showed that this process is first order in **608a** (Figure VI-7). Thermolysis of this complex in the presence of 1 eq. of BHT resulted in the same distribution of products in the same time period, providing evidence against generation of free aryl radicals. Similarly, thermolysis of **608b** in benzene resulted in the formation of **604b**, **605b**, and **6D** in a 1:1:1 ratio (Scheme VI-5, Bottom; Figure VI-9).

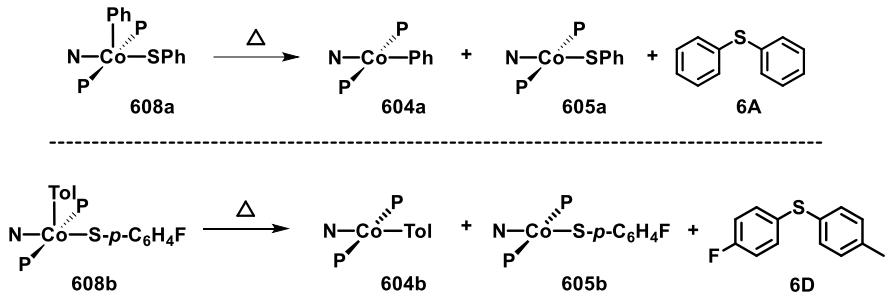

Scheme VI-5. Top: Thermolysis of **608a** and observed products. Bottom: Thermolysis of **608b** and observed products.

Attempting to determine whether the C-S bond formation step happened at a single Co center, thermolysis of **608a** in a 1:1 ratio with **608b** was carried out. In principle, strict unimolecular C-S reductive elimination should lead to only two diarylasulfide products as a result of this thermolysis. In the event, formation of four diarylsulfides was instead observed, along with the four expected Co^{II} products: **604a**, **604b**, **605a**, and **605b** (Scheme VI-6). ^{19}F NMR analysis during the course of the reaction at 80 °C revealed the formation of the Co(III) crossover product **608c** (Figure VI-11). This suggested that during the thermolysis, thiolate ligands can exchange between the Co(III) centers prior to RE. This exchange would then lead to the formation of crossover diarylsulfides, even if RE happens unimolecularly, and thus prevent us from firmly excluding crossover via other pathways. Performing this reaction at double the initial concentration of Co^{III} complexes still showed **608c** during thermolysis and a very similar distribution of Co^{II} products and diaryl sulfides after the reaction had completed.

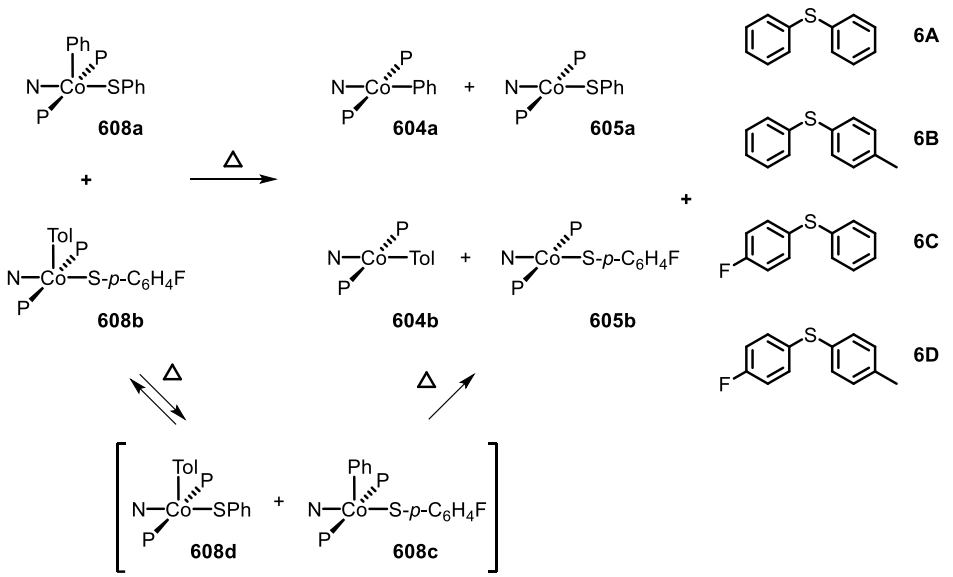

Scheme VI-6. Thermolysis of a mixture of **608a** and **608b**.

The thiolate exchange between Co(III) complexes could occur in at least two non-exclusive ways: 1) direct thiolate exchange between two Co(III) complexes, 2) via exchange between Co(II) and Co(III) thiolate complexes. To probe the ability of Co(III) to exchange thiolate ligands with Co(II), **608a** was thermolyzed in the presence of 1 eq. **605b**. *In situ* ^{19}F NMR observation at 80 °C revealed the formation **608c** during the reaction (Scheme VI-7). After the thermolysis was complete, 6% of the total starting fluorinated thiolate was found as **6C** demonstrating that Co^{II} and Co^{III} can swap thiolates. The conditions required for the observation of thiolate swapping between two Co(III) complexes inevitably led to at least some Co(II) thiolate, which prevented us from establishing whether Co(III) thiolate complexes can exchange thiolates without the involvement of Co(II).

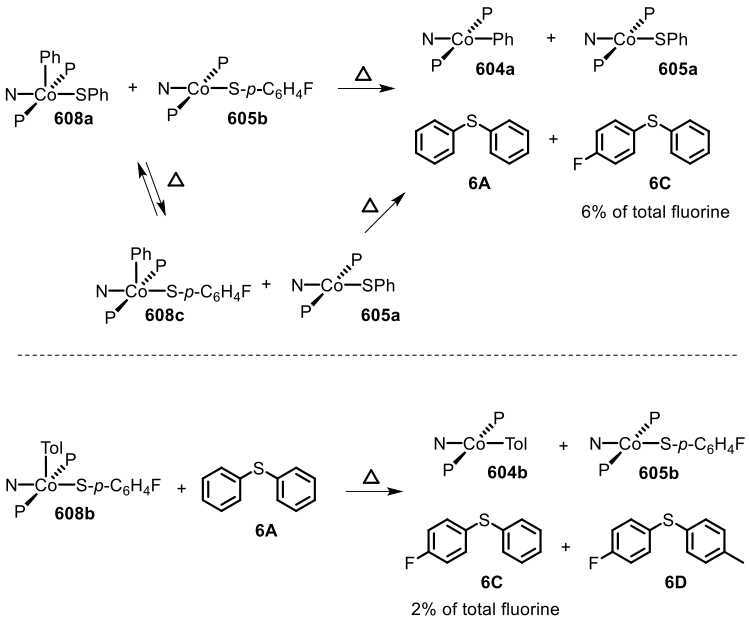

Scheme VI-7. Top: Thermolysis of **608a** in the presence of **605b** and observed products. Bottom: Thermolysis of **608b** in the presence of **6A** and observed products.

6.2.6 Comproportionation Hypothesis and Reactions with Co^{I} Compounds

By analogy with our work on pincer rhodium complexes,[18,30,183b]. we envisioned that after the concerted C–S reductive elimination from **608a**, an unsaturated **614** fragment would be generated. We further hypothesized that this unsaturated (PNP)Co species **614** undergoes rapid comproprotionation with the remaining **608a** to generate the observed Co(II) products.[221] To test this hypothesis, **609** was combined with **608a** in benzene at ambient temperature. An immediate color change to green was observed upon mixing, indicating the formation of (PNP)Co^{II} complexes. ^{1}H NMR spectroscopic observation confirmed the formation of **604a** and **605a** in a 1:1 ratio. Similarly, mixing freshly made **610** with **608a** resulted in an immediate comproportionation producing **604a** and **605a** in

a 1:1 ratio by ^{1}H NMR spectroscopy (Scheme VI-8). In this case, free triphenylphosphine was also observed by ^{1}H and ^{31}P{^{1}H} NMR spectroscopy.

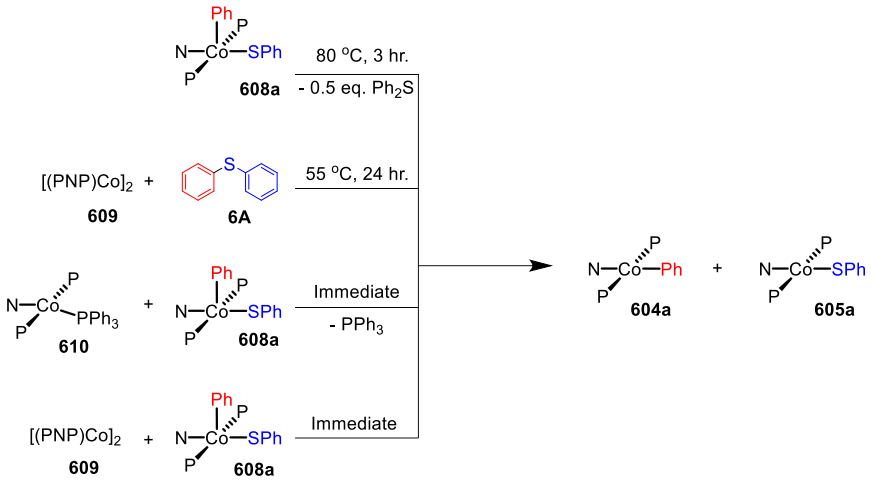

Scheme VI-8. Reaction pathways shown to generate a 1:1 mixture of **604a** and **605a**.

6.2.7 Reversibility of C–S RE

Treatment of **609** with diphenyl sulfide (**6A**) and heating overnight in a 55 °C oil bath resulted in the formation of **604a** and **605a** in a 1:1 ratio (Scheme VI-8). This experiment shows that Co(I) here can cleave a C–S bond in a diarylsulfide, suggesting that C-S RE might be reversible. A related observation is that thermolysis of **608b** in the presence of **6A** resulted in the formation of a small amount of **6C** in addition to **6D** (Scheme VI-7, bottom); which can be interpreted as occasional trapping of a Co(I) species formed in the RE of **6D** by Ph_2S (**A**) as opposed to by the Co(III) starting material **608b**. By way of a control experiment, thermolysis of **604b** and **605b** with **6A** at 80 °C for 7 d resulted in no detectable change, establishing that Co^{II} compounds do not react with a diarylsulfide.

In order to gain some insight into whether this C-S cleavage by Co(I) occurs via concerted OA, we subjected **609** to thermolysis with 2-isopropylphenyl-4'-fluorophenyl sulfide (**6E**). Based on what we learned of the preferences of the (PNP)Rh system in OA with aryl halides,[18,30,31b] it seemed reasonable to assume that the concerted OA mechanism with (PNP)Co should favor the C-S bond unencumbered by the *ortho*-isopropyl substituent (C^F-S, Scheme VI-9). DFT calculations predicted that homolytic cleavage of the C^F-S bond is 1.6 kcal/mol less thermodynamically favorable than the cleavage of the C–S bond connecting to the 2-isopropylphenyl substituent (C^R-S, Scheme VI-9). Thus, a radical abstraction mechanism for the C-S cleavage might be expected to favor the cleavage of C^R-S.

Heating the mixture of **609** with **6E** in at 80 °C for three days resulted in the complete consumption of **609** with the formation of a 1:1 mixture of **604c** and **605c** (Scheme VI-9). **605b** was not observed by either ^{1}H or ^{19}F NMR spectroscopy. Treatment of this solution with anhydrous HCl resulted in the formation of **603** along with **604c** with presumed liberation of 2-isopropylthiophenol. GC-MS and APCI-MS analysis of this solution revealed the formation of 2-isopropylthiophenol and **6E** as the only two volatile components; *p*-FC_6H_4SH was not detected. We did not detect any biaryl or bisulfide products. These observations show that only C^F–S bond was cleaved, consistent with a concerted OA C–S activation pathway.[222]

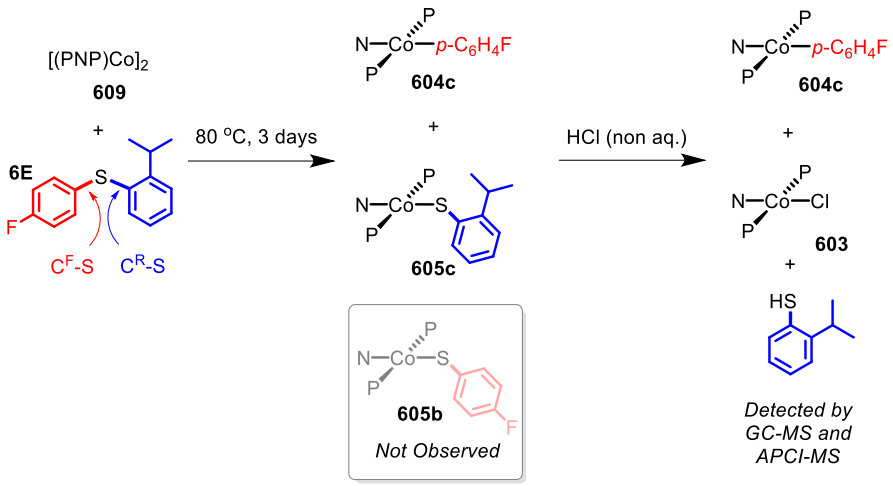

Scheme VI-9. Thermolysis of $[(PNP)Co]_2$ (**607**) with 2-isopropylphenyl-4'-fluorophenyl sulfide (**6E**) and the following treatment with non-aqueous HCl.

6.2.8 DFT Calculations

In order to gain better understanding of the system, DFT calculations were carried to address a few salient points. The geometries were optimized using [B3LYP/LANL2DZ/6-31G(d) level of theory in the gas phase] and the energies for these geometries were then determined with [M06/SDD/6-311+G(d,p)] method incorporating the benzene solvent effect via SMD model. Further details are given in the Supporting Information. We first evaluated the thermodynamics of the overall observed reaction. Conversion of 1 equiv of **608a** into a 0.5:0.5:0.5 mixture of **604a**: **605a**: **6A** was calculated to be favorable by -22.1 kcal/mol in free energy. The geometries of **604a** and **605a** in the doublet ground state were approximately square-planar geometry and consistent with the X-ray structure of **603b**. The calculated structure of **608a** reproduced the overall geometry determined in the XRD study, as well.

We then considered the monomeric Co(I) intermediates in the reaction. Both the "naked" (PNP)Co fragment (**614**) and its SPh_2 adduct (**615**) were calculated to favor a triplet ground state (by 15.5 kcal/mol and 9.9 kcal/mol in free energy, respectively). The geometry of the triplet (PNP)Co(SPh_2) (**615t**) about Co is decidedly not planar, and can be described as attempting to approach tetrahedral within the constraint of the pincer. The array of donor atoms in **615t** is the same as in the low-spin singlet **605a**, but all the calculated bond distances to Co are considerably longer, especially that for the C-S bond (2.538 Å in **615t** vs 2.264 Å in **605a**).

The reductive C-S coupling in **608a** to give singlet (PNP)Co(SPh_2) (**615s**) is nearly ergoneutral, but the conversion of **608a** to **615t** is favorable on the enthalpy (by 4.5 kcal/mol) and on the free energy (by 9.5 kcal/mol) surfaces. The dissociation of SPh_2 from **615t** to give triplet **614t** and free **6A** is endothermic, but is of course favored entropically, resulting in a favorable free energy of dissociation. Thus the complete RE from **608a** to give **614t** and **6A** is quite exoergic by 13.6 kcal/mol, which is less favorable than the formation of a mixture of **604a:605a:6A**.

The dimerization of **614t** to form **609** was calculated to be enthalpically favorable, but disfavored entropically and overall endoergic (by 2.8 kcal/mol per Co). This is consistent with the experimental observation of the dimer **609** as the ground state. The electronic structure of **609** with the calculated lowest energy is that of an open-shell singlet.

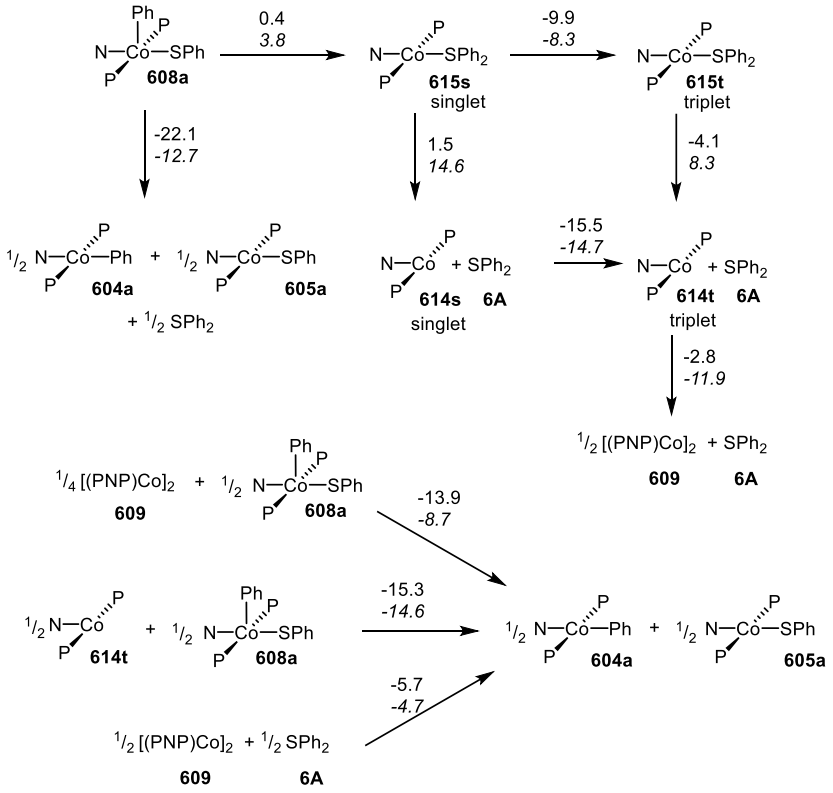

Scheme VI-10. DFT calculated energies for the various transformations. Reaction free energies (at 298 K) are given over the arrows on top; reaction enthalpies in italic below. All the energies are in kcal/mol. Normalized per one mole of Co.

The thermodynamics of the standalone Co(I)/Co(III) comproprotionation reactions were calculated to be consistent with our hypothesis outlined above. The reaction of **614t** with **608a** to give **604a** and **605a** was found to be exothermic and exoergic (by -14.6 and -15.3 kcal/mol, respectively). A similar comproportionation starting from **609** instead of **614t** was also found to be favorable (by -13.9 kcal/mol per mole of Co).

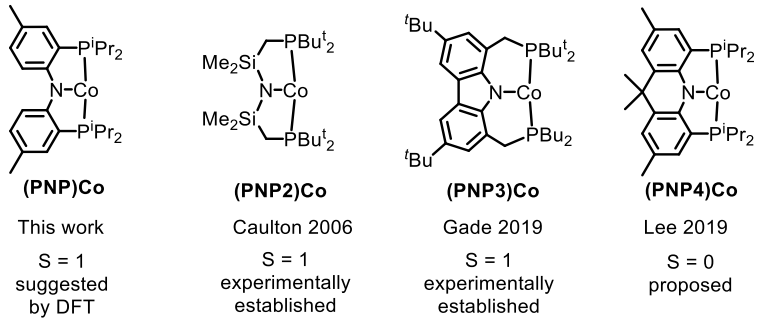

Figure VI-4. Examples of three-coordinate Co complexes supported by various anionic PNP ligands.

The substantial (ca. 15 kcal/mol) calculated preference for the triplet state of (PNP)Co (**614t**) is at odds with the recent report by Lee and coworkers, which presented three-coordinate (PNP4)Co as a singlet species (Figure VI-4).[223] This interpretation by Lee et al. is also at odds with the unambiguously established triplet ground states for the (PNP2)Co and (PNP3)Co by the Caulton[224] and Gade groups,[220] respectively (Figure VI-4). Both (PNP2)Co[224] and (PNP3)Co[220] were isolated and fully characterized, including by X-ray crystallography, magnetic moment measurement, as well as by elemental analysis for (PNP3)Co. (PNP4)Co was purported to be isolated, but no structural determination or magnetic moment was reported, and satisfactory elemental analysis was not obtained. (PNP4)Co was analyzed by DFT calculations as a singlet, but the calculations examining the viability of the triplet state were not carried out. Given these facts and the very close similarity of the PNP and PNP4 ligands, it would be very surprising indeed if they led to different spin state preferences in **614** vs (PNP4)Co. Although we do not observe free 612, it is also worth pointing out that even its adduct with PPh_3 (**610**) does not present as a low-spin complex based on the appearance of its

NMR spectra. It is possible that the (PNP4)Co system needs to be reexamined more closely.

For the C-S reductive coupling en route to (PNP)Co(SPh_2) from **608a**, a transition state was found, lying 24.8 kcal/mol above **608a** in free energy (**6TS**, Figure VI-5). This transformation requires spin crossover in the process, which we propose happens after the singlet **6TS** on the reaction coordinate. A singlet state of the reductive coupling product (PNP)Co(SPh_2) (**615s**) is only 0.4 kcal/mol endergonic relative to **608a**. However, **615t** is lower in energy still. The activation barrier magnitude calculated by DFT agrees qualitatively with the experimental observations. The observed half-life of 0.6 h at 80 °C corresponds to ca. 26 kcal/mol in free energy barrier ($\Delta G^{\ddagger}_{298}$).

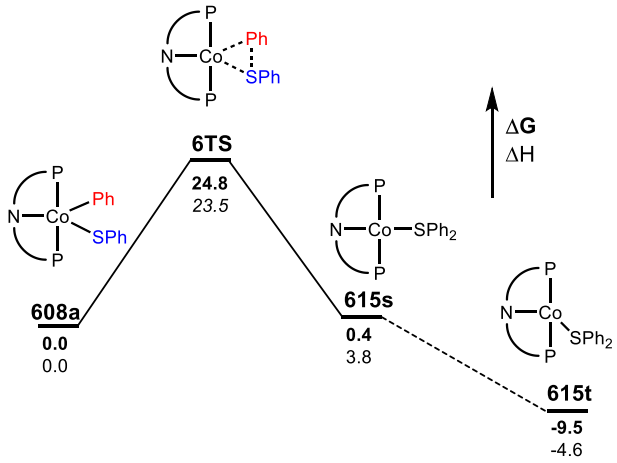

Figure VI-5. Representation of the reaction coordinate for the RE of SPh_2 (**6A**) from (PNP)Co(Ph)(SPh) (**606a**)

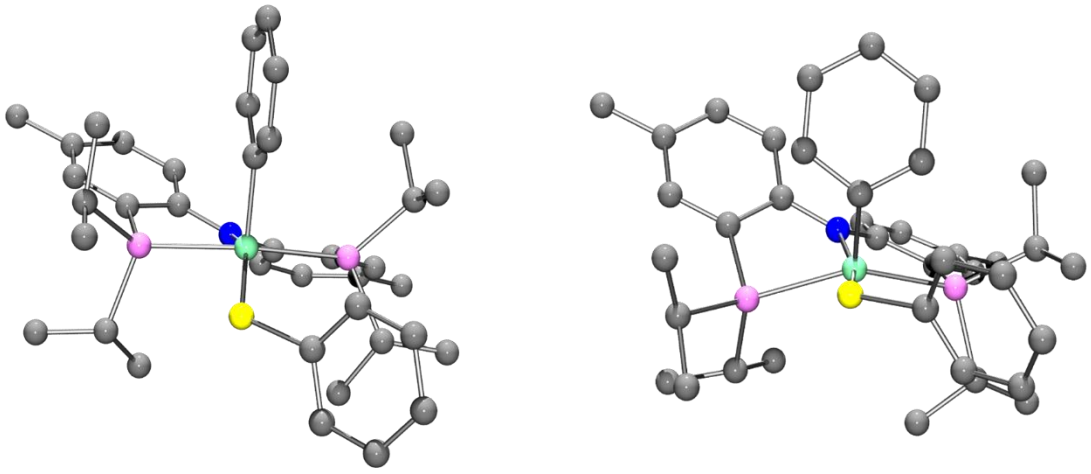

Figure VI-6. DFT calculated structures of **608a** (left) and the **6TS** (right).

Examination of the geometry of the **6TS** (Figure VI-6) shows that it can be thought of as reflecting the migration of the Co-bound Ph group onto the S atom, which in turn is brought more closely into the plane defined by P/N/P/Co. The Co-S distance in **6TS** is actually slightly shorter than in **608a**, and much shorter than calculated in **615t**. The Co-C_{Ph} distance elongates by ca. 0.13 Å in **6TS** (2.055 Å) vs **608a** (1.929 Å), while the newly forming C-S distance (2.085 Å) is about 0.29 Å longer than the expected C-S distances of ca. 1.80 Å in Ph_2S or its complexes. The other geometric feature of **6TS** that needs to be emphasized is the necessary rotation of the Co-bound phenyl ring from edge-on relative to S in **608a** to side-on in 6TS. The hindrance of this rotation by the iPr groups is a major contributor to the magnitude of the activation barrier. This is a rather general observation for the reductive elimination of R-X from five-coordinate d^6 complexes (pincer)M(R)(X) where R = aryl or alkenyl, first articulated by Goldman and Krogh-Jespersen for the

(PCP)Ir system.[225] We previously discussed this issue for the closely related RE reactions from (PNP)Rh(Ar)(X) complexes.[18,183b,208]

Lastly, we considered the experimental observations of the apparent reversibility of C–S RE in reactions of **6A** with Co(I) complexes. Thermodynamically, the experimentally observed reaction of **609** with **6A** to give **604a** and **605a** was indeed calculated to be favorable. At first glance, the microscopic reverse C-S OA might appear kinetically feasible as the energy of the singlet **615s** is similar to that of **608a**. However, given that 1) **613t**, 2) **612t** + free SPh_2, and 3) **607** + free SPh_2 are all considerably lower in energy than the singlet (PNP)Co(SPh_2), the barriers for the microscopic reverse C-S OA starting from these states are prohibitively high.

In rationalization, three possibilities might be considered. First, it is possible that our DFT calculation do not accurately describe the relative energies of the species in different spin states. The second option is that the reaction of **6A** with **609** proceeds as a C–S OA within the dimer, without the formation of monomeric intermediates. The putative single C–S OA dicobalt product may then comproportionate intramolecularly to give **604a** and **605a** without the intermediacy of free **608a**. This reaction pathway would thus not be a microscopic reverse of the monomolecular C-S RE. The complexity of the many potential pathways that would need to be considered to properly analyze the reaction of **609** with **6A** has deterred us from pursuing this problem computationally within the scope of this report.

6.3 Conclusion

In summary, (PNP)Co complexes relevant to cross-coupling reactions were prepared and fully characterized. These complexes were synthesized in a method analogous to the corresponding rhodium complexes, and much to our delight, C–S reductive elimination was successfully achieved.

Interestingly, the Co(I)/Co(III) comproportionation observed here directly mimics the Ni(0)/Ni(II) comproportionation observed and studied by the Hazari group.[74] The similarly further underscores the close parallels in reactivity that exist between group 9 metals in the d^8/d^6 manifold and the group 10 metals in the d^{10}/d^8 manifold.

We were able to prevent intramolecular reductive elimination of the Co–Ph with the central donor of the pincer by switching from a central aryl donor to an amido central donor; however, it appears that the PNP supporting ligand does not have a strong enough ligand field strength to prevent promotion of an electron from the [(PNP)Co] fragment to a triplet ground state resulting in a swift comproportionation reaction which removes catalytically competent cobalt complexes from the reaction.

6.4 Experimental

6.4.1 General Considerations

Unless otherwise specified, all manipulations were performed either inside an argon filled glove box, or by using rigorous Schlenk techniques. Pentane, THF, diethyl ether, and toluene were purified using a PureSolv MD-5 Solvent Purification System and were stored over 4Å molecular sieves in an argon-filled glove box. C_6D_6 was dried over

NaK, benzophenone, and 18-crown-6 then stored in an argon-filled glove box over 4Å molecular sieves prior to use. All other chemicals were used as received from commercial vendors. $^{Me}PN^{H}P^{iPr}$ (**201a**),[21] 4-tolyllithium,[17e] $(PPh_3)_3CoCl$,[60] and $(PPh_3)_2Co(N(TMS)_2)$ (**611**)[61] were prepared according to literature procedures. Authentic samples of 4-$FC_6H_4SC_6H_5$, 4-$FC_6H_4SC_6H_4$-4'-CH_3, $C_6H_5SC_6H_4$-4-CH_3, and 4-FC_6H_4S-2'-$^{i}PrC_6H_4$ were prepared using a (POCOP)Rh catalyst previously reported by our group and their spectra match that previously reported.[18,226]

All NMR spectra were acquired on a Bruker 400 spectrometer (^{1}H NMR, 400.2 MHz) and Varian Inova 500 (^{1}H NMR, 499.703 MHz; ^{13}C NMR, 125.697 MHz; ^{31}P NMR, 202.265 MHz, ^{19}F NMR, 470.135) in denoted solvents. All chemical shifts are reported in δ (ppm). All ^{1}H and ^{13}C NMR spectra were referenced internally to the residual solvent signal (C_6D_6 at δ 7.16 for ^{1}H and δ 128.06 for ^{13}C NMR). ^{19}F NMR spectra were referenced externally to neat trifluoroacetic acid δ -78.55. ^{31}P NMR spectra were externally referenced to an 85% phosphoric acid solution δ 0. Elemental analyses were performed by CALI Labs, Inc. (Highland Park, NJ). Note: All half-widths were acquired with an applied line broadening of 2 Hz; for peaks which overlap, the half-widths were best estimated by taking the frequency difference from the center of the resonance to the half-max of the unobstructed side of the peak and multiplying that value by two.

GC-FID method

Column parameters: HP-5; 30 meters; I.D. 0.32 mm; Film 0.25 µm

Injection parameters: split-splitless 200-fold split (0.05 min); 1 µL injection; port temp. 250 °C.

Temperature gradient: 80 °C (1 min.), then ramp 20 °C/min to 210 °C (total time 8.5 min).

Mobile phase: carrier gas, helium; make-up gas, argon. Constant flow; 4.0 mL/min

Detector parameters: temp. 300 °C; FID gas, hydrogen and air.

GC-MS method

Column parameters: DB-5MS; 30 meters; I.D. 0.25 mm; Film 0.25 µm.

Injection parameters: split-splitless (splitless injection); 1 µL injection; port temp. 225 °C

Temperature gradient: 50 °C (3 min.), then ramp 20 °C/min to 300 °C and hold for 3 min. (total time 18.50 min.)

Mobile phase: carrier gas, helium. Constant flow, 1.5 ml/min

Detector parameters: MS Transfer Line 250 °C; mass range 30-500 amu; 70 eV filament

6.4.2 Synthesis and Characterization

NaSPh, NaSC$_6$H$_4$-4-F, & NaS-2-^{i}PrC$_6$H$_4$. To a Schlenk flask was added NaH (~5 mmol), THF (20 mL), and the corresponding thiol (1.5 eq. v. NaH). The reaction was allowed to stir overnight resulting in a colorless solution. Volatiles were removed *in vacuo* and the residue was completely dissolved in 10 mL THF. Pentane (10 mL) was added to the solution resulting in the immediate precipitation of the sodium thiolate. The salt was

collected on a glass frit and washed with pentane and diethyl ether prior to drying *in vacuo*. All thiophenolate salts were stored in an Ar-filled glove box and used without further purification in accordance with literature precedent.[227]

(PNP)Co(Ph) (604a). In an Ar-filled glove box, a 50 mL Schlenk flask was charged with **603** (1.168 g, 2.23 mmol) and 15 mL toluene. After all the solid was dissolved, the flask was placed into a -35 °C freezer for 30 min. Phenyllithium (1.25 mL of a 1.8 M solution in hexanes, 2.25 mmol) was added in one portion. This solution was allowed to stir overnight. The solution was filtered through a pad of Celite and the volatiles were removed *in vacuo*. The residue was dissolved in 2 mL of toluene and layered with 4 mL of pentane. The flask was then placed in a -35 °C freezer overnight affording a green solid. The solid was washed with cold isooctane and then dried under vacuum at room temperature. Yield: 689 mg (55%). ^{1}H NMR (C_6D_6, 500 MHz): δ 39.6-36.7 (overlapping, $\Delta\nu_{1/2}$ = 180 Hz, $\Delta\nu_{1/2}$ = 960 Hz, 6H), 23.39 ($\Delta\nu_{1/2}$ = 42 Hz, 6H), 14.90 ($\Delta\nu_{1/2}$ = 310 Hz, 12H), 7.49 ($\Delta\nu_{1/2}$ = 21 Hz, 2H), 0.09 ($\Delta\nu_{1/2}$ = 1000 Hz, 12H), -13.99 ($\Delta\nu_{1/2}$ = 70 Hz, 2H), -28.91 ($\Delta\nu_{1/2}$ = 130 Hz, 2H), -92.51 ($\Delta\nu_{1/2}$ = 990 Hz, 2H).

(PNP)Co(SPh) (605a). In an Ar-filled glove box, a 20 mL scintillation vial was charged with **603** (152 mg, 0.291 mmol) and 10 mL THF. To this solution, NaSPh (63 mg, 0.48 mmol) was added. The solution changed from deep blue to dark green over 30 minutes. The reaction was left to stir overnight. The volatiles were removed *in vacuo* and the product was extracted with 10 mL of pentane and filtered through a plug of Celite. The volatiles were removed again, yielding a green solid. Yield: 43 mg (74%). ^{1}H NMR (C_6D_6, 500 MHz): δ 25.21 ($\Delta\nu_{1/2}$ = 190 Hz, 6H), 23.84 ($\Delta\nu_{1/2}$ = 280 Hz, 2H), 10.89 ($\Delta\nu_{1/2}$ = 49

Hz, 2H), 9.42 ($\Delta\nu_{1/2}$ = 1400 Hz, 2H), 6.82 ($\Delta\nu_{1/2}$ = 52 Hz, 3H), 5.7-2.2 (overlapping, $\Delta\nu_{1/2}$ = 400 Hz, $\Delta\nu_{1/2}$ = 700 Hz, 25 H), -10.49 ($\Delta\nu_{1/2}$ = 520 Hz, 2H), -20.49 ($\Delta\nu_{1/2}$ = 380 Hz, 2H).

(PNP)Co(Tol) (604b). In an Ar-filled glove box, a 50 mL Schlenk flask was charged with **603** (1.366 g, 2.61 mmol) and 15 mL THF. Freshly prepared 4-tolyllithium (0.256 g, 2.64 mmol) was weighed into a scintillation vial and dissolved in 15 mL THF. Both of these solutions were placed into a -35 °C freezer within the glove box. After one hour, the 4-tolyllithium solution was pipetted into the Schlenk flask and the mixture was stirred overnight. The volatiles were removed *in vacuo* and the residue was dissolved in 15 mL toluene. After Celite filtration, the volatiles were removed *in vacuo* and the resulting solid was dissolved in 5 mL of pentane. This pentane solution was placed into a -35 °C freezer overnight affording green precipitate. Yield: 1.023 g (68%) The supernatant was concentrated and placed back into the freezer yielding an additional 0.254 g (85% overall). ^{1}H NMR (C_6D_6, 500 MHz): δ 39.6-36.2 (overlapping, $\Delta\nu_{1/2}$ = 180 Hz, $\Delta\nu_{1/2}$ = 860 Hz, 6H), 23.56 ($\Delta\nu_{1/2}$ = 34 Hz, 6H), 14.80 ($\Delta\nu_{1/2}$ = 320 Hz, 12H), 7.53 ($\Delta\nu_{1/2}$ = 17 Hz, 2H), 0.15 ($\Delta\nu_{1/2}$ = 870 Hz, 12H), -8.09 ($\Delta\nu_{1/2}$ = 14 Hz, 3H, tolyl CH_3), -12.65 ($\Delta\nu_{1/2}$ = 46 Hz, 2H), -29.04 ($\Delta\nu_{1/2}$ = 110 Hz, 2H), -93.76 ($\Delta\nu_{1/2}$ = 1000 Hz, 2H). Elem. Anal. Calcd. for $C_{33}H_{47}CoNP_2$: C, 68.50; H, 8.19. Found: C, 68.17; H, 7.85.

(PNP)Co(S-4-C_6H_4F) (605b). In an Ar-filled glove box, a 25 mL Schlenk flask was charged with **603** (0.209 g, 0.398 mmol) and 10 mL of THF. Sodium 4-fluorothiophenolate (0.083 g, 0.55 mmol) was added and the solution was allowed to stir overnight. The volatiles were removed *in vacuo* and the residue was extracted with 10 mL pentane. The solution was passed through a plug of Celite and then dried under vacuum.

Yield: 0.210 g (85%). ^{1}H NMR (C_6D_6, 500 MHz): δ 25.51 ($\Delta\nu_{1/2}$ = 200 Hz, 6H), 23.69 ($\Delta\nu_{1/2}$ = 260 Hz, 2H), 11.04 ($\Delta\nu_{1/2}$ = 50 Hz, 2H), 8.60 ($\Delta\nu_{1/2}$ = 1100 Hz, 2H), 6.48 ($\Delta\nu_{1/2}$ = 52 Hz, 2H), 5.8-2.3 (overlapping, $\Delta\nu_{1/2}$ = 400 Hz, $\Delta\nu_{1/2}$ = 600 Hz, 24H), -9.24 ($\Delta\nu_{1/2}$ = 460 Hz, 2H), -20.73 ($\Delta\nu_{1/2}$ = 380 Hz, 2H). ^{19}F NMR (C_6D_6, 470 MHz): δ -117.4.

(PNP)Co(*p*-C_6H_4F) (604c). In an Ar-filled glove box, a 50 mL Schlenk flask was charged with **603** (0.262 g, 0.50 mmol) and 20 mL of THF. This solution was placed into a -35 °C freezer for 40 minutes. A 1 M solution of 4-fluorophenylmagnesium bromide (1.0 mL, 1.0 mmol) was added rapidly dropwise and the reaction was stirred overnight. The volatiles were removed *in vacuo* and the hard residue was extracted with 20 mL pentane overnight while stirring. The solution was filtered through a pad of Celite and the volatiles were removed yielding a dark green solid. Yield: 227 mg (78%) ^{1}H NMR (C_6D_6, 500 MHz): δ 39.06 & 37.80 (overlapping, $\Delta\nu_{1/2}$ = 170 Hz, $\Delta\nu_{1/2}$ = 1100 Hz, 6H), 24.20 ($\Delta\nu_{1/2}$ = 41 Hz, 6H), 14.91 ($\Delta\nu_{1/2}$ = 350 Hz, 12H), 7.75 ($\Delta\nu_{1/2}$ = 22 Hz, 2H), 0.19 ($\Delta\nu_{1/2}$ = 1100 Hz, 12H), -11.56 ($\Delta\nu_{1/2}$ = 51 Hz, 2H), -29.83 ($\Delta\nu_{1/2}$ = 120 Hz, 2H), -93.68 ($\Delta\nu_{1/2}$ = 1200 Hz, 2H). ^{19}F NMR (C_6D_6, 470 MHz): δ -160.0.

(PNP)Co(S-2-^{i}PrC$_6$H$_4$) (605c). In an Ar-filled glove box, a 20 mL scintillation vial was charged with **603** (0.148 g, 0.282 mmol) and 10 mL THF. In a separate vial, sodium 2-isopropylphenylthiolate was dissolved in 5 mL THF. The thiolate solution was pipetted into the vial containing the cobalt complex and allowed to stir overnight. The volatiles were removed *in vacuo* and the residue was dissolved in pentane. After Celite filtration, the volatiles were removed again yielding a green solid. Yield: 112 mg (63%). ^{1}H NMR (C_6D_6, 400 MHz): δ 24.53 ($\Delta\nu_{1/2}$ = 250 Hz, overlap, 4H), 23.83 ($\Delta\nu_{1/2}$ = 380 Hz,

overlap, 2H), 10.71 ($\Delta\nu_{1/2}$ = 50 Hz, overlap, 2H), 10.52 ($\Delta\nu_{1/2}$ = 80 Hz, overlap, 1H), 6.4-4.0 (overlapping, $\Delta\nu_{1/2}$ = 90 Hz, $\Delta\nu_{1/2}$ = 600 Hz, 12H), 3.8-2.1 (overlapping $\Delta\nu_{1/2}$ = 80 Hz, $\Delta\nu_{1/2}$ = 850 Hz, 12H), -1.66 ($\Delta\nu_{1/2}$ = 70 Hz, 5H), -15.91 ($\Delta\nu_{1/2}$ = 940 Hz, 2H), -19.90 ($\Delta\nu_{1/2}$ = 430 Hz, 2H).

(PNP)Co(PPh$_3$) (610). In an Ar-filled glove box, a J. Young Tube was charged with **611** (0.017 g, 0.022 mmol) and 600 μL C_6D_6. To this solution was added **201a** (0.011 g, 0.026 mmol). Immediate ^{1}H NMR observation revealed the appearance of new paramagnetically shifted resonances. This compound could not be isolated because over time, the complexes freely lose triphenylphosphine and make **609**, even at -35 °C. ^{1}H NMR (C_6D_6, 500 MHz): δ 76.65 ($\Delta\nu_{1/2}$ = 1600 Hz, 2H), 22.55 ($\Delta\nu_{1/2}$ = 120 Hz, 6H), 21.00 ($\Delta\nu_{1/2}$ = 130 Hz, 2H), 15.53 ($\Delta\nu_{1/2}$ = 120 Hz, 2H), 9.34 ($\Delta\nu_{1/2}$ = 160 Hz, 6H), 3.99 ($\Delta\nu_{1/2}$ = 220 Hz, 12H), 3.30 ($\Delta\nu_{1/2}$ = 200 Hz, 16H), -8.65 ($\Delta\nu_{1/2}$ = 360 Hz, 5H) -13.43 ($\Delta\nu_{1/2}$ = 140 Hz, 2H).

(PNP)Co(Ph)(OAc) (606a). In an Ar-filed glove box, a 20 mL scintillation was charged with **604a** (0.550 g, 0.974 mmol) and 10 mL toluene. Bis(acetoxyiodo)benzene (0.183 g, 0.57 mmol) was added in one portion and the solution was allowed to stir overnight. The volatiles were removed *in vacuo*. The residue was dissolved in toluene and filtered through a pad of Celite. The volatiles were removed again, and the resulting solid was dissolved in pentane and placed into a -35 °C freezer to afford a tan precipitate. Yield: 0.269 g (44%). ^{1}H NMR (C_6D_6, 500 MHz): δ 7.46 (dt, *J* = 8.4 Hz, *J* = 2.0 Hz, 2H), 7.06 (dt, *J* = 7.8 Hz, *J* = 1.4 Hz, 1H), 7.01 (dd, *J* = 5.2 Hz, *J* = 3.2 Hz, 2H), 6.93 (td, *J* = 7.5 Hz, *J* = 1.9 Hz, 1H), 6.89 (tt, *J* = 7.0 Hz, *J* = 1.0 Hz, 1H), 6.78 (ddd, *J* = 7.9 Hz, *J* = 7.0

Hz, *J* = 1.9 Hz, 1H), 6.67 (dd, *J* = 8.5 Hz, *J* = 1.8 Hz, 2H), 6.62 (ddd, *J* = 7.9 Hz, *J* = 1.8 Hz, *J* = 0.8 Hz, 1H), 2.48 (m, 2H), 2.15 (s, 8H, overlapping tolyl methyl and methine resonances), 1.69 (s, 3H, OAc–CH_3), 1.37 (dvt, *J* = 6.3 Hz, *J* = 7.3 Hz, 6H, P–CH–($C\mathit{H}_3$)$_2$), 1.28 (dvt, *J* = 6.4 Hz, *J* = 6.3 Hz, 6H, P–CH–($C\mathit{H}_3$)$_2$), 1.04 (dvt, *J* = 7.2 Hz, *J* = 7.2 Hz, 6H, P–CH–($C\mathit{H}_3$)$_2$), 0.59 (dvt, *J* = 6.8 Hz, *J* = 6.8 Hz, 6H, P–CH–($C\mathit{H}_3$)$_2$). $^{13}C\{^1H\}$ NMR (C_6D_6, 125 MHz): δ 183.2 (t, *J* = 1.8 Hz, C=O), 159.3 (t, *J* = 10.8 Hz), 140.4 (br s), 135.6 (t, *J* = 2.3 Hz), 131.84 (s), 131.41 (overlapping signals), 125.96 (t, *J* = 2.5 Hz), 124.70 (t, *J* = 3.0 Hz), 124.60 (t, *J* = 2.3 Hz), 123.28 (br s), 122.88 (overlapping doublets, *J* = 19.8 Hz, *J* = 19.8 Hz), 119.84 (t, *J* = 4.5 Hz), 23.81 (t, J= 10.7 Hz, P–*C*H–(CH_3)$_2$), 23.04 (br s, OAc–*C*H_3), 22.6 (t, *J* = 7.6 Hz, P–*C*H–(CH_3)$_2$), 20.72 (s, Ar-*C*H_3), 19.2 (t, *J* = 2.1 Hz, P–CH–($C\mathit{H}_3$)$_2$), 18.6 (br s, P–CH–($C\mathit{H}_3$)$_2$), 17.88 (br s, two overlapping P–CH–($C\mathit{H}_3$)$_2$). $^{31}P\{^1H\}$ NMR (C_6D_6, 202 MHz): δ 40.1. Elem. Anal. Calcd for $C_{34}H_{48}CoNO_2P_2$: C, 65.48; H, 7.76. Found: C, 65.38; H, 7.56.

(PNP)Co(Tol)(OAc) (606b). In an Ar-filed glove box, a 50 mL scintillation was charged with **604b** (0.219 g, 0.378 mmol) and 30 mL toluene. Bis(acetoxyiodo)benzene (0.063 g, 0.20 mmol) was added in one portion and the solution was allowed to stir overnight. The volatiles were removed *in vacuo*. The residue was dissolved in pentane and filtered through a plug of Celite. The volatiles were removed again, and the resulting solid was dissolved in 1 mL of pentane and placed into a -35 °C freezer to afford a brown-tan precipitate. Yield: 0.160 g (65%). ^1H NMR (C_6D_6, 500 MHz): δ 7.46 (dt, *J* = 8.5 Hz, *J* = 2.1 Hz, 2H), 7.02 (dd, *J* = 5.4 Hz, *J* = 3.2 Hz, 2H), 6.94 (dd, *J* = 8.1 Hz, *J* = 1.6 Hz, 1H), 6.83 (dd, *J* = 8.2 Hz, *J* = 1.9 Hz, 1H), 6.67 (dd, *J* = 8.5 Hz, *J* = 1.9 Hz, 2H), 6.61 (dd, *J* =

8.1 Hz, *J* = 1.8 Hz, 1H), 6.47 (dq, *J* = 8.0 Hz, *J* = 2.0 Hz , 1H), 2.49 (m, 2H, P–C*H*–$(CH_3)_2$), 2.21 (s, 3H, tolyl–CH_3), 2.16 (s, 8H, overlapping backbone tolyl methyl and methine resonances), 1.70 (s, 3H, OAc–CH_3), 1.38 (dvt, *J* = 7.3 Hz, *J* = 7.3 Hz, 6H, P–CH–(C*H*$_3)_2$). $^{13}C\{^1H\}$ NMR (C_6D_6, 125 MHz): δ 183.18 (t, *J* = 1.7 Hz, C=O), 159.42 (t, *J* = 10.9 Hz), 140.10 (t, *J* =1.9 Hz), 135.26 (t, *J* = 2.3 Hz), 131.92 (t, *J* = 2.0 Hz), 131.84 (s), 131.36 (s), 127.01 (t, *J* = 2.7 Hz), 125.73 (t, *J* = 2.5 Hz), 124.62 (t, *J* = 3.0 Hz), 122.99 (overlapping doublets, *J* = 19.6 Hz, *J* = 19.8 Hz), 119.81 (t, *J* = 4.6 Hz), 23.78 (t, *J* = 10.5 Hz, P–*C*H–$(CH_3)_2$), 23.04 (s, OAc–CH_3), 22.65 (t, *J* = 7.5 Hz, P–*C*H–$(CH_3)_2$), 20.72 (s, backbone tolyl methyls), 20.69 (s, tolyl–CH_3), 19.17 (t, *J* = 2.2 Hz, P–CH–(*C*$H_3)_2$), 18.64 (s, P–CH–(*C*$H_3)_2$), 17.96 (s, P–CH–(*C*$H_3)_2$), 17.93 (s, P–CH–(*C*$H_3)_2$). $^{31}P\{^1H\}$ NMR (C_6D_6, 202 MHz): δ 40.1 (br s). Elem. Anal. Calcd. for $C_{35}H_{50}CoNO_2P_2$: C, 65.93; H, 7.90. Found: C, 66.22; H, 7.57.

(PNP)Co(Ph)(I) (607a). **Method A:** In an Ar-filled glove box, **606a** (0.100 g, 0.161 mmol) was dissolved in ca. 10 mL of 1:1 mixture of toluene/C_6H_6. To this solution Me_3SiI (23 μL, 0.16 mmol) was added and the reaction was left to stir for 1 h. The volatiles were then removed and the product was extracted with ca. 30 mL of pentane and filtered through a pad of celite on a glass frit. The volatiles were removed and a blue-green solid was obtained (101 mg, 90%). **Method B:** In an Ar-filled glove box, a 25 mL Schlenk flask was charged with **604a** (0.218 g, 0.386 mmol) and 20 mL of toluene. To this flask, a solution of freshly sublimed I_2 (1.0 mL of a 0.19 M solution in THF, 0.19 mmol) was added in one portion. After four hours, the volatiles were removed *in vacuo*. The residue was dissolved in 4 mL pentane and placed into a -35 °C freezer inside the glovebox. The

supernatant was decanted, and the solids were dried *in vacuo*. Yield: 0.152 g (57%). ^{1}H NMR (C_6D_6, 500 MHz): δ 7.86 (d, *J* = 8.6 Hz, 2H), 7.17 (overlapped, 3H), 6.72 (dd, *J* = 8.6 Hz, *J* = 2.0 Hz, 2H), 6.52 (br t, *J* =7.1 Hz, 1H), 6.38 (ddd, *J* = 8.9 Hz, *J* = 7.1 Hz, *J* = 2.0 Hz, 1H), 6.14 (ddd, *J* = 9.0 Hz, *J* = 7.2 Hz, *J* = 2.0 Hz, 1H), 5.92 (d, *J* = 8.2 Hz, 1H), 4.06 (observed hept., *J* = 6.8 Hz, 2H, P–C*H*–$(CH_3)_2$), 2.67 (m, 2H, P–C*H*–$(CH_3)_2$), 2.11 (s, 6H, backbone tolyl methyls), 1.67 (br d, *J* = 6.1 Hz, 6H, P–CH–(C*H*$_3)_2$), 1.24 (br d, *J* = 6.5 Hz, 6H, P–CH–(C*H*$_3)_2$), 0.73 (br d, *J* = 5.5 Hz, 6H, P–CH–(C*H*$_3)_2$), 0.37 (br d, *J* = 6.2 Hz, 6H, P–CH–(C*H*$_3)_2$). ^{13}C{^{1}H} NMR (C_6D_6, 125 MHz): δ 162.61 (br s), 152.19 (s), 136.19 (s), 132.88 (s), 131.43 (s), 126.04 (s), 125.44 (s), 123.70 (s), 122.99 (br s), 122.67 (s), 27.02 (br s, P–*C*H–$(CH_3)_2$), 24.83 (br s, P–*C*H–$(CH_3)_2$), 20.61 (s, backbone tolyl methyls), 18.66 (s, P–CH–(*C*H$_3)_2$), 18.62 (s, P–CH–(*C*H$_3)_2$), 17.56 (s, P–CH–(*C*H$_3)_2$), 17.39 (s, P–CH–(*C*H$_3)_2$). ^{31}P{^{1}H} NMR (C_6D_6, 202 MHz): δ 37.7 (br s).

(PNP)Co(Ph)(SPh) (608a). In an Ar-filled glove box, a 20 mL scintillation vial was charged with **606a** (0.269 g, 0.431 mmol) and 10 mL of toluene. To this solution, Me_3SiI (23 μL, 0.16 mmol) was added and the reaction was left to stir overnight. The volatiles were removed *in vacuo*. The residue was dissolved in THF and sodium thiophenolate (0.097 g, 0.73 mmol) was added to the solution. After three hours, the volatiles were then removed and the product was extracted with 20 mL of pentane and filtered through a pad of Celite. The volatiles were removed and a dark blue-green solid was obtained. Yield: 187 mg (64%). ^{1}H NMR (C_6D_6, 500 MHz): δ 7.88 (d, *J* = 8.6 Hz, 2H), 7.80 (overlapping, 3H), 7.10 (br s, 2H), 6.99 (m, 3H), 6.76 (ddd, *J* = 8.6 Hz, *J* = 2.1 Hz, *J* = 0.6 Hz, 1H), 6.62 (br t, *J* = 7.0 Hz, 1H), 6.57 (br s, 1H), 6.28 (br s, 1H), 6.01 (br

s, 1H), 2.89 (observed hept. J = 6.9 Hz, 2H, P–C*H*–$(CH_3)_2$), 2.49 (m, 2H, P–C*H*–$(CH_3)_2$), 2.16 (s, 6H, backbone tolyl methyls), 1.26 (br d, J = 5.9 Hz, 6H, P–CH–(*C*$H_3)_2$), 1.12 (br d, J = 5.7 Hz, 6H, P–CH–(*C*$H_3)_2$), 0.95 (br d, J = 6.1 Hz, 6H, P–CH–(*C*$H_3)_2$), 0.44 (br d, J = 5.9 Hz, 6H, P–CH–(*C*$H_3)_2$). $^{13}C\{^1H\}$ NMR (C_6D_6, 125 MHz): δ 162.01 (br), 149.07 (br), 146.65 (br), 139.90 (br), 135.93 (two overlapping signals), 132.29 (two overlapping signals), 131.31 (two overlapping signals) 126.73, 125.76 (br), 124.83 (br), 124.74, 123.52, 121.48, 25.84 (br, P–*C*H–$(CH_3)_2$), 24.80 (br, P–*C*H–$(CH_3)_2$), 20.56 (s, backbone tolyl methyls), 20.00 (s, P–CH–(*C*$H_3)_2$), 18.07 (s, P–CH–(*C*$H_3)_2$), 17.71 (s, P–CH–(*C*$H_3)_2$), 17.29 (s, P–CH–(*C*$H_3)_2$). $^{31}P\{^1H\}$ NMR (C_6D_6, 202 MHz): δ 31.1 (br s). Elem. Anal. Calcd for $C_{38}H_{50}CoNP_2S$: C, 67.74; H, 7.48. Found: C, 67.85; H, 7.18.

(PNP)Co(Tol)(SAr^F) (608b). In an Ar-filled glove box, a 20 mL scintillation vial was charged with **606b** (65 mg, 0.10 mmol) and 10 mL toluene. To this solution was added trimethylsilyliodide (20 μL, 0.14 mmol) in one portion and the solution was allowed to stir overnight. The volatiles were removed *in vacuo*. The residue was dissolved in THF and sodium 4-fluorothiophenolate (0.033 g, 0.22 mmol) was added. After 30 minutes, the volatiles were removed and the residue was dissolved in 10 mL pentane and filtered through a pad of Celite. The filtrate was dried *in vacuo* resulting in a dark blue solid. Yield: 0.063 g (88%). ^1H NMR (C_6D_6, 500 MHz): δ 7.87 (d, J = 8.6 Hz, 2H), 7.60 (overlapping, dd, J = 8.7 Hz, J = 5.5 Hz, and broad singlet, 3H), 7.10 (s, 2H), 6.77 (dd, J = 8.6 Hz, J = 1.6 Hz 2H), 6.69 (t, J = 8.7 Hz, 2H) 6.45 (br s, 1H), 6.12 (br s, 1H), 5.86 (br s, 1H), 2.84 (observed hept. J = 6.9 Hz, 2H, P–C*H*–$(CH_3)_2$), 2.46 (m, 2H, P–C*H*–$(CH_3)_2$), 2.18 (s, 6H, backbone tolyl methyls), 2.02 (s, 3H, tolyl–CH_3) 1.23 (br d, J = 4.4 Hz, 6H, P–CH–

(CH_3)$_2$), 1.12 (br d, J = 5.8 Hz, 6H, P–CH–(CH_3)$_2$), 0.92 (br d, J = 5.4 Hz, 6H, P–CH–(CH_3)$_2$), 0.44 (br d, J = 5.3 Hz, 6H, P–CH–(CH_3)$_2$). $^{13}C\{^1H\}$ NMR (C_6D_6, 125 MHz): δ 162.02 (br, C–N), 161.7 (d, J = 243 Hz, *C*–F), 148.30 (br), 141.3 (br), 139.57 (br), 137.20 (d, J = 7.1 Hz, C_6H_4F), 132.47, 132.27, 131.30, 126.78, 125.85 (br), 121.53, 114.91 (d, J = 21 Hz, C_6H_4F), 25.79 (br, P–*C*H–(CH_3)$_2$), 24.81 (br, P–*C*H–(CH_3)$_2$), 20.57 (s, backbone tolyl methyls), 20.28 (s, Co–C_6H_4–*C*H_3), 19.95 (s, P–CH–(CH_3)$_2$), 18.10 (s, P–CH–(CH_3)$_2$), 17.67 (s, P–CH–(CH_3)$_2$), 17.27 (s, P–CH–(CH_3)$_2$). $^{31}P\{^1H\}$ NMR (C_6D_6, 202 MHz): δ 30.2 (br s). ^{19}F NMR (C_6D_6, 470 MHz): δ -119.4.

Spectroscopic observation of (PNP)Co(Ph)(SAr^F) (608c). In an Ar-filled glove box, a 10 mL Schlenk flask was charged with **606a** (10 mg, 0.016 mmol) and 5 mL of toluene. To this solution, Me_3SiI (10 μL, 0.07 mmol) was added and the reaction was left to stir overnight. The volatiles were removed *in vacuo*. The residue was dissolved in THF and sodium 4-fluorothiophenolate (0.030 g, 0.019 mmol) was added. After 30 minutes, the volatiles were removed. The residue was dissolved in C_6D_6 for spectroscopic analysis. ^1H NMR (C_6D_6, 500 MHz): δ 7.87 (d, J = 8.6 Hz, 2H), 7.71 (br s, 1H, Co–Ph), 7.58 (dd, J = 8.8 Hs, J = 5.5 Hz, 2H), 7.09 (br s, 2H), 6.76 (dd, J = 8.6 Hz, J = 1.6 Hz, 2H), 6.67 (t, J = 8.8 Hz, 2H), 6.62 (br t, J = 7.0 Hz, 1H, Co–Ph), 6.57 (br s, 1H, Co–Ph), 6.27 (br s, 1H, Co–Ph), 5.99 (br s, 1H, Co–Ph), 2.84 (observed hept. J = 6.9 Hz, 2H, P–C*H*–(CH_3)$_2$), 2.45 (m, 2H, P–C*H*–(CH_3)$_2$), 2.17 (s, 6H, backbone tolyl methyls), 1.22 (br d, J = 5.7 Hz, 6H, P–CH–(CH_3)$_2$), 1.12 (br d, J = 5.5 Hz, 6H, P–CH–(CH_3)$_2$), 0.91 (br d, J = 5.6 Hz, 6H, P–CH–(CH_3)$_2$), 0.41 (br d, J = 5.5 Hz, 6H, P–CH–(CH_3)$_2$). ^{19}F NMR (C_6D_6, 470 MHz): δ -119.3.

6.4.3 Probing the Mechanism of C–S Elimination From (PNP)Co

Thermolysis of 608a. 608a (4 mg, 0.006 mmol) was dissolved in 600 μL of C_6D_6 in a J. Young tube. To this solution, 1,4-dioxane (2 μL, 0.023 mmol) was added using a syringe to serve as an internal standard. A ^{1}H NMR spectrum of the mixture was acquired and then the NMR tube was placed in an 80 °C oil bath for three hours. The final mixture contained: **604a** (46% of initial **608a**), **605a** (46% of initial **608a**) and **6A** (48% of initial **608a**) as observed by ^{1}H NMR spectroscopy.

***In situ* monitoring of consumption of 608a. 608a** (15 mg, 0.022 mmol) was dissolved in 500 μL of C_6D_6 in a J. Young tube. To this solution, 1.4-dioxane (5 μL, 0.058 mmol) was added using a syringe to serve as an internal standard. The tube was heated to 80 °C inside the NMR and monitored continually by ^{1}H NMR spectroscopy. The consumption of **608a** versus the internal standard as monitored by ^{1}H NMR spectroscopy fits a first order correlation.

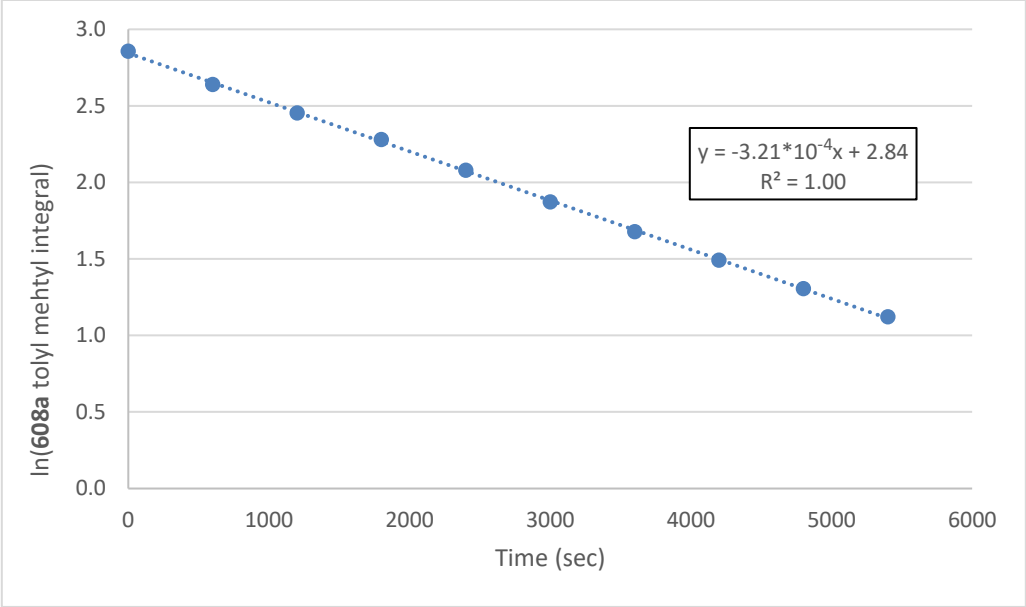

Figure VI-7. Plot of ln(**608a** integral) versus time.

Thermolysis of 608b. **608b** (40 mg, 0.057 mmol) was dissolved in 600 μL of C_6D_6 in a J. Young tube. A ^{1}H NMR spectrum of the mixture was acquired and then the NMR tube was placed in an 80 °C oil bath overnight. The final mixture contained: **604b, 605b**, and **6D** in a 1.0:1.0:1.0 ratio as observed by ^{1}H and ^{19}F NMR spectroscopy.

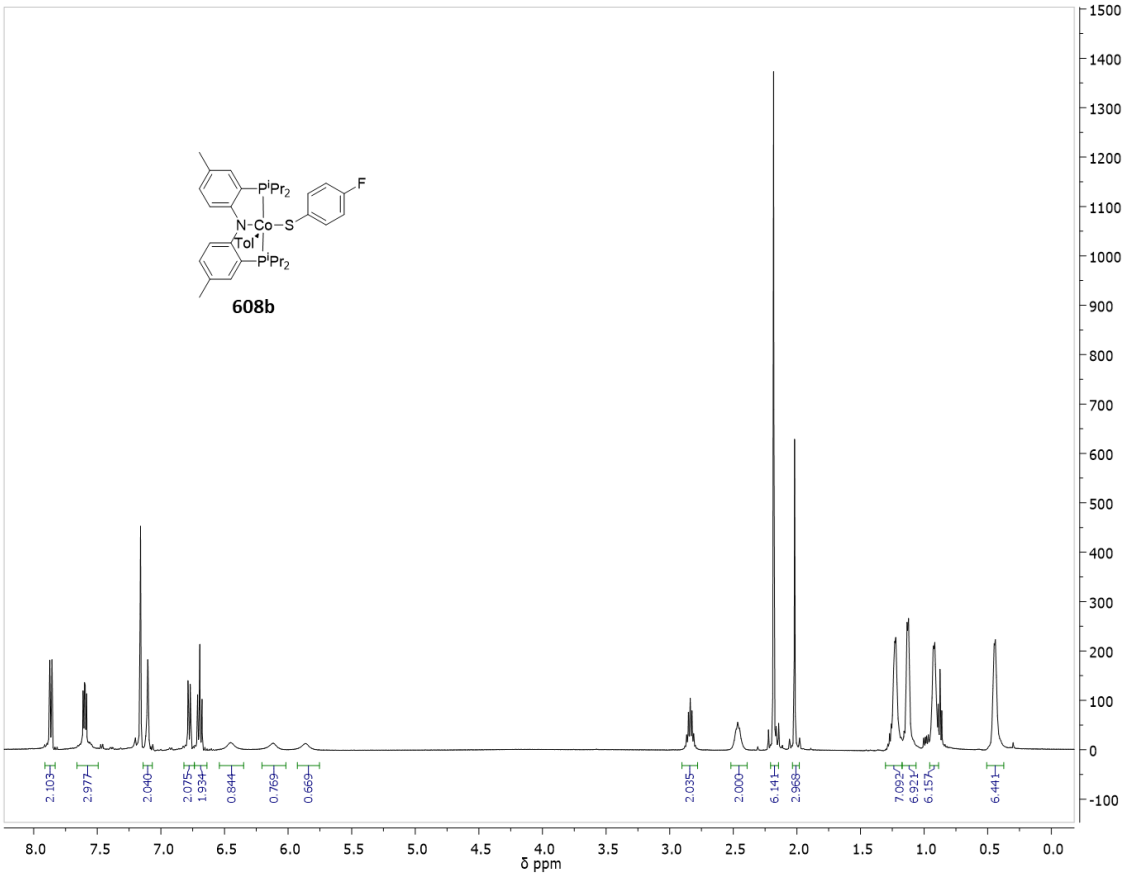

Figure VI-8. ^{1}H NMR (500 MHz, C_6D_6) spectrum of **608b** before thermolysis.

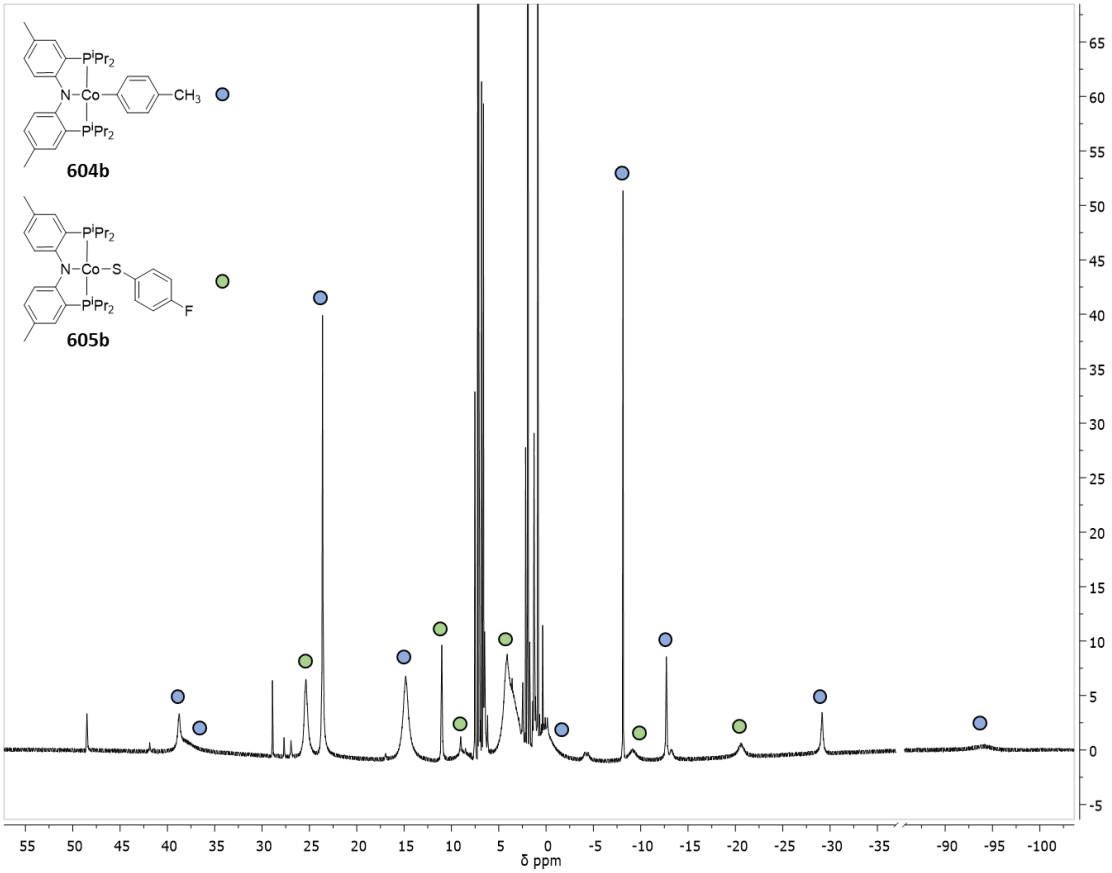

Figure VI-9. ^{1}H NMR (500 MHz, C_6D_6) of the thermolyzed **608b**.

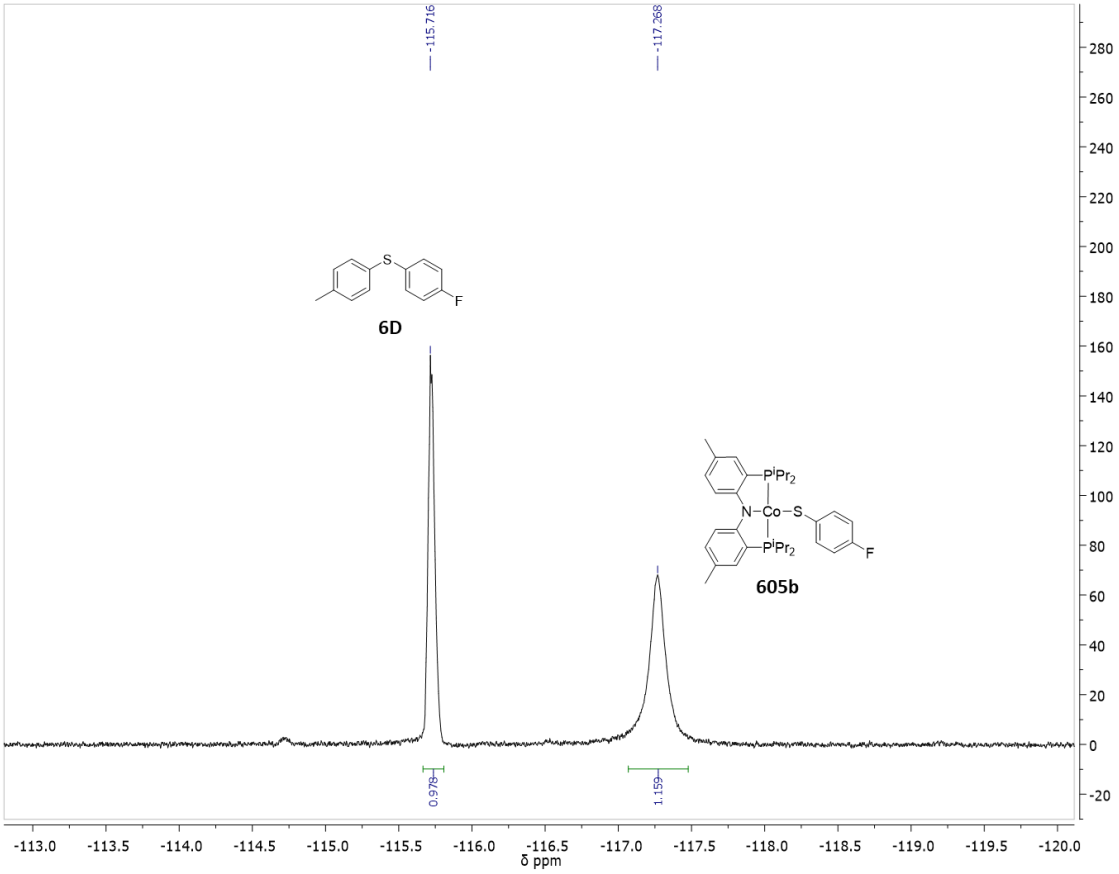

Figure VI-10. ^{19}F NMR (470 MHz, C_6D_6) of the thermolyzed **608b**.

Thermolysis of 608a with BHT as a radical inhibitor. 608a (4 mg, 0.006 mmol) and 2,6-di-*tert*-butyl-4-methylphenol (BHT) (2 mg, 0.009 mmol) were dissolved in 600 μL of C_6D_6 in a J. Young tube. To this solution, 1.4-dioxane (2 μL, 0.023 mmol) was added using a syringe to serve as an internal standard. A ^{1}H NMR spectrum of the mixture was acquired and then the NMR tube was placed in an 80 °C oil bath for three hours. The final mixture contained: **604a** (46% of initial **608a**), **605a** (46% of initial **608a**) and **6A** (45% of initial **608a**) as observed by ^{1}H NMR spectroscopy.

Thermolysis of a 1:1 mixture of 608a & 608b. In an Ar-filled glove box, a J. Young tube was charged with C_6D_6 (200 μL), **608a** (100 μL of a 0.15 M solution in C_6D_6, 0.015 mmol), **608b** (100 μL of a 0.14 M solution in C_6D_6, 0.014 mmol), and benzotrifluoride (100 μL of a 0.12 M solution in C_6D_6, 0.012 mmol) as a ^{19}F NMR referencing standard. The solution was then heated to 80 °C in an NMR spectrometer. ^{1}H and ^{19}F NMR spectra were acquired every ten minutes. *In situ* variable temperature ^{19}F NMR spectroscopy revealed the formation of **605b**, **6D**, **6C**, and the scrambled Co^{III}: **608c**. After thermolysis, ^{1}H NMR spectroscopy revealed the four expected (PNP)Co(X) species: **604a**, **604b**, **605a**, and **605b.** The four diaryl sulfides: **6A**, **6B**, **6C**, and **6D** were observed by GC-FID. This experiment was repeated with double the concentration of the two Co(III) complexes and, consistent with the first experiment, scrambling of thiolates in the Co^{III} complexes occurred, and the same distribution of final products were observed. Note: Figure VI-12 shows a ^{19}F NMR spectrum of a mixture of independently prepared **608b**

and **608c**, showing that these two compounds give two resolved signals, as they do in the thermolysis reaction mixture.

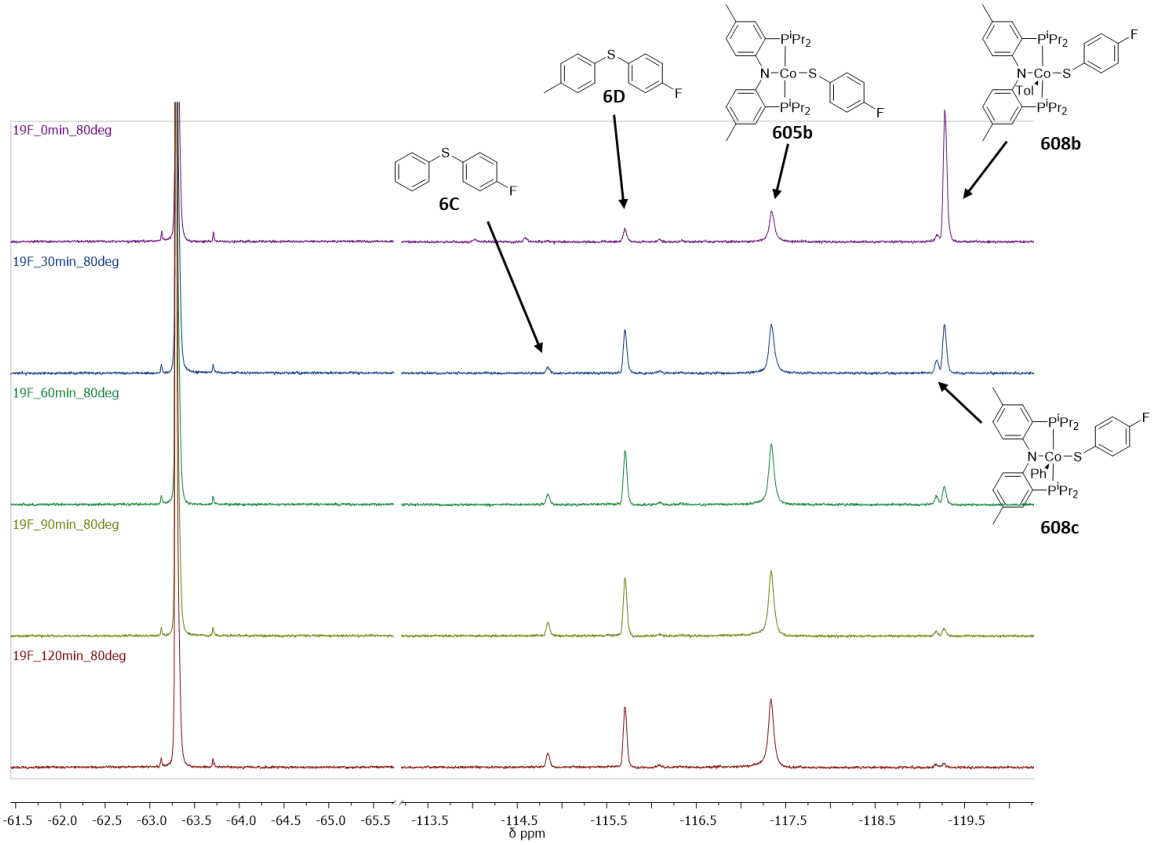

Figure VI-11. Variable temperature ^{19}F NMR (470 MHz, C_6D_6) observation of the mixed thermolysis of **608a** with **608b** (29mM and 28 mM initial concentrations respectively). Timepoints shown are at 30 minute intervals.

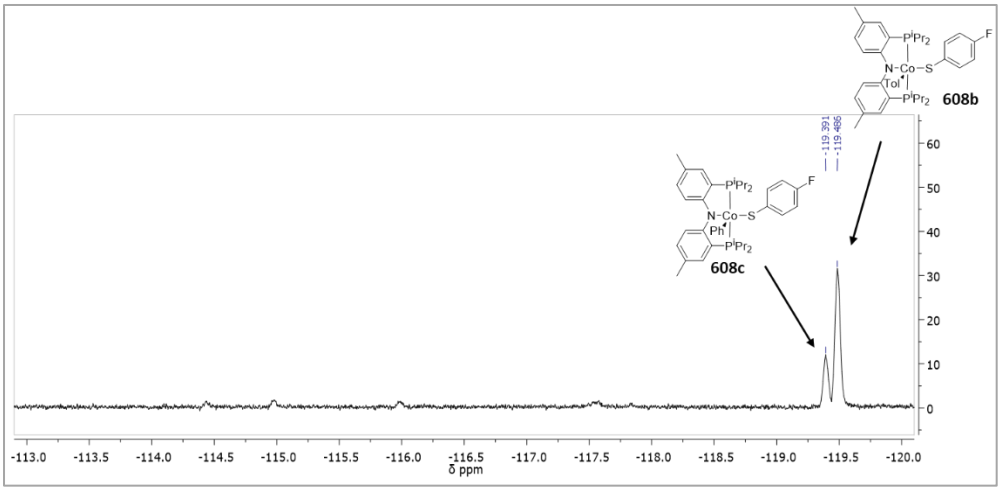

Figure VI-12. ^{19}F (470 MHz, C_6D_6) of a pure sample of **608b** spiked with **608c**.

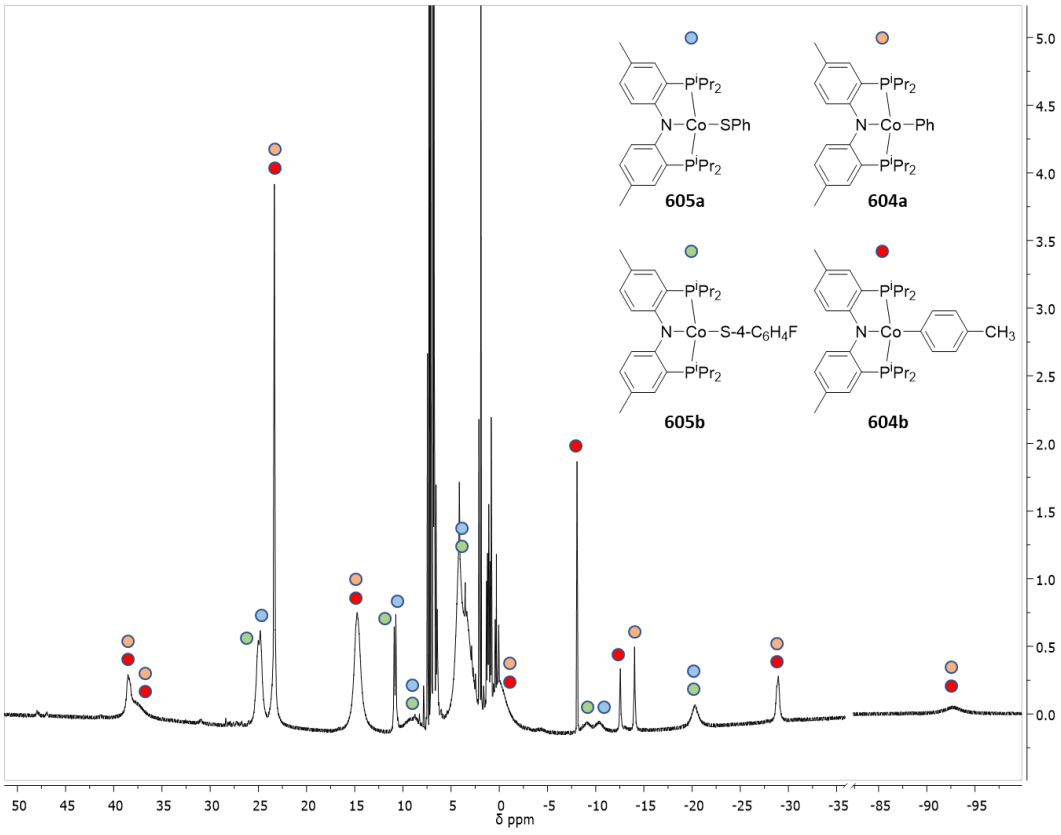

Figure VI-13. ^{1}H NMR (500 MHz, C_6D_6) of the mixed thermolysis of **608a** with **608b** after cooling to room temperature. The four expected Co(II) products are observed.

Thermolysis of 608b with 6A. In an Ar-filled glove box, a J. Young tube was charged with **608b** (200 μL of a 0.14 M solution in C_6D_6, 0.028 mmol), and **6A** (10 μL, 0.059 mmol) then diluted with C_6D_6. The mixture was thermolyzed in an 80 °C oil bath for two days. **6C**, and **6D** were both observed by ^{19}F NMR spectroscopy. **6C** constituted approximately 2% of the fluorinated diarylsulfides that were formed.

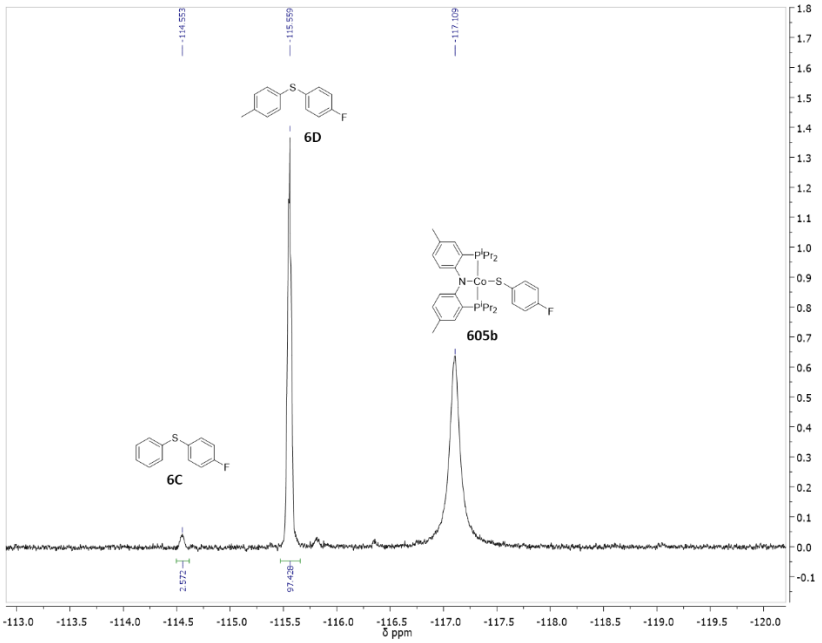

Figure VI-14. ^{19}F NMR (470 MHz, C_6D_6) spectrum showing the resultant mixture of thermolysis of **608b** with **6A**

Thermolysis of 608a with 605b. In an Ar-filled glovebox, a J. Young tube was charged with **608a** (18 mg, 0.027 mmol) and **605b** (17 mg, 0.028 mmol) then diluted with C_6D_6. In situ ^{19}F NMR spectroscopy at 80 °C revealed the formation of **608c** during the reaction This mixture was heated overnight in an 80 °C oil bath. ^{1}H NMR spectroscopy revealed the formation of **605a**, and **604a** in a 1.0:0.95 ratio in addition to **605b**. ^{19}F NMR

spectroscopy revealed the formation of **6C** containing 6% of the total available fluorinated thiolate indicating that Co^{II} and Co^{III} complexes can exchange thiolate ligands.

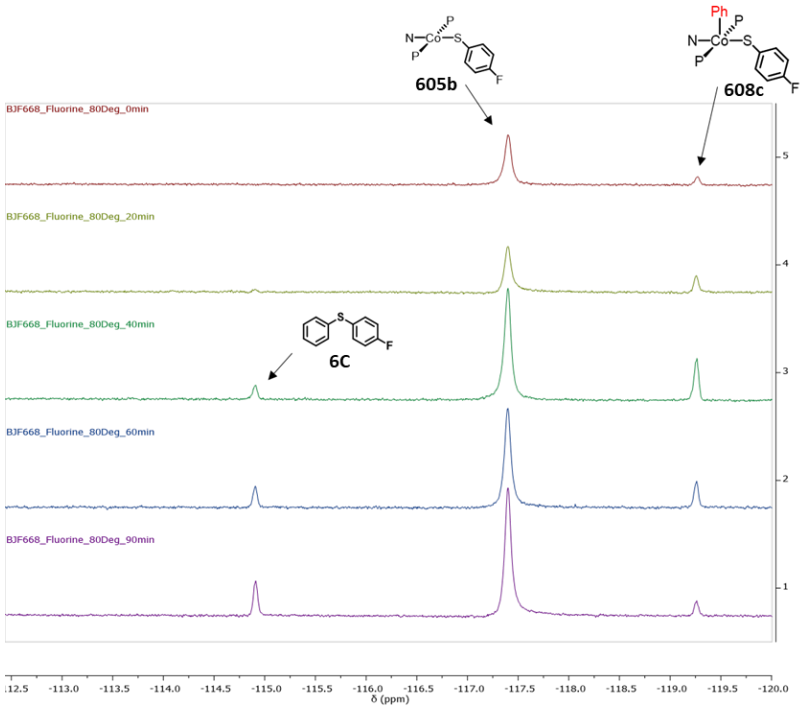

Figure VI-15. ^{19}F NMR (470 MHz, C_6D_6) *in situ* spectra of thermolysis of a 1:1 mixture of **608a** and **605b.**

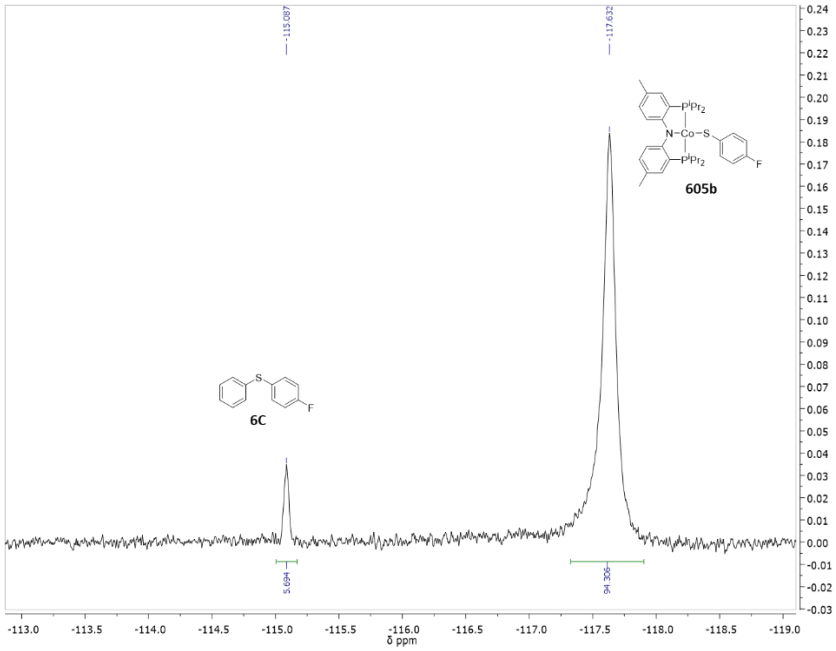

Figure VI-16. ^{19}F NMR (470 MHz, C_6D_6) after thermolysis of **608a** in the presence of **605b** showing the produced fluorinated diarylsulfide **6C**.

Thermolysis of 604b and 605b with 6A. In an Ar-filled glove box, a J. Young tube was charged with **604b** (21mg, 0.036 mmol), **605b** (21 mg, 0.035 mmol), and **6A** (16 µL, 0.096 mmol) then diluted with C_6D_6. The mixture was thermolyzed in an 80 °C oil bath for seven days. Only **604b**, **605b**, and **6A** were observed by ^1H and ^{19}F NMR spectroscopy indicating that Co^{II} complexes cannot activate diaryl sulfides.

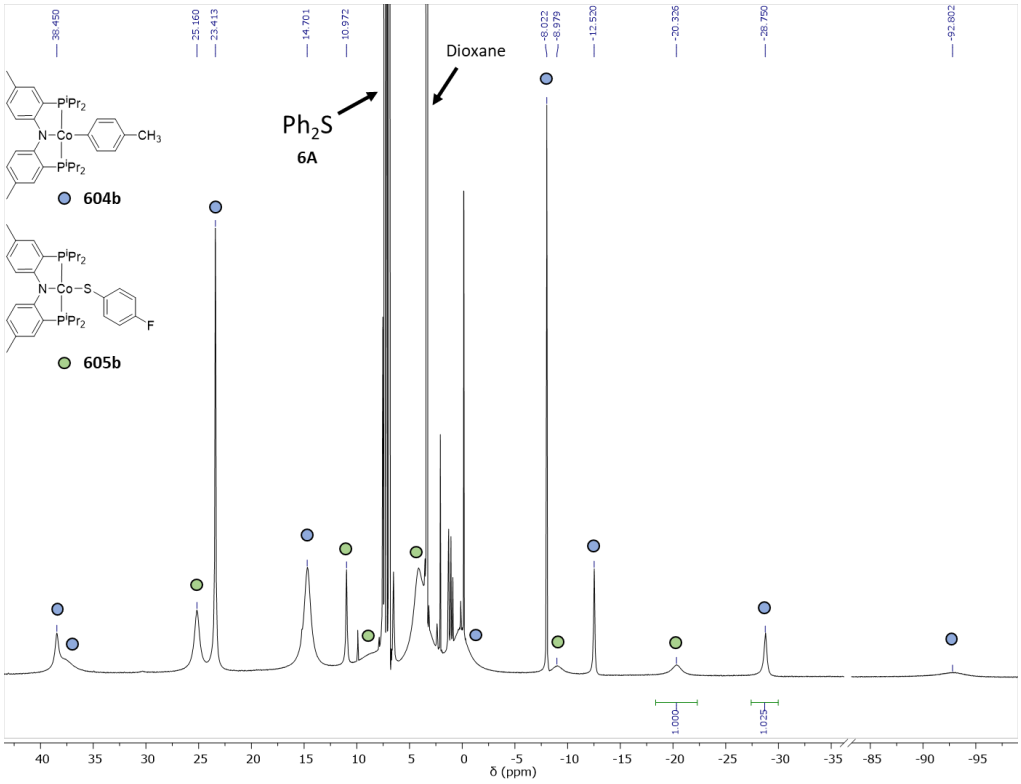

Figure VI-17. ^{1}H NMR (400 MHz, C_6D_6) spectrum of the seven-day thermolysis of **604b**, **605b**, and **6A**. Only the starting materials are observed.

6.4.4 Reactions of Co^{I} Compounds

Reaction of 609 with 608a. In an Ar-filled glove box, a J. Young tube was charged with **609** (23 mg, 0.047 mmol (PNP)Co) and **608a** (50 mg, 0.074 mmol). The solids were dissolved with C_6D_6. An immediate color change was observed upon mixing resulting in a green solution indicative of (PNP)Co^{II} complexes. ^{1}H NMR spectroscopy revealed the formation of **604a** and **605a** in a 1.0:1.0 ratio.

Reaction of 610 with 608a. In an Ar-filled glove box, a J. Young tube was charged with $(N(SiMe_3)_2)Co(PPh_3)_2$ (**611**) (17 mg, 0.022 mmol) and $^{Me}PN^{H}P^{iPr}$ (11 mg, 0.025

mmol) in C_6D_6. A ^1H NMR spectrum was acquired showing formation of **610**. **608a** (50 mg, 0.074 mmol) was then added and an immediate color change was observed upon mixing resulting in a green solution indicative of (PNP)Co^{II} complexes. ^1H NMR spectroscopy revealed the formation of **604a** and **605a** in a 1.0:1.0 ratio.

Reaction of 609 with PPh_3 and subsequent addition of tris(4-methoxyphenyl)phosphine. In an Ar-filled glove box, a J. Young tube was charged with **609** (20 mg, 0.042 mmol (PNP)Co) and triphenylphosphine (131 mg, 0.50 mmol) then diluted with C_6D_6. No reaction was observed after 3 days at room temperature. The solution was then heated to 55 °C overnight resulting in complete conversion to **610**. The tube was then brought back into the glove box and tris(4-methoxyphenyl)phosphine (176 mg, 0.50 mmol) was added. ^1H NMR spectroscopy revealed a second set of paramagnetically shifted resonances indicating that the phosphine is associated with the metal center.

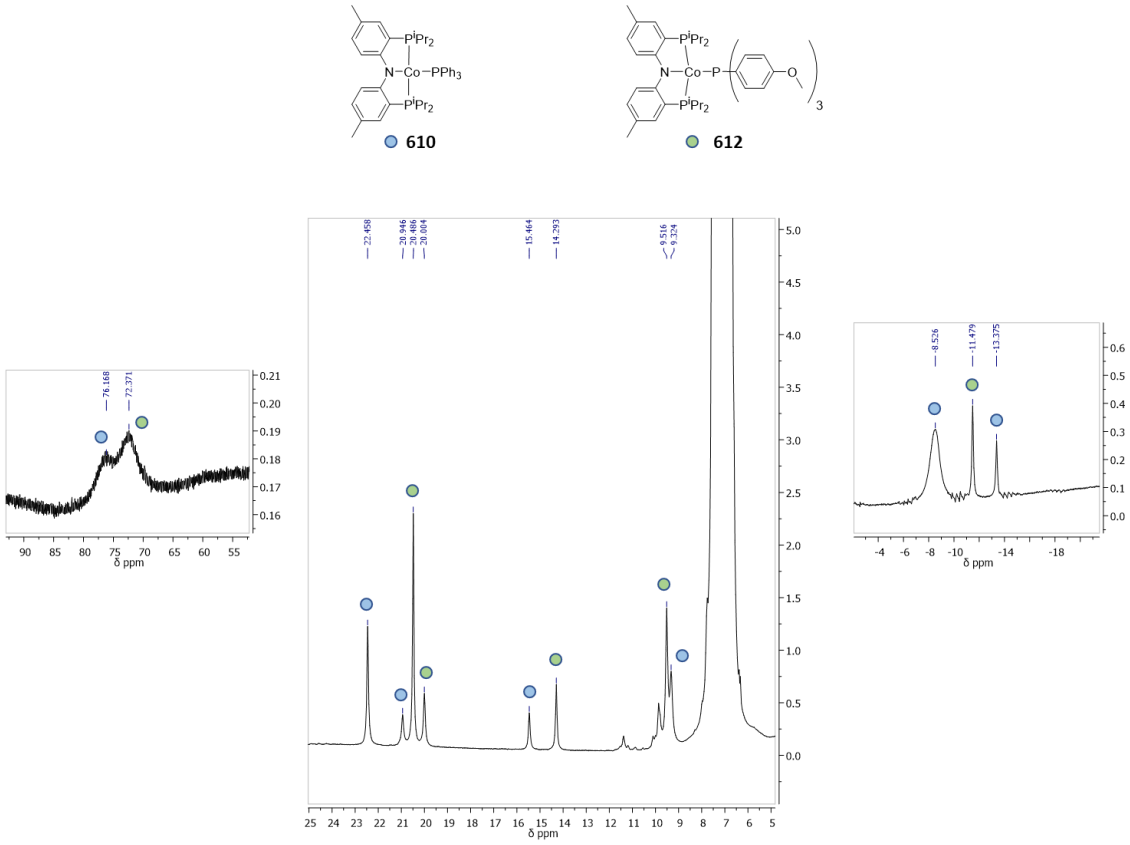

Figure VI-18. ^{1}H NMR (500 MHz, C_6D_6) of **609** after adding PPh_3 and then tris (4-methoxyphenyl)phosphine showing closely related paramagnetically shifted ^{1}H NMR resonances.

Reaction of 609 with 6A. In an Ar-filled glove box, a J. Young tube was charged with **609** (23 mg, 0.046 mmol (PNP)Co) and **6A** (18 μL, 0.10 mmol) then diluted with C_6D_6. The solution was heated at 55 °C overnight resulting in consumption of the **607** and formation of **605a** and **604a** in a 1.0:1.1 ratio as observed by ^{1}H NMR spectroscopy.

Reaction of 609 with 6E. In an Ar-filled glove box, a J. Young tube was charged with **609** (23 mg, 0.046 mmol (PNP)Co) and **6E** (125 μL of 0.40 M stock solution in C_6D_6, 0.05 mmol). The solution was heated in an 55 °C oil bath overnight resulting in little change by ^{1}H, and ^{19}F NMR spectroscopy. The solution was then heated in an 80 °C oil bath for three days resulting in complete consumption of **609**. Two paramagnetic products were identified by ^{1}H and ^{19}F NMR spectroscopy as **604c** and **605c** in a 1:1 ratio ratio. No (PNP)Co(S-4-C_6H_4F) was observed by ^{1}H nor ^{19}F NMR spectroscopy.

The solution was treated with 50 μL of 2N HCl in diethyl ether after which, **603** and **604c** were observed as the major (PNP)Co^{II} complexes in solution by ^{1}H NMR spectroscopy. APCI-MS and GC-MS of the solution revealed only **6E** and 2-isopropylthiophenol. No 4-fluorothiophenol was observed by these methods indicating that only the S–C^{ArF} bond was cleaved which is consistent with an oxidative addition C–S activation pathway.

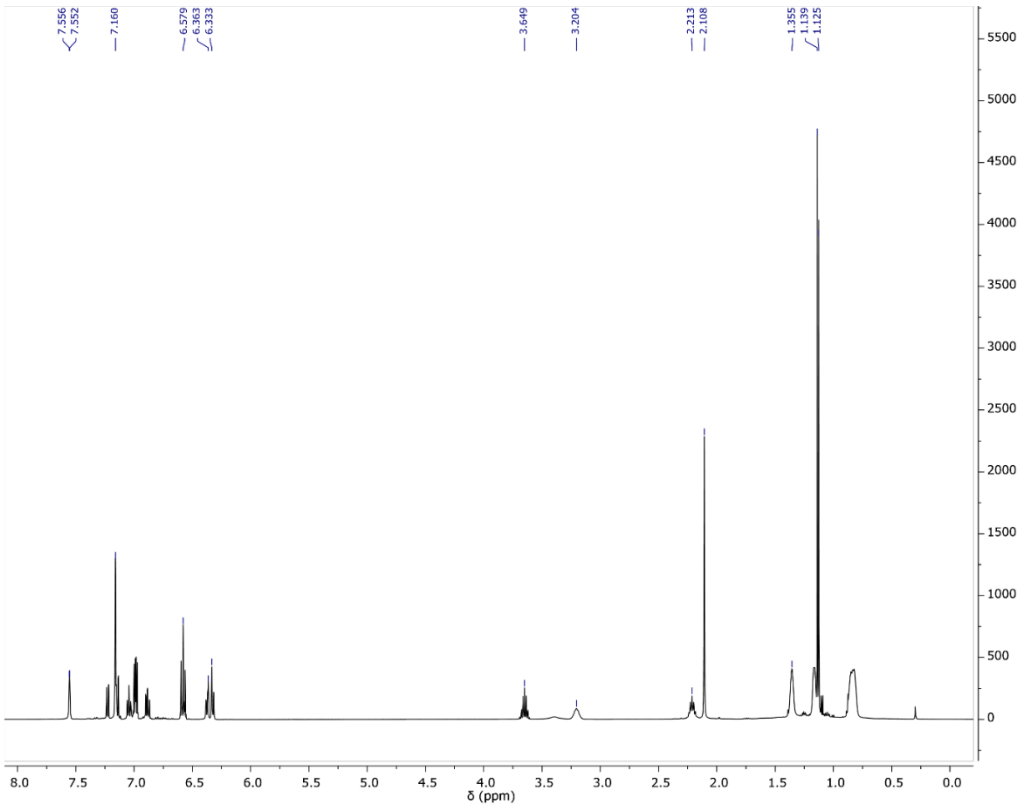

Figure VI-19. ^{1}H NMR (500 MHz, C_6D_6) of **609** and **6E** before heating. Sample contains residual THF and silicone grease.

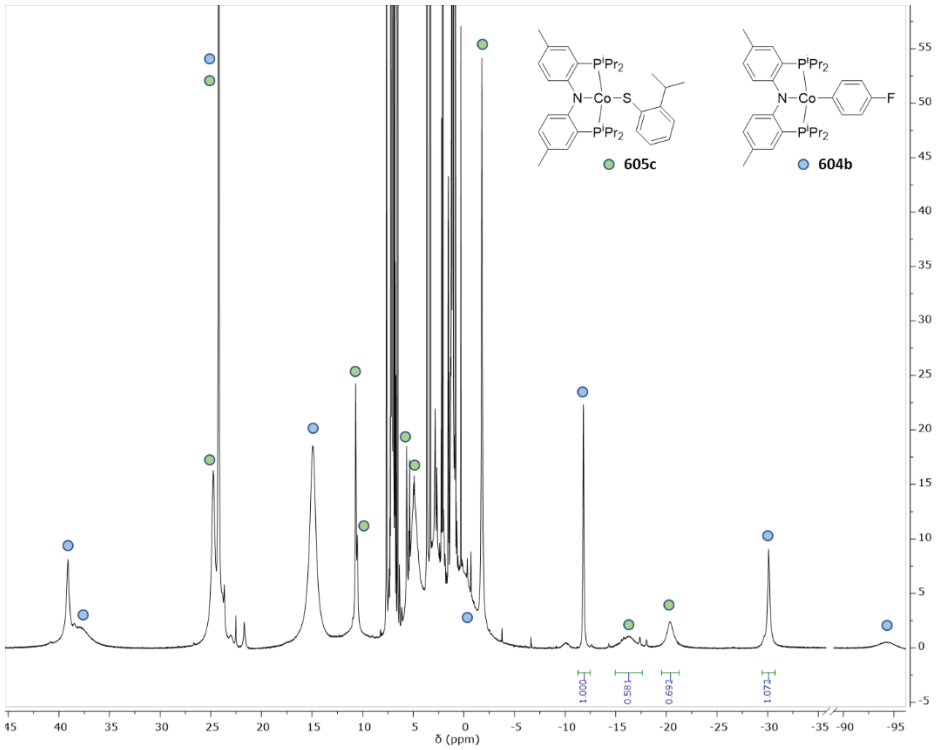

Figure VI-20. ^{1}H NMR (500 MHz, C_6D_6) of **609** and **6E** after heating at 80 °C for three days.

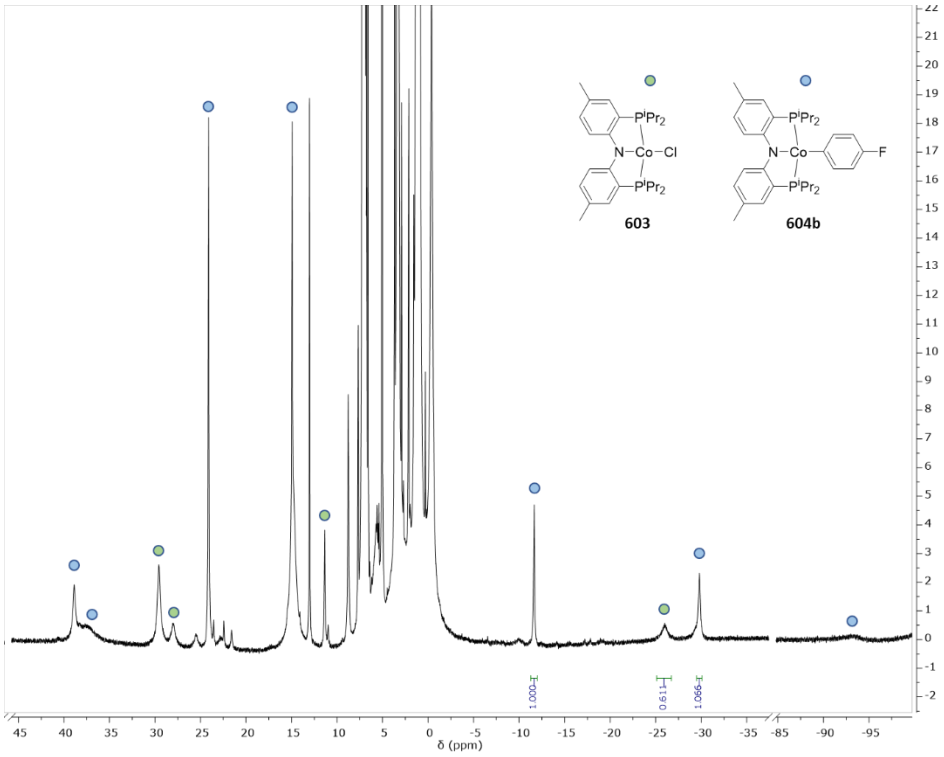

Figure VI-21. ^{1}H NMR (500 MHz, C_6D_6) of **609** and **6E** after heating at 80 °C for three days and then treating with anhydrous HCl in diethyl ether.

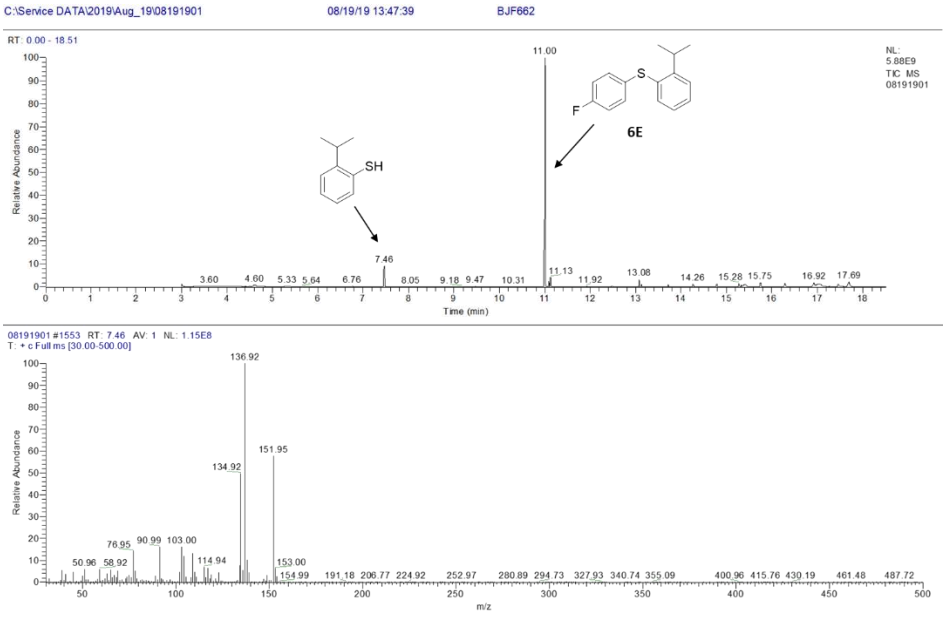

Figure VI-22. GC-MS of the reaction solution resulting from treatment with HCl. GC trace (top). Mass spectrum at a retention time of 7.46 minutes (bottom).

6.4.5 Computational Details

All computations were carried out with the Gaussian09 program.[172] All of the geometries were fully optimized by B3LYP[228] functional with LANL2DZ pseudopotentials and basis set for Co atom and 6-31G(d) basis set for the other atoms in the gas phase. Wave function of each structure was tested for SCF stability using standard methods15 and the structure was reoptimized if necessary. In particular, structures **614s**, **615s**, and **609** were calculated to be open-shell singlet, which lies lower in energy than their respective closed-shell singlet counterparts. Harmonic vibrational frequency calculations at the same level of theory were performed to ensure that either a minimum (for intermediates) or a first-order saddle point (for transition states) was obtained, and also to evaluate the zero-point vibrational energy and thermal corrections at 298.15 K The

single-point energies and solvent effects were computed with the M06[173] functional using the SDD pseudopotentials and basis set for Co atom and the 6-311+G(d,p) basis set for the other atoms based on the gas-phase optimized structures. The solvation energies were evaluated by a self-consistent reaction field (SCRF) using the SMD implicit solvent model.[229] Unless otherwise specified, the energies reported in this paper are Gibbs free energies under 298.15 K and 1 atm with solvent effect corrections.

6.4.6 X-Ray Crystallography

X-ray structural determination details for (^{Me}PNP^{iPr})Co(Tol) (604b). CCDC Deposition #1868267. Data collection method: A Leica MZ 75 microscope was used to identify a suitable brown block with very well-defined faces with dimensions (max, intermediate, and min) 0.272 x 0.183 x 0.074 mm^3 from a representative sample of crystals of the same habit. The crystal mounted on a nylon loop was then placed in a cold nitrogen stream (Oxford) maintained at 110 K.

A BRUKER APEX 2 X-ray (three-circle) diffractometer was employed for crystal screening, unit cell determination, and data collection. The goniometer was controlled using the APEX2 software suite, v2008-6.0.[135] The sample was optically centered with the aid of a video camera such that no translations were observed as the crystal was rotated through all positions. The detector was set at 6.0 cm from the crystal sample (APEX2, 512x512 pixel). The X-ray radiation employed was generated from a Mo sealed X-ray tube (K_α = 0.70173Å with a potential of 40 kV and a current of 40 mA).

Sixty data frames were taken at widths of 1.0°. These reflections were used in the auto-indexing procedure to determine the unit cell. A suitable cell was found and refined by nonlinear least squares and Bravais lattice procedures. The unit cell was verified by examination of the *h k l* overlays on several frames of data. No super-cell or erroneous reflections were observed. After careful examination of the unit cell, an extended data collection procedure (5 sets) was initiated using omega scans.

Data reduction, structure solution, and refinement methods: Integrated intensity information for each reflection was obtained by reduction of the data frames with the program APEX2.[135] The integration method employed a three-dimensional profiling algorithm and all data were corrected for Lorentz and polarization factors, as well as for crystal decay effects. Finally, the data was merged and scaled to produce a suitable data set. The absorption correction program SADABS[174] was employed to correct the data for absorption effects.

Systematic reflection conditions and statistical tests of the data suggested the space group $P2_1/c$. A solution was obtained readily using XT/XS in APEX2.[135,138] Hydrogen atoms were placed in idealized positions and were set riding on the respective parent atoms. All non-hydrogen atoms were refined with anisotropic thermal parameters. Absence of additional symmetry and voids were confirmed using PLATON (ADDSYM).[139] The structure was refined (weighted least squares refinement on F^2) to convergence.[138,140] Olex2 was employed for the final data presentation and structure plots.[140]

X-ray structural determination details for (^{Me}PNP^{iPr})Co(Ph)(OAc) (606a). CCDC Deposition #1868268. A dark purple, multi-faceted crystal of suitable size and quality (0.10 x 0.05 x 0.02 mm) was selected using an optical microscope and mounted onto a nylon loop. Low temperature (150 K) X-ray data were obtained on a Bruker APEX2 CCD based diffractometer (Mo sealed X-ray tube, K_α = 0.71073 Å). All diffractometer manipulations, including data collection, integration and scaling were carried out using the Bruker APEX2 software.[135] An absorption correction was applied using SADABS.[174] The structure was initially solved in the monoclinic *C2/c* space group using XS[138] (incorporated in SHELXTL). The solution was refined by full-matrix least squares on F^2. No additional symmetry was found using ADDSYM incorporated into the PLATON program.[139] All non-hydrogen atoms were refined with anisotropic thermal parameters. The structure was refined (weighted least squares refinement on F^2) and the final least-squares refinement converged to R_1 = 0.0299 ($I > 2\sigma(I)$, 6839 data) and wR_2 = 0.0805 (F^2, 7986 data, 383 parameters).

X-ray structural determination details for (^{Me}PNP^{iPr})Co(Ph)(SPh) (608a). CCDC Deposition #1868266. A Leica MZ 75 microscope was used to identify a suitable blue block with very well-defined faces with dimensions (max, intermediate, and min) 0.646 x 0.296 x 0.152 mm^3 from a representative sample of crystals of the same habit. The crystal mounted on a nylon loop was then placed in a cold nitrogen stream (Oxford) maintained at 110 K.

A BRUKER APEX 2 X-ray (three-circle) diffractometer was employed for crystal screening, unit cell determination, and data collection. The goniometer was controlled using the APEX2 software suite, v2008-6.0.[135] The sample was optically centered with the aid of a video camera such that no translations were observed as the crystal was rotated through all positions. The detector was set at 6.0 cm from the crystal sample (APEX2, 512x512 pixel). The X-ray radiation employed was generated from a Mo sealed X-ray tube (K_α = 0.70173Å with a potential of 40 kV and a current of 40 mA).

Sixty data frames were taken at widths of 1.0°. These reflections were used in the auto-indexing procedure to determine the unit cell. A suitable cell was found and refined by nonlinear least squares and Bravais lattice procedures. The unit cell was verified by examination of the *h k l* overlays on several frames of data. No super-cell or erroneous reflections were observed. After careful examination of the unit cell, an extended data collection procedure (6 sets) was initiated using omega scans.

Data reduction, structure solution, and refinement methods. Integrated intensity information for each reflection was obtained by reduction of the data frames with the program APEX2.[135] The integration method employed a three-dimensional profiling

algorithm and all data were corrected for Lorentz and polarization factors, as well as for crystal decay effects. Finally, the data was merged and scaled to produce a suitable data set. The absorption correction program SADABS[174] was employed to correct the data for absorption effects.

Systematic reflection conditions and statistical tests of the data suggested the space group $P2_1/n$. A solution was obtained readily using XT/XS in APEX2.[135,138] Hydrogen atoms were placed in idealized positions and were set riding on the respective parent atoms. All non-hydrogen atoms were refined with anisotropic thermal parameters. Absence of additional symmetry and voids were confirmed using PLATON (ADDSYM).[139] The structure was refined (weighted least squares refinement on F^2) to convergence.[138,140] Olex2 was employed for the final data presentation and structure plots.[140]

CHAPTER VII

ATTEMPTED OXIDATIVE ADDITION TO THE PNP COBALT FRAGMENT

7.1 Introduction

In the previous chapter, the intermediacy of a T-shaped (PNP)Co fragment was demonstrated. T-shaped intermediates of this type are high-energy d^8 metal complexes which are typically thought to have a closed-shell singlet electronic configuration with an empty $d_{x^2-y^2}$ orbital. Our group has previously shown that pincer-ligated, T-shaped Rh,[30,31b,230] Ir,[231] and Pd[232] complexes are competent in the activation of Ar–X bonds (X = H or Hal) and have designed a wide variety of precursors to which can generate T-shaped intermediates either upon the addition of a promoter or by heating (Figure VII-1). This chapter and the next outline multiple attempts at harnessing the (PNP)Co fragment **614** for use in oxidative addition and ultimately catalysis. Attempts at closing the C–S coupling catalytic cycle are disclosed here and the reactivity of **614** with various aryl halides and radical traps will be demonstrated.

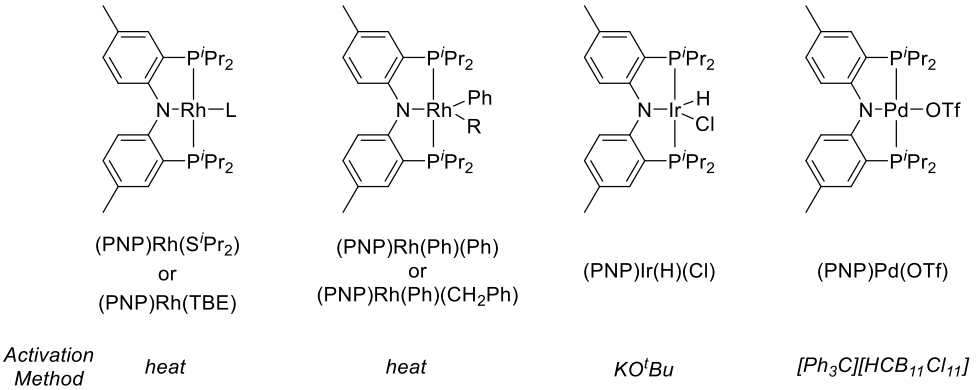

Figure VII-1. (PNP)M complexes produced by the Ozerov group to generate unsaturated, T-shaped metal complexes and their corresponding activation methods.

7.2 Results and Discussion

7.2.1 Production of and Evidence for the Existence of a T-Shaped Cobalt Fragment

Thermolysis of the isolated and characterized (PNP)Co(Ph)(SPh) (**608a**) produces the unsaturated (PNP)Co fragment (**614**). This fragment has not been observed spectroscopically as it rapidly comproportionates with the **608a** starting material. However, performing the thermolysis of **608a** under an atmosphere of CO at 80 °C overnight results in the full conversion of **608a** to (PNP)Co(CO)$_2$ (**701**) with no detectable paramagnets in solution. In this case, instead of solely the expected diphenyl sulfide product, diphenylthioester (2:1 PhC(O)SPh (**7A**):Ph$_2$S (**6A**)) was also observed (Scheme VII-1).

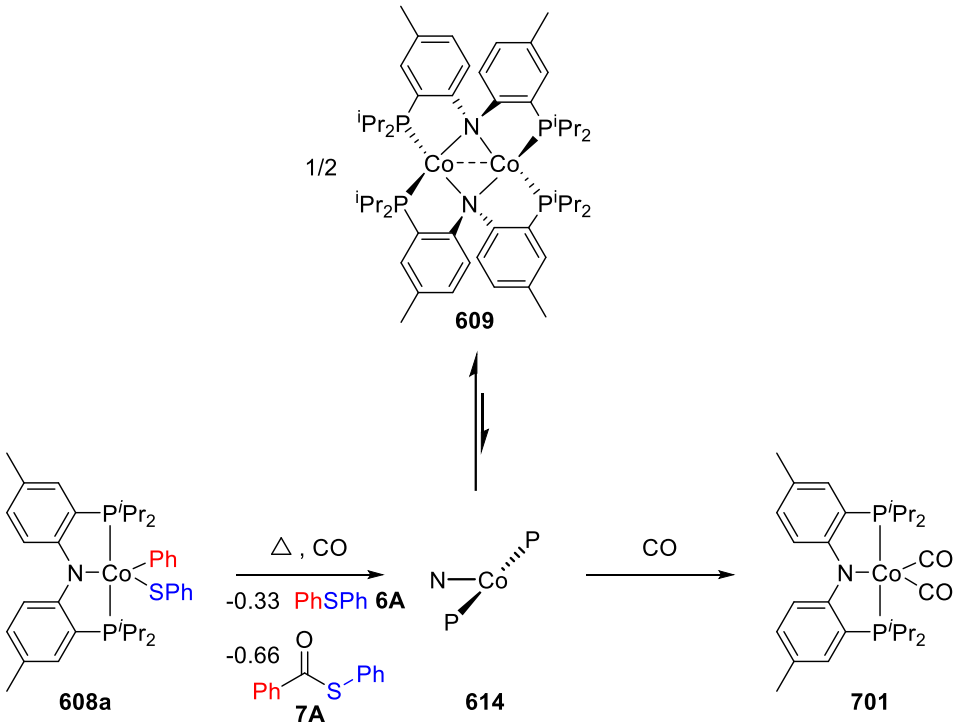

Scheme VII-1. Thermolysis of **608a** under an atmosphere and the production of **701**.

614 was also proposed by Mindiola and coworkers to be in equilibrium with **609** (Scheme VII-1) and it follows that the reaction of **609** with excess CO will produce **701**.[215] Furthermore, our reaction between **609** and diphenyl sulfide to produce **604a** and **605a** (Section 6.2.7) demonstrates that the dimer, at least at elevated temperatures, exhibits some degree of unsaturation about the metal center.

7.2.2 Production of the Cobalt Fragment in the Presence of Aryl Halides

For (PNP)Co to be a suitable platform for catalysis, the rate of oxidative addition must outcompete the rate of comproportionation and other undesirable single electron chemistry. In an effort to establish the reactivity of the (PNP)Co fragment, **609** was used as an isolable form of (PNP)Co. Treatment of **609** with *p*-FC_6H_4I and heating overnight produced **604c** and (PNP)Co(I) (**702**) in a 1:5 ratio (Scheme VII-9). This observation initially gave us some confidence that the (PNP)Co fragment would be able to perform oxidative addition after C–S elimination from **608a**; however, our interest was piqued by the unequal ratio of Co^{II} -aryl to Co^{II} -halide. The Budzelaar group has published on the behavior of (PDI)CoN_2 (**703**) in reactions with alkyl and aryl halides (Scheme VII-2). These reactions result in a deficiency of (PDI)Co(R) (**705**) vs (PDI)Co(X) (**704**) similar to our shortage of **604c** vs. **702** with apparent loss of the carbonaceous fragment.[233] The authors go on to describe this as a radical halogen atom abstraction after which the radical fragment can undergo multiple side reactions. Additionally described is the notion that an unequal ratio of Co(X) to Co(R) is a hallmark for radical behavior which appeared detrimental to the prospect of OA to **614**. One interesting detail in the Budzelaar papers is

that for reactions performed in C_6D_6, no coupling of the radical fragment R• with solvent was observed by GC/MS (*vide infra*).

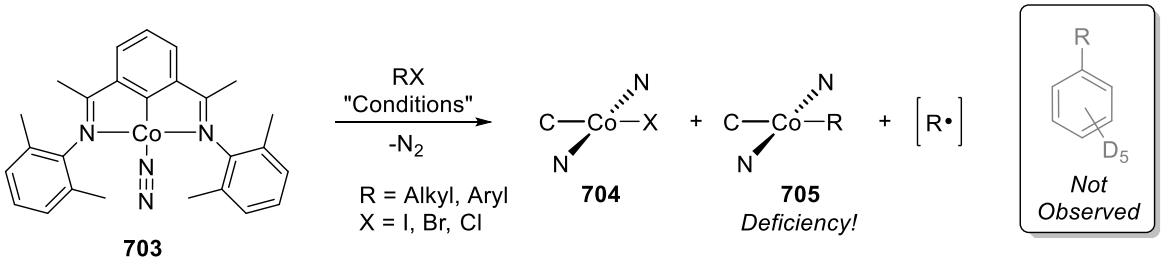

Scheme VII-2. Treatment of (PDI)Co(N_2) (**703**) with alkyl/aryl halides and observed products.

The results of the reaction between **609** and *p*-FC_6H_4I in conjunction with the report by the Budzelaar group indicate that the (PNP)Co system may activate aryl halides via radical halogen atom abstraction. Nevertheless, the attempted activation of aryl halides after RE from **608a** was attempted. Thermolysis of **608a** and 10 eq. *p*-FC_6H_4I in benzene at 80 °C for two hours afforded ~6-8% **607a** (Scheme VII-3). The identifiable paramagnetically shifted ^{1}H NMR resonances were attributable to **604a**, **605a**, **702**, and **604c** (Figure VII-12). As **604c** overlaps with other, more abundant paramagnets in solution, identifying it was difficult; however, it appears that **604c** was present, yet constituted only a small amount of the available (PNP)Co in solution. Of note is that neither **706** nor **604c** were observed by ^{19}F NMR spectroscopy.

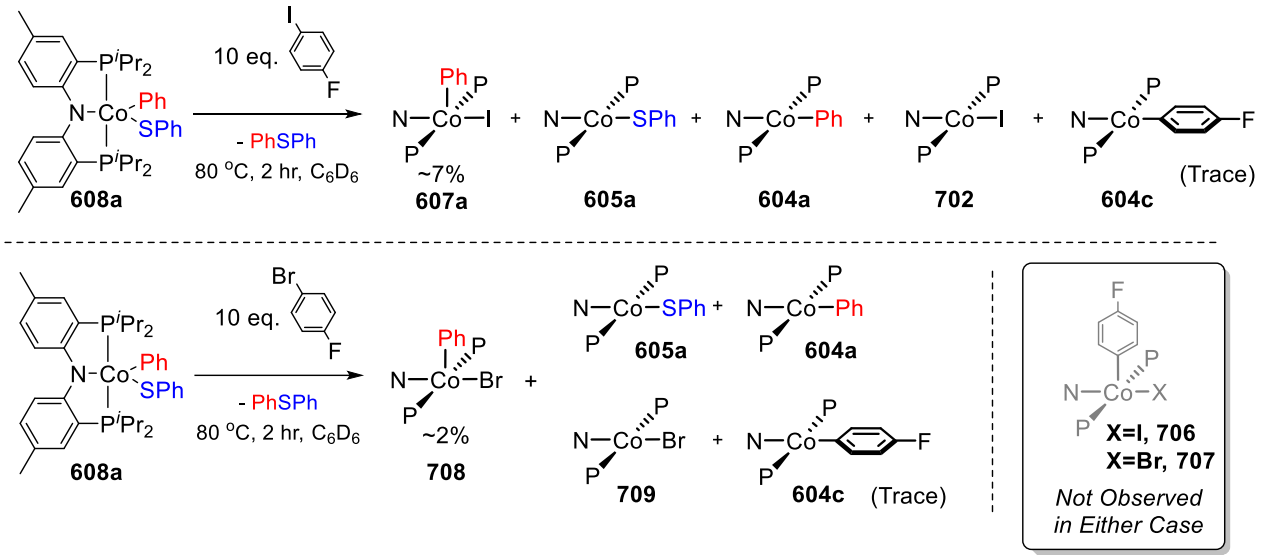

Scheme VII-3. Top: Thermolysis of 608a with *p*-C_6H_4I (10 eq.) and observed products. Bottom: Thermolysis of 608a with *p*-C_6H_4Br and observed products.

After heating this mixture overnight at 80 °C, all the cobalt-containing diamagnets were gone with **605a**, **604a**, **604c**, and **702** being the only identifiable paramagnetic species in solution in a 1.0:1.0:0.1:1.5 ratio (see section 7.2.4 for discussion of fluorophenyl deficiency). Performing the same experiment in the presence of 2 eq. BHT (v. (PNP)Co) gives no change in the observed products. Increasing the number of equivalents of *p*-FC_6H_4I v. (PNP)Co to 100 eq. instead of 10 eq. increased the amount of **607a** observed after two hours of thermolysis from ~7% to ~15% with the same distribution of Co^{II} complexes.

Among the series Cl, Br, I, iodoarenes are the easiest substrate for oxidative addition, yet also the most likely to afford radical reactivity. We moved to aryl bromides in an attempt to achieve oxidative addition instead of performing a single electron transformation. Thermolyzing **608a** in the presence of 10 eq. of *p*-FC_6H_4Br yielded no

oxidative addition product; however, some single electron chemistry was still observed. Two hours into thermolysis, unsurprisingly yielded no **707**; however, a small amount (<2%) of (PNP)Co(Ph)(Br) (**708**) was observed. After thermolysis, diamagnetic cobalt complexes were consumed leaving (PNP)Co(Br) (**709**), **605a**, and **604a** in a 0.2:1.0:1.0 ratio as observed by ^{1}H NMR spectroscopy. Some small disturbances in the baseline of the ^{1}H NMR spectrum could be attributed to (PNP)Co(p-C_6H_4F); however, they were far too small to integrate reliably (trace). Thermolysis of **608a** in the presence of *p*-FC_6H_4Cl was not attempted. The diminishing amount of (PNP)Co(Ph)(X) observed by ^{1}H NMR spectroscopy two hours of thermolysis attests to the degree of difficulty of homolytic cleavage of the C–Hal bond of *p*-FC_6H_4I vs. *p*-FC_6H_4Br.[234] The operative comproportionation event retains its swift rate resulting in fewer observed Co^{III} complexes as the difficulty of C–X cleavage is increased (Scheme VII-4). Presumably, this trend would follow and from iodo- (7% **607a**) to bromo- (<2% **708**) and then to chloro-substituted arenes where it is likely that no **712** would be observed after 2 hours.

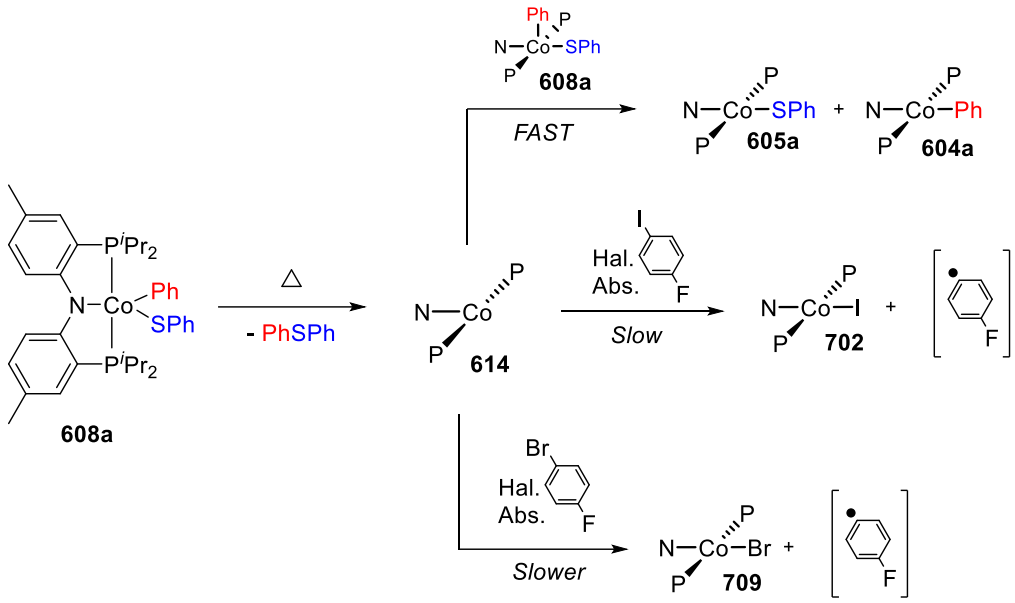

Scheme VII-4. Relative rates of the reactions which consume **614**.

*7.2.3 Ligand Exchange about (PNP)Co^{III} and Stability Testing of **607a***

Various reaction pathways for the generation of **607a** in the thermolysis **608a** in the presence of *p*-FC_6H_4I have been considered: 1) by oxidative addition of *p*-FC_6H_4I to **614** followed by a halogen-for-thiolate scrambling event with **608a** yielding **607a** and **710** (Scheme VII-5, Top). 2) iodine atom abstraction from *p*-FC_6H_4I by **604a** (Scheme VII-5, Middle), 3) iodine atom abstraction from *p*-FC_6H_4I by **614** forming **702** followed by a halogen-for-thiolate scrambling event with **608a** generating **605a** and **607a** (Scheme VII-5, Bottom).

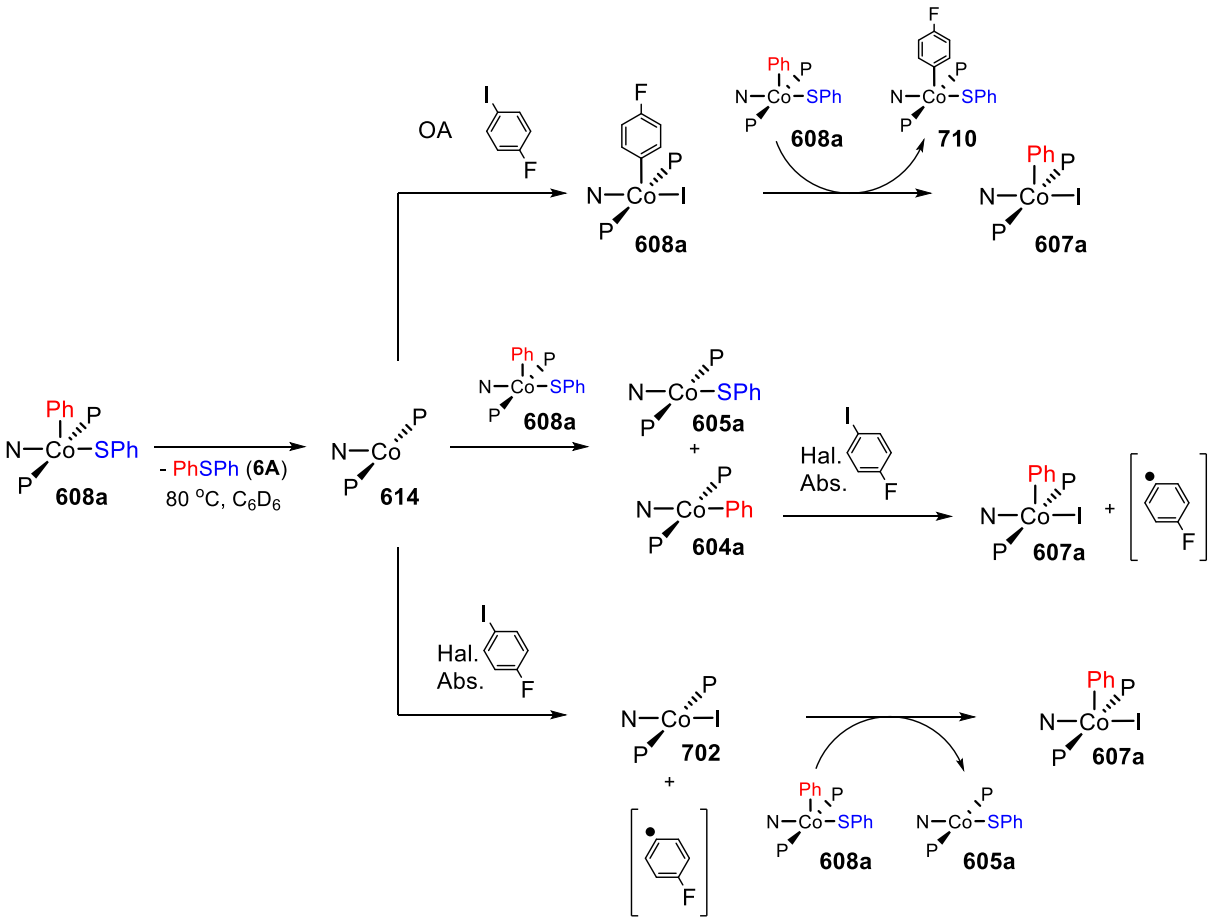

Scheme VII-5. Potential reactions to explain formation of **607a** in the thermolysis of **608a** with *p*-FC_6H_4I.

To explore the possibility that a Co^{II} complex interacted with *p*-FC_6H_4I (Scheme VII-5, Middle), 29 eq. of *p*-FC_6H_4I was added to a previously thermolyzed sample of **608a** in a J. Young tube. This mixture was then heated for three more days, at which point, only *p*-FC_6H_4I, **604a**, and **605a** were observed by ^{1}H and ^{19}F spectroscopy indicating that **604a** is incapable of activating *p*-FC_6H_4I.

As the ability of thiolates to scramble between (PNP)Co centers has been previously demonstrated (See section 6.2.5), we elected to move our search there. Halogen

atom abstraction from *p*-FC_6H_4I by **614** would form **702** with concomitant ejection of a fluorophenyl radical (Scheme VII-5, bottom). Exploring the potential for thiolate-for-halide scrambling between **608a** and **702** would be rather difficult considering that at 80 °C, where thiolate exchange takes place, **608a** actively undergoes reductive elimination. We elected instead to look for thiolate-for-halide exchange between **607a** and **605b**. The thermolysis of these two compounds in benzene at 80 °C overnight afforded **6C**, yet also produced many unidentifiable paramagnetic resonances (Scheme VII-6).

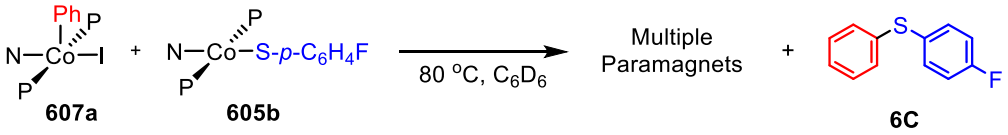

Scheme VII-6. Thermolysis of **608a** and **605b** and observed diarylsulfide product.

Intrigued by the sheer number of paramagnetic resonances in the ^{1}H NMR spectrum originating from the reaction of **607a** and **605b**, we decided to delve further into the stability of **607a**.

609 was added to a sample of **607a** resulting in an immediate reaction yielding a green solution of Co^{II} complexes **604a** and **702** in a 1.0:0.4 ratio (for a similar comproportionation event with **609**, see section 6.2.6). This indicates that **607a** is sensitive to the presence of unsaturated Co^{I} complexes (Scheme VII-7). Moreover, thermolyzing a pure sample of **607a** at 80 °C overnight resulted in the complete consumption of **607a** yielding **604a**, **702** in a 1.0:0.6 ratio along with a host of other paramagnets, establishing that **607a** is also thermally sensitive (Scheme VII-7). The origin of the deficiency of **702**

in both cases was not explored further. Between comproportionation and thermal degradation, >95% of the resonances from Figure VII-15 can be accounted for.

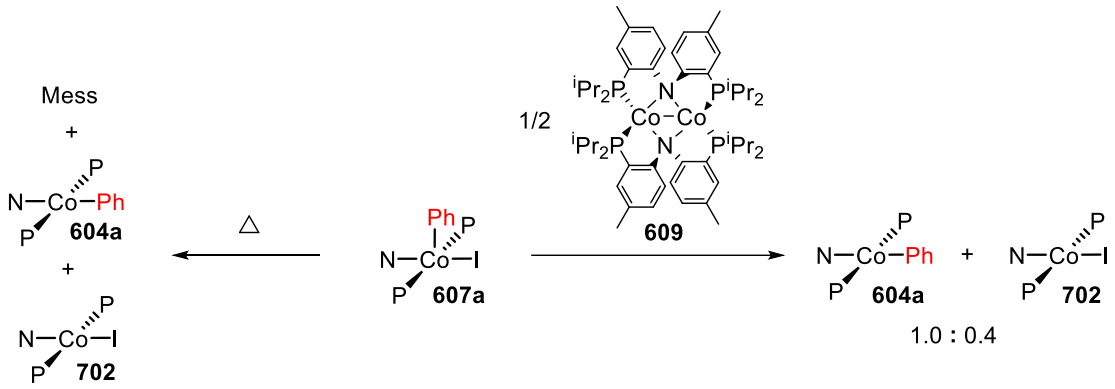

Scheme VII-7. Probing the instability of **607a** to heat and unsaturated Co^{I}.

Ideally, reacting **614** with a substrate sensitive to the presence of radicals would allow us to distinguish between the two pathways. A great deal of study has been devoted to the study of 2-allyloxyiodobenzene (**7B**) as a mechanistic probe for reactions involving halogen atom abstraction and the cyclization of the corresponding aryl radical to form 3-methyl-2,3-dihydrobenzofuran (**7C**),[235] including isotopically labeled studies.[236] Thermolyzing **608a** in the presence of **7B** resulted in the formation of **604a**, **605a**, and **702** in a 1.0:1.0:0.5 ratio (Scheme VII-8). No other identifiable paramagnetic resonances were observed including that for the expected (PNP)Co(2,3-dihydrobenzofuranyl-3-methyl) complex **711**. A small amount of **7C**[237] **(**~3% of the total 2-allyloxyiodobenzene) was observed in the ^{1}H NMR spectrum was indicating that an aryl radical is likely generated during the reaction. GC-MS analysis of the mixture supported this assignment as multiple compounds with the m/z ratio 132 were detected. While the observation of **7C** is consistent with iodine atom abstraction followed by isomerization, it is not conclusive support for

solely halogen atom abstraction. **7C** could be formed also be formed by OA of the aryl iodide and 1,2 insertion of the pendant 2-allyl substituent,[236] albeit unlikely for this system. Organic products from the iodine atom abstraction from **7B** such as the homocoupling product of the 2,3-dihydrobenzofuranyl-3-methyl radical, 1,2-bis-(2,3-dihydrobenzofuran-3-yl)ethane (**7D**), was not observed. The product resulting from deuterium atom abstraction from solvent (**7E**) or radical addition to solvent (**7F**) were also not observed. Treatment of **604a** with **7B** resulted in the formation of trace amounts of **702** and no other observable products (Scheme VII-8, Bottom) which is generally consistent with the lack of reaction between Co^{II} and *p*-FC_6H_4I. Note: Although 604a cannot activate aryl iodides effectively, it can accept Cl• from chloroform, trityl chloride, or α,α-dichlorotoluene (in a similar fashion to I• from I_2 see section 6.2.2) to form (PNP)Co(Ph)(Cl) (**712**).

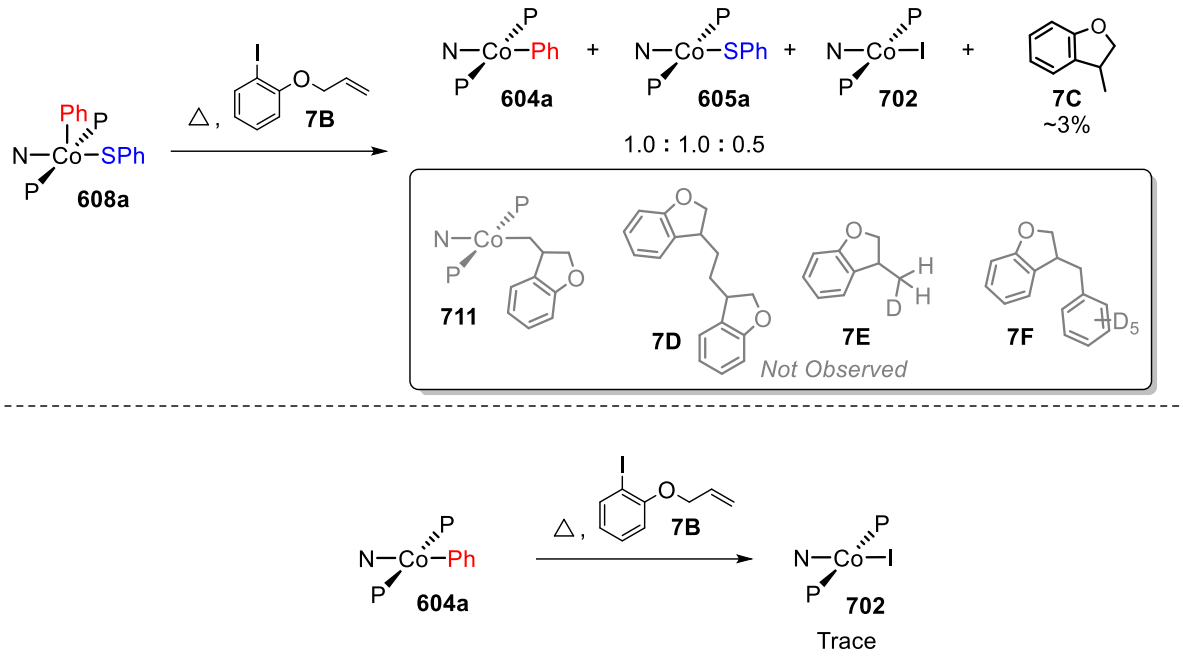

Scheme VII-8. Top: Thermolysis of 608a with 2-allyloxyoiodobenzene and observed products. Bottom: Thermolysis of 604a with 2-allyloxyiodobenzene resulting very poor conversion.

It appears (PNP)Co reacts with aryl halides predominantly via halogen atom abstraction. Whether or not the radical pathway operates through an outer sphere electron transfer to the aryl halide forming a radical anion or whether single electron processes are in competition with a two-electron oxidative addition remains to be discovered.

7.2.4 Reactions between [(PNP)Co]$_2$ and Halogenated Arenes and the Fate of •C$_6$H$_4$F

To avoid the added complexity of thiolate swapping and potential for involvement of the diarylsulfide product, the reactions between **609** and halogenated arenes was studied. Combining **609** with either *p*-FC$_6$H$_4$I, *p*-FC$_6$H$_4$Br, or *p*-FC$_6$H$_4$Cl and thermolyzing the mixture in benzene at 80 °C overnight resulted in the formation of a 1:5 mixture of **604c** and (PNP)Co(X) (X = I **702**, Br **709**, Cl **603** respectively). The consistent

1:5 ratio of **604c** and (PNP)Co(X) across the series of aryl halides supports the generation of a free aryl radical, the reactivity of which is halide-unrelated, thus resulting in the same distribution of products in each case. The thermolysis of **609** and *p*-FC_6H_4Cl was repeated in the absence of light resulting again in the same 1:5 distribution of Co^{II} products (Scheme VII-9).

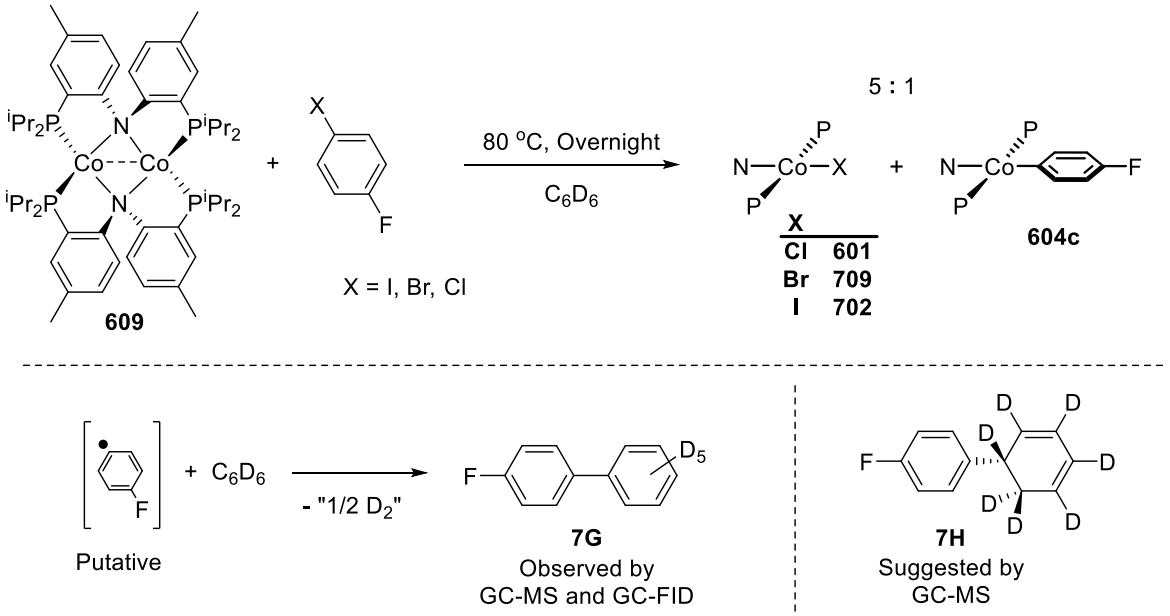

Scheme VII-9. Top: Treatment of **609** with 4-fluorohalobenzenes and observed products. Bottom: Fate of fluorophenyl radical ejected from the reaction of 609 with 4-fluorohalobenzenes.

GC-MS analysis of these reaction mixtures revealed 4-d_5-phenyl-1-fluorobenzene (**7G**). The presence of this compound helps to elucidate the lack of **604c** which would be the expected as a product of comproportionation after oxidative addition of a fluorinated halobenzene. However, given the previous observations and single electron behavior of **609**, **7G** is presumably formed by the radical addition of a 4-fluorophenyl radical[238] to a molecule of C_6D_6 (solvent) after halogen atom abstraction from 4-fluoro-1-halobenzene

by an unsaturated (PNP)Co fragment. A second peak in the GC trace was observed and tentatively assigned to 4'-fluoro-1,2-dihydro-1,1'biphenyl-1,2,2,3,4,5,6-d_7 (**7H**; m/z = 181), the de-deuteration of which would evolve D_2 and regenerate aromaticity, which may explain the fate of some of the •D; however, the unequal ratio of the organic products does not allow for total mass balance. The GC-MS trace of the products of the reaction of **609** with *p*-FC_6H_4Cl in the absence of light were nearly identical to the traces resulting from the reaction of **609** with the three 4-fluorohalobenzenes in the presence of light.

In the reactions of **608a** (Section 7.2.2) with both *p*-FC_6H_4I and *p*-FC_6H_4Br, a small amount of 4-fluorodiphenylsulfide (**6C**) was confirmed by ^{19}F NMR spectroscopy as well as by GC-MS and GC-FID. This presumably forms by abstraction of a thiolyl radical from **608a**. Also located by both GC-MS and GC-FID in both reactions was **7G** (Scheme VII-10). Again, the presence of **7G** helps elucidate the lack of **604c**. The fate of •D from C_6D_6 in the thermolysis reactions with **608a** is currently unknown; however, the mass balance for this reaction was not unity. There exist paramagnetic complexes in solution that have yet to be identified. The expected radical recombination product, 4,4'-difluorobiphenyl, was not observed by gas chromatography or ^{19}F NMR spectroscopy (Scheme VII-10). This observation is in agreement with the experimental observation that the addition of BHT does not change the observed distribution of products. The fluorophenyl radical reacts with the bulk solvent much more readily than the 2 eq. of BHT that is present.

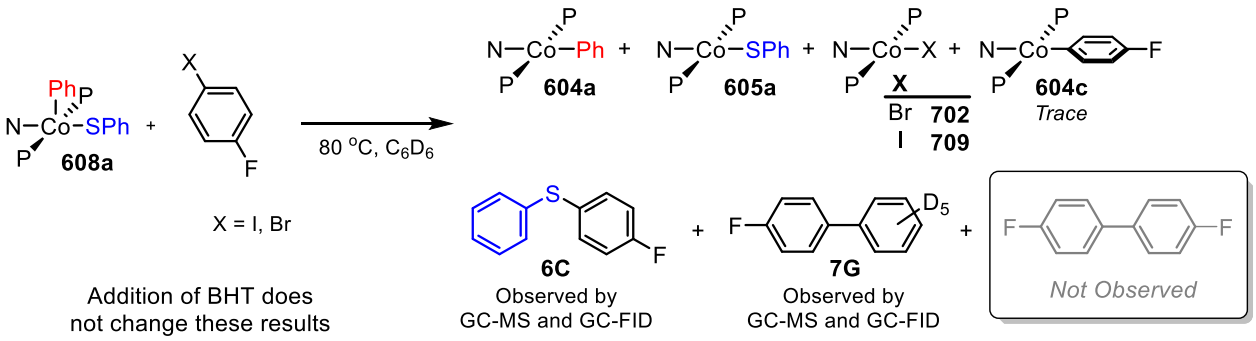

Scheme VII-10. Reaction of **608a** with 4-fluorohalobenzene and observed products.

Lastly, thermolyzing a mixture of **609** and 2-allyloxyiodobenzene at 80 °C overnight resulted in the complete consumption of **609** and the formation of (PNP)Co(I) and a trace amount of 2-methylbenzofuran. Akin to above, **711**, **7D**, **7E**, and **7F** were not observed (Scheme VII-11). Also, no paramagnets other than **702** were detected by ^{1}H NMR spectroscopy leaving the fate of the 2-allyloxyphenyl radical a mystery.

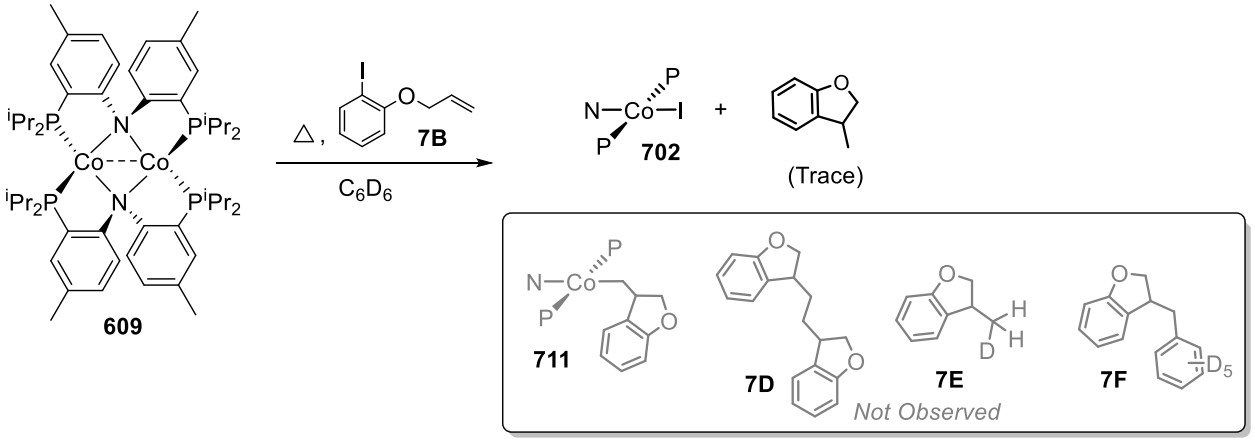

Scheme VII-11. Reaction of 609 with 2-allyloxyiodobenzene and observed products.

7.2.4 Single Electron Reactivity of Co^{II} Complexes Involving Thiolates

In developing a better synthetic method to arrive at **608a**, **604a** was treated with 0.5 eq. diphenyldisulfide (7I) and left overnight. Unfortunately, no reaction progressed at room temperature, but heating overnight resulted in the 1:1:1 formation of **6A**, **604a**, and **605a** (Scheme VII-12, top). Presumably, this reaction proceeds by the radical addition of •SPh to **604a** forming **608a**. The subsequent reductive elimination from Co^{III} forms **614** which then undergoes comproportionation with **608a**. If radical addition to **604a** is rapid, temperature and reaction time optimization may result in this being a viable synthetic route to produce **608a**; however, the current method is not.

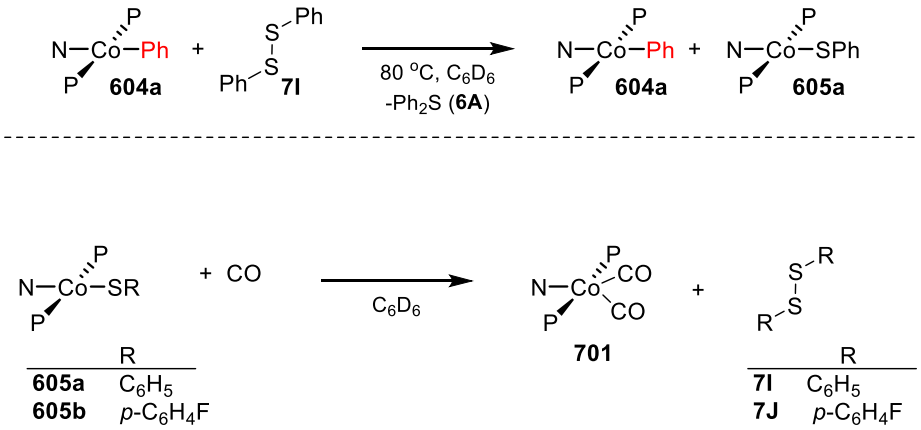

Scheme VII-12. Top: Reaction of 604a with **7I** and observed products. Bottom: Reaction of Co^{II} thiolates with CO and observed products.

When synthesizing potential byproducts for the trapping experiment with CO, **605a** was treated with CO yielding a surprising product. Upon exposure to CO, **605a** produces **701** and **7I**. The net reaction is as if the addition of CO labilizes a thiolyl radical which dimerizes forming the disulfide. Treating **605b** with CO yields a similar result forming bis(4-fluorophenyl)disulfide **7J** and **701** (Scheme VII-12, Bottom).

7.3 Conclusion

In conclusion, the potential for oxidative addition to **614** was explored and control experiments including the thermolysis and comproportionation of **607a** have resulted in the elucidation of the pathway that **614** takes when provided with 4-fluoroiodobenzene in an attempted catalytic reaction. In providing the (PNP)Co system discussed in Chapter VI with an aryl halide, it has been demonstrated that halogen atom abstraction is the predominant pathway leaving little in the way of catalytically relevant cobalt complexes. The future of this ligand scaffold in carbon–heteroatom cross-coupling is grim; however, there may be a future for **614** in radical initiated polymerization reactions or radical induced cyclization reactions where the bond strength of a given starting material is high as **609** has been demonstrated to activate difficult C–X bonds including C_{Ar}–Cl bonds.

7.4 Experimental

7.4.1 General Considerations

Unless otherwise specified, all manipulations were performed under an argon atmosphere using standard Schlenk line or glovebox techniques. Toluene, ether, tetrahydrofuran (THF), pentane, diethyl ether, and isooctane were dried and deoxygenated (by purging) using an Innovative Technologies MD-5 solvent purification system and stored over molecular sieves in an Ar-filled glovebox. C_6D_6 and hexanes were dried over and distilled from a NaK/Ph_2CO/18-crown-6 mixture and stored over molecular sieves in an Ar-filled glovebox. Me_3SiCl, *p*-FC_6H_4Cl, *p*-FC_6H_4Br, and *p*-FC_6H_4I were vacuum transferred from CaH_2 prior to use and stored in an Ar-filled glovebox Me_3SiCl was stored

in a -35 °C freezer within the glovebox. **609** was synthesized according to a literature procedure[215] All other chemicals were used as received from commercial vendors. NMR spectra were recorded on a Varian NMRS 500 spectrometer (^{1}H NMR, 499.686 MHz; ^{13}C NMR, 125.659 MHz; ^{31}P NMR, 202.298 MHz; ^{19}F NMR, 470.111 MHz), a Bruker 400 spectrometer (^{1}H NMR, 400.2 MHz), and a Varian Inova 300 spectrometer (^{1}H NMR, 299.951 MHz; ^{13}C NMR, 75.413 MHz; ^{31}P NMR, 121.425 MHz). All ^{1}H and ^{13}C NMR spectra were referenced internally to the residual solvent signal (C_6D_6 at δ 7.16 for ^{1}H NMR and δ 128.06 for ^{13}C NMR). ^{31}P NMR spectra were referenced externally using 85% H_3PO_4 at δ 0. ^{19}F NMR spectra were referenced externally using neat CF_3CO_2H at δ −78.55. Elemental analyses were performed by CALI Laboratories, Inc. (Parsippany, NJ).

7.4.2 Synthesis and Characterization

(PNP)Co(Ph)(Cl) (712). **Method A:** In an Ar-filled glove box, **606a** (0.014 g, 0.022 mmol) was dissolved in 5 mL of pentane. To this solution, Me_3SiCl (3.1 μL, 0.022 mmol) was added and the reaction was left to stir for 12 h. The volatiles were then removed and the product was extracted with ca. 5 mL of pentane and filtered through a pad of Celite on a glass frit. The volatiles were removed and a blue-green solid was obtained (0.010 g, 76%). **Method B:** In an Ar-filled glove box, a 10 mL Schlenk flask was charged with **604a** (0.104 g, 0.184 mmol) and 10 mL of diethyl ether. To this solution was added $CDCl_3$ (75 μL, 0.93 mmol). The following day, the volatiles were removed *in vacuo*. The residue was extracted with pentane and filtered through a plug of Celite. Removal of the volatiles afforded the desired product. Yield: 0.073 g (64%). **Method C:** Spectroscopically

identified. In an Ar-filled glove box, a J. Young tube was charged with **604a** (0.022 g, 0.038 mmol) and trityl chloride (0.018 g, 0.065 mmol) in C_6D_6. Instantaneous, clean conversion to the desired product was observed; however, the inability to separate the product from Gomberg's dimer[239] rendered this method unusable. **Method D:** Spectroscopically identified: In an Ar-filled glove box, a J. Young tube was charged with **604a** (0.022 g, 0.039 mmol) and α,α-dichlorotoluene (25 μL, 0.19 mmol) in C_6D_6. Conversion to the desired product was observed within 10 min. ^{1}H NMR (C_6D_6, 500 MHz): δ 7.78 (d, *J* = 8.6 Hz, 2H), 7.31 (d, *J* = 8.3 Hz, 1H), 7.13 (br s, 2H), 6.72 (ddd, *J* = 8.6 Hz, *J* = 2.1 Hz, *J* = 0.6 Hz, 2H) 6.61 (tt, *J* = 7.1 Hz, *J* = 0.9 Hz, 1H), 6.53 (ddd, *J* = 8.3 Hz, *J* = 7.1 Hz, *J* = 2.1 Hz, 1H), 6.26 (ddd, *J* = 8.3 Hz, *J* = 7.1 Hz, *J* = 2.1 Hz, 1H), 5.93 (dd, *J* = 8.3 Hz, *J* = 1.0 Hz, 1H), 3.39 (observed hept, *J* = 6.9 Hz, 2H, P–C*H*–$(CH_3)_2$), 2.42 (mult, *J* = 7.1 Hz, 2H, P–C*H*–$(CH_3)_2$), 2.16 (s, 6H), 1.51 (d, *J* = 6.1 Hz, 6H, P–CH–$(CH_3)_2$), 1.18 (d, *J* = 6.6 Hz, 6H, P–CH–$(CH_3)_2$), 0.96 (d, 5.6 Hz, 6H, P–CH–$(CH_3)_2$), 0.40 (d, *J* = 6.2 Hz, 6H, P–CH–$(CH_3)_2$). ^{13}C{^{1}H} NMR (C_6D_6, 125 MHz): δ 161.80 (br), 145.42 (s), 138.28 (s), 132.20 (s), 131.26 (overlapping signals) 125.69 (s), 124.87 (s), 123.84 (s), 122.43 (s), 122.24 (br), 24.79 (br, P–*C*H–$(CH_3)_2$), 24.34 (br, P–*C*H–$(CH_3)_2$), 20.41 (s, backbone tolyl methyls), 19.25 (s, P–CH–(CH$_3$)$_2$), 17.54 (s, P–CH–(CH$_3$)$_2$), 17.16 (s, P–CH–(CH$_3$)$_2$), 17.14 (s, P–CH–(CH$_3$)$_2$). ^{31}P{^{1}H} NMR (C_6D_6, 202 MHz): δ 25.1 (br s).

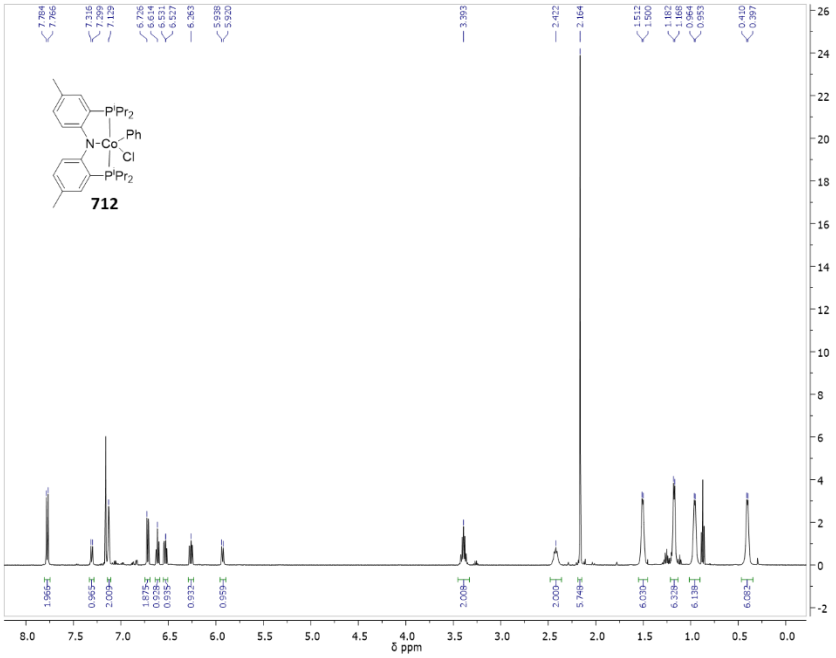

Figure VII-2. ^{1}H NMR (500 MHz, C_6D_6) spectrum of **712**. Sample contains residual pentane.

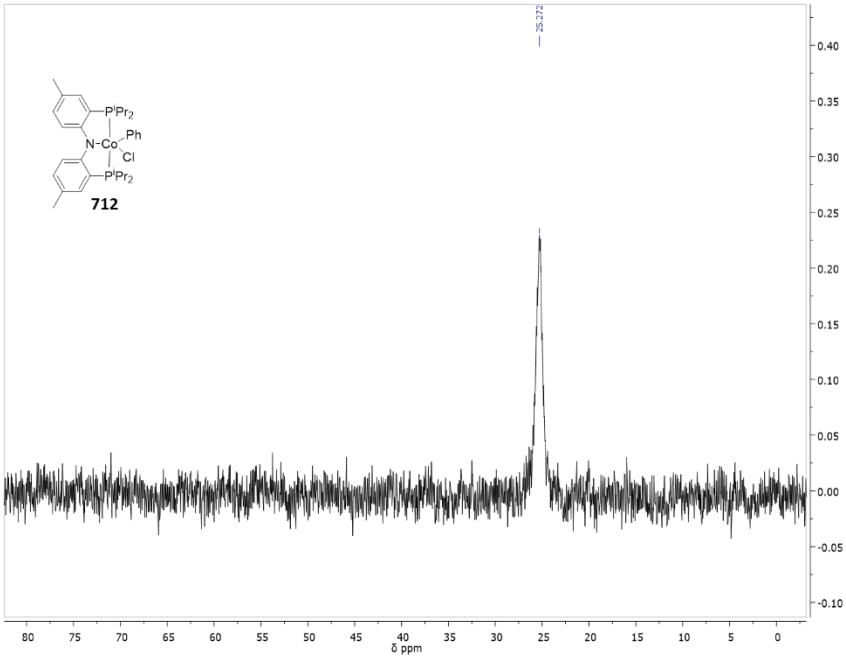

Figure VII-3. $^{31}P\{^{1}H\}$ NMR (202 MHz, C_6D_6) spectrum of **712**.

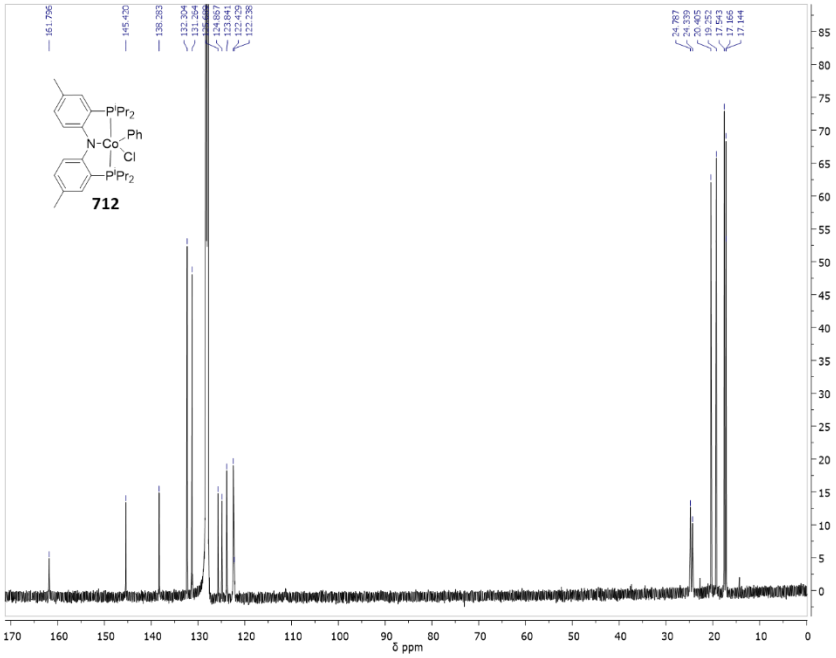

Figure VII-4. $^{13}C\{^{1}H\}$ NMR (125 MHz, C_6D_6) spectrum of **712**.

Spectroscopic observation of (PNP)Co(*p*–C_6H_4F)(I) (706). In an Ar-filled glove box, a 20 mL scintillation vial was charged with **604c** (58 mg, 0.10 mmol) and 10 mL toluene. To this vial, a solution of freshly sublimed I_2 (0.25 mL of a 0.19 M solution in THF, 0.049 mmol) was added in one portion. After four hours, the volatiles were removed *in vacuo*. The residue was dissolved in C_6D_6 for spectroscopic analysis. ^{1}H NMR (C_6D_6, 500 MHz): δ 7.80 (2H), 7.01 (1H, Co–C_6H_5F), 6.70 (2H), 6.25 (1H, Co–C_6H_5F), 6.00 (1H, Co–C_6H_5F), 5.76 (1H, Co–C_6H_5F), 3.99 (2H, P–C*H*–$(CH_3)_2$), 2.61 (2H, P–C*H*–$(CH_3)_2$), 2.11 (6H, tolyl–CH_3), 1.60 (6H, P–CH–(CH_3)$_2$), 1.21 (6H, P–CH–(CH_3)$_2$), 0.64 (6H, P–CH–(CH_3)$_2$), 0.30 (6H, P–CH–(CH_3)$_2$). $^{31}P\{^{1}H\}$ NMR (C_6D_6, 202 MHz): δ 36.7 (br s). ^{19}F NMR (C_6D_6, 470 MHz): δ -124.8.

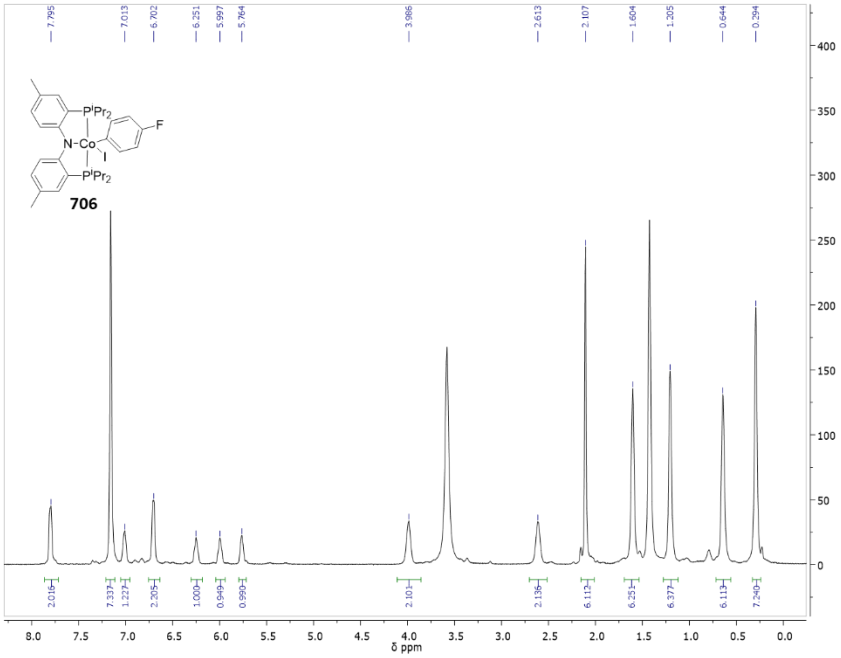

Figure VII-5. ^{1}H NMR (500 MHz, C_6D_6) spectrum of (PNP)Co(*p*-C_6H_4F)(I) (**706**). Sample contains a large amount of THF.

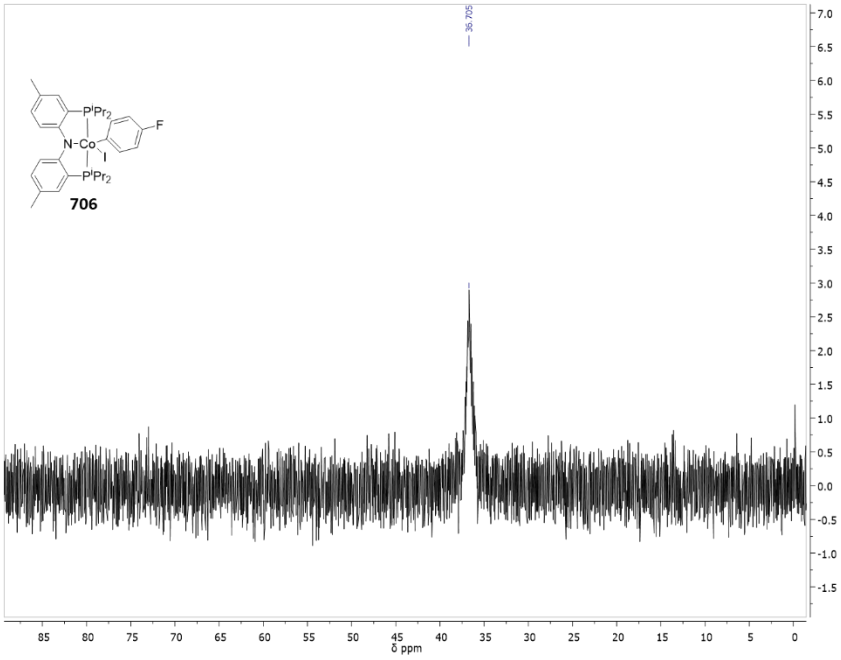

Figure VII-6. $^{31}P\{^{1}H\}$ NMR (202 MHz, C_6D_6) spectrum of (PNP)Co(*p*-C_6H_4F)(I) (**706**).

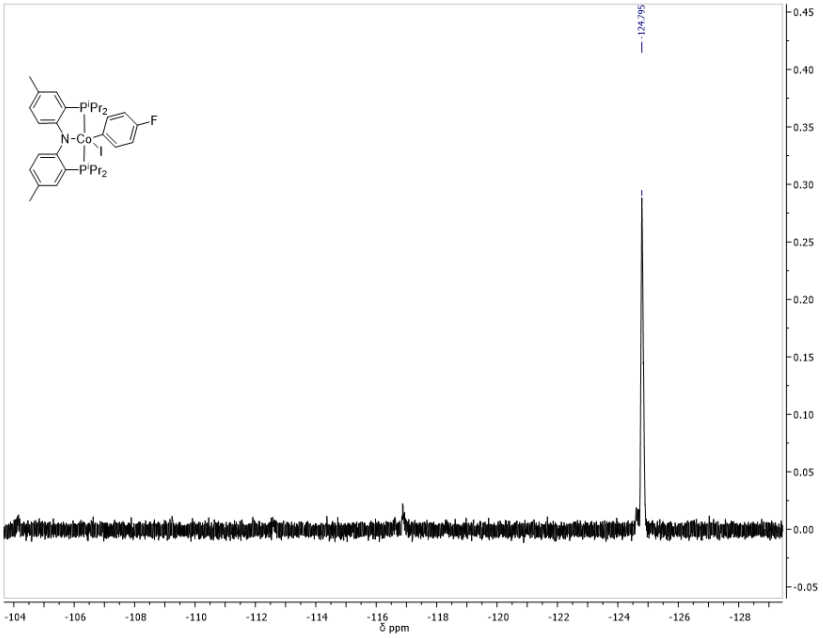

Figure VII-7. ^{19}F NMR (470 MHz, C_6D_6) spectrum of (PNP)Co(*p*-C_6H_4F)(I) (**706**).

7.4.3 Experiments to Probe the Mechanism of Aryl Halide Activation by (PNP)Co

Reaction of 609 with *p*-FC_6H_4I. In an Ar-filled glove box, **609** (21 mg, 0.043 mmol (PNP)Co) and *p*-FC_6H_4I (57 mg, 0.26 mmol) were weighed into two separate vials. *p*-FC_6H_4I was diluted with C_6D_6 and transferred onto the cobalt complex. The dissolved mixture was transferred to a J. Young tube and heated in a 55 °C oil bath for two days. ^{1}H and ^{19}F NMR spectroscopy revealed the formation of **604c** and **702**. Integrations in the ^{1}H NMR spectrum showed a 1:5 ratio. GC-MS of the reaction mixture showed a trace with a m/z = 177 with no fragments as would be expected for **7G**.

Reaction of 609 with *p*-FC_6H_4Cl. In an Ar-filled glove box, **609** (25 mg, 0.052 mmol (PNP)Co) and *p*-C_6H_4Cl (20 µL, 0.18 mmol) were combined in a J. Young tube. This mixture was heated in an 80 °C oil bath overnight resulting in the formation of 604c and 603 in a 1:5 ratio as observed by ^1H NMR spectroscopy. GC-MS of the reaction mixture showed a trace with a m/z = 177 with no fragments as would be expected for **7G**.

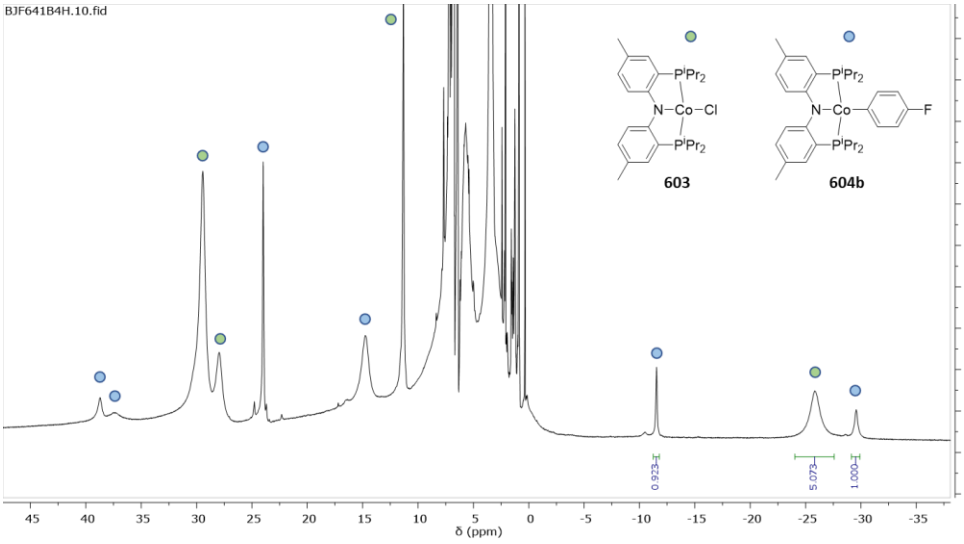

Figure VII-8. ^1H NMR (400 MHz, C_6D_6) spectrum after thermolysis of **609** with *p*-C_6H_4Cl.

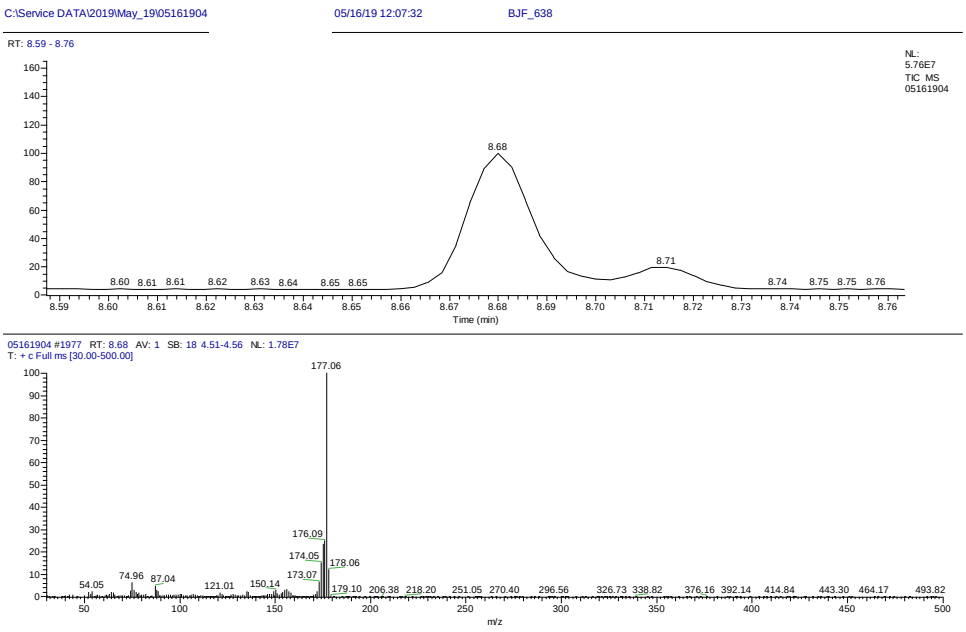

Figure VII-9. Top: Portion of GC trace of reaction mixture resulting from thermolysis of **609** with *p*-C_6H_4Cl. Bottom: Mass spectrum corresponding to GC trace at 8.68 min. m/z = 177 as expected for **7G**

Thermolysis of 608a with 10 eq. *p*-FC_6H_4I. In an Ar-filled glove box, a J. Young tube was charged with C_6D_6 (380 μL), **608a** (60 μL of a 0.15 M solution in C_6D_6, 0.009 mmol), *p*-FC_6H_4I (10 μL, 0.09 mmol), and an internal standard stock solution (50 μL) containing 1,4-dioxane (0.099 M, 0.005 mmol) as a ^1H NMR standard and benzotrifluoride (0.407 M, 0.02 mmol) as a ^{19}F NMR standard. A ^1H NMR spectrum was acquired upon mixing. The solution was then heated in an 80 °C oil bath for two hours. ^1H NMR observation revealed 6-8% conversion to **607a**. Also observed by ^1H NMR spectroscopy were **604a**, **605a**, **604c**, and **702** in a 1.0:1.0:trace:1.5 ratio.

Thermolysis of 608a with 100 eq. *p*-FC_6H_4I. In an Ar-filled glove box, a J. Young tube was charged with C_6D_6 (30 μL), **608a** (100 μL of a 0.15 M solution in C_6D_6, 0.015

mmol), *p*-FC_6H_4I (170 μL, 1.5 mmol), and an internal standard stock solution (200 μL) containing 1,4-dioxane (0.099 M, 0.039 mmol) as a ^1H NMR standard and benzotrifluoride (0.407 M, 0.16 mmol) as a ^{19}F NMR standard. A ^1H NMR spectrum was acquired upon mixing. The solution was then heated in an 80 °C oil bath for two hours. ^1H NMR observation revealed 15-18% conversion to **607a**. Also observed by ^1H NMR spectroscopy were **605a**, **604a**, **702** in a 1.0:1.6:1.3 ratio and **604c** which could not be integrated due to overlapping ^1H NMR resonances.

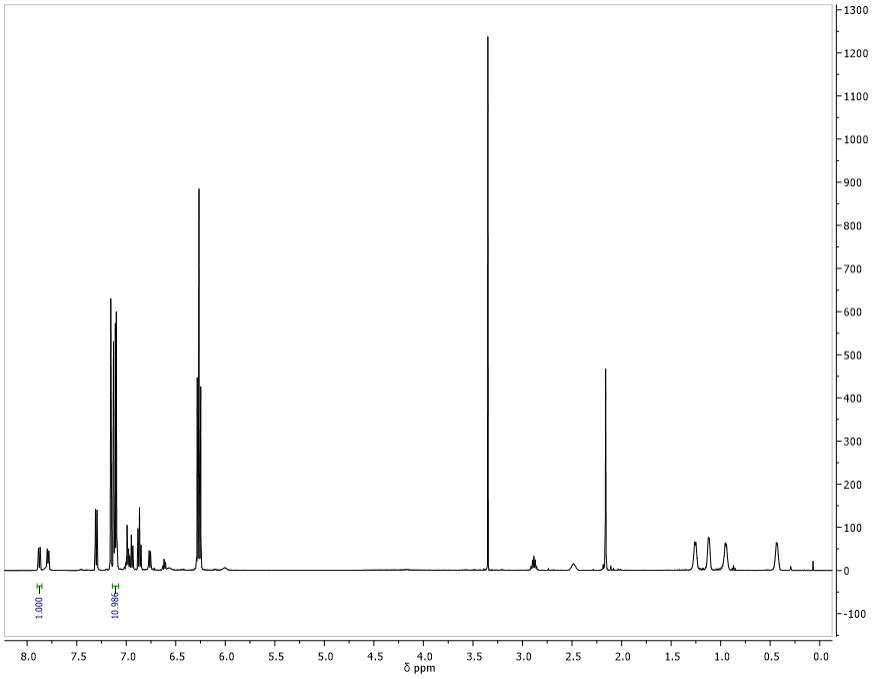

Figure VII-10. ^1H NMR (500 MHz, C_6D_6) spectrum of (PNP)Co(Ph)(SPh) (**608a**) and *p*-FC_6H_4I (10 eq.) prior to thermolysis. Dioxane (3.35 ppm) and benzotrifluoride added as internal standards.

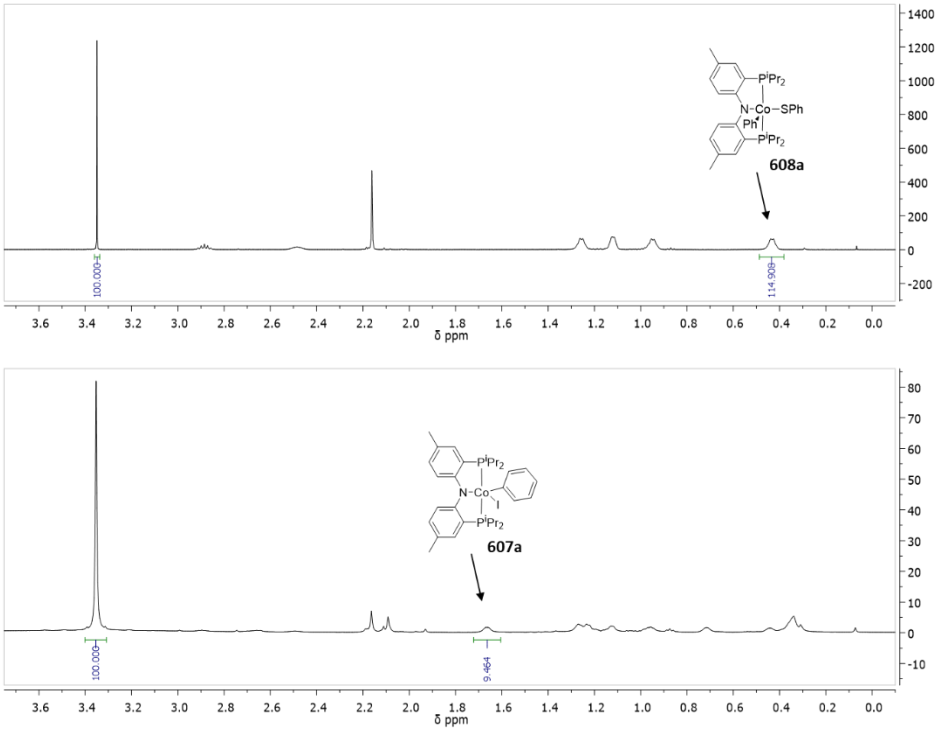

Figure VII-11. ^{1}H NMR (500 MHz, C_6D_6) Top: Aliphatic region of a mixture of 608a and *p*-FC_6H_4I before thermolysis. Bottom: Aliphatic region after thermolysis The integrated methyl resonances were selected because they were removed from overlapping resonances.

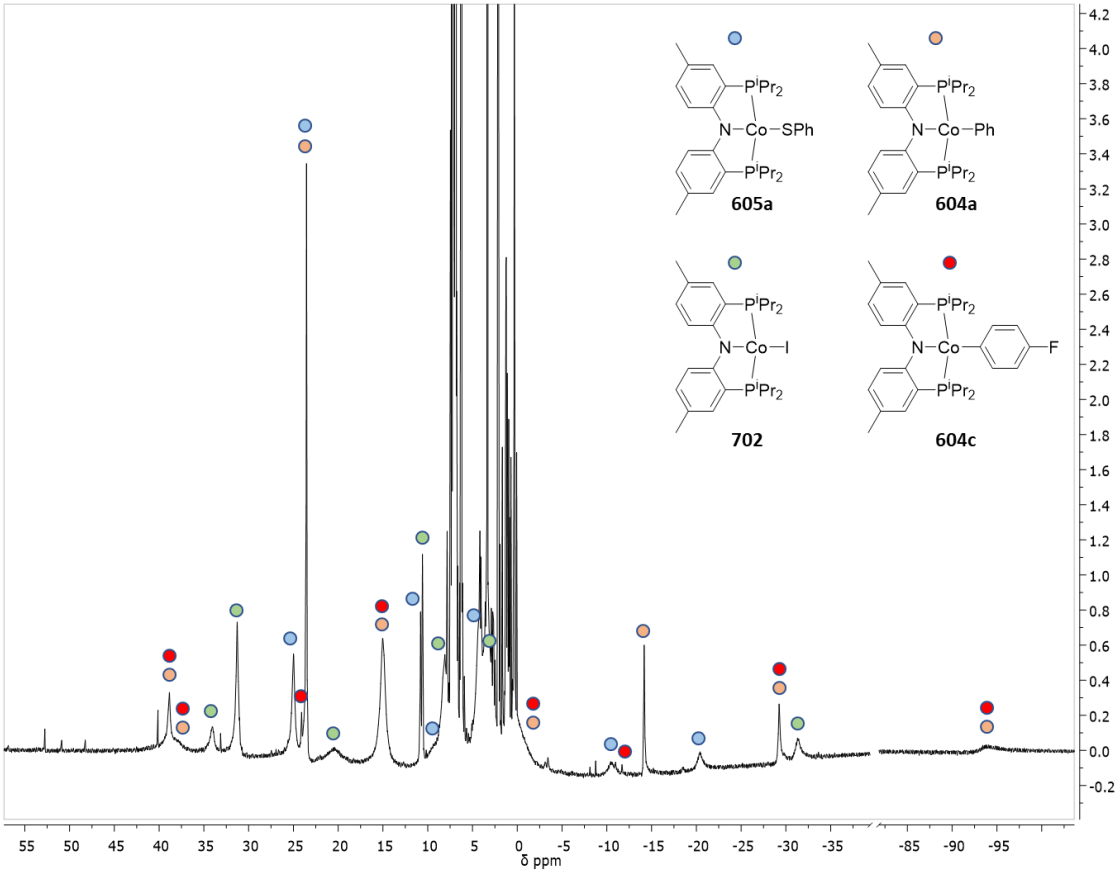

Figure VII-12. Expanded view of the ^{1}H NMR (500 MHz, C_6D_6) window of the thermolyzed mixture of **608a** with *p*-FC_6H_4I (10 eq.) showing four identifiable (PNP)Co(X) compounds with paramagnetically shifted ^{1}H NMR resonances.

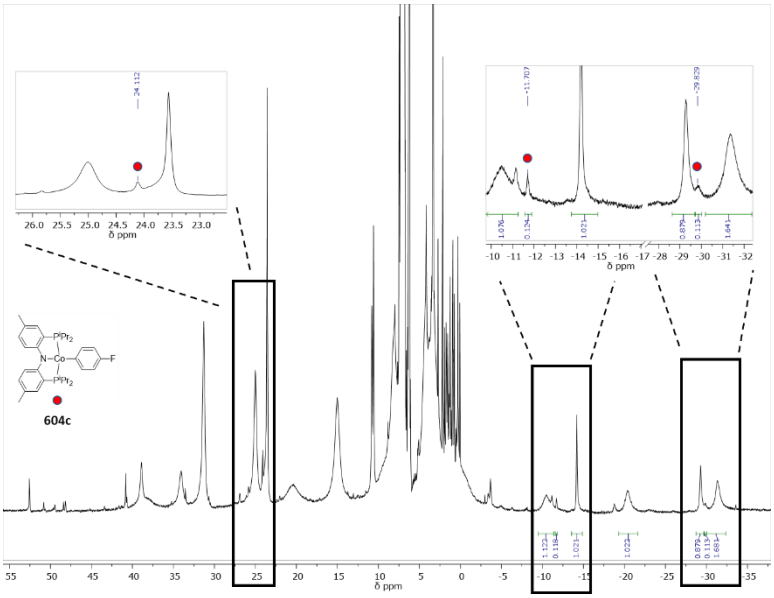

Figure VII-13. Expanded ^{1}H NMR (500 MHz, C_6D_6) spectral window of the thermolyzed mixture of **608a** with *p*-FC_6H_4I (10 eq.) showing **604c** as designated by red dots.

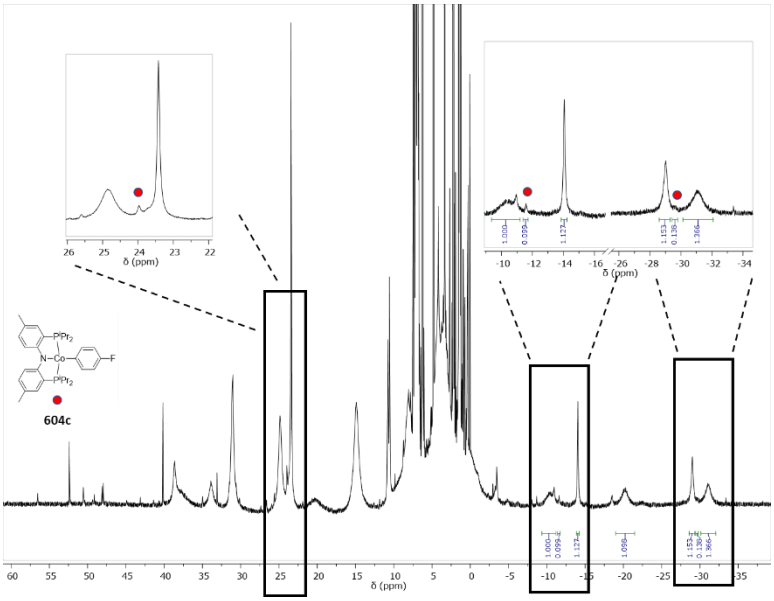

Figure VII-14. Expanded ^{1}H NMR (400 MHz, C_6D_6) spectral window of the thermolyzed mixture of **608a** with *p*-FC_6H_4I and BHT (2 eq.) **605a**, **604a**, **604c**, and **702** yielded in a 1.0:1.1:0.1:1.4 ratio. Nearly identical to the thermolysis reaction performed in the absence of BHT. **604c** designated by red dots.

Thermolysis of 604c with 5 eq. *p*-FC_6H_4I. In an Ar-filled glove box, a J. Young tube was charged with **604c** (41 mg, 0.071 mmol), *p*-FC_6H_4I (40 μL, 0.35 mmol), and C_6D_6. The tube was heated in an 80 °C oil bath for three days. After three days, only the starting materials were observed by ^1H and ^{19}F NMR spectroscopy.

Thermolysis of a 1:1 mixture of 604a and 605a with *p*-FC_6H_4I. In an Ar-filled glovebox, a J. Young tube was charged with C_6D_6 (360 μL), **608a** (60 μL of a 0.15 M solution in C_6D_6, 0.009 mmol), and an internal standard stock solution (50 μL) containing 1,4-dioxane (0.099 M, 0.005 mmol) and benzotrifluoride (0.407 M, 0.02 mmol). The solution was then heated in an 80 °C oil bath for three days. ^1H NMR spectroscopy revealed the expected **605a** and **604a**. The J. Young tube was brought back into the glove box and *p*-FC_6H_4I (30 μL, 0.26 mmol) was added by microsyringe. The mixture was then heated to 80 °C for three days and no change was observed by ^{19}F or ^1H NMR spectroscopy.

Thermolysis of 607a with 605b in C_6D_6. In an Ar-filled glove box, a J. Young tube was charged with **607a** (21 mg, 0.030 mmol), **605b** (19 mg, 0.030 mmol), and 600 μL. This tube was heated overnight in an 80 °C oil bath resulting in the complete consumption of **607a** and observation of **6C** by ^{19}F NMR spectroscopy. A large number of paramagnetic complexes were observed by ^1H NMR spectroscopy.

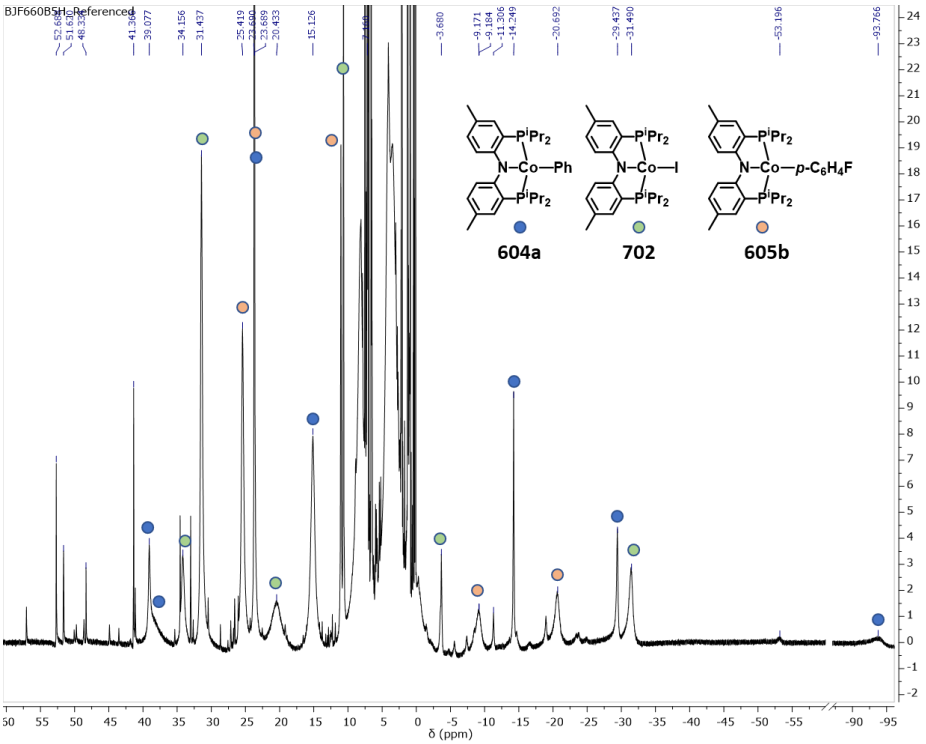

Figure VII-15. ^{1}H NMR (500 MHz, C_6D_6) spectrum of the mixture resulting from the thermolysis of **607a** with **605b**.

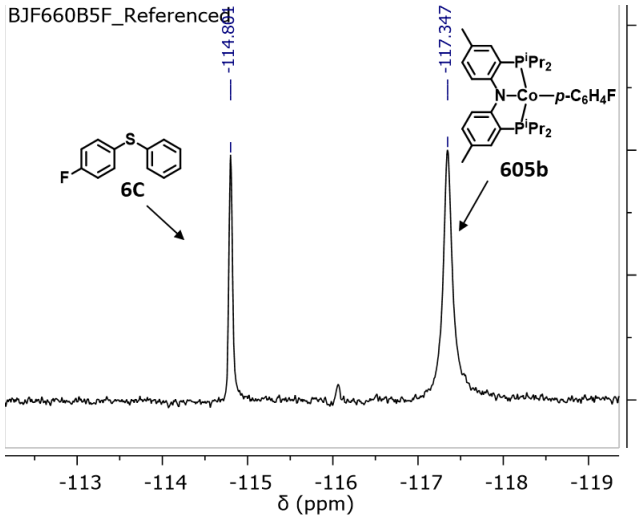

Figure VII-16. ^{19}F NMR (470 MHz, C_6D_6) spectrum of the mixture resulting from the thermolysis of **607a** with **605a**.

7.4.4 Stability Testing of (PNP)Co(Ph)(I)

Thermolysis of 607a in C_6D_6. In an Ar-filled glove box, a J. Young tube was charged with **607a** (40 mg, 0.064 mmol) and 600 µL of C_6D_6. The tube was heated for two days in an 80 °C oil bath resulting in the complete decomposition of **607a** and appearance of **604a** and **702** along with other unidentified paramagnets.

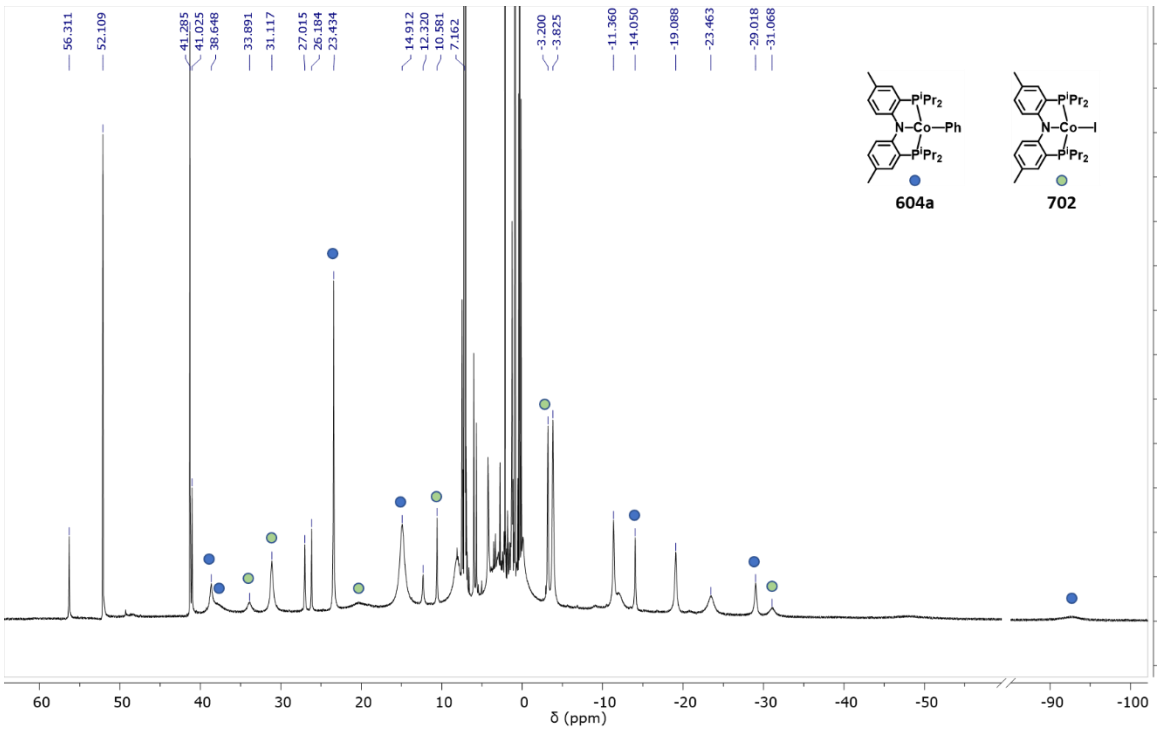

Figure VII-17. ^{1}H NMR (400MHz, C_6D_6) spectrum resulting from the thermolysis of **607a** in benzene.

Reaction of 607a with 609 in C_6D_6. In an Ar-filled glove box, a J. Young tube was charged with **607a** (20 mg, 0.029 mmol), **609** (17 mg, 0.034 mmol (PNP)Co), and 600 µL of C_6D_6. The solution in the tube immediately turned green and ^{1}H NMR spectroscopy revealed the formation of **604a** and **702**.

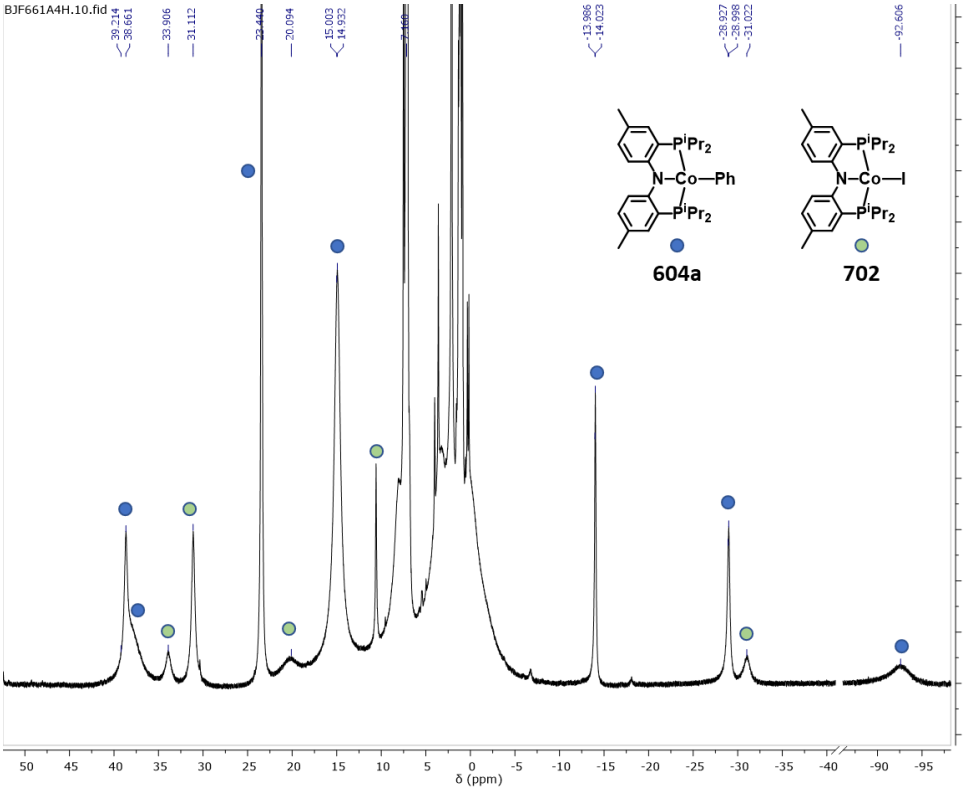

Figure VII-18. ^{1}H NMR (400 MHz, C_6D_6) resulting from the comproportionation between **607a** and **609**.

7.4.5 Single Reactivity of Cobalt Complexes with Disulfides

Reaction of 604a with PhSSPh. In an Ar-filled glovebox, a J. Young tube was charged with **604a** (32 mg, 0.057 mmol) and diphenyl disulfide (100 μL of a 0.29 M solution in C_6D_6, 0.029 mmol) then diluted with C_6D_6. No reaction was observed after sitting overnight. The tube was placed in an 80 °C oil bath overnight resulting in formation of **6A**, **604a,** and **605a**.

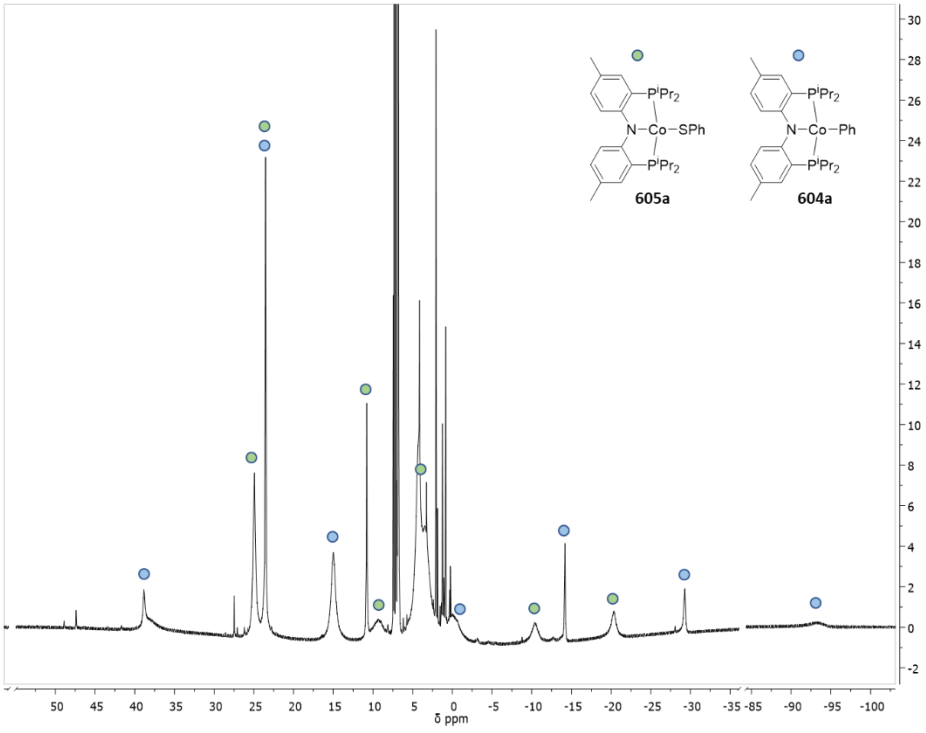

Figure VII-19. ^{1}H NMR (500 MHz, C_6D_6) spectrum showing the resultant mixture of thermolysis of **604a** with **7I**.

Reaction of a 1:1:1 mixture of 604b, 605b, and 6D with CO. In an Ar-filled glovebox, a J. Young tube was charged with **608b** (20 mg, 0.028 mmol) and C_6D_6 (600 µL). The tube was placed in an 80 °C oil bath overnight resulting in formation of **6D**, **604b,** and **605b** in a 1:1:1 ratio (see Section 6.2.5). This solution was subjected to three freeze-pump-thaw cycles and backfilled with 1 atm CO. ^{19}F NMR spectroscopy revealed the formation of 6D and 7J in a 1.0:0.5 ratio with concomitant formation of **701** as observed by ^{1}H and $^{31}P\{^{1}H\}$ NMR spectroscopy. **604b** persists in the presence of CO as observed by ^{1}H NMR spectroscopy.

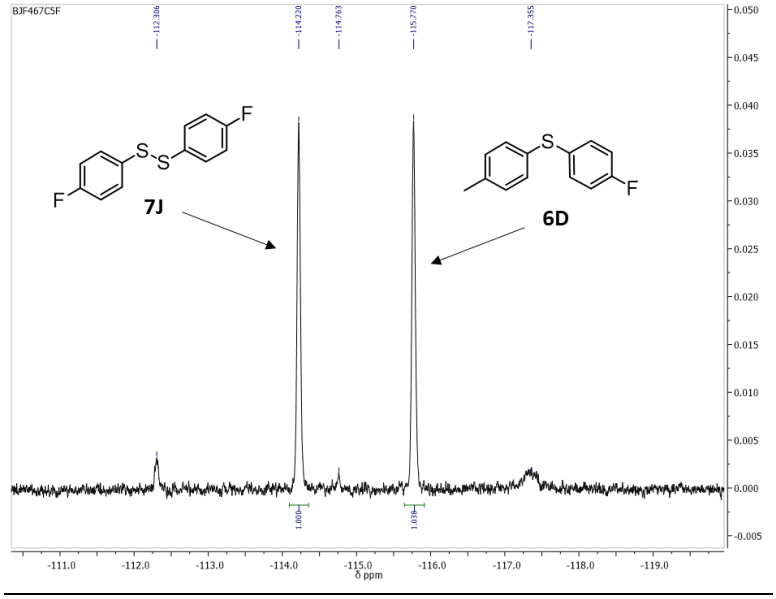

Figure VII-20. ^{19}F NMR (470 MHz, C_6D_6) spectrum of the products of thermolysis of **608b** after addition of 1 atm CO revealing **7J** and **6D** in a 0.5:1.0 ratio (note two fluorines on **7J**)

CHAPTER VIII

REACTIONS OF PNP LIGATED COBALT COMPLEXES WITH ALCOHOLS AND THEIR DERIVATIVES

8.1 Introduction

To produce a catalytic cycle using (PNP)Co we turned our sights toward alcohol dehydrogenation. We hypothesized that cobalt complexes containing oxygenous substituents would be advantageous for alcohol dehydrogenation. Selection of (PNP)Co as a platform for the dehydrogenation of alcohols was multifaceted. Firstly, the central amido of the PNP ligand has shown basic behavior in our group which may prove adept at O–H bond activation.[240] Secondly, the SOMO of Co^{II} should be a better size match for mixing with the HOMO of the PNP ligand resulting in a delocalized molecular orbital and increasing the ease of oxidation. The electrochemical oxidation of the PNP ligand has been extensively studied and shown to be easily oxidizable. Potentially the redox capabilities of the supporting ligand coupled with the size match of the Co^{II} SOMO would allow for aerobic oxidation of the (PNP)Co(X) species. The aerobic oxidation of the ligand in this scenario would result in an oxidation of cobalt creating a "Co^{III}-like" species without the need for an added reductant.

A closely related reaction that we were interested in was the activation of C–O bonds of esters derived from alcohols. These reactions are powerful in organic synthesis as the use of these C–O bonds in cross-coupling are typically orthogonal to the cross-coupling reactions of aryl halides. Our group has had success with a PNP ligated rhodium

complex for the activation of aryl esters[31c] which gave us some confidence that (PNP)Co would be a suitable platform for C–O activation. By building on our paradigm that Group 9 M^{I}/M^{III} catalysis can mimic Group 10 M^{0}/M^{II} chemistry (predominantly of Ni in this case), we applied our cobalt complexes to the cleavage of ester C–O bonds. This was especially interesting as there have been very few examples of cobalt mediated ester cleavage in the literature. And of the examples that do exist, none of them can cleave the C–O bond of an aryl ester. The Yamamoto group has the first example of cobalt mediated cleavage of esters (Scheme VIII-1, Top Left).[81] In their experiments, treating a cobalt hydride complex (**801**) with vinyl acetate for one day at room temperature resulted in the loss of N_2, ethylene and a trace amount of ethane. The cobalt acetate product was not isolated, only proposed due to a loss of PPh_3 from the cobalt material as observed by IR spectroscopy. Satisfactory elemental analysis for the purported ligandless "Co(OAc)" or the pyridine adduct (from attempted purification) was not obtained.[81] Use of **801** in the cleavage of allyl esters was reported by Srivastava (Scheme VIII-1, Top Right). In this report, the cobalt complex cleaves the allyl C–O bond yielding propylene and produces the corresponding tris(triphenylphosphine)cobalt carboxylate. The cobalt carboxylates were characterized by elemental analysis and IR spectroscopy. Some ^{1}H NMR data was reported but was not necessarily enlightening as there are no extraordinarily diagnostic signals.[80] In a second report by the Yamamoto group, the use of cobalt compounds **801** or **802** in the cleavage of aryl esters was recorded. This aligns with our interests; however, the aryl C–O bond in this system was left untouched as compounds **801** and **802** undergo exclusive cleavage of the acyl C–O bond producing tris(triphenylphosphine)cobalt

phenoxide (**803**) (Scheme VIII-1, Bottom).[241] In this case, the cobalt containing by product was characterized by X-ray crystallography as well as by direct synthesis of an authentic sample of **803**.

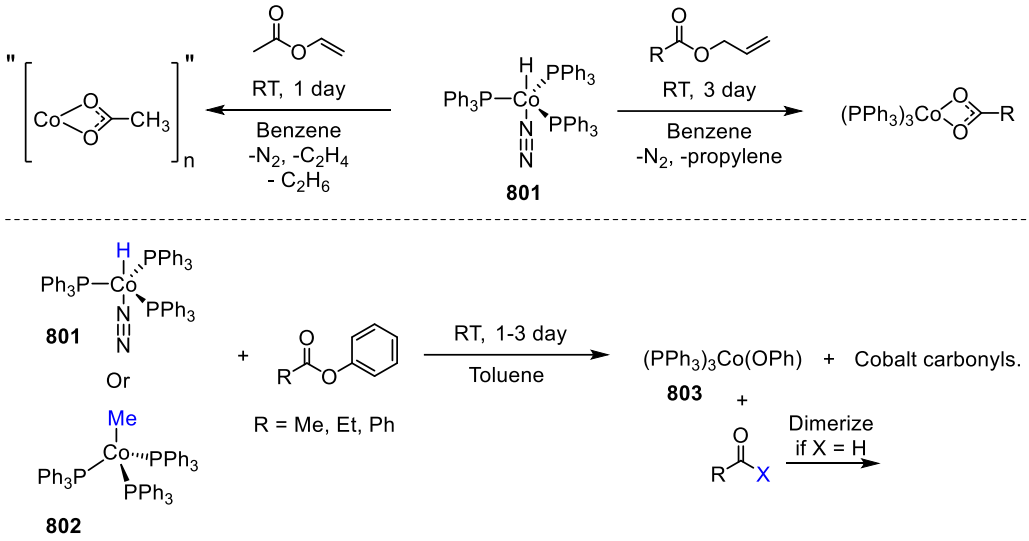

Scheme VIII-1. Top: Reactions of **801** in the cleavage of vinyl and allyl acetates. Bottom: Reaction of **801** and **802** in the cleavage of aryl carboxylates yielding **803**, cobalt carbonyls, and carbonyl-containing organic byproducts.

More recently, cobalt salts have found use in the allylation or vinylation of aryl halides or carbonyl compounds. In 2003, the Gosmini group reported the use of $CoBr_2$ in the allylation of functionalized aryl halides. Allylating aryl bromides required the use of 20 mol% CoBr and multiple stoichiometric equivalents of reductant (Zn). The increasing difficulty of functionalizing aryl chlorides required the use of a trimetallic system including 10 eq. of Mn powder and added $FeBr_2$ to what was an already quite complex system. Although this system was capable of allylating aryl halides, substantial amounts of byproducts were observed including the products of protonolysis and aryl homocoupling (Scheme VIII-2, Top).[242] Cobalt mediated vinylation of aryl halides was

disclosed which included the addition of a bipyridine supporting ligand. Vinylation of aryl halides did not require the use of a trimetallic system, but still necessitated the use of 10 eq. of Mn powder (Scheme VIII-2, middle).[243] The $CoBr_2$/Zn from the allylation of aryl bromides was adapted for the allylation of carbonyl compounds which required more $CoBr_2$ and less reductant (Scheme VIII-2, Bottom).[244] Electrochemical methods for the vinylation of aryl halides using vinylic acetates were also disclosed.[245]

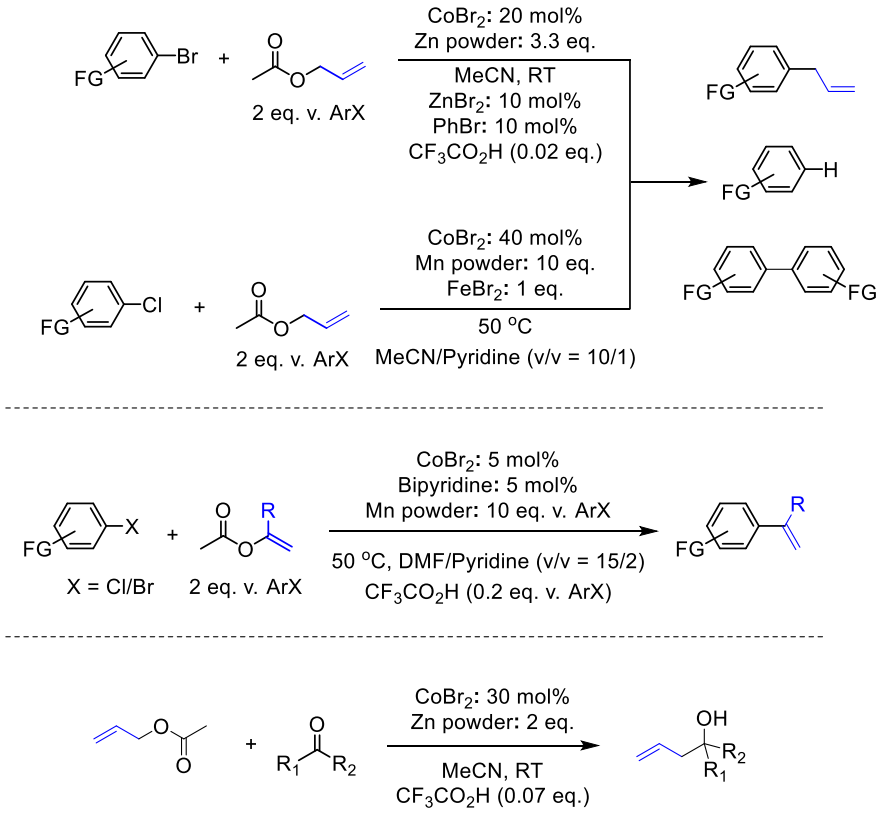

Scheme VIII-2. Publications by the Gosmini group. Top: Allylation of aryl halides using cobalt. Middle: Vinylation of aryl halides using cobalt. Bottom: Allylation of carbonyl compounds using cobalt. Excess reductant is used in each case.

To the best of our knowledge, these seven publications are the only examples of cobalt mediated ester cleavage in the literature, none of which cleave the aryl C–O bond of an aryl ester. Thus, an example of cobalt mediated cleavage of aryl esters with well-defined intermediates would be of high impact and would establish precedent upon which future cobalt-mediated catalysis could be built.

8.2 Results and Discussion

8.2.1 Synthesis of (PNP)Co(OR) Complexes for ROH Dehydrogenation and Unfortunate Lability of the PNP Ligand

Treatment of **603** with sodium acetate gratifyingly yielded a new set of paramagnetically shifted ^{1}H NMR resonances were obtained that were tentatively assigned as (PNP)Co(OAc) (**804**) (Scheme VIII-3). However, only partial conversion to **804** was observed, even in a large excess (>20 eq.) of NaOAc. The Hazari group has had similar issues exchanging chloride for acetate at Co^{II}.[246]

Excess **201a** may become problematic when trying to establish a well-defined system for aerobic alcohol oxidation as free **201a** could act as an auxiliary stabilizing ligand (via P or P=O), become oxidized itself, or act as a base at the central amine. Attempts to remove excess **201a** with MeI failed as indicated by the formation of **702** resulting from nucleophilic character at the cobalt acetate. Attempts to directly insert $Co(OAc)_2$ into **201a** also resulted in partial conversion to the desired **804**. It was later realized that an equilibrium exists between **804** with free acetic acid and **201a** with $Co(OAc)_2$ as depicted in (Scheme VIII-3). Addition of HOAc to (PNP)Co(OAc) will expel

cobalt from (PNP)Co(OAc) resulting in **201a** and $Co(OAc)_2$. Ejection of cobalt from the pincer ligand here is also in agreement with observations from the Hazari group in that acidic protons or oxidizing conditions can eject cobalt from a pincer scaffold.[246] An X-ray quality crystal was grown from the mixture of **201a** and **804** resulting in structural characterization of **804** as we have assigned it (Figure VIII-1).

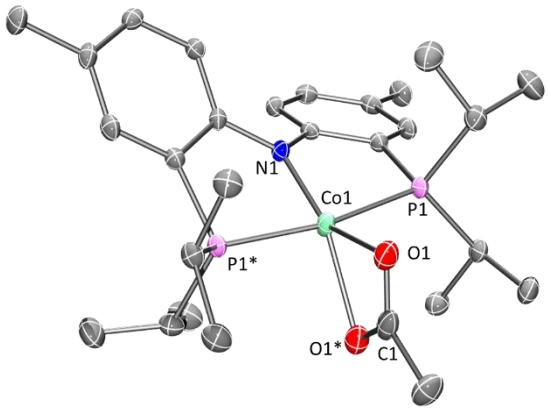

Figure VIII-1. POV-Ray rendition of Ortep plot (50% probability ellipsoids) of (PNP)Co(OAc) (**804**). Hydrogen atoms are omitted for clarity. Selected bond distances (Å) and angles (deg) for **804**: Co1-P1, 2.2223(5); Co1-N1, 1.9144(16); Co1-O1, 2.1372(12); P1-Co1-P1*, 169.15(2); N1-Co1-O1, 149.19(4); O1-Co1-O1*, 61.61(7).

Adventitious water in the $Co(OAc)_2$ mired the synthesis of **804** from **201a-Li** and $Co(OAc)_2$, resulting in the same mixture of **804** and free **201a**. Treatment of **603** with AgOAc resulted in only partial formation of **804** and addition of excess AgOAc resulted in decomposition of the (PNP)Co complexes presumably from oxidation of the supporting ligand. Swapping acetate for pivalate (Scheme VIII-3) made no difference as (PNP)Co(OPiv) (**805**) was plagued by a similar equilibrium exemplified by the broadness of the resonances in Figure VIII-3 versus the sharp resonances for **805** originating from the cleavage of phenyl pivalate (Figure VIII-11). Incidentally, the frequency for some

resonances are shifted by the exchange (see Figure VIII-3 0.98 ppm & -8.43 ppm v. Figure VIII-11 -3.74 & -10.21 ppm).

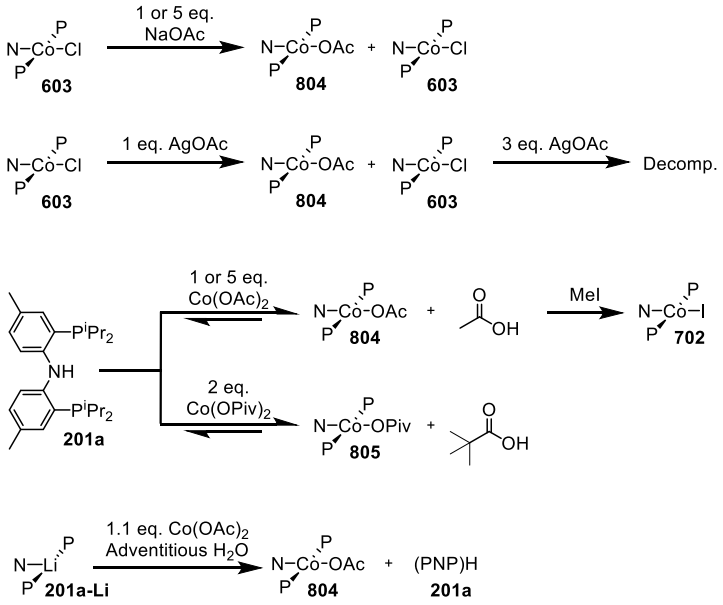

Scheme VIII-3. Attempts at synthesizing (PNP)Co(OAc) (**804**) and (PNP)Co(OPiv) (**805**).

Given the difficulty of synthesizing analytically pure **804**, we set our eyes on a (PNP)Co^{II} alkoxide. Treatment of **603** with NaO^{i}Pr formed *in situ* yielded complete consumption of **603** and the appearance of a new set of paramagnetically shifted ^{1}H NMR resonances tentatively assigned as (PNP)Co(O^{i}Pr) (**806**). To confirm the existence of **806**, Me_3SiCl was added to the mixture. Distillation of the volatiles allowed isopropoxytrimethylsilane to be observed ^{1}H NMR spectroscopy. The dark blue residue was dissolved in C_6D_6 and was found by ^{1}H NMR spectroscopy to be **603**. In a similar synthetic route, (PNP)Co(OTf) (**807**) was produced by treatment of **806** with Me_3SiOTf. Synthesis of **807** in this manner contrasts with the attempted synthesis of **807** from **603**

and Me_3SiOTf which exists as an equilibrium. Even the addition of >50 eq. Me_3SiOTf to **603** yields only partial conversion to the desired **807**. **807** was crystallographically determined to be a κ^1 triflate of the expected square planar geometry; though, the X-ray data was not of publishable quality.

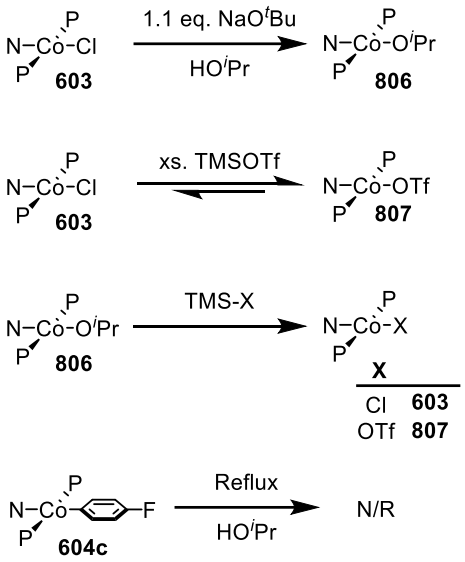

Scheme VIII-4. Synthesis of (PNP)Co(O^{i}Pr) (**806**) and (PNP)Co(OTf) (**807**).

8.2.2 Attempted Alcohol Dehydrogenation Reactions

For a model test substrate, 4-fluorobenzyl alcohol was selected as the fluorine provides an NMR handle and oxidation of the alcohol to either the aldehyde or carboxylic acid results in a large change in the ^{19}F chemical shift. Dissolving **806** in 4-fluorobenzyl alcohol results in a new set of paramagnetically shifted ^1H NMR resonances. The identity of this new complex was not investigated; however, it is likely an equilibrium between **806** and (PNP)Co(4-fluorophenylmethoxide) (**808**). Exposing this mixture to O_2

consumed all the paramagnetic material; however, the alcohol appears unchanged. No evidence of alcohol oxidation was observed. The notable peak was a $^{31}P\{^{1}H\}$ NMR resonance at 60 ppm which has not been identified.

Unfortunately, exposure of **806** to air resulted in the expulsion of cobalt from the ligand and oxidized **201a** was observed by $^{31}P\{^{1}H\}$ NMR spectroscopy.[246] This spelled the end for our endeavor into aerobic alcohol dehydrogenation as the cobalt material of interest falls out of the supporting ligand upon exposure to air.

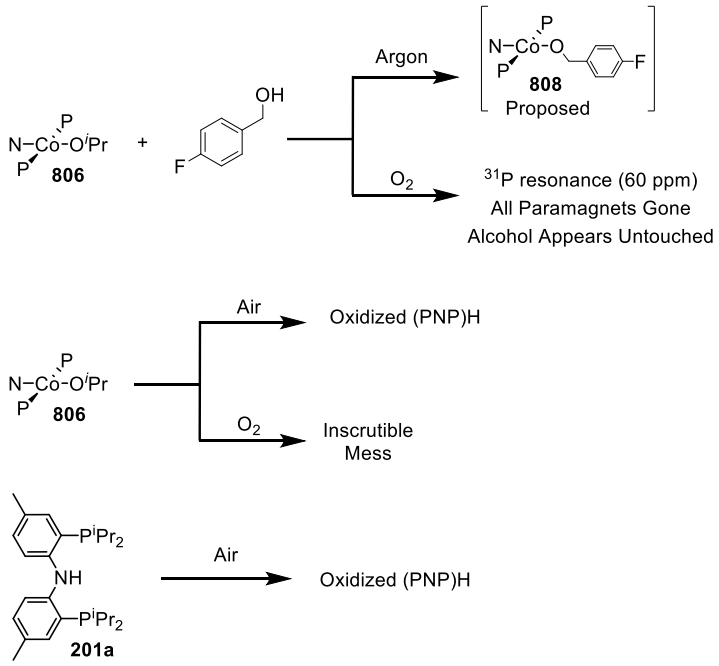

Scheme VIII-5. Attempted alcohol dehydrogenation reactions.

8.2.2 Attempted Ester Cleavage Reactions

As in Chapter VII, **609** was used as a surrogate for the unsaturated cobalt fragment **614**. The synthesis of **609** was modified from published procedures in that **603** was treated

with Mg^0 resulting in the formation of **609** and $MgCl_2$•THF. The $MgCl_2$ proved difficult to remove initially which had negative future implications (*vide infra*). Attempting the reaction of **603** with Mg^0 in toluene resulted in a small amount of **604b**. Of note is that Co^0 powder could not insert into the PNP ligand, although perhaps not surprisingly.

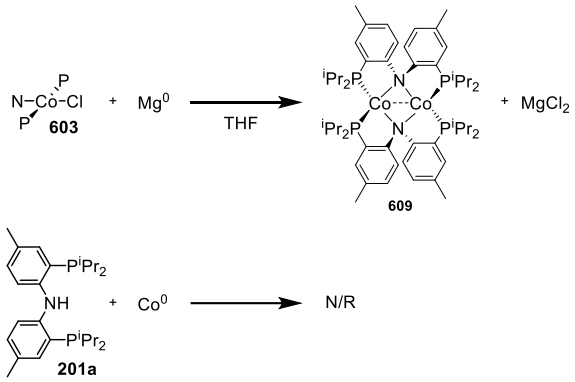

Scheme VIII-6. Alternate synthesis of **609** and attempted synthesis from cobalt (0) powder.

Treatment of **609** with naphthyl pivalate and heating to 80 °C overnight resulted in the formation of **805** and (PNP)Co(2-naphthyl) (**809**) in a 0.5:1.0 ratio. Also observed in this reaction was **603**. The origin of **603** in this case is unknown; however, it is possible that **805** is sensitive to the presence of chlorinated solvents. Also possible is $MgCl_2$•THF carried over from the synthesis of **609** may exchange chloride for carboxylates at substitutionally labile Co^{II} complexes resulting in a deficiency of **805** and observation of **603**. In either case, this obscures the results of (PNP)Co mediated ester cleavage.

Treatment of **609** with phenyl pivalate resulted in the formation of **805** and **604a** in a 1.0:1.4 ratio with no observed **603** indicating at best an undesirable side reaction, and

at worst, a radical reaction mechanism. Notably, literature exists for the radical deprotection of pivaloxyl protecting groups.[247]

In a similar reaction with 4-methoxyphenylpivalate, a 1.3:1.0 ratio was observed between **603** and (PNP)Co(*p*-C_6H_4OMe) (**810**) apparently swapping the selectivity for the more abundant fragment. Also observed in this case was ~3% **613** which is in contrast to nickel mediated cleavage of pivalic esters in which no acyl C–O bond cleavage is observed.[97] In this case, no **805** was observed. The lack of **805** in this case is likely due to the degradation pathways discussed prior. Assumedly, all **603** generated here originated as **805**.

Moving away from pivalates to explore the breadth of the reactivity available to (PNP)Co, the C–O bond cleavage of phenyl acetate was attempted resulting in **603**, **604a**, one unidentified paramagnet, and **613** (~24% of original (PNP)Co). The moderate amount of **613** in this case was not surprising as the decreased steric encumbrance of the methyl group may allow cobalt to activate the acyl C–O bond. The existence of **613** ostensibly requires ejection of a methyl group; however, no methyl containing products were identified, albeit not all products were identified.

The attempted C–O cleavage of coumarin proceeded similarly in that a large amount of **613** (~45% of original (PNP)Co) was observed. In this case, very few paramagnets were observed the most abundant of which was **603**. An unidentified $^{31}P\{^1H\}$ NMR signal appeared at 31 ppm and a vinyl resonance in the ^1H NMR was left unassigned. Potentially, hydrogenating the parent coumarin and installing a methyl group alpha to the carbonyl would allow for cleaner, more selective reactivity. Lastly, dissolving **609** in

either diphenyl ether or anisole and heating to 180 °C or 160 °C respectively yielded no C–O cleavage. A small amount of propylene was observed in the NMR tube in each of these cases which was likely produced from cannibalization of the isopropyl phosphine donors of the pincer ligand.

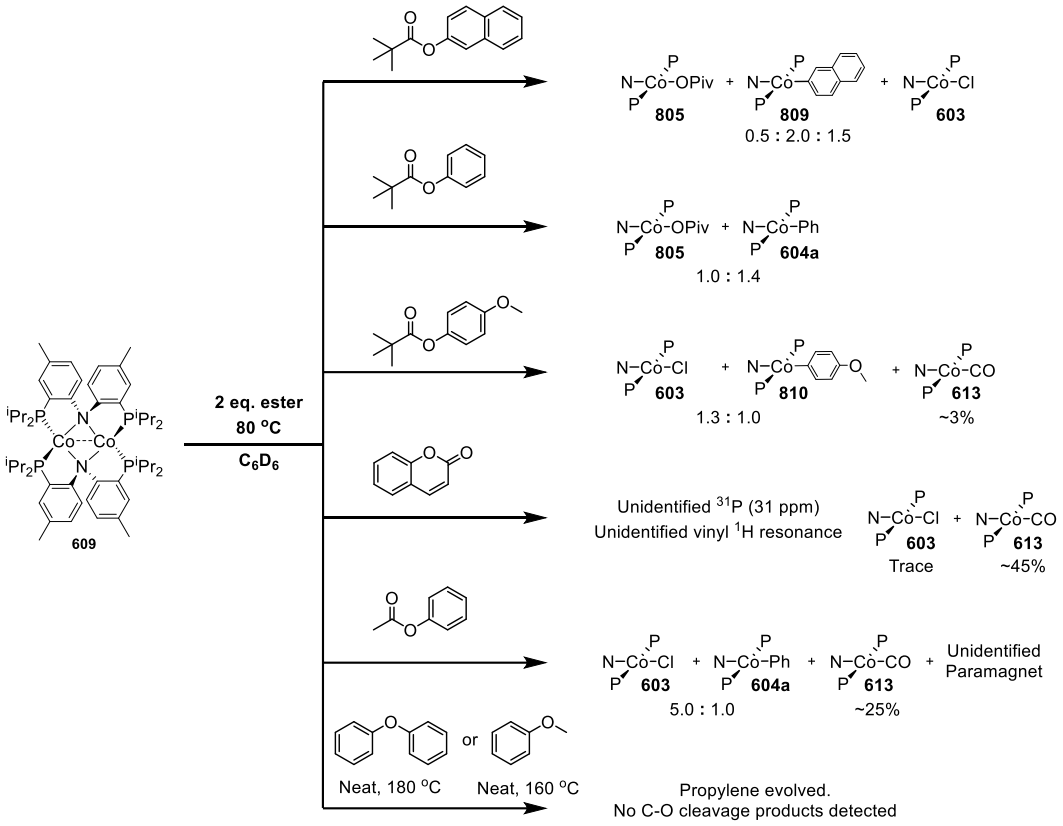

Scheme VIII-7. Attempted C–O bond cleavage reactions mediated by (PNP)Co

8.3 Conclusion

New (PNP)Co complexes were synthesized and their effectiveness at the aerobic dehydrogenation of 4-fluorobenzyl alcohol was tested. (PNP)Co(OiPr) was found to be unfit for aerobic oxidation reactions as the cobalt center does not remain ligated by the PNP ligand. This is likely detrimental to the use of (PNP)Co for aerobic oxidation

reactions. The lability of ligands about Co^{II} has previously been discussed (see Section 6.2.5 & Section 7.2.3). This work outlines the lability of the **201a** on Co^{II} when presented with acidic protons as is the case with the equilibrium between **201a** with $Co(OAc)_2$ and **804** and acetic acid demonstrates.

The use of the (PNP)Co system in the cleavage of aryl esters was explored and **609** was found to cleave the aryl C–O bond of esters; however, this was complicated by the presence of chlorinated materials which exchanged the (PNP)Co carboxylates for chlorides. Furthermore, the unequal ratio of the two cobalt fragments is indicative of a radical pathway, or at a minimum, an undesirable side reaction. Given our results in the reactions between **609** and aryl halides, involvement of a single electron pathway would not be surprising.

8.4 Experimental

8.4.1 General Considerations

Unless otherwise specified, all manipulations were performed either inside an argon-filled glove box, or by using Schlenk techniques. Pentane, THF, and toluene were dried using a PureSolv MD-5 Solvent Purification System and were stored over 4Å molecular sieves in an argon-filled glove box. C_6D_6 was dried over NaK, benzophenone, and 18-crown-6 then stored in an argon-filled glove box over 4Å molecular sieves prior to use. Naphthyl pivalate, phenyl pivalate, and 4-methoxyphenylpivalate were prepared by reactions of the corresponding alcohol with pivaloyl chloride,[85] vacuum distilled, and stored in an argon-filled glove box over 4Å molecular sieves prior to use. The **201a**,[21]

$Co(OPiv)_2$,[102,248] and **609**[215] were synthesized according to literature procedures. 2-naphthyllithium was synthesized according to a literature procedure for 4-tolyllithium.[17e] All other chemicals were used as received from commercial vendors. All NMR spectra were acquired on a Bruker 400 spectrometer (^{1}H NMR, 400.09 MHz; ^{13}C NMR, 100.60 MHz; ^{31}P NMR, 161.96 MHz), and Varian Inova 500 (^{1}H NMR, 499.703 MHz; ^{13}C NMR, 125.697 MHz; ^{31}P NMR, 202.265 MHz) in denoted solvents. All chemical shifts are reported in δ (ppm). All ^{1}H and ^{13}C NMR spectra were referenced internally to the residual solvent signal (C_6D_6 at δ 7.16 for ^{1}H and δ 128.06 for ^{13}C NMR). ^{31}P NMR spectra were externally referenced to an 85% phosphoric acid solution δ 0. Elemental analyses were performed by CALI Labs, Inc. (Highland Park, NJ).

8.4.2 Synthesis and Characterization

(PNP)Co(OAc) (804). In an Ar-filled glove box, a 50 mL culture tube was charged with **201a** (1.164 g, 2.7 mmol), $Co(OAc)_2$ (950 mg, 5.4 mmol), and fluorobenzene (15 mL). This tube was placed into an 80 °C oil bath overnight. The solution was filtered through a pad of Celite and the volatiles of the filtrate were removed *in vacuo*. The residue was extracted with pentane (20 mL), filtered through a pad of Celite, and placed into a -35 °C freezer within the glovebox for two days. The supernatant was decanted, and solids were washed with pentane and dried *in vacuo* yielding 680 mg of a mixture of **201a** and **804**. ^{1}H NMR (C_6D_6, 500 MHz): δ 22.70 (br s, 2H), 18.91 (s, 6H), 6.53 (br s, 12H), 4.05 (br s, 4H), 3.04 (br s, 12H), -13.56 (br s, 12H).

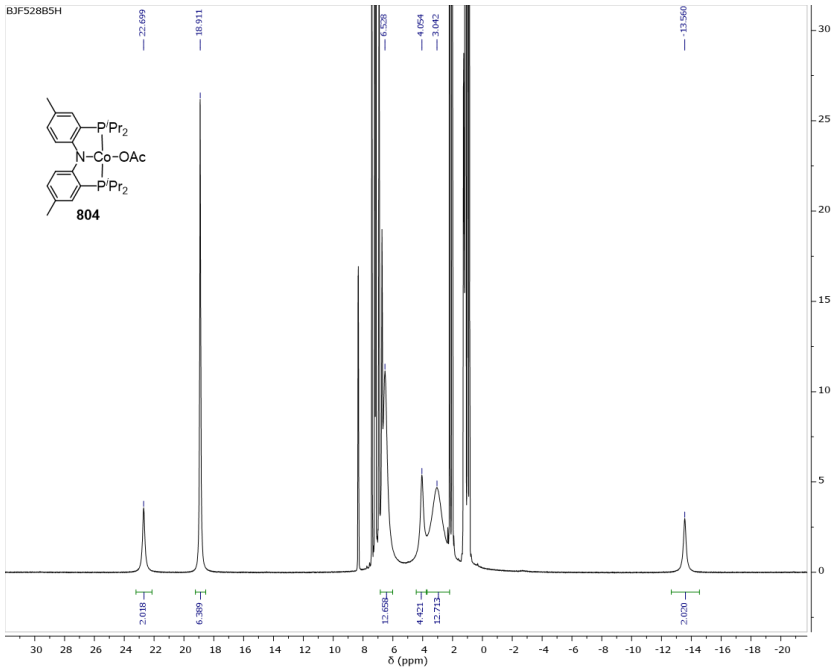

Figure VIII-2. ^{1}H NMR (500 MHz, C_6D_6) spectrum of **804**. Sample contains non-metallated **201a**

(PNP)Co(OPiv) (805). In an Ar-filled glove box, a 50 mL culture tube was charged with **201a** (330 mg, 0.77 mmol), $Co(OPiv)_2$ (400 mg, 1.5 mmol). Toluene (20 mL) was added and the suspension was stirred overnight. The suspension was filtered through a pad of Celite and the volatiles from the filtrate were evaporated *in vacuo* yielding 348 mg of a mixture of **201a** and **805**. ^{1}H NMR (C_6D_6, 500 MHz): δ 20.34 (br, 2H), 16.84 (br, 6H, 11.33 (br, 2H), 8.30 (br, 2H), 3.85 (br, 12H), 2.95 (br, 12H), 0.99 (br, 12H), -8.43 (br, 2H)

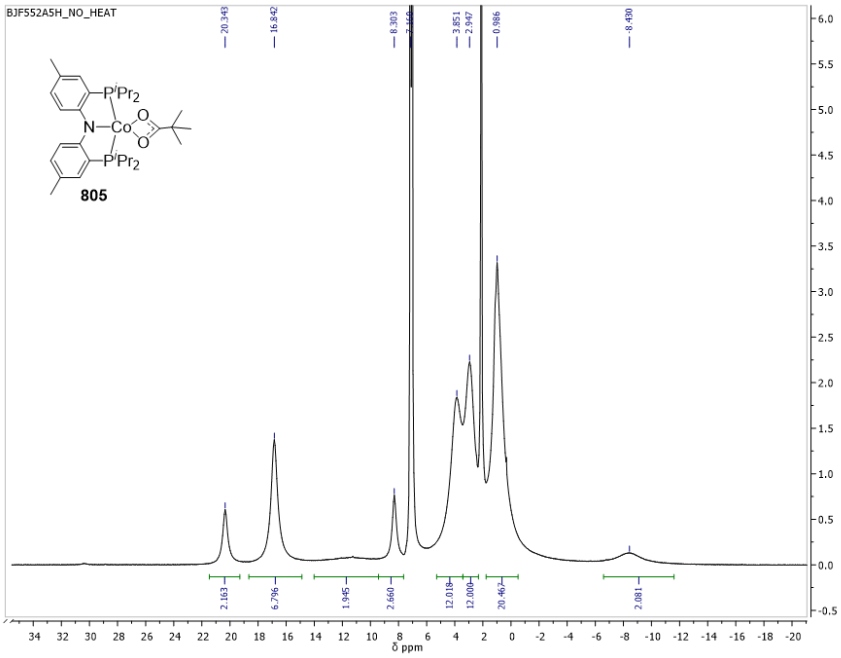

Figure VIII-3. ^{1}H NMR (500 MHz, C_6D_6) spectrum of **805** with free pivalic acid.

(PNP)Co(O^{i}Pr) (806). In an Ar-filled glove box, a 50 mL Schlenk flask was charged with **603** (638 mg, 1.2 mmol) and dissolved in ^{i}PrOH (25 mL). To this solution was added NaO^{t}Bu (130 mg, 1.3 mmol), and the mixture was stirred overnight. The volatiles were removed *in vacuo* and the residue was dissolved in toluene and filtered through a pad of Celite. All volatiles were removed *in vacuo* yielding **806** (503 mg 75%) of >90% purity. ^{1}H NMR spectroscopy revealed full conversion of **603** to **806**. **806** was recrystallized from a saturated pentane solution (53 mg, 8%). Notably **806** is highly soluble in pentane which precluded its isolation on large scale from pentane.

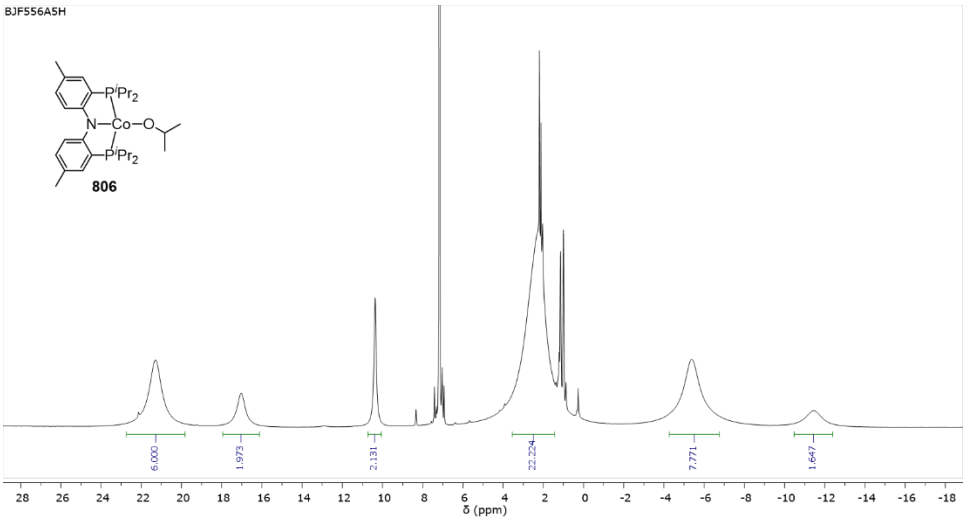

Figure VIII-4. ^{1}H NMR (500 MHz, C_6D_6) spectrum of **806**.

(PNP)Co(OTf) (807). In an Ar-filled glove box, a scintillation vial was charged with **806** (175 mg, 0.32 mmol) and dissolved in toluene. To this solution was added TMSOTf (60 µL, 0.33 mmol). The solution was stirred overnight and the volatiles were removed in vacuo. ^{1}H NMR spectroscopy revealed complete conversion to **807**. The residue was taken up in pentane (not all dissolved) and placed into a -35 °C freezer in the glovebox yielding **807** as a dark blue-green powder (76 mg, 38%). The supernatant still contained **807**. ^{1}H NMR (C_6D_6, 400 MHz): δ 35.63 (br, 6H), 31.75 (br, 2H), 14.61 & 13.34 (overlap 6H), 6.58 (br, 12H), 3.62 (br, 12H), -34.48 (br, 2H).

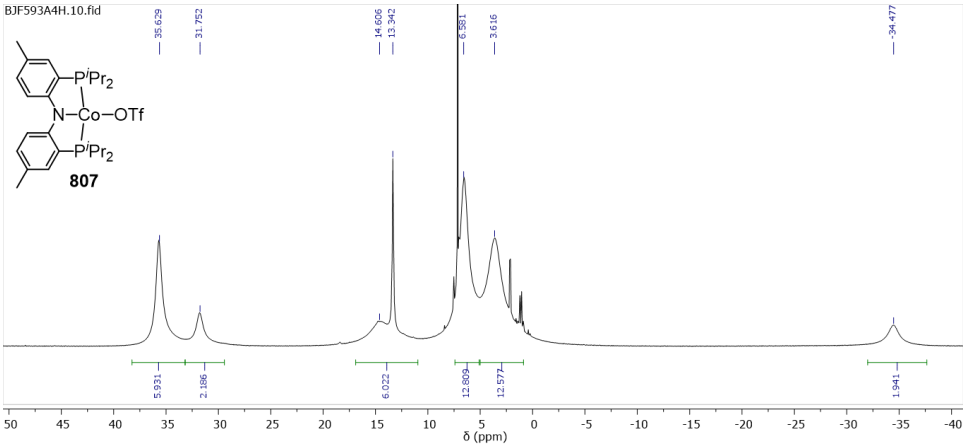

Figure VIII-5. ^{1}H NMR (500 MHz, C_6D_6) spectrum of **807**. Sample contains isopropoxytrimethylsilane.

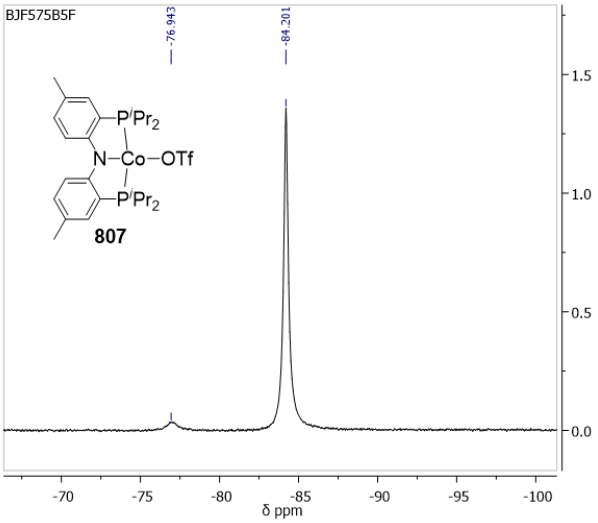

Figure VIII-6. ^{19}F NMR (470 MHz, C_6D_6) spectrum of **807**. Sample contains residual TMSOTf.

Spectroscopic observation of (PNP)Co(2-naphthyl) (809). In an Ar-filled glove box, a scintillation vial was charged with **603** (190 mg, 0.36 mmol) and placed into a -35 °C freezer within the glovebox. A separate vial was charged with 2-naphthyllithium (51 mg, 0.38 mmol) and placed into the freezer as well. After 30 minutes, the 2-

naphthyllithium solution was pipetted slowly into the solution of **603** resulting in an immediate color change from dark blue to green. This solution was stirred overnight after which the volatiles were removed *in vacuo*. The residue was extracted with pentane and filtered through a plug of Celite. Evaporation of the volatiles yielded **809** as a dusty green powder. ^{1}H NMR (C_6D_6, 400 MHz): δ 38.53 & 37.36 (br overlap, 5H), 30.33 (br, 1H), 23.80 (6H), 14.82 (12H), 0.3 (br, 12H), -4.11 (1H), -11.06 (1H), -29.18 (br overlap, 2H), -90.74 (br, 1H).

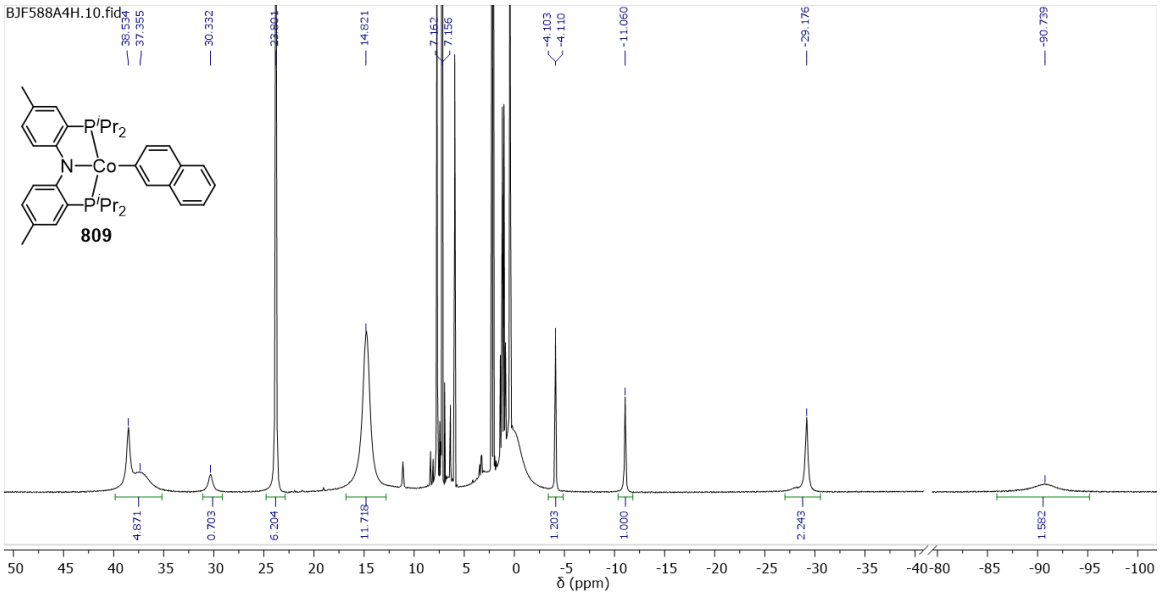

Figure VIII-7. ^{1}H NMR (400 MHz, C_6D_6) spectrum of **809**.

8.4.2 Reactions of Co^{II} Complexes En Route to Alcohol Dehydrogenation

Reaction between 603 and TMSOTf. In an Ar-filled glove box, a J. Young tube was charged with **603** (28 mg, 0.053 mmol), TMSOTf (100 µL, 0.55 mmol), and C_6D_6

(600 µL). ^{1}H NMR spectroscopic analysis revealed a mixture of **603** and **807**. Additional TMSOTf (ca. 1 mL) was added via Pasteur pipette. The solution was heated overnight in a 50 °C oil bath. ^{1}H NMR spectroscopic analysis again revealed a mixture of **603** and **807**.

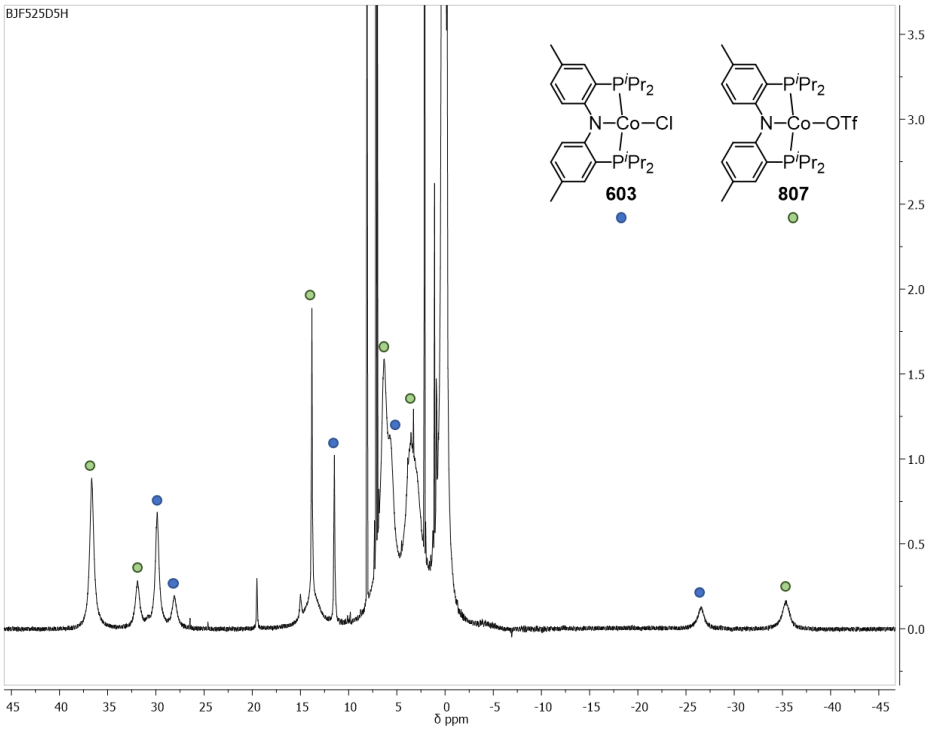

Figure VIII-8. ^{1}H NMR (500 MHz, C_6D_6) spectrum of the resultant mixture from addition of >100 eq. TMSOTf to **603**.

Reaction between 806 and 4-fluorobenzyl alcohol under argon. In an Ar-filled glove box, a J. Young tube was charged with **806** (41 mg, 0.074 mmol) and 4-fluorobenzyl alcohol (100 µL, 0.92 mmol). ^{1}H NMR spectroscopic analysis revealed a new set of paramagnetically shifted resonances which do not correspond to **806**.

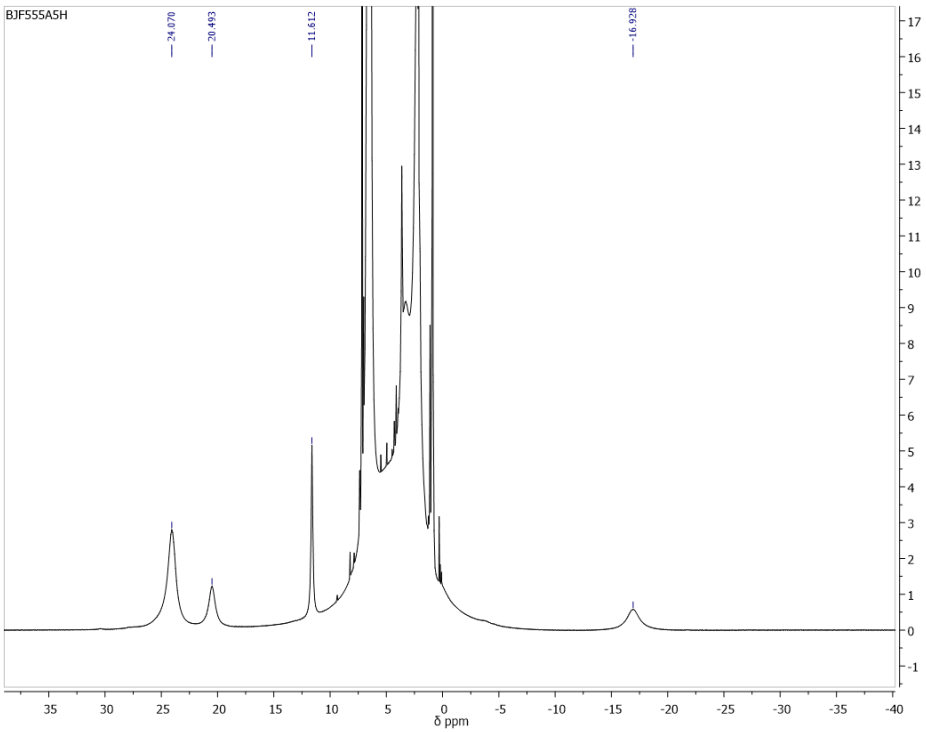

Figure VIII-9. ^{1}H NMR (500 MHz, C_6D_6) spectrum of an unknown paramagnet resulting from the addition of 4-fluorobenzyl alcohol to **806**.

Exposure of 806 to Air. A sample of **806** dissolved in toluene was brought out of an argon-filled glove box and allowed to stir open to air overnight. ^{31}P{^{1}H} NMR spectroscopic analysis revealed the formation of oxidized **201a** indicating that cobalt had fallen out of the supporting ligand.

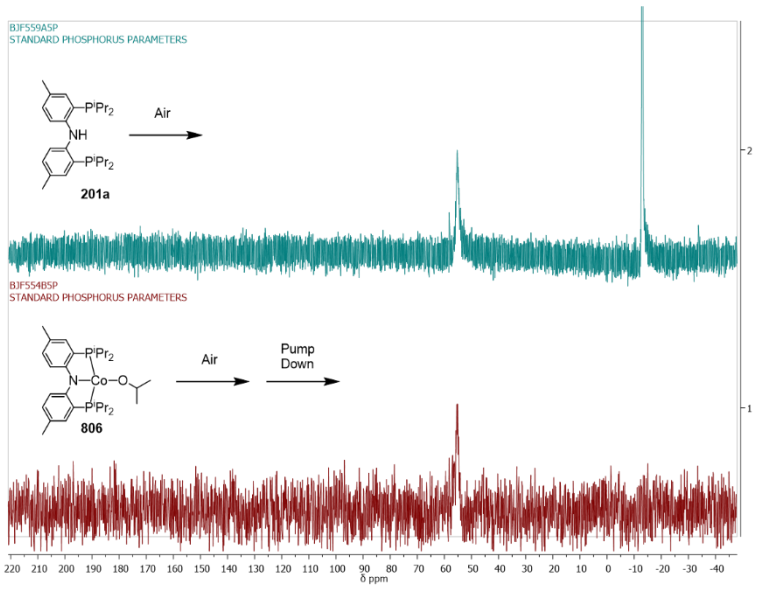

Figure VIII-10. Top: $^{31}P\{^{1}H\}$ NMR (202 MHz, C_6D_6) spectrum of a partially oxidized sample of **201a**. Bottom: $^{31}P\{^{1}H\}$ NMR (202 MHz, C_6D_6) spectrum of the solution resulting from exposure of **806** to air.

8.4.3 Attempts at Cobalt Mediated Ester C–O Bond Cleavage

General Procedure for Cobalt Mediated Ester Cleavage. In an Ar-filled glove box, a J. Young tube was charged with **609** (~0.05 mmol (PNP)Co), dioxane (10 µL, 0.11 mmol), the corresponding ester (~2 eq. v. (PNP)Co), and 600 µL C_6D_6. The tube was heated in an 80 °C oil bath overnight and then analyzed by ^{1}H NMR spectroscopy.

Reaction of 609 with naphthyl pivalate. In accordance with the general procedure, 609 was treated with naphthyl pivalate.

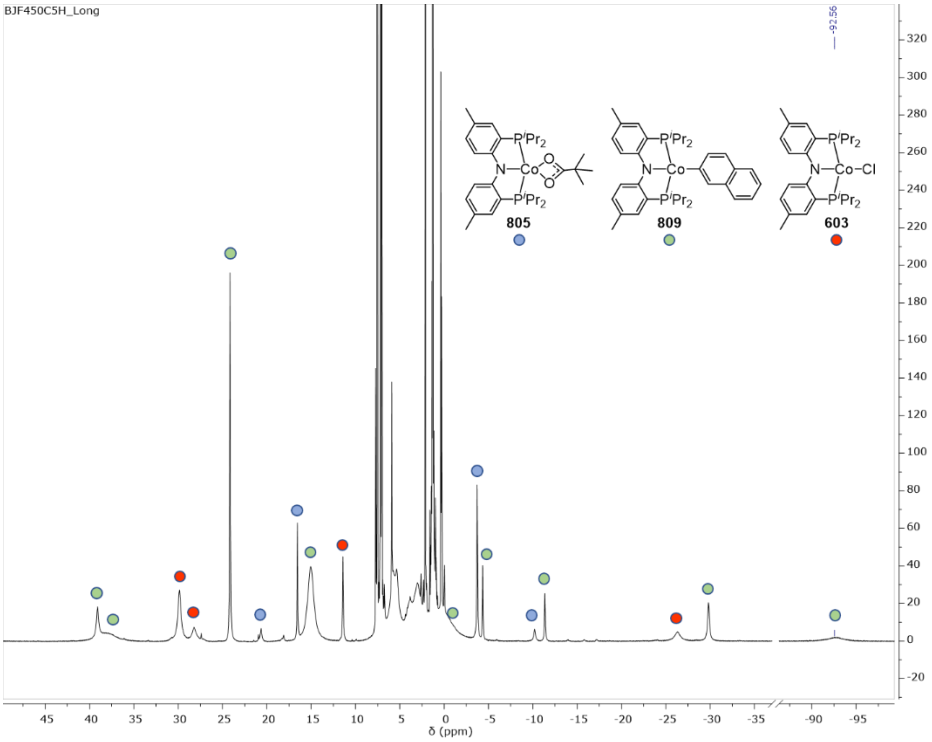

Figure VIII-11. ^{1}H NMR (500 MHz, C_6D_6) spectrum of the products of thermolysis between **609** and naphthyl pivalate.

Reaction of 609 with phenyl pivalate. In accordance with the general procedure, 609 was treated with phenyl pivalate.

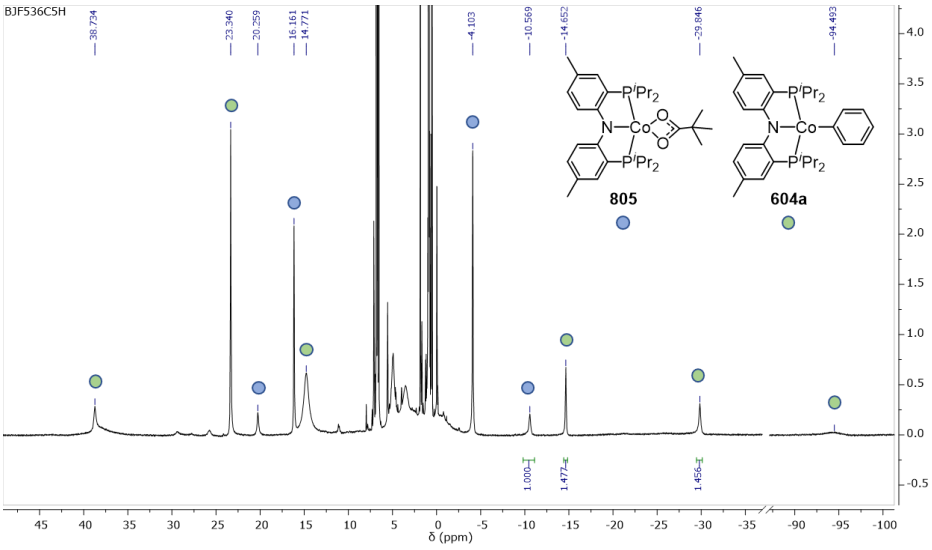

Figure VIII-12. ^{1}H NMR (500 MHz, C_6D_6) spectrum of the products of thermolysis between **609** and phenyl pivalate.

Reaction of 609 with 4-methoxyphenyl pivalate. 609 was treated with 4-methoxyphenyl pivalate in accordance with the general procedure except the thermolysis was performed over 48 hours. (PNP)Co(*p*-C_6H_4OMe) was identified by similarity to **604a** and **604b**.

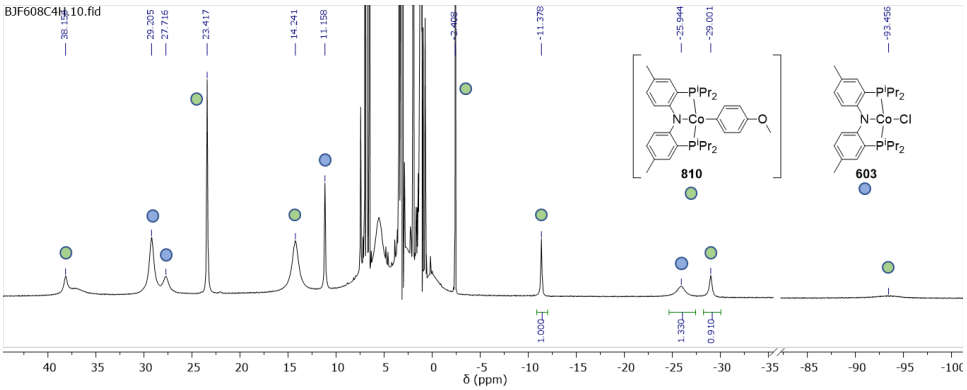

Figure VIII-13. ^{1}H NMR (400 MHz, C_6D_6) spectrum of the products of thermolysis between **609** and 4-methoxyphenyl pivalate

Reaction of 609 with phenyl acetate. In accordance with the general procedure, 609 was treated with phenyl acetate.

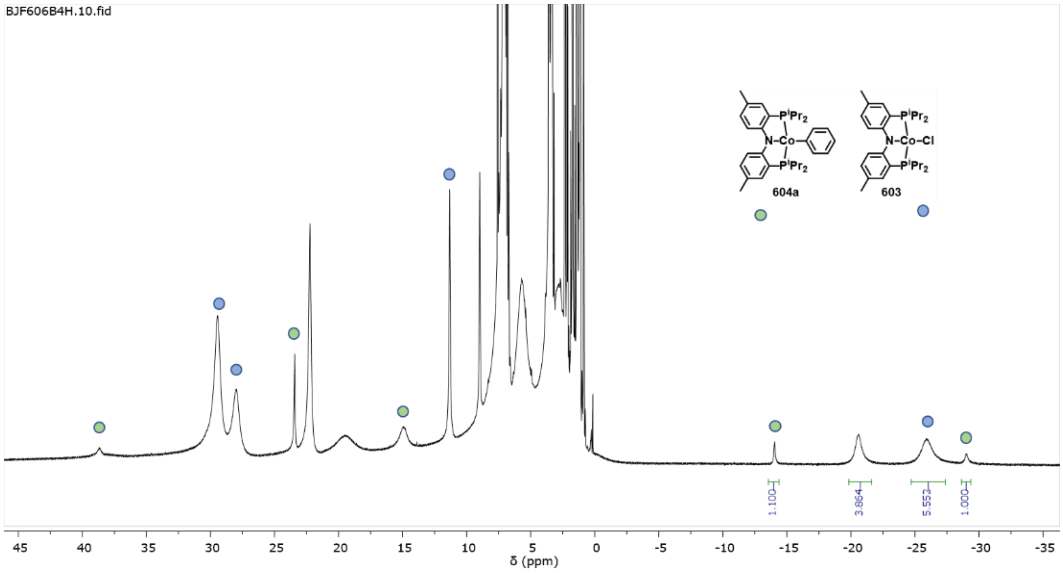

Figure VIII-14. ^{1}H NMR (400 MHz, C_6D_6) spectrum of the products of thermolysis between **609** and phenyl acetate. Unknown paramagnetic resonances do not have dots.

Reaction of 609 with coumarin. 609 was treated with coumarin in accordance with the general procedure except the thermolysis was performed over 48 hours.

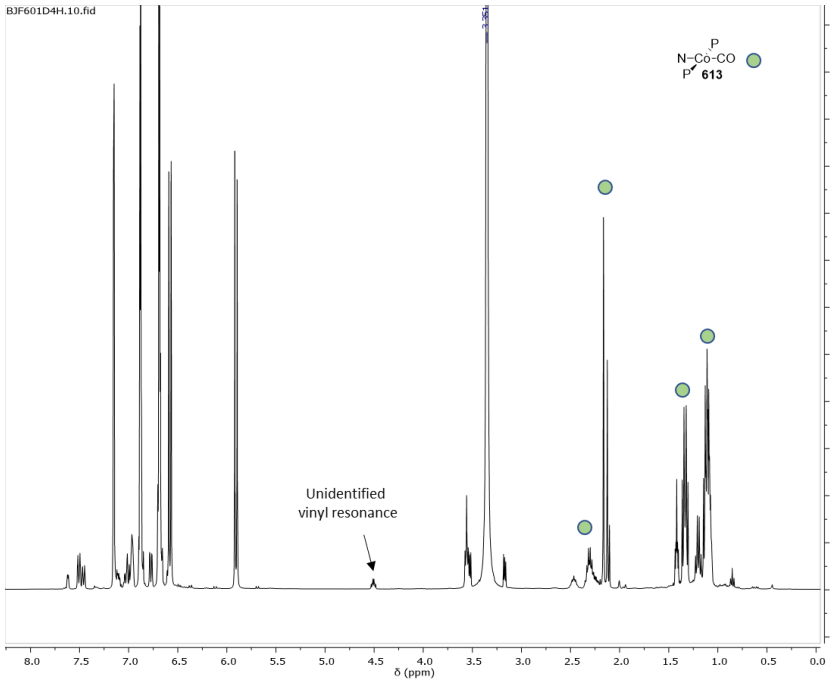

Figure VIII-15. ^{1}H NMR (400 MHz, C_6D_6) spectrum of the products of thermolysis between **609** and coumarin.

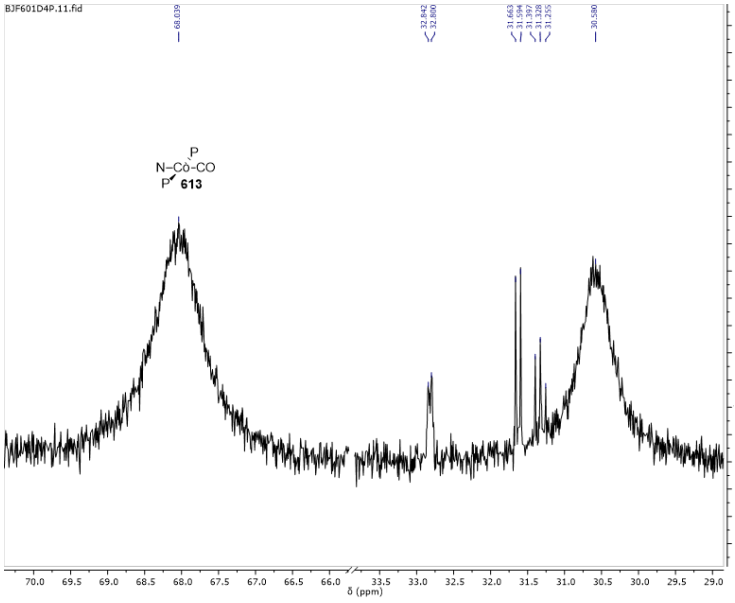

Figure VIII-16. $^{31}P\{^{1}H\}$ NMR (162 MHz, C_6D_6) spectrum of the products of thermolysis between **609** and coumarin. Resonances from 30-33 ppm were not identified.

CHAPTER IX

CONCLUSION

A complete kinetic investigation into the mechanism of DHBTA has been accomplished using a variety of PNP ligated iridium complexes. This investigation yielded numerous interesting findings including a plausible mechanism for the DHBTA reaction involving the rate-limiting rotation of a σ-complex of pinacolborane. One widely applicable finding from this study was slow egress of dihydrogen produced in solution within a standard 5 mm J. Young NMR tube in the absence of agitation.

To make iridium catalyzed borylation of terminal alkynes a more widely available route of alkynylboronate synthesis, we developed an air stable precatalyst. This precatalyst has many advantages including its synthesis which requires only commercially available starting materials. It was found that the DHBTA reaction can withstand a moderate amount of air and moisture provided that sufficient pinacolborane is present. This precatalyst achieved the same catalytic resting state in solution as the air-sensitive iridium complexes used for the kinetic investigations. Reactions using this catalyst were performed with minimal air-free techniques; nevertheless, DHBTA persisted. Notably, the DHBTA reaction persists under air in a closed vial with an excess amount of HBpin.

Initially, the synthesis and characterization of PSiP complexes of cobalt was performed with an eye toward developing a cross-coupling catalyst. Unfortunately, this system was difficult to metallate with cobalt halide salts. Satisfyingly, dicobalt octacarbonyl was found to insert into the Si–H bond of the proligand at room temperature

yielding a (PSiP$^{i\text{Pr}}$)Co dicarbonyl. Removal of these carbonyl ligands proved difficult and as such, we elected to explore the possibility of synthesizing a cobalt silylene. Our endeavors in this area were successful and we were able to demonstrate an example of a rare base-free silylene complex of cobalt. However, our goal of cross-coupling with cobalt remained unfulfilled.

Given our previous success in catalytic C–S bond formation with both (POCOP)Rh(Ar)(SAr') and (PNP)Rh(Ar)(SAr'), an investigation into similar reactions with the base metal analog, cobalt, was performed. To directly apply the rhodium chemistry to cobalt, (POCOP)Co(Ph)(SPh) was synthesized; however, thermolysis of this compound was found to result in reductive elimination of the Co–Ph with the supporting ligand. To increase the difficulty of elimination with the supporting ligand, the PNP ligand was adopted. Gratifyingly, this new ligand scaffold afforded the desired C–S coupling product. Unfortunately, the system is plagued by a single electron comproportionation event which sequesters catalytically active cobalt in the form of inactive Co^{II}.

Providing (PNP)Co(Ph)(SPh) with aryl halides during thermolysis would ideally have led to capture of the (PNP)Co fragment by oxidative addition in a manner akin to the (PNP)Rh fragment. However, halogen atom abstraction from the aryl halide substrate was operative here resulting in the formation of Co^{II} halides and concomitant ejection of an aryl radical. Radical trapping experiments support the existence of aryl radicals and coupling of the proposed radical with solvent was observed. These investigations, although lacking catalysis, have produced a series of paramagnetic cobalt complexes which will aid in the characterization of new paramagnetic pincer cobalt complexes.

Lastly, the (PNP)Co system was applied to the cleavage of aryl ester C–O bonds with the intention of using the aryl fragment as a cross-coupling partner. Expectedly, these reactions also yielded complexes of Co^{II}. Notably, the ratios of products in these cases were not 1:1 indicating that some radical processes may be operative. Nevertheless, this work presents the only example of cobalt-mediated ester C_{Ar}–O bond cleavage to date.

REFERENCES

(1) Negishi, E.; de Meijere, A. *Handbook of Organopalladium Chemistry for Organic Synthesis*. Wiley-Interscience: New York, 2002.

(2) Hartwig, J. F. *Organotransition Metal Chemistry: From Bonding to Catalysis*. University Science Books: Sausalito, CA, 2009; pp 877-965.

(3) a) Negishi, E.-i. Magical Power of Transition Metals: Past, Present, and Future (Nobel Lecture). *Angew. Chem. Int. Ed.* **2011,** *50*, 6738-6764. b) Suzuki, A. Cross-Coupling Reactions Of Organoboranes: An Easy Way To Construct C-C Bonds (Nobel Lecture). *Angew. Chem. Int. Ed.* **2011,** *50*, 6722-6737.

(4) Hartwig, J. F. Carbon−Heteroatom Bond-Forming Reductive Eliminations of Amines, Ethers, and Sulfides. *Acc. Chem. Res.* **1998,** *31*, 852-860.

(5) Hartwig, J. F. Transition Metal Catalyzed Synthesis of Arylamines and Aryl Ethers from Aryl Halides and Triflates: Scope and Mechanism. *Angew. Chem. Int. Ed.* **1998,** *37*, 2046-2067.

(6) Old, D. W.; Wolfe, J. P.; Buchwald, S. L. A Highly Active Catalyst for Palladium-Catalyzed Cross-Coupling Reactions: Room-Temperature Suzuki Couplings and Amination of Unactivated Aryl Chlorides. *J. Am. Chem. Soc.* **1998,** *120*, 9722-9723.

(7) a) Molnár, A. *Palladium-Catalyzed Coupling Reactions: Practical Aspects and Future Developments*. Wiley-VCH: Weinheim, Germany, 2013. b) Tsuji, J. *Palladium Reagents in Catalysis: New Perspectives for the 21st Century*. Wiley: Hoboken, NJ, 2004.

(8) Hartwig, J. F. *Organotransition Metal Chemistry: From Bonding to Catalysis*. University Science Books: Sausalito, CA, 2009; pp 261-320.

(9) Hartwig, J. F. *Organotransition Metal Chemistry: From Bonding to Catalysis*. University Science Books: Sausalito, CA, 2009; pp 321-348.

(10) Crabtree, R. H. *The Organometallic Chemistry of the Transition Metals*. 6th ed.; John Wiley & Sons, Inc.: Hoboken, NJ, 2014; pp 163-184.

(11) a) Sun, C.-L.; Krause, H.; Fürstner, A. A Practical Procedure for Iron-Catalyzed Cross-Coupling Reactions of Sterically Hindered Aryl-Grignard Reagents with Primary Alkyl Halides. *Adv. Synth. Catal.* **2014,** *356*, 1281-1291. b) Bedford, R. B.; Carter, E.; Cogswell, P. M.; Gower, N. J.; Haddow, M. F.; Harvey, J. N.; Murphy, D. M.; Neeve, E. C.; Nunn, J. Simplifying Iron–Phosphine Catalysts for Cross-Coupling Reactions. *Angew. Chem. Int. Ed.* **2013,** *52*, 1285-1288. c) Schoch, R.; Desens, W.; Werner, T.; Bauer, M. X-ray Spectroscopic Verification of the Active Species in Iron-Catalyzed Cross-Coupling Reactions. *Chem. Eur. J.* **2013,** *19*, 15816-15821. d) Lefèvre, G.; Jutand, A. Activation of Aryl and Heteroaryl Halides by an Iron(I) Complex Generated in the Reduction of [Fe(acac)$_3$] by PhMgBr: Electron Transfer versus Oxidative Addition. *Chem. Eur. J.* **2014,** *20*, 4796-4805. e) Guisán-Ceinos, M.; Tato, F.; Buñuel, E.; Calle, P.; Cárdenas, D. J. Fe-Catalysed Kumada-Type Alkyl–Alkyl Cross-Coupling. Evidence for the Intermediacy of Fe(I) Complexes. *Chem. Sci.* **2013,** *4*, 1098-1104. f) Hedström, A.; Lindstedt, E.; Norrby, P.-O. On the Oxidation State of Iron in Iron-Mediated C–C Couplings. *J. Organomet. Chem.* **2013,** *748*, 51-55.

(12) a) Diccianni, J. B.; Diao, T. Mechanisms of Nickel-Catalyzed Cross-Coupling Reactions. *Trends in Chemistry* **2019,** *1*, 830-844. b) Wang, Z.-X.; Liu, N. Nickel-Catalyzed Cross-Coupling with Pincer Ligands. *Eur. J. Inorg. Chem.* **2012,** *2012*, 901-911. c) Joshi-Pangu, A.; Biscoe, M. R. The Use of Tertiary Alkylmagnesium Nucleophiles in Ni-Catalyzed Cross-Coupling Reactions. *Synlett* **2012,** *2012*, 1103-1107.

(13) a) Thapa, S.; Shrestha, B.; Gurung, S. K.; Giri, R. Copper-Catalysed Cross-Coupling: an Untapped Potential. *Org. Biomol. Chem.* **2015,** *13*, 4816-4827. b) Evano, G.; Blanchard, N. *Copper-Mediated Cross-Coupling Reactions*. Wiley: 2014.

(14) Cahiez, G.; Moyeux, A. Cobalt-Catalyzed Cross-Coupling Reactions. *Chem. Rev.* **2010,** *110*, 1435-1462.

(15) Peris, E.; Crabtree, R. H. Key factors in pincer ligand design. *Chem. Soc. Rev.* **2018,** *47*, 1959-1968.

(16) Morales-Morales, D.; Jensen, C. M. *The Chemistry of Pincer Compounds*. Elsevier: Amsterdam, 2007.

(17) a) Gerber, L. C. H.; Watson, L. A.; Parkin, S.; Weng, W.; Foxman, B. M.; Ozerov, O. V. Bis(methylidene) Complex of Tantalum Supported by a PNP Ligand. *Organometallics* **2007,** *26*, 4866-4868. b) Gatard, S.; Chen, C.-H.; Foxman, B. M.; Ozerov, O. V. Oxidative Addition Reactions of Silyl Halides with the (PNP)Rh Fragment. *Organometallics* **2008,** *27*, 6257-6263. c) Whited, M. T.; Grubbs, R. H. Oxygen-Atom Transfer from Carbon Dioxide to a Fischer Carbene at (PNP)Ir. *J. Am. Chem. Soc.* **2008,** *130*, 5874-5875. d) Whited, M. T.; Zhu, Y.; Timpa, S. D.; Chen, C.-H.; Foxman, B. M.; Ozerov, O. V.; Grubbs, R. H. Probing the C−H Activation of Linear and Cyclic Ethers at (PNP)Ir. *Organometallics* **2009,** *28*, 4560-4570. e) DeMott, J. C.; Bhuvanesh, N.; Ozerov, O. V. Frustrated Lewis Pair-Like Splitting of Aromatic C–H Bonds and Abstraction of Halogen Atoms by a Cationic $[(^{F}PNP)Pt]^{+}$ Species. *Chem. Sci.* **2013,** *4*, 642-649. f) Davidson, J. J.; DeMott, J. C.; Douvris, C.; Fafard, C. M.; Bhuvanesh, N.; Chen, C.-H.; Herbert, D. E.; Lee, C.-I.; McCulloch, B. J.; Foxman, B. M.; Ozerov, O. V. Comparison of the Electronic Properties of Diarylamido-Based PNZ Pincer Ligands: Redox Activity at the Ligand and Donor Ability Toward the Metal. *Inorg. Chem.* **2015,** *54*, 2916-2935. g) Pell, C. J.; Shih, W.-C.; Gatard, S.; Ozerov, O. V. Formation of (PNP)Rh Complexes Containing Covalent Rhodium–Zinc Bonds in Studies of Potential Rh-Catalysed Negishi Coupling. *Chem. Commun.* **2017,** *53*, 6456-6459. h) Kosanovich, A. J.; Shih, W.-C.; Ozerov, O. V. Synthesis and Characterization of Unsaturated Manganese(I) and Rhenium(I) Dicarbonyl Complexes Supported by an Anionic PNP Pincer. *J. Organomet. Chem.* **2019,** *897*, 1-6.

(18) Timpa, S. D.; Pell, C. J.; Ozerov, O. V. A Well-Defined (POCOP)Rh Catalyst for the Coupling of Aryl Halides with Thiols. *J. Am. Chem. Soc.* **2014,** *136*, 14772-14779.

(19) Press, L. P.; Kosanovich, A. J.; McCulloch, B. J.; Ozerov, O. V. High-Turnover Aromatic C–H Borylation Catalyzed by POCOP-Type Pincer Complexes of Iridium. *J. Am. Chem. Soc.* **2016,** *138*, 9487-9497.

(20) Roland, C. D.; Li, H.; Abboud, K. A.; Wagener, K. B.; Veige, A. S. Cyclic polymers from alkynes. *Nat. Chem.* **2016,** *8*, 791-796.

(21) Fan, L.; Foxman, B. M.; Ozerov, O. V. N−H Cleavage as a Route to Palladium Complexes of a New PNP Pincer Ligand. *Organometallics* **2004,** *23*, 326-328.

(22) Jansen, A.; Pitter, S. Synthesis of Hemilabile P,N Ligands: ω-2-Pyridyl-n-alkylphosphines. *Monatsh. Chem.* **1999,** *130*, 783-794.

(23) a) Rybtchinski, B.; Ben-David, Y.; Milstein, D. Unexpected Isomerization of a cis- into a trans-Dihydride Complex. A Neutral Late Transition Metal Complex as a Hydride Donor. *Organometallics* **1997,** *16*, 3786-3793. b) Shih, W.-C.; Ozerov, O. V. One-Pot Synthesis of 1,3-Bis(phosphinomethyl)arene PCP/PNP Pincer Ligands and Their Nickel Complexes. *Organometallics* **2015,** *34*, 4591-4597.

(24) DeMott, J. C.; Gu, W.; McCulloch, B. J.; Herbert, D. E.; Goshert, M. D.; Walensky, J. R.; Zhou, J.; Ozerov, O. V. Silyl–Silylene Interplay in Cationic PSiP Pincer Complexes of Platinum. *Organometallics* **2015,** *34*, 3930-3933.

(25) Shih, W.-C.; Gu, W.; MacInnis, M. C.; Timpa, S. D.; Bhuvanesh, N.; Zhou, J.; Ozerov, O. V. Facile Insertion of Rh and Ir into a Boron–Phenyl Bond, Leading to Boryl/Bis(phosphine) PBP Pincer Complexes. *J. Am. Chem. Soc.* **2016,** *138*, 2086-2089.

(26) a) Chen, L.; Ren, P.; Carrow, B. P. Tri(1-adamantyl)phosphine: Expanding the Boundary of Electron-Releasing Character Available to Organophosphorus Compounds. *J. Am. Chem. Soc.* **2016,** *138*, 6392-6395. b) Ikawa, T.; Barder, T. E.; Biscoe, M. R.; Buchwald, S. L. Pd-Catalyzed Amidations of Aryl Chlorides Using Monodentate Biaryl Phosphine Ligands: A Kinetic, Computational, and Synthetic Investigation. *J. Am. Chem. Soc.* **2007,** *129*, 13001-13007.

(27) a) Burdett, J. K.; Albright, T. A. Trans Influence and Mutual Influence of Ligands Coordinated to a Central Atom. *Inorg. Chem.* **1979,** *18*, 2112-2120. b) Manojlovic-Muir, L. J.; Muir, K. W. The trans-Influence of Ligands in Platinum(II) Complexes. The Significance of the Bond Length Data. *Inorg. Chim. Acta* **1974,** *10*, 47-49.

(28) Wang, D. Y.; Choliy, Y.; Haibach, M. C.; Hartwig, J. F.; Krogh-Jespersen, K.; Goldman, A. S. Assessment of the Electronic Factors Determining the Thermodynamics of "Oxidative Addition" of C–H and N–H Bonds to Ir(I) Complexes. *J. Am. Chem. Soc.* **2016,** *138*, 149-163.

(29) a) Lam, W. H.; Shimada, S.; Batsanov, A. S.; Lin, Z.; Marder, T. B.; Cowan, J. A.; Howard, J. A. K.; Mason, S. A.; McIntyre, G. J. Accurate Molecular Structures of 16-Electron Rhodium Hydrido Boryl Complexes: Low-Temperature Single-

Crystal X-ray and Neutron Diffraction and Computational Studies of [$(PR_3)_2$RhHCl(Boryl)] (Boryl = Bpin, Bcat). *Organometallics* **2003,** *22*, 4557-4568. b) Oliván, M.; Eisenstein, O.; Caulton, K. G. New Access to Vinylidenes from Ruthenium Polyhydrides. *Organometallics* **1997,** *16*, 2227-2229. c) Riehl, J. F.; Jean, Y.; Eisenstein, O.; Pelissier, M. Theoretical study of the structures of electron-deficient d^6 ML_5 complexes. Importance of a p-donating ligand. *Organometallics* **1992,** *11*, 729-737.

(30) Gatard, S.; Çelenligil-Çetin, R.; Guo, C.; Foxman, B. M.; Ozerov, O. V. Carbon−Halide Oxidative Addition and Carbon−Carbon Reductive Elimination at a (PNP)Rh Center. *J. Am. Chem. Soc.* **2006,** *128*, 2808-2809.

(31) a) Foley, B. J.; Palit, C. M.; Timpa, S. D.; Ozerov, O. V. Synthesis of (POCOP)Co(Ph)(X) Pincer Complexes and Observation of Aryl–Aryl Reductive Elimination Involving the Pincer Aryl. *Organometallics* **2018,** *37*, 3803-3812. b) Puri, M.; Gatard, S.; Smith, D. A.; Ozerov, O. V. Competition Studies of Oxidative Addition of Aryl Halides to the (PNP)Rh Fragment. *Organometallics* **2011,** *30*, 2472-2482. c) Zhu, Y.; Smith, D. A.; Herbert, D. E.; Gatard, S.; Ozerov, O. V. C–H and C–O Oxidative Addition in Reactions of Aryl Carboxylates with a PNP Pincer-Ligated Rh(I) Fragment. *Chem. Commun.* **2012,** *48*, 218-220.

(32) Gutiérrez, E.; Hudson, S. A.; Monge, A.; Nicasio, M. C.; Paneque, M.; Ruiz, C. Organometallic Derivatives of Ni(II) with Poly(pyrazolyl)borate Ligands. *J. Organomet. Chem.* **1998,** *551*, 215-227.

(33) Ghosh, R.; Emge, T. J.; Krogh-Jespersen, K.; Goldman, A. S. Combined Experimental and Computational Studies on Carbon−Carbon Reductive Elimination from Bis(hydrocarbyl) Complexes of (PCP)Ir. *J. Am. Chem. Soc.* **2008,** *130*, 11317-11327.

(34) a) Koizumi, T.-a.; Yamazaki, A.; Yamamoto, T. Reductive elimination of C_6F_5–C_6F_5 in the reaction of bis(pentafluorophenyl)palladium(II) complexes with protic acids. *Dalton Trans.* **2008**, 3949-3952. b) Hughes, R. P.; Ward, A. J.; Golen, J. A.; Incarvito, C. D.; Rheingold, A. L.; Zakharov, L. N. Synthesis, Molecular Structures, And Chemistry Of Some New Palladium(II) And Platinum(II) Complexes With Pentafluorophenyl Ligands. *Dalton Trans.* **2004**, 2720-2727. c) Bartolomé, C.; Villafañe, F.; Martín-Alvarez, J. M.; Martínez-Ilarduya, J. M.; Espinet, P. [$Pd(Fmes)_2$(tmeda)]: A Case of Intermittent C-H···F-C Hydrogen-Bond Interaction in Solution. *Chem. Eur. J.* **2013,** *19*, 3702-3709. d) Osakada, K.; Onodera, H.; Nishihara, Y. Diarylpalladium Complexes with a Cis Structure.

Formation via Transmetalation of Arylboronic Acids with an Aryliodopalladium Complex and Intramolecular Coupling of the Aryl Ligands, Affording Unsymmetrical Biaryls. *Organometallics* **2005,** *24*, 190-192.

(35) a) Miller, S. L.; Chotana, G. A.; Fritz, J. A.; Chattopadhyay, B.; Maleczka, R. E.; Smith, M. R. C–H Borylation Catalysts that Distinguish Between Similarly Sized Substituents Like Fluorine and Hydrogen. *Org. Lett.* **2019,** *21*, 6388-6392. b) Obligacion, J. V.; Semproni, S. P.; Chirik, P. J. Cobalt-Catalyzed C–H Borylation. *J. Am. Chem. Soc.* **2014,** *136*, 4133-4136. c) Syed, Z. H.; Chen, Z.; Idrees, K. B.; Goetjen, T. A.; Wegener, E. C.; Zhang, X.; Chapman, K. W.; Kaphan, D. M.; Delferro, M.; Farha, O. K. Mechanistic Insights into C–H Borylation of Arenes with Organoiridium Catalysts Embedded in a Microporous Metal–Organic Framework. *Organometallics* **2020**. d) Ishiyama, T.; Takagi, J.; Ishida, K.; Miyaura, N.; Anastasi, N. R.; Hartwig, J. F. Mild Iridium-Catalyzed Borylation of Arenes. High Turnover Numbers, Room Temperature Reactions, and Isolation of a Potential Intermediate. *J. Am. Chem. Soc.* **2002,** *124*, 390-391. e) Dai, H.-X.; Yu, J.-Q. Pd-Catalyzed Oxidative ortho-C–H Borylation of Arenes. *J. Am. Chem. Soc.* **2012,** *134*, 134-137. f) Structure, Properties, and Preparation of Boronic Acid Derivatives. In *Boronic Acids*, pp 1-133. g) Takagi, J.; Sato, K.; Hartwig, J. F.; Ishiyama, T.; Miyaura, N. Iridium-Catalyzed C–H Coupling Reaction of Heteroaromatic Compounds with bis(pinacolato)diboron: Regioselective Synthesis of Heteroarylboronates. *Tetrahedron Lett.* **2002,** *43*, 5649-5651.

(36) Mkhalid, I. A. I.; Barnard, J. H.; Marder, T. B.; Murphy, J. M.; Hartwig, J. F. C−H Activation for the Construction of C−B Bonds. *Chem. Rev.* **2010,** *110*, 890-931.

(37) a) Hartwig, J. F. Regioselectivity of the borylation of alkanes and arenes. *Chem. Soc. Rev.* **2011,** *40*, 1992-2002. b) Hartwig, J. F. Borylation and Silylation of C–H Bonds: A Platform for Diverse C–H Bond Functionalizations. *Acc. Chem. Res.* **2012,** *45*, 864-873.

(38) a) Furukawa, T.; Tobisu, M.; Chatani, N. C–H Functionalization at Sterically Congested Positions by the Platinum-Catalyzed Borylation of Arenes. *J. Am. Chem. Soc.* **2015,** *137*, 12211-12214. b) Légaré, M.-A.; Courtemanche, M.-A.; Rochette, É.; Fontaine, F.-G. Metal-free catalytic C-H bond activation and borylation of heteroarenes. *Science* **2015,** *349*, 513-516. c) Mazzacano, T. J.; Mankad, N. P. Base Metal Catalysts for Photochemical C–H Borylation That Utilize Metal–Metal Cooperativity. *J. Am. Chem. Soc.* **2013,** *135*, 17258-17261. d) Schaefer, B. A.; Margulieux, G. W.; Small, B. L.; Chirik, P. J. Evaluation of Cobalt Complexes Bearing Tridentate Pincer Ligands for Catalytic C–H Borylation. *Organometallics* **2015,** *34*, 1307-1320.

(39) a) Beletskaya, I.; Pelter, A. Hydroborations catalysed by transition metal complexes. *Tetrahedron* **1997,** *53*, 4957-5026. b) Dhillon, R. S. *Hydroboration and Organic Synthesis*. Springer-Verlag: Berlin, 2007.

(40) Trost, B. M.; Ball, Z. T. Addition of Metalloid Hydrides to Alkynes: Hydrometallation with Boron, Silicon, and Tin. *Synthesis* **2005,** *2005*, 853-887.

(41) Chen, H.; Schlecht, S.; Semple, T. C.; Hartwig, J. F. Thermal, Catalytic, Regiospecific Functionalization of Alkanes. *Science* **2000,** *287*, 1995-1997.

(42) Brown, J. M.; Lloyd-Jones, G. C. Vinylborane Formation in Rhodium-Catalyzed Hydroboration of Vinylarenes. Mechanism versus Borane Structure and Relationship to Silation. *J. Am. Chem. Soc.* **1994,** *116*, 866-878.

(43) Olsson, V. J.; Szabó, K. J. Selective One-Pot Carbon–Carbon Bond Formation by Catalytic Boronation of Unactivated Cycloalkenes and Subsequent Coupling. *Angew. Chem. Int. Ed.* **2007,** *46*, 6891-6893.

(44) Ishiyama, T.; Ishida, K.; Takagi, J.; Miyaura, N. Palladium-Catalyzed Benzylic C–H Borylation of Alkylbenzenes with Bis(pinacolato)diboron or Pinacolborane. *Chem. Lett.* **2001,** *30*, 1082-1083.

(45) Brown, H. C.; Bhat, N. G.; Srebnik, M. A Simple, General Synthesis of 1-Alkynyldiisopropoxyboranes. *Tetrahedron Lett.* **1988,** *29*, 2631-2634.

(46) Lee, C.-I.; Zhou, J.; Ozerov, O. V. Catalytic Dehydrogenative Borylation of Terminal Alkynes by a SiNN Pincer Complex of Iridium. *J. Am. Chem. Soc.* **2013,** *135*, 3560-3566.

(47) Lee, C.-I.; DeMott, J. C.; Pell, C. J.; Christopher, A.; Zhou, J.; Bhuvanesh, N.; Ozerov, O. V. Ligand Survey Results in Identification of PNP Pincer Complexes of Iridium as Long-Lived and Chemoselective Catalysts for Dehydrogenative Borylation of Terminal Alkynes. *Chem. Sci.* **2015,** *6*, 6572-6582.

(48) Hall, D. G. *Boronic Acids: Preparation and Applications in Organic Synthesis, Medicine and Materials*. 2nd ed.; Wiley-VCH: Weinheim, 2012.

(49) Hebrard, F.; Kalck, P. Cobalt-Catalyzed Hydroformylation of Alkenes: Generation and Recycling of the Carbonyl Species, and Catalytic Cycle. *Chem. Rev.* **2009,** *109*, 4272-4282.

(50) a) Blanco-Urgoiti, J.; Añorbe, L.; Pérez-Serrano, L.; Domínguez, G.; Pérez-Castells, J. The Pauson–Khand reaction, a powerful synthetic tool for the synthesis of complex molecules. *Chem. Soc. Rev.* **2004,** *33*, 32-42. b) Pauson, P. L.; Khand, I. U. Uses of cobalt-carbonyl acetylene complexes in organic synthesis. *Ann. N.Y. Acad. Sci.* **1977,** *295*, 2-14.

(51) Schore, N. E., The Pauson–Khand Cycloaddition Reaction for Synthesis of Cyclopentenones. In *Organic Reactions*, John Wiley & Sons, Inc.: 1991; pp 1-90.

(52) a) Nicholas, K. M. Chemistry and Synthetic Utility of Cobalt-Complexed Propargyl Cations. *Acc. Chem. Res.* **1987,** *20*, 207-214. b) Teobald, B. J. The Nicholas Reaction: The Use of Dicobalt Hexacarbonyl-Stabilised Propargylic Cations in Synthesis. *Tetrahedron* **2002,** *58*, 4133-4170.

(53) Maity, A.; Hyun, S.-M.; Powers, D. C. Oxidase catalysis via aerobically generated hypervalent iodine intermediates. *Nat. Chem.* **2018,** *10*, 200-204.

(54) De, S. K. Cobalt(II) Chloride As A Novel and Efficient Catalyst for the Synthesis of 1,2,5-Trisubstituted Pyrroles Under Solvent-Free Conditions. *Heteroat. Chem* **2008,** *19*, 592-595.

(55) Kharasch, M. S.; Fuchs, C. F. Factors Influencing the Course and Mechanisms of Grignard Reactions. XI. The Effect of Metallic Halides on the Reaction of Grignard Reagents with Vinyl Halides and Substituted Vinyl Halides. *J. Am. Chem. Soc.* **1943,** *65*, 504-507.

(56) Yoshino, T.; Matsunaga, S. (Pentamethylcyclopentadienyl)cobalt(III)-Catalyzed C–H Bond Functionalization: From Discovery to Unique Reactivity and Selectivity. *Adv. Synth. Catal.* **2017,** *359*, 1245-1262.

(57) Moselage, M.; Li, J.; Ackermann, L. Cobalt-Catalyzed C–H Activation. *ACS Catal.* **2016,** *6*, 498-525.

(58) Bürger, H.; Wannagat, U. Silylamido-Derivate von Eisen und Kobalt. *Monatsh. Chem.* **1963,** *94*, 1007-1012.

(59) Tsutsui, M.; Zeiss, H. π-Complexes of the Transition Metals. XIV. Acetylenic Condensations on Manganese(II) and Cobalt(II). *J. Am. Chem. Soc.* **1961,** *83*, 825-827.

(60) Wakatsuki, Y.; Yamazaki, H. (1,3-Butadiene-1,4-diyl)(η^5-cyclopentadienyl)-(triphenylphosphine)Cobalt* With Various Substituents. *Inorg. Synth.* **1989,** *26*, 190.

(61) Brennan, M. R.; Kim, D.; Fout, A. R. A Synthetic and Mechanistic Investigation Into the Cobalt(I) Catalyzed Amination of Aryl Halides. *Chem. Sci.* **2014,** *5*, 4831-4839.

(62) Klein, H.-F.; Karsch, H. H. Methyltetrakis(trimethylphosphin)kobalt und seine Derivate. *Chem. Ber.* **1975,** *108*, 944-955.

(63) Gosser, L. W.; Cushing, M. A., Jr. π-Cyclooctenyl-π-1,5-cyclooctadienecobalt. *Inorg. Synth.* **1977,** *17*, 112.

(64) a) Wang, S.; Chen, S.-Y.; Yu, X.-Q. C–H functionalization by high-valent Cp*Co(III) catalysis. *Chem. Commun.* **2017,** *53*, 3165-3180. b) Chirila, P. G.; Whiteoak, C. J. Recent advances using [Cp*Co(CO)I_2] catalysts as a powerful tool for C–H functionalisation. *Dalton Trans.* **2017,** *46*, 9721-9739.

(65) Arevalo, R.; Chirik, P. J. Enabling Two-Electron Pathways with Iron and Cobalt: From Ligand Design to Catalytic Applications. *J. Am. Chem. Soc.* **2019,** *141*, 9106-9123.

(66) Kamigaito, M.; Ando, T.; Sawamoto, M. Metal-Catalyzed Living Radical Polymerization. *Chem. Rev.* **2001,** *101*, 3689-3746.

(67) Barata-Vallejo, S.; Postigo, A. Metal-mediated radical perfluoroalkylation of organic compounds. *Coord. Chem. Rev.* **2013,** *257*, 3051-3069.

(68) Lin, Q.; Diao, T. Mechanism of Ni-Catalyzed Reductive 1,2-Dicarbofunctionalization of Alkenes. *J. Am. Chem. Soc.* **2019,** *141*, 17937-17948.

(69) Nalesnik, T. E.; Freudenberger, J. H.; Orchin, M. Radical hydroformylation and hydrogenation of cyclopropenes with $HCo(CO)_4$ and $HMn(CO)_5$. *J. Organomet. Chem.* **1982,** *236*, 95-100.

(70) Nesbit, M. A.; Suess, D. L. M.; Peters, J. C. E–H Bond Activations and Hydrosilylation Catalysis with Iron and Cobalt Metalloboranes. *Organometallics* **2015,** *34*, 4741-4752.

(71) Alawisi, H.; Al-Afyouni, K. F.; Arman, H. D.; Tonzetich, Z. J. Aldehyde Decarbonylation by a Cobalt(I) Pincer Complex. *Organometallics* **2018,** *37*, 4128-4135.

(72) Lin, C.-Y.; Power, P. P. Complexes of Ni(I): a "Rare" Oxidation State of Growing Importance. *Chem. Soc. Rev.* **2017,** *46*, 5347-5399.

(73) Guard, L. M.; Mohadjer Beromi, M.; Brudvig, G. W.; Hazari, N.; Vinyard, D. J. Comparison of dppf-Supported Nickel Precatalysts for the Suzuki–Miyaura Reaction: The Observation and Activity of Nickel(I). *Angew. Chem. Int. Ed.* **2015,** *54*, 13352-13356.

(74) Beromi, M. M.; Nova, A.; Balcells, D.; Brasacchio, A. M.; Brudvig, G. W.; Guard, L. M.; Hazari, N.; Vinyard, D. J. Mechanistic Study of an Improved Ni Precatalyst for Suzuki–Miyaura Reactions of Aryl Sulfamates: Understanding the Role of Ni(I) Species. *J. Am. Chem. Soc.* **2017,** *139*, 922-936.

(75) Ishizu, J.; Yamamoto, T.; Yamamoto, A. Selective Cleavage of C–O Bonds in Esters Through Oxidative Addition to Nickel(0) Complexes. *Chem. Lett.* **1976,** *5*, 1091-1094.

(76) Yamamoto, T.; Ishizu, J.; Kohara, T.; Komiya, S.; Yamamoto, A. Oxidative Addition of Aryl Carboxylates to Nickel(0) Complexes Involving Cleavage of the Acyl-Oxygen Bond. *J. Am. Chem. Soc.* **1980,** *102*, 3758-3764.

(77) Li, Z.; Zhang, S.-L.; Fu, Y.; Guo, Q.-X.; Liu, L. Mechanism of Ni-Catalyzed Selective C−O Bond Activation in Cross-Coupling of Aryl Esters. *J. Am. Chem. Soc.* **2009,** *131*, 8815-8823.

(78) Rosen, B. M.; Quasdorf, K. W.; Wilson, D. A.; Zhang, N.; Resmerita, A.-M.; Garg, N. K.; Percec, V. Nickel-Catalyzed Cross-Couplings Involving Carbon−Oxygen Bonds. *Chem. Rev.* **2011,** *111*, 1346-1416.

(79) a) Ittel, S. D.; Tolman, C. A.; English, A. D.; Jesson, J. P. The Chemistry of 2-Naphthyl Bis[bis(dimethylphosphino)ethane] Hydride Complexes of Iron, Ruthenium, and Osmium. 2. Cleavage of sp and sp^3 Carbon-Hydrogen, Carbon-Oxygen, and Carbon-Halogen Bonds. Coupling of Carbon Dioxide and Acetonitrile. *J. Am. Chem. Soc.* **1978,** *100*, 7577-7585. b) Li, B.-J.; Xu, L.; Wu, Z.-H.; Guan, B.-T.; Sun, C.-L.; Wang, B.-Q.; Shi, Z.-J. Cross-Coupling of Alkenyl/Aryl Carboxylates with Grignard Reagent via Fe-Catalyzed C−O Bond Activation. *J. Am. Chem. Soc.* **2009,** *131*, 14656-14657.

(80) Srivastava, R. S. Carbon–Oxygen Bond Cleavage in Allylic Esters Promoted by Low-Valent Transition-Metal Hydride Complexes. *Appl. Organomet. Chem.* **1993,** *7*, 607-611.

(81) Komiya, S.; Yamamoto, A. Carbon-Oxygen Bond Cleavage of Alkenyl Carboxylate Promoted by Transition Metal Hydrides. *J. Organomet. Chem.* **1975,** *87*, 333-339.

(82) Nagayama, K.; Shimizu, I.; Yamamoto, A. Oxidative Addition of Aryl and Benzyl Trifluoroacetates to Zerovalent Palladium Complexes with Two Modes of C–O Bond Cleavage Processes. *Bull. Chem. Soc. Jpn.* **1999,** *72*, 799-803.

(83) Ben Halima, T.; Zhang, W.; Yalaoui, I.; Hong, X.; Yang, Y.-F.; Houk, K. N.; Newman, S. G. Palladium-Catalyzed Suzuki–Miyaura Coupling of Aryl Esters. *J. Am. Chem. Soc.* **2017,** *139*, 1311-1318.

(84) a) Kundu, S.; Choi, J.; Wang, D. Y.; Choliy, Y.; Emge, T. J.; Krogh-Jespersen, K.; Goldman, A. S. Cleavage of Ether, Ester, and Tosylate C(sp^3)–O Bonds by an Iridium Complex, Initiated by Oxidative Addition of C–H Bonds. Experimental and Computational Studies. *J. Am. Chem. Soc.* **2013,** *135*, 5127-5143. b) Stanley, L. M.; Bai, C.; Ueda, M.; Hartwig, J. F. Iridium-Catalyzed Kinetic Asymmetric

Transformations of Racemic Allylic Benzoates. *J. Am. Chem. Soc.* **2010,** *132*, 8918-8920.

(85) Quasdorf, K. W.; Tian, X.; Garg, N. K. Cross-Coupling Reactions of Aryl Pivalates with Boronic Acids. *J. Am. Chem. Soc.* **2008,** *130*, 14422-14423.

(86) Guo, L.; Hsiao, C.-C.; Yue, H.; Liu, X.; Rueping, M. Nickel-Catalyzed C_{sp2}–C_{sp3} Cross-Coupling via C–O Bond Activation. *ACS Catal.* **2016,** *6*, 4438-4442.

(87) Ohtsuki, A.; Yanagisawa, K.; Furukawa, T.; Tobisu, M.; Chatani, N. Nickel/N-Heterocyclic Carbene-Catalyzed Suzuki–Miyaura Type Cross-Coupling of Aryl Carbamates. *J. Org. Chem.* **2016,** *81*, 9409-9414.

(88) Hie, L.; Fine Nathel, N. F.; Hong, X.; Yang, Y.-F.; Houk, K. N.; Garg, N. K. Nickel-Catalyzed Activation of Acyl C−O Bonds of Methyl Esters. *Angew. Chem. Int. Ed.* **2016,** *55*, 2810-2814.

(89) Quasdorf, K. W.; Antoft-Finch, A.; Liu, P.; Silberstein, A. L.; Komaromi, A.; Blackburn, T.; Ramgren, S. D.; Houk, K. N.; Snieckus, V.; Garg, N. K. Suzuki−Miyaura Cross-Coupling of Aryl Carbamates and Sulfamates: Experimental and Computational Studies. *J. Am. Chem. Soc.* **2011,** *133*, 6352-6363.

(90) Quasdorf, K. W.; Riener, M.; Petrova, K. V.; Garg, N. K. Suzuki−Miyaura Coupling of Aryl Carbamates, Carbonates, and Sulfamates. *J. Am. Chem. Soc.* **2009,** *131*, 17748-17749.

(91) Tobisu, M.; Chatani, N. Devising Boron Reagents for Orthogonal Functionalization through Suzuki–Miyaura Cross-Coupling. *Angew. Chem. Int. Ed.* **2009,** *48*, 3565-3568.

(92) a) Muto, K.; Yamaguchi, J.; Itami, K. Nickel-Catalyzed C–H/C–O Coupling of Azoles with Phenol Derivatives. *J. Am. Chem. Soc.* **2012,** *134*, 169-172. b) Muto, K.; Yamaguchi, J.; Lei, A.; Itami, K. Isolation, Structure, and Reactivity of an Arylnickel(II) Pivalate Complex in Catalytic C–H/C–O Biaryl Coupling. *J. Am. Chem. Soc.* **2013,** *135*, 16384-16387.

(93) a) Ehle, A. R.; Zhou, Q.; Watson, M. P. Nickel(0)-Catalyzed Heck Cross-Coupling via Activation of Aryl C–OPiv Bonds. *Org. Lett.* **2012,** *14*, 1202-1205. b) Srinivas, H. D.; Zhou, Q.; Watson, M. P. Enantiospecific, Nickel-Catalyzed Cross-Couplings of Allylic Pivalates and Arylboroxines. *Org. Lett.* **2014,** *16*, 3596-3599. c) Zhou, Q.; Srinivas, H. D.; Dasgupta, S.; Watson, M. P. Nickel-Catalyzed Cross-Couplings of Benzylic Pivalates with Arylboroxines: Stereospecific Formation of Diarylalkanes and Triarylmethanes. *J. Am. Chem. Soc.* **2013,** *135*, 3307-3310.

(94) Guan, B.-T.; Wang, Y.; Li, B.-J.; Yu, D.-G.; Shi, Z.-J. Biaryl Construction via Ni-Catalyzed C−O Activation of Phenolic Carboxylates. *J. Am. Chem. Soc.* **2008,** *130*, 14468-14470.

(95) Dawans, F.; Marechal, J. C.; Teyssie, P. Bis(π-allylnickel haloacetates). *J. Organomet. Chem.* **1970,** *21*, 259-261.

(96) Gu, Y.; Martín, R. Ni-Catalyzed Stannylation of Aryl Esters via C−O Bond Cleavage. *Angew. Chem. Int. Ed.* **2017,** *56*, 3187-3190.

(97) Lu, Q.; Yu, H.; Fu, Y. Mechanistic Study of Chemoselectivity in Ni-Catalyzed Coupling Reactions between Azoles and Aryl Carboxylates. *J. Am. Chem. Soc.* **2014,** *136*, 8252-8260.

(98) Shimasaki, T.; Tobisu, M.; Chatani, N. Nickel-Catalyzed Amination of Aryl Pivalates by the Cleavage of Aryl C-O Bonds. *Angew. Chem. Int. Ed.* **2010,** *49*, 2929-2932.

(99) Hartwig, J. F. Evolution of C–H Bond Functionalization from Methane to Methodology. *J. Am. Chem. Soc.* **2016,** *138*, 2-24.

(100) Cho, J.-Y.; Tse, M. K.; Holmes, D.; Maleczka, R. E.; Smith, M. R. Remarkably Selective Iridium Catalysts for the Elaboration of Aromatic C-H Bonds. *Science* **2002,** *295*, 305-308.

(101) Preshlock, S. M.; Ghaffari, B.; Maligres, P. E.; Krska, S. W.; Maleczka, R. E.; Smith, M. R. High-Throughput Optimization of Ir-Catalyzed C–H Borylation: A Tutorial for Practical Applications. *J. Am. Chem. Soc.* **2013,** *135*, 7572-7582.

(102) Obligacion, J. V.; Bezdek, M. J.; Chirik, P. J. C(sp^2)–H Borylation of Fluorinated Arenes Using an Air-Stable Cobalt Precatalyst: Electronically Enhanced Site Selectivity Enables Synthetic Opportunities. *J. Am. Chem. Soc.* **2017,** *139*, 2825-2832.

(103) Obligacion, J. V.; Chirik, P. J. Mechanistic Studies of Cobalt-Catalyzed C(sp^2)–H Borylation of Five-Membered Heteroarenes with Pinacolborane. *ACS Catal.* **2017,** *7*, 4366-4371.

(104) Dombray, T.; Werncke, C. G.; Jiang, S.; Grellier, M.; Vendier, L.; Bontemps, S.; Sortais, J.-B.; Sabo-Etienne, S.; Darcel, C. Iron-Catalyzed C–H Borylation of Arenes. *J. Am. Chem. Soc.* **2015,** *137*, 4062-4065.

(105) Chen, H.; Schlecht, S.; Semple, T. C.; Hartwig, J. F. Thermal, Catalytic, Regiospecific Functionalization of Alkanes. *Science* **2000,** *287*, 1995-1997.

(106) Murphy, J. M.; Lawrence, J. D.; Kawamura, K.; Incarvito, C.; Hartwig, J. F. Ruthenium-Catalyzed Regiospecific Borylation of Methyl C−H Bonds. *J. Am. Chem. Soc.* **2006,** *128*, 13684-13685.

(107) Chen, H.; Hartwig, J. F. Catalytic, Regiospecific End-Functionalization of Alkanes: Rhenium-Catalyzed Borylation under Photochemical Conditions. *Angew. Chem. Int. Ed.* **1999,** *38*, 3391-3393.

(108) Coapes, R. B.; Souza, F. E. S.; Thomas, R. L.; Hall, J. J.; Marder, T. B. Rhodium catalysed dehydrogenative borylation of vinylarenes and 1,1-disubstituted alkenes without sacrificial hydrogenation—a route to 1,1-disubstituted vinylboronates. *Chem. Commun.* **2003**, 614-615.

(109) Larsen, M. A.; Cho, S. H.; Hartwig, J. Iridium-Catalyzed, Hydrosilyl-Directed Borylation of Unactivated Alkyl C–H Bonds. *J. Am. Chem. Soc.* **2016,** *138*, 762-765.

(110) Larsen, M. A.; Wilson, C. V.; Hartwig, J. F. Iridium-Catalyzed Borylation of Primary Benzylic C–H Bonds without a Directing Group: Scope, Mechanism, and Origins of Selectivity. *J. Am. Chem. Soc.* **2015,** *137*, 8633-8643.

(111) a) León, T.; Fernández, E. The Pauson–Khand reaction using alkynylboronic esters: solving a long-standing regioselectivity issue. *Chem. Commun.* **2016,** *52*, 9363-9366. b) Jiao, J.; Nishihara, Y. Alkynylboron compounds in organic synthesis. *J. Organomet. Chem.* **2012,** *721-722*, 3-16. c) Browne, D. L.; Vivat, J. F.; Plant, A.; Gomez-Bengoa, E.; Harrity, J. P. A. Investigation of the Scope and Regiochemistry of Alkynylboronate Cycloadditions with Sydnones. *J. Am. Chem. Soc.* **2009,** *131*, 7762-7769. d) Nishihara, Y.; Suetsugu, M.; Saito, D.; Kinoshita, M.; Iwasaki, M. Synthesis of Cyclic 1-Alkenylboronates via Zr-Mediated Double Functionalization of Alkynylboronates and Sequential Ru-Catalyzed Ring-Closing Olefin Metathesis. *Org. Lett.* **2013,** *15*, 2418-2421. e) Kirkham, J. D.; Leach, A. G.; Row, E. C.; Harrity, J. P. A. Investigation of the Origins of Regiochemical Control in [4+2] Cycloadditions of 2-Pyrones and Alkynylboronates. *Synthesis* **2012,** *44*, 1964-1973.

(112) Tsuchimoto, T.; Utsugi, H.; Sugiura, T.; Horio, S. Alkynylboranes: A Practical Approach by Zinc-Catalyzed Dehydrogenative Coupling of Terminal Alkynes with 1,8-Naphthalenediaminatoborane. *Adv. Synth. Catal.* **2015,** *357*, 77-82.

(113) Romero, E. A.; Jazzar, R.; Bertrand, G. Copper-Catalyzed Dehydrogenative Borylation of Terminal Alkynes with Pinacolborane. *Chem. Sci.* **2017,** *8*, 165-168.

(114) Wei, D.; Carboni, B.; Sortais, J.-B.; Darcel, C. Iron-Catalyzed Dehydrogenative Borylation of Terminal Alkynes. *Adv. Synth. Catal.* **2018,** *360*, 3649-3654.

(115) Procter, R. J.; Uzelac, M.; Cid, J.; Rushworth, P. J.; Ingleson, M. J. Low-Coordinate NHC–Zinc Hydride Complexes Catalyze Alkyne C–H Borylation and Hydroboration Using Pinacolborane. *ACS Catal.* **2019,** *9*, 5760-5771.

(116) Pell, C. J.; Ozerov, O. V. Catalytic Dehydrogenative Borylation of Terminal Alkynes by POCOP-Supported Palladium Complexes. *Inorg. Chem. Front.* **2015,** *2*, 720-724.

(117) Zhou, J.; Lee, C.-I.; Ozerov, O. V. Computational Study of the Mechanism of Dehydrogenative Borylation of Terminal Alkynes by SiNN Iridium Complexes. *ACS Catal.* **2018,** *8*, 536-545.

(118) Weng, W.; Guo, C.; Moura, C.; Yang, L.; Foxman, B. M.; Ozerov, O. V. Competitive Activation of N−C and C−H Bonds of the PNP Framework by Monovalent Rhodium and Iridium. *Organometallics* **2005,** *24*, 3487-3499.

(119) Fan, L.; Yang, L.; Guo, C.; Foxman, B. M.; Ozerov, O. V. N−C Cleavage in Pincer PNP Complexes of Palladium. *Organometallics* **2004,** *23*, 4778-4787.

(120) Ozerov, O. V.; Guo, C.; Papkov, V. A.; Foxman, B. M. Facile Oxidative Addition of N−C and N−H Bonds to Monovalent Rhodium and Iridium. *J. Am. Chem. Soc.* **2004,** *126*, 4792-4793.

(121) Huacuja, R.; Herbert, D. E.; Fafard, C. M.; Ozerov, O. V. A terminal palladium fluoride complex supported by an anionic PNP pincer ligand. *J. Fluorine Chem.* **2010,** *131*, 1257-1261.

(122) Young, C. L., Hydrogen and Deuterium. In *IUPAC Sulubility Data Series*, Pergamon Press.: Oxford, 1981; Vol. 5/6, pp 159-160.

(123) Gallego, M. G.; Sierra, M. A. Kinetic Isotope Effects in the Study of Organometallic Reaction Mechanisms. *Chem. Rev.* **2011,** *111*, 4857-4963.

(124) Hansch, C.; Leo, A.; Taft, R. W. A survey of Hammett substituent constants and resonance and field parameters. *Chem. Rev.* **1991,** *91*, 165-195.

(125) a) He, C.; Ke, J.; Xu, H.; Lei, A. Synergistic Catalysis in the Sonogashira Coupling Reaction: Quantitative Kinetic Investigation of Transmetalation. *Angew. Chem. Int. Ed.* **2013,** *52*, 1527-1530. b) Hung, Y.-T.; Chen, M.-T.; Huang, M.-H.; Kao, T.-Y.; Liu, Y.-S.; Liang, L.-C. Catalytic Sonogashira Couplings Mediated by an Amido Pincer Complex of Palladium. *Inorg. Chem. Front.* **2014,** *1*, 405-413. c) Kotzabasaki, V.; Lykakis, I. N.; Gryparis, C.; Psyllaki, A.; Vasilikogiannaki, E.; Stratakis, M. Gold-Catalyzed Dehydrogenative Cycloaddition of Tethered 1,*n*-Dihydrodisilanes to Alkynes. *Organometallics* **2013,** *32*, 665-672. d) Powers, A. R.; Ghiviriga, I.; Abboud, K. A.; Veige, A. S. Au-iClick Mirrors the Mechanism of Copper Catalyzed Azide–Alkyne Cycloaddition (CuAAC). *Dalton Trans.* **2015,** *44*, 14747-14752.

(126) Lee, C.-I.; Shih, W.-C.; Zhou, J.; Reibenspies, J. H.; Ozerov, O. V. Synthesis of Triborylalkenes from Terminal Alkynes by Iridium-Catalyzed Tandem C□H Borylation and Diboration. *Angew. Chem. Int. Ed.* **2015,** *54*, 14003-14007.

(127) Gregor, L. C.; Chen, C.-H.; Fafard, C. M.; Fan, L.; Guo, C.; Foxman, B. M.; Gusev, D. G.; Ozerov, O. V. Heterolytic splitting of H–X bonds at a cationic (PNP)Pd center. *Dalton Trans.* **2010,** *39*, 3195-3202.

(128) Rosini, G. P.; Wang, K.; Patel, B.; Goldman, A. S. A mechanistic study of thermal C-H reductive elimination from a six-coordinate d^6 iridium complex. *Inorg. Chim. Acta* **1998,** *270*, 537-542.

(129) Webster, C. E.; Fan, Y.; Hall, M. B.; Kunz, D.; Hartwig, J. F. Experimental and Computational Evidence for a Boron-Assisted, σ-Bond Metathesis Pathway for Alkane Borylation. *J. Am. Chem. Soc.* **2003,** *125*, 858-859.

(130) a) Haines, B. E.; Saito, Y.; Segawa, Y.; Itami, K.; Musaev, D. G. Flexible Reaction Pocket on Bulky Diphosphine–Ir Complex Controls Regioselectivity in para-Selective C–H Borylation of Arenes. *ACS Catal.* **2016,** *6*, 7536-7546. b) Huang, G.; Kalek, M.; Liao, R.-Z.; Himo, F. Mechanism, reactivity, and selectivity of the iridium-catalyzed C(sp3)–H borylation of chlorosilanes. *Chem. Sci.* **2015,** *6*, 1735-1746. c) Tamura, H.; Yamazaki, H.; Sato, H.; Sakaki, S. Iridium-Catalyzed Borylation of Benzene with Diboron. Theoretical Elucidation of Catalytic Cycle Including Unusual Iridium(V) Intermediate. *J. Am. Chem. Soc.* **2003,** *125*, 16114-16126. d) Zhong, R.-L.; Sakaki, S. sp^3 C–H Borylation Catalyzed by Iridium(III) Triboryl Complex: Comprehensive Theoretical Study of Reactivity, Regioselectivity, and Prediction of Excellent Ligand. *J. Am. Chem. Soc.* **2019,** *141*, 9854-9866.

(131) a) Alcaraz, G.; Grellier, M.; Sabo-Etienne, S. Bis σ-Bond Dihydrogen and Borane Ruthenium Complexes: Bonding Nature, Catalytic Applications, and Reversible Hydrogen Release. *Acc. Chem. Res.* **2009,** *42*, 1640-1649. b) Esteruelas, M. A.; Fernández, I.; García-Yebra, C.; Martín, J.; Oñate, E. Elongated σ-Borane versus σ-Borane in Pincer–POP–Osmium Complexes. *Organometallics* **2017,** *36*, 2298-2307. c) Hartwig, J. F.; Cook, K. S.; Hapke, M.; Incarvito, C. D.; Fan, Y.; Webster, C. E.; Hall, M. B. Rhodium Boryl Complexes in the Catalytic, Terminal Functionalization of Alkanes. *J. Am. Chem. Soc.* **2005,** *127*, 2538-2552. d) Hebden, T. J.; Denney, M. C.; Pons, V.; Piccoli, P. M. B.; Koetzle, T. F.; Schultz, A. J.; Kaminsky, W.; Goldberg, K. I.; Heinekey, D. M. σ-Borane Complexes of Iridium: Synthesis and Structural Characterization. *J. Am. Chem. Soc.* **2008,** *130*, 10812-10820. e) Pandey, K. K. Transition metal–σ-borane complexes. *Coord. Chem. Rev.* **2009,** *253*, 37-55.

(132) Lambert, J. B.; Larson, E. G.; Bosch, R. J.; TeVrucht, M. L. E. Stereomutation in the Seyferth reaction. *J. Am. Chem. Soc.* **1985,** *107*, 5443-5447.

(133) Ammann, C.; Meier, P.; Merbach, A. A simple multinuclear NMR thermometer. *Journal of Magnetic Resonance (1969)* **1982,** *46*, 319-321.

(134) Iluc, V. M.; Fedorov, A.; Grubbs, R. H. H/D Exchange Processes Catalyzed by an Iridium-Pincer Complex. *Organometallics* **2012,** *31*, 39-41.

(135) *APEX2 "Program for Data Collection on Area Detectors"*, BRUKER AXS Inc.: 5465 East Cheryl Parkway, Madison, WI 53711-5373 USA.

(136) Sheldrick, G. M. *"Cell_Now (version **2008**/1): Program for Obtaining Unit Cell Constants from Single Crystal Data"*, University of Göttingen, Germany.

(137) Sheldrick, G. M. *TWINABS, "Program for Absorption Correction of Area Detector Frames*, BRUKER AXS Inc.: 5465 East Cheryl Parkway, Madison, WI 53711-5373 USA.

(138) a) Sheldrick, G. M. A Short History of SHELX. *Acta Cryst.* **2008,** *A64*, 112-122. b) Sheldrick, G. M. SHELXT - Integrated Space-Group and Crystal-Structure Determination. *Acta Cryst.* **2015,** *A71*, 3-8. c) Sheldrick, G. M. Crystal Structure Refinement With SHELXL. *Acta Cryst.* **2015,** *C71*, 3-8.

(139) Spek, A. L. Single-Crystal Structure Validation with the Program PLATON. *J. Appl. Crystallogr.* **2003,** *36*, 7-13.

(140) Dolomanov, O. V.; Bourhis, L. H.; Gildea, R. J.; Howard, J. A. K.; Puschmann, H. OLEX2: a Complete Structure Solution, Refinement, and Analysis Program. *J. Appl. Crystallogr.* **2009,** *42*, 339-341.

(141) Krautwald, S.; Bezdek, M. J.; Chirik, P. J. Cobalt-Catalyzed 1,1-Diboration of Terminal Alkynes: Scope, Mechanism, and Synthetic Applications. *J. Am. Chem. Soc.* **2017,** *139*, 3868-3875.

(142) a) Allen, K. E.; Heinekey, D. M.; Goldman, A. S.; Goldberg, K. I. Regeneration of an Iridium(III) Complex Active for Alkane Dehydrogenation Using Molecular Oxygen. *Organometallics* **2014,** *33*, 1337-1340. b) Schiwek, C.; Meiners, J.; Förster, M.; Würtele, C.; Diefenbach, M.; Holthausen, M. C.; Schneider, S. Oxygen Reduction with a Bifunctional Iridium Dihydride Complex. *Angew. Chem. Int. Ed.* **2015,** *54*, 15271-15275. c) Williams, B. D.; Kaminsky, W.; Mayer, J. M.; Goldberg, K. I. Reactions of iridium hydride pincer complexes with dioxygen: new dioxygen complexes and reversible O_2 binding. *Chem. Commun.* **2008**, 4195-4197.

(143) Bolaño, T.; Esteruelas, M. A.; Gay, M. P.; Oñate, E.; Pastor, I. M.; Yus, M. An Acyl-NHC Osmium Cooperative System: Coordination of Small Molecules and Heterolytic B–H and O–H Bond Activation. *Organometallics* **2015,** *34*, 3902-3908.

(144) a) Melnick, J. G.; Radosevich, A. T.; Villagrán, D.; Nocera, D. G. Decarbonylation of ethanol to methane, carbon monoxide and hydrogen by a [PNP]Ir complex. *Chem. Commun.* **2010,** *46*, 79-81. b) Whited, M. T.; Grubbs, R. H. A Catalytic Cycle for Oxidation of tert-Butyl Methyl Ether by a Double C−H Activation-Group Transfer Process. *J. Am. Chem. Soc.* **2008,** *130*, 16476-16477.

(145) a) Ghosh, R.; Kanzelberger, M.; Emge, T. J.; Hall, G. S.; Goldman, A. S. Dinitrogen Complexes of Pincer-Ligated Iridium. *Organometallics* **2006,** *25*, 5668-5671. b) Lee, D. W.; Kaska, W. C.; Jensen, C. M. Mechanistic Features of Iridium Pincer Complex Catalyzed Hydrocarbon Dehydrogenation Reactions: Inhibition upon Formation of a μ-Dinitrogen Complex. *Organometallics* **1998,** *17*, 1-3.

(146) Merola, J. S.; Husebo, T. L.; Matthews, K. E. Aqueous Organometallic Chemistry of mer-$Ir(H)^2(PMe^3)_3X$ Complexes. *Organometallics* **2012,** *31*, 3920-3929.

(147) Herde, J. L.; Lambert, J. C.; Senoff, C. V.; Cushing, M. A. Cyclooctene and 1,5-cyclooctadiene Complexes of Iridium(I). *Inorganic Synthesis* **2007,** *15*, 18-20.

(148) a) Okazaki, M.; Tobita, H.; Ogino, H. Reactivity of silylene complexes. *Dalton Trans.* **2003**, 493-506. b) Waterman, R.; Hayes, P. G.; Tilley, T. D. Synthetic Development and Chemical Reactivity of Transition-Metal Silylene Complexes. *Acc. Chem. Res.* **2007,** *40*, 712-719.

(149) Glaser, P. B.; Tilley, T. D. Catalytic Hydrosilylation of Alkenes by a Ruthenium Silylene Complex. Evidence for a New Hydrosilylation Mechanism. *J. Am. Chem. Soc.* **2003,** *125*, 13640-13641.

(150) Lee, V. Y.; Aoki, S.; Yokoyama, T.; Horiguchi, S.; Sekiguchi, A.; Gornitzka, H.; Guo, J.-D.; Nagase, S. Toward a Silicon Version of Metathesis: From Schrock-Type Titanium Silylidenes to Silatitanacyclobutenes. *J. Am. Chem. Soc.* **2013,** *135*, 2987-2990.

(151) Handwerker, H.; Leis, C.; Probst, R.; Bissinger, P.; Grohmann, A.; Kiprof, P.; Herdtweck, E.; Bluemel, J.; Auner, N.; Zybill, C. Reversible intramolecular base-stabilization in silylene (silanediyl) complexes: surprising reactivity for silylene coordination compounds with a dynamic N•••Si•••N bond. *Organometallics* **1993,** *12*, 2162-2176.

(152) Price, J. S.; Emslie, D. J. H.; Britten, J. F. Manganese Silylene Hydride Complexes: Synthesis and Reactivity with Ethylene to Afford Silene Hydride Complexes. *Angew. Chem. Int. Ed.* **2017,** *56*, 6223-6227.

(153) a) Smith, P. W.; Tilley, T. D. Base-Free Iron Hydrosilylene Complexes via an α-Hydride Migration that Induces Spin Pairing. *J. Am. Chem. Soc.* **2018,** *140*, 3880-3883. b) Tobita, H.; Matsuda, A.; Hashimoto, H.; Ueno, K.; Ogino, H. Direct Evidence for Extremely Facile 1,2- and 1,3-Group Migrations in an $FeSi_2$ System. *Angew. Chem. Int. Ed.* **2004,** *43*, 221-224.

(154) Iluc, V. M.; Hillhouse, G. L. Arrested 1,2-Hydrogen Migration from Silicon to Nickel upon Oxidation of a Three-Coordinate Ni(I) Silyl Complex. *J. Am. Chem. Soc.* **2010,** *132*, 11890-11892.

(155) a) Whited, M. T.; Deetz, A. M.; Boerma, J. W.; DeRosha, D. E.; Janzen, D. E. Formation of Chlorosilyl Pincer-Type Rhodium Complexes by Multiple Si–H Activations of Bis(phosphine)/Dihydrosilyl Ligands. *Organometallics* **2014,** *33*, 5070-5073. b) Whited, M. T.; Deetz, A. M.; Donnell, T. M.; Janzen, D. E. Examining the role of Rh/Si cooperation in alkene hydrogenation by a pincer-type [P_2Si]Rh complex. *Dalton Trans.* **2016,** *45*, 9758-9761. c) Whited, M. T.; Zhang, J.; Ma, S.; Nguyen, B. D.; Janzen, D. E. Silylene-assisted hydride transfer to CO_2 and CS_2 at a [P_2Si]Ru pincer-type complex. *Dalton Trans.* **2017,** *46*, 14757-14761.

(156) a) Korshin, E. E.; Leitus, G.; Shimon, L. J. W.; Konstantinovski, L.; Milstein, D. Silanol-Based Pincer Pt(II) Complexes: Synthesis, Structure, and Unusual Reactivity. *Inorg. Chem.* **2008,** *47*, 7177-7189. b) Mitton, S. J.; McDonald, R.; Turculet, L. Synthesis and Characterization of Neutral and Cationic Platinum(II) Complexes Featuring Pincer-like Bis(phosphino)silyl Ligands: Si−H and Si−Cl Bond Activation Chemistry. *Organometallics* **2009,** *28*, 5122-5136. c) Takaya, J.; Iwasawa, N. Hydrocarboxylation of Allenes with CO_2 Catalyzed by Silyl Pincer-Type Palladium Complex. *J. Am. Chem. Soc.* **2008,** *130*, 15254-15255.

(157) Li, Y.; Krause, J. A.; Guan, H. Cobalt POCOP Pincer Complexes via Ligand C–H Bond Activation with $Co_2(CO)_8$: Catalytic Activity for Hydrosilylation of Aldehydes in an Open vs a Closed System. *Organometallics* **2018,** *37*, 2147-2158.

(158) Corey, J. Y.; Braddock-Wilking, J. Reactions of Hydrosilanes with Transition-Metal Complexes: Formation of Stable Transition-Metal Silyl Compounds. *Chem. Rev.* **1999,** *99*, 175-292.

(159) Addison, A. W.; Rao, T. N.; Reedijk, J.; van Rijn, J.; Verschoor, G. C. Synthesis, structure, and spectroscopic properties of copper(II) compounds containing nitrogen–sulphur donor ligands; the crystal and molecular structure of aqua[1,7-bis(N-methylbenzimidazol-2′-yl)-2,6-dithiaheptane]copper(II) perchlorate. *J. Chem. Soc., Dalton Trans.* **1984**, 1349-1356.

(160) a) Cui, P.; Iluc, V. M. Redox-induced umpolung of transition metal carbenes. *Chem. Sci.* **2015,** *6*, 7343-7354. b) Shih, W.-C.; Ozerov, O. V. Synthesis and Characterization of PBP Pincer Iridium Complexes and Their Application in Alkane Transfer Dehydrogenation. *Organometallics* **2017,** *36*, 228-233.

(161) Weng, W.; Chen, C.-H.; Foxman, B. M.; Ozerov, O. V. Palladium Complexes of a $P_2C=$ Ligand Containing a Central Carbene Moiety. *Organometallics* **2007,** *26*, 3315-3320.

(162) Azhakar, R.; Ghadwal, R. S.; Roesky, H. W.; Hey, J.; Stalke, D. Facile Access to Transition-Metal–Carbonyl Complexes with an Amidinate-Stabilized Chlorosilylene Ligand. *Chemistry – An Asian Journal* **2012,** *7*, 528-533.

(163) Wang, W.; Inoue, S.; Enthaler, S.; Driess, M. Bis(silylenyl)- and Bis(germylenyl)-Substituted Ferrocenes: Synthesis, Structure, and Catalytic Applications of

Bidentate Silicon(II)–Cobalt Complexes. *Angew. Chem. Int. Ed.* **2012,** *51*, 6167-6171.

(164) Handford, R. C.; Smith, P. W.; Tilley, T. D. Activations of all Bonds to Silicon (Si–H, Si–C) in a Silane with Extrusion of [CoSiCo] Silicide Cores. *J. Am. Chem. Soc.* **2019,** *141*, 8769-8772.

(165) a) Straus, D. A.; Zhang, C.; Quimbita, G. E.; Grumbine, S. D.; Heyn, R. H.; Tilley, T. D.; Rheingold, A. L.; Geib, S. J. Silyl and Diphenylsilylene Derivatives of (η^5-C_5Me_5)(PMe_3)$_2$Ru. Evidence for the Base-Free Silylene Complex [(η^5-C_5Me_5)(PMe_3)$_2$Ru=$SiPh_2$]$^+$. *J. Am. Chem. Soc.* **1990,** *112*, 2673-2681. b) Grumbine, S. K.; Tilley, T. D.; Arnold, F. P.; Rheingold, A. L. Base-Free Silylene Complexes without π-Donor Stabilization. Molecular Structure of [Cp*(PMe_3)$_2$Ru=$SiMe_2$][$B(C_6F_5)_4$]. *J. Am. Chem. Soc.* **1994,** *116*, 5495-5496.

(166) Wiberg, K. B. Application of the Pople-Santry-Segal CNDO Method to the Cyclopropylcarbinyl and Cyclobutyl Cation and to Bicyclobutane. *Tetrahedron* **1968,** *24*, 1083-1096.

(167) Corey, J. Y. Reactions of Hydrosilanes with Transition Metal Complexes. *Chem. Rev.* **2016,** *116*, 11291-11435.

(168) Morris, R. H. Estimating the Acidity of Transition Metal Hydride and Dihydrogen Complexes by Adding Ligand Acidity Constants. *J. Am. Chem. Soc.* **2014,** *136*, 1948-1959.

(169) a) Esteruelas, M. A.; Oliván, M.; Vélez, A. POP-Pincer Silyl Complexes of Group 9: Rhodium versus Iridium. *Inorg. Chem.* **2013,** *52*, 12108-12119. b) Möller, S.; Fey, O.; Malisch, W.; Seelbach, W. Metallo-silanole und metallo-siloxane VII. Zur oxofunktionalisierung von Ruthenio-hydridosilanen mit dimethyldioxiran: Darstellung der ersten Ruthenio-silanole. *J. Organomet. Chem.* **1996,** *507*, 239-244.

(170) Chien, J. C. W.; Tsai, W. M.; Rausch, M. D. Isospecific polymerization of propylene catalyzed by *rac*-ethylenebis(indenyl)methylzirconium "cation". *J. Am. Chem. Soc.* **1991,** *113*, 8570-8571.

(171) Straus, D. A.; Zhang, C.; Tilley, T. D. Trityl tetraphenylborate as a reagent in organometallic chemistry. *J. Organomet. Chem.* **1989,** *369*, C13-C17.

(172) Frisch, M. J.; Trucks, G. W.; Schlegel, H. B.; Scuseria, G. E.; Robb, M. A.; Cheeseman, J. R.; Scalmani, G.; Barone, V.; Petersson, G. A.; Nakatsuji, H.; Li, X.; Caricato, M.; Marenich, A. V.; Bloino, J.; Janesko, B. G.; Gomperts, R.; Mennucci, B.; Hratchian, H. P.; Ortiz, J. V.; Izmaylov, A. F.; Sonnenberg, J. L.; Williams; Ding, F.; Lipparini, F.; Egidi, F.; Goings, J.; Peng, B.; Petrone, A.; Henderson, T.; Ranasinghe, D.; Zakrzewski, V. G.; Gao, J.; Rega, N.; Zheng, G.; Liang, W.; Hada, M.; Ehara, M.; Toyota, K.; Fukuda, R.; Hasegawa, J.; Ishida, M.; Nakajima, T.; Honda, Y.; Kitao, O.; Nakai, H.; Vreven, T.; Throssell, K.; Montgomery Jr., J. A.; Peralta, J. E.; Ogliaro, F.; Bearpark, M. J.; Heyd, J. J.; Brothers, E. N.; Kudin, K. N.; Staroverov, V. N.; Keith, T. A.; Kobayashi, R.; Normand, J.; Raghavachari, K.; Rendell, A. P.; Burant, J. C.; Iyengar, S. S.; Tomasi, J.; Cossi, M.; Millam, J. M.; Klene, M.; Adamo, C.; Cammi, R.; Ochterski, J. W.; Martin, R. L.; Morokuma, K.; Farkas, O.; Foresman, J. B.; Fox, D. J. *Gaussian 09, Revision D.01*, Wallingford, CT, 2009.

(173) Zhao, Y.; Truhlar, D. G. The M06 suite of density functionals for main group thermochemistry, thermochemical kinetics, noncovalent interactions, excited states, and transition elements: two new functionals and systematic testing of four M06-class functionals and 12 other functionals. *Theor. Chem. Acc.* **2008,** *120*, 215-241.

(174) Sheldrick, G. M. *SADABS (version **2008**/1): Program for Absorption Correction of Area Detector Frames*, BRUKER AXS Inc.: 5465 East Cheryl Parkway, Madison, WI 53711-5373 USA.

(175) *CrystalClear*, Rigaku: The Woodlands, TX, 2011.

(176) Farrugia, L. J. WinGX and ORTEP for Windows: an Update. *J. Appl. Crystallogr.* **2012,** *45*, 849-854.

(177) *Persistence of Vision Raytracer*, version 3.6; Persistence of Vision Pty. Ltd.: Williamstown, Victoria, Australia, 2004.

(178) a) Han, F.-S. Transition-metal-catalyzed Suzuki–Miyaura cross-coupling reactions: a remarkable advance from palladium to nickel catalysts. *Chem. Soc. Rev.* **2013,** *42*, 5270-5298. b) Netherton, M. R.; Fu, G. C. Nickel-Catalyzed Cross-

Couplings of Unactivated Alkyl Halides and Pseudohalides with Organometallic Compounds. *Adv. Synth. Catal.* **2004,** *346*, 1525-1532. c) Tasker, S. Z.; Standley, E. A.; Jamison, T. F. Recent Advances in Homogeneous Nickel Catalysis. *Nature* **2014,** *509*, 299-309.

(179) Surry, D. S.; Buchwald, S. L. Diamine ligands in copper-catalyzed reactions. *Chem. Sci.* **2010,** *1*, 13-31.

(180) a) Bauer, I.; Knölker, H.-J. Iron Catalysis in Organic Synthesis. *Chem. Rev.* **2015,** *115*, 3170-3387. b) Cassani, C.; Bergonzini, G.; Wallentin, C.-J. Active Species and Mechanistic Pathways in Iron-Catalyzed C–C Bond-Forming Cross-Coupling Reactions. *ACS Catal.* **2016,** *6*, 1640-1648.

(181) a) Miao, J.; Ge, H. Recent Advances in First-Row-Transition-Metal-Catalyzed Dehydrogenative Cou-pling of C(sp^3)–H Bonds. *Eur. J. Org. Chem.* **2015,** *2015*, 7859-7868. b) Rudolph, A.; Lautens, M. Secondary Alkyl Halides in Transition-Metal-Catalyzed Cross-Coupling Reactions. *Angew. Chem. Int. Ed.* **2009,** *48*, 2656-2670. c) Su, B.; Cao, Z.-C.; Shi, Z.-J. Exploration of Earth-Abundant Transition Metals (Fe, Co, and Ni) as Catalysts in Unreactive Chemical Bond Activations. *Acc. Chem. Res.* **2015,** *48*, 886-896.

(182) a) Bullock, R. M. *Catalysis Without Precious Metals*. Wiley: 2010. b) Chirik, P. J. Carbon–Carbon Bond Formation in a Weak Ligand Field: Leveraging Open-Shell First-Row Transition-Metal Catalysts. *Angew. Chem. Int. Ed.* **2017,** *56*, 5170-5181.

(183) a) Timpa, S. D.; Fafard, C. M.; Herbert, D. E.; Ozerov, O. V. Catalysis of Kumada–Tamao–Corriu coupling by a (POCOP)Rh pincer complex. *Dalton Trans.* **2011,** *40*, 5426-5429. b) Timpa, S. D.; Pell, C. J.; Zhou, J.; Ozerov, O. V. Fate of Aryl/Amido Complexes of Rhodium(III) Supported by a POCOP Pincer Ligand: C–N Reductive Elimination, β-Hydrogen Elimination, and Relevance to Catalysis. *Organometallics* **2014,** *33*, 5254-5262.

(184) Gatard, S.; Guo, C.; Foxman, B. M.; Ozerov, O. V. Thioether, Dinitrogen, and Olefin Complexes of (PNP)Rh: Kinetics and Thermodynamics of Exchange and Oxidative Addition Reactions. *Organometallics* **2007,** *26*, 6066-6075.

(185) a) Mao, J.; Liu, F.; Wang, M.; Wu, L.; Zheng, B.; Liu, S.; Zhong, J.; Bian, Q.; Walsh, P. J. Cobalt–Bisoxazoline-Catalyzed Asymmetric Kumada Cross-

Coupling of Racemic α-Bromo Esters with Aryl Grignard Reagents. *J. Am. Chem. Soc.* **2014,** *136*, 17662-17668. b) Smith, A. L.; Hardcastle, K. I.; Soper, J. D. Redox-Active Ligand-Mediated Oxidative Addition and Reductive Elimination at Square Planar Cobalt(III): Multielectron Reactions for Cross-Coupling. *J. Am. Chem. Soc.* **2010,** *132*, 14358-14360.

(186) Hiroyuki, H.; Minoru, U.; Hiroto, Y.; Hideki, Y.; Koichiro, O. Cobalt-catalyzed Cross-coupling Reactions of Aryl Bromides with Alkyl Grignard Reagents. *Chem. Lett.* **2008,** *37*, 1178-1179.

(187) Wong, Y.-C.; Jayanth, T. T.; Cheng, C.-H. Cobalt-Catalyzed Aryl−Sulfur Bond Formation. *Org. Lett.* **2006,** *8*, 5613-5616.

(188) Amatore, M.; Gosmini, C. Efficient Cobalt-Catalyzed Formation of Unsymmetrical Biaryl Compounds and Its Application in the Synthesis of a Sartan Intermediate. *Angew. Chem. Int. Ed.* **2008,** *47*, 2089-2092.

(189) Wei, J.; Liu, K.-M.; Duan, X.-F. Cobalt-Catalyzed Biaryl Couplings via C–F Bond Activation in the Absence of Phosphine or NHC Ligands. *J. Org. Chem.* **2017,** *82*, 1291-1300.

(190) Xu, H.; Bernskoetter, W. H. Mechanistic Considerations for C–C Bond Reductive Coupling at a Cobalt(III) Center. *J. Am. Chem. Soc.* **2011,** *133*, 14956-14959.

(191) Fryzuk, M. D. The 1992 Alcan Award Lecture Excursions around the periodic table: ligand design in inorganic chemistry. *Can. J. Chem.* **1992,** *70*, 2839-2845.

(192) Ingleson, M. J.; Pink, M.; Fan, H.; Caulton, K. G. Exploring the Reactivity of Four-Coordinate PNPCoX with Access to Three-Coordinate Spin Triplet PNPCo. *Inorg. Chem.* **2007,** *46*, 10321-10334.

(193) Lian, Z.; Xu, X.; Sun, H.; Chen, Y.; Zheng, T.; Li, X. Imine-assisted C–F bond activation using low-valent cobalt compounds supported by trimethylphosphine ligands and formation of novel organic fluorides. *Dalton Trans.* **2010,** *39*, 9523-9529.

(194) Neely, J. M.; Bezdek, M. J.; Chirik, P. J. Insight into Transmetalation Enables Cobalt-Catalyzed Suzuki–Miyaura Cross Coupling. *ACS Cent. Sci.* **2016,** *2*, 935-942.

(195) a) Obligacion, J. V.; Semproni, S. P.; Pappas, I.; Chirik, P. J. Cobalt-Catalyzed C(sp^2)-H Borylation: Mechanistic Insights Inspire Catalyst Design. *J. Am. Chem. Soc.* **2016,** *138*, 10645-10653. b) Semproni, S. P.; Hojilla Atienza, C. C.; Chirik, P. J. Oxidative Addition and C–H Activation Chemistry with a PNP Pincer-Ligated Cobalt Complex. *Chem. Sci.* **2014,** *5*, 1956-1960.

(196) a) Ibrahim, A. D.; Entsminger, S. W.; Fout, A. R. Insights into a Chemoselective Cobalt Catalyst for the Hydroboration of Alkenes and Nitriles. *ACS Catal.* **2017,** *7*, 3730-3734. b) Ibrahim, A. D.; Entsminger, S. W.; Zhu, L.; Fout, A. R. A Highly Chemoselective Cobalt Catalyst for the Hydrosilylation of Alkenes using Tertiary Silanes and Hydrosiloxanes. *ACS Catal.* **2016,** *6*, 3589-3593. c) Tokmic, K.; Fout, A. R. Alkyne Semihydrogenation with a Well-Defined Nonclassical Co–H_2 Catalyst: A H_2 Spin on Isomerization and E-Selectivity. *J. Am. Chem. Soc.* **2016,** *138*, 13700-13705. d) Tokmic, K.; Jackson, B. J.; Salazar, A.; Woods, T. J.; Fout, A. R. Cobalt-Catalyzed and Lewis Acid-Assisted Nitrile Hydrogenation to Primary Amines: A Combined Effort. *J. Am. Chem. Soc.* **2017,** *139*, 13554-13561. e) Tokmic, K.; Markus, C. R.; Zhu, L.; Fout, A. R. Well-Defined Cobalt(I) Dihydrogen Catalyst: Experimental Evidence for a Co(I)/Co(III) Redox Process in Olefin Hydrogenation. *J. Am. Chem. Soc.* **2016,** *138*, 11907-11913.

(197) a) Hartwig, J. F. Evolution of a Fourth Generation Catalyst for the Amination and Thioetherification of Aryl Halides. *Acc. Chem. Res.* **2008,** *41*, 1534-1544. b) Sayah, M.; Organ, M. G. Potassium Isopropoxide: For Sulfination It is the Only Base You Need! *Chem. Eur. J.* **2013,** *19*, 16196-16199.

(198) Guenifa, F.; Hadjadj, N.; Zeghouan, O.; Bendjeddou, L.; Maerazig, H. 4-(Dimethylamino)pyridinium trichlorido[4-(dimethylamino)pyridine-κN]cobaltate(II). *Acta Cryst.* **2013,** *E69*, m379-m380.

(199) Hebden, T. J.; St. John, A. J.; Gusev, D. G.; Kaminsky, W.; Goldberg, K. I.; Heinekey, D. M. Preparation of a Dihydrogen Complex of Cobalt. *Angew. Chem. Int. Ed.* **2011,** *50*, 1873-1876.

(200) Fryzuk, M. D.; Leznoff, D. B.; Thompson, R. C.; Rettig, S. J. One-Electron Transformations of Paramagnetic Cobalt Complexes. Synthesis and Structure of

Cobalt(II) Amidodiphosphine Halide and Alkyl Complexes and Their Reaction with Alkyl Halides. *J. Am. Chem. Soc.* **1998,** *120*, 10126-10135.

(201) Fryzuk, M. D.; MacNeil, P. A. Hybrid multidentate ligands. Tridentate amidophosphine complexes of nickel(II) and palladium(II). *J. Am. Chem. Soc.* **1981,** *103*, 3592-3593.

(202) Murugesan, S.; Stöger, B.; Carvalho, M. D.; Ferreira, L. P.; Pittenauer, E.; Allmaier, G.; Veiros, L. F.; Kirchner, K. Synthesis and Reactivity of Four- and Five-Coordinate Low-Spin Cobalt(II) PCP Pincer Complexes and Some Nickel(II) Analogues. *Organometallics* **2014,** *33*, 6132-6140.

(203) Zanardi, A.; Novikov, M. A.; Martin, E.; Benet-Buchholz, J.; Grushin, V. V. Direct Cupration of Fluoroform. *J. Am. Chem. Soc.* **2011,** *133*, 20901-20913.

(204) Shih, W.-C.; Gu, W.; MacInnis, M. C.; Herbert, D. E.; Ozerov, O. V. Boryl/Borane Interconversion and Diversity of Binding Modes of Oxygenous Ligands in PBP Pincer Complexes of Rhodium. *Organometallics* **2017,** *36*, 1718-1726.

(205) Jaynes, B. S.; Ren, T.; Liu, S.; Lippard, S. J. Tuning the stereochemistry of pentacoordinate cobalt(III) halide complexes: a rare case of trigonal bipyramidal stereochemistry for cobalt(III). *J. Am. Chem. Soc.* **1992,** *114*, 9670-9671.

(206) Klein, H.-F.; Li, X.; Flörke, U.; Haupt, H.-J. Hydrido(acylenolato)cobalt(III)-Verbindungen mit Trimethylphosphan- Liganden: Insertionsreaktionen mit Alkinen und die ersten Carbonylcobalt(III)-Komplexe / Hydrido(acylenolato)cobalt(III) Compounds Containing Trimethylphosphane Ligands: Insertion Reactions with Alkynes and the First Carbonylcobalt(III) Complexes. *Zeitschrift für Naturforschung B* **2000,** *55*, 707-717.

(207) Greig, L. M.; Slawin, A. M. Z.; Smith, M. H.; Philp, D. The dynamic covalent chemistry of mono- and bifunctional boroxoaromatics. *Tetrahedron* **2007,** *63*, 2391-2403.

(208) Timpa, S. D.; Zhou, J.; Bhuvanesh, N.; Ozerov, O. V. Potential Carbon–Fluorine Reductive Elimination from Pincer-Supported Rh(III) and Dominating Side Reactions: Theoretical and Experimental Examination. *Organometallics* **2014,** *33*, 6210-6217.

(209) Morales-Morales, D.; Redón, R.; Yung, C.; Jensen, C. M. Dehydrogenation of Alkanes Catalyzed by an Iridium Phosphinito PCP Pincer Complex. *Inorg. Chim. Acta* **2004,** *357*, 2953-2956.

(210) a) Desnoyer, A. N.; Love, J. A. Recent advances in well-defined, late transition metal complexes that make and/or break C–N, C–O and C–S bonds. *Chem. Soc. Rev.* **2017,** *46*, 197-238. b) Hartwig, J. F. Carbon–Heteroatom Bond Formation Catalysed by Organometallic Complexes. *Nature* **2008,** *455*, 314-322. c) Ritleng, V.; Henrion, M.; Chetcuti, M. J. Nickel N-Heterocyclic Carbene-Catalyzed C–Heteroatom Bond Formation, Reduction, and Oxidation: Reactions and Mechanistic Aspects. *ACS Catal.* **2016,** *6*, 890-906. d) Zeng, Q.; Zhang, L.; Zhou, Y. Advances in Selective Carbon-Heteroatom Coupling Reactions. *Chem. Rec.* **2018,** *18*, 1278-1291.

(211) Hazari, N.; Melvin, P. R.; Beromi, M. M. Well-Defined Nickel and Palladium Precatalysts for Cross-Coupling. *Nat. Rev. Chem.* **2017,** *1*, 1-16.

(212) a) Chirik, P.; Morris, R. Getting Down to Earth: The Renaissance of Catalysis with Abundant Metals. *Acc. Chem. Res.* **2015,** *48*, 2495-2495. b) Hayler, J. D.; Leahy, D. K.; Simmons, E. M. A Pharmaceutical Industry Perspective on Sustainable Metal Catalysis. *Organometallics* **2019,** *38*, 36-46.

(213) a) Duong, H. A.; Yeow, Z.-H.; Tiong, Y.-L.; Mohamad Kamal, N. H. B.; Wu, W. Cobalt-Catalyzed Cross-Coupling Reactions of Aryl Triflates and Lithium Arylborates. *J. Org. Chem.* **2019,** *84*, 12686-12691. b) Liu, S.; Huang, W.; Wang, D.; Wei, P.; Shen, Q. Cobalt-Catalyzed Cross-Coupling of Lithium (Hetero)Aryl Zincates with Heteroaryl Chlorides and Bromides. *Organic Chemistry Frontiers* **2019,** *6*, 2630-2634. c) Lutter, F. H.; Grokenberger, L.; Spieß, P.; Hammann, J. M.; Karaghiosoff, K.; Knochel, P. Cobalt-Catalyzed Cross-Coupling of Functionalized Alkylzinc Reagents with (Hetero)Aryl Halides. *Angew. Chem. Int. Ed.* **2020,** *59*, 5546-5550.

(214) a) Léonard, N. G.; Palmer, W. N.; Friedfeld, M. R.; Bezdek, M. J.; Chirik, P. J. Remote, Diastereoselective Cobalt-Catalyzed Alkene Isomerization–Hydroboration: Access to Stereodefined 1,3-Difunctionalized Indanes. *ACS Catal.* **2019,** *9*, 9034-9044. b) Muhammad, S. R.; Nugent, J. W.; Tokmic, K.; Zhu, L.; Mahmoud, J.; Fout, A. R. Electronic Ligand Modifications on Cobalt Complexes and Their Application toward the Semi-Hydrogenation of Alkynes and Para-Hydrogenation of Alkenes. *Organometallics* **2019,** *38*, 3132-3138. c) Pabst, T. P.; Obligacion, J. V.; Rochette, É.; Pappas, I.; Chirik, P. J. Cobalt-Catalyzed

Borylation of Fluorinated Arenes: Thermodynamic Control of C(sp^2)-H Oxidative Addition Results in ortho-to-Fluorine Selectivity. *J. Am. Chem. Soc.* **2019,** *141*, 15378-15389.

(215) Fout, A. R.; Basuli, F.; Fan, H.; Tomaszewski, J.; Huffman, J. C.; Baik, M.-H.; Mindiola, D. J. A Co_2N_2 Diamond-Core Resting State of Cobalt(I): A Three-Coordinate CoI Synthon Invoking an Unusual Pincer-Type Rearrangement. *Angew. Chem. Int. Ed.* **2006,** *45*, 3291-3295.

(216) Guard, L. M.; Hebden, T. J.; Linn, D. E.; Heinekey, D. M. Pincer-Supported Carbonyl Complexes of Cobalt(I). *Organometallics* **2017,** *36*, 3104-3109.

(217) Krishnan, V. M.; Arman, H. D.; Tonzetich, Z. J. Preparation and Reactivity of a Square-Planar PNP Cobalt(II)–Hydrido Complex: Isolation of the First {Co–NO}^{8}–Hydride. *Dalton Trans.* **2018,** *47*, 1435-1441.

(218) Kuriyama, S.; Arashiba, K.; Tanaka, H.; Matsuo, Y.; Nakajima, K.; Yoshizawa, K.; Nishibayashi, Y. Direct Transformation of Molecular Dinitrogen into Ammonia Catalyzed by Cobalt Dinitrogen Complexes Bearing Anionic PNP Pincer Ligands. *Angew. Chem. Int. Ed.* **2016,** *55*, 14291-14295.

(219) Ingleson, M. J.; Pink, M.; Caulton, K. G. Reducing Power of Three-Coordinate Cobalt(I). *J. Am. Chem. Soc.* **2006,** *128*, 4248-4249.

(220) Merz, L. S.; Blasius, C. K.; Wadepohl, H.; Gade, L. H. Square Planar Cobalt(II) Hydride versus T-Shaped Cobalt(I): Structural Characterization and Dihydrogen Activation with PNP–Cobalt Pincer Complexes. *Inorg. Chem.* **2019**.

(221) a) Obligacion, J. V.; Zhong, H.; Chirik, P. J. Insights into Activation of Cobalt Pre-Catalysts for C(sp2)−H Functionalization. *Isr. J. Chem.* **2017,** *57*, 1032-1036. b) Rummelt, S. M.; Zhong, H.; Léonard, N. G.; Semproni, S. P.; Chirik, P. J. Oxidative Addition of Dihydrogen, Boron Compounds, and Aryl Halides to a Cobalt(I) Cation Supported by a Strong-Field Pincer Ligand. *Organometallics* **2019,** *38*, 1081-1090. c) Socol, S. M.; Verkade, J. G. Steric and electronic effects in cobalt(II) disproportionation with phosphorus ligands. *Inorg. Chem.* **1986,** *25*, 2658-2663.

(222) Sandford, C.; Fries, L. R.; Ball, T. E.; Minteer, S. D.; Sigman, M. S. Mechanistic Studies into the Oxidative Addition of Co(I) Complexes: Combining Electroanalytical Techniques with Parameterization. *J. Am. Chem. Soc.* **2019,** *141*, 18877-18889.

(223) Choi, J.; Lee, Y. A Low-Spin Three-Coordinate Cobalt(I) Complex and Its Reactivity toward H2 and Silane. *Angew. Chem. Int. Ed.* **2019,** *58*, 6938-6942.

(224) Ingleson, M.; Fan, H.; Pink, M.; Tomaszewski, J.; Caulton, K. G. Three-Coordinate Co(I) Provides Access to Unsaturated Dihydrido-Co(III) and Seven-Coordinate Co(V). *J. Am. Chem. Soc.* **2006,** *128*, 1804-1805.

(225) Ghosh, R.; Zhang, X.; Achord, P.; Emge, T. J.; Krogh-Jespersen, K.; Goldman, A. S. Dimerization of Alkynes Promoted by a Pincer-Ligated Iridium Complex. C−C Reductive Elimination Inhibited by Steric Crowding. *J. Am. Chem. Soc.* **2007,** *129*, 853-866.

(226) Cristau, H. J.; Chabaud, B.; Chêne, A.; Christol, H. Synthesis of Diaryl Sulfides by Nickel(II)-Catalyzed Arylation of Arenethiolates. *Synthesis* **1981,** *1981*, 892-894.

(227) Scattolin, T.; Senol, E.; Yin, G.; Guo, Q.; Schoenebeck, F. Site-Selective C−S Bond Formation at C−Br over C−OTf and C−Cl Enabled by an Air-Stable, Easily Recoverable, and Recyclable Palladium(I) Catalyst. *Angew. Chem. Int. Ed.* **2018,** *57*, 12425-12429.

(228) a) Becke, A. D. Density-Functional Exchange-Energy Approximation With Correct Asymptotic Behavior. *Physical Review A* **1988,** *38*, 3098-3100. b) Lee, C.; Yang, W.; Parr, R. G. Development of the Colle-Salvetti Correlation-Energy Formula into a Functional of the Electron Density. *Physical Review B* **1988,** *37*, 785-789.

(229) Marenich, A. V.; Cramer, C. J.; Truhlar, D. G. Universal Solvation Model Based on Solute Electron Density and on a Continuum Model of the Solvent Defined by the Bulk Dielectric Constant and Atomic Surface Tensions. *The Journal of Physical Chemistry B* **2009,** *113*, 6378-6396.

(230) Pell, C. J.; Zhu, Y.; Huacuja, R.; Herbert, D. E.; Hughes, R. P.; Ozerov, O. V. Fluorocarbene, Fluoroolefin, and Fluorocarbyne Complexes of Rh. *Chem. Sci.* **2017,** *8*, 3178-3186.

(231) Fan, L.; Parkin, S.; Ozerov, O. V. Halobenzenes and Ir(I): Kinetic C−H Oxidative Addition and Thermodynamic C−Hal Oxidative Addition. *J. Am. Chem. Soc.* **2005,** *127*, 16772-16773.

(232) Zhu, Y.; Chen, C.-H.; Fafard, C. M.; Foxman, B. M.; Ozerov, O. V. Net Heterolytic Cleavage of B–H and B–B Bonds Across the N–Pd Bond in a Cationic (PNP)Pd Fragment. *Inorg. Chem.* **2011,** *50*, 7980-7987.

(233) a) Zhu, D.; Budzelaar, P. H. M. Binuclear Oxidative Addition of Aryl Halides. *Organometallics* **2010,** *29*, 5759-5761. b) Zhu, D.; Korobkov, I.; Budzelaar, P. H. M. Radical Mechanisms in the Reaction of Organic Halides with Diiminepyridine Cobalt Complexes. *Organometallics* **2012,** *31*, 3958-3971.

(234) a) Streitwieser, A.; Heathcock, C.; Kosower, E. *Introduction to Organic Chemistry*. 4th ed.; Pearson: 1999. b) Luo, Y.-R. *Comprehensive Handbook of Chemical Bond Energies*. 1st ed.; CRC Press: Boca Raton, 2007.

(235) a) Sambiagio, C.; Marsden, S. P.; Blacker, A. J.; McGowan, P. C. Copper catalysed Ullmann type chemistry: from mechanistic aspects to modern development. *Chem. Soc. Rev.* **2014,** *43*, 3525-3550. b) Uyeda, C.; Tan, Y.; Fu, G. C.; Peters, J. C. A New Family of Nucleophiles for Photoinduced, Copper-Catalyzed Cross-Couplings via Single-Electron Transfer: Reactions of Thiols with Aryl Halides Under Mild Conditions (O °C). *J. Am. Chem. Soc.* **2013,** *135*, 9548-9552. c) Tan, Y.; Muñoz-Molina, J. M.; Fu, G. C.; Peters, J. C. Oxygen nucleophiles as reaction partners in photoinduced, copper-catalyzed cross-couplings: O-arylations of phenols at room temperature. *Chem. Sci.* **2014,** *5*, 2831-2835. d) Olivero, S.; Duñach, E. Selectivity in the Tandem Cyclization – Carboxylation Reaction of Unsaturated Haloaryl Ethers Catalyzed by Electrogenerated Nickel Complexes. *Eur. J. Org. Chem.* **1999,** *1999*, 1885-1891.

(236) Creutz, S. E.; Lotito, K. J.; Fu, G. C.; Peters, J. C. Photoinduced Ullmann C–N Coupling: Demonstrating the Viability of a Radical Pathway. *Science* **2012,** *338*, 647-651.

(237) Pan, X.; Lacôte, E.; Lalevée, J.; Curran, D. P. Polarity Reversal Catalysis in Radical Reductions of Halides by N-Heterocyclic Carbene Boranes. *J. Am. Chem. Soc.* **2012,** *134*, 5669-5674.

(238) Nicovich, J. M.; Ravishankara, A. R. Reaction of Hydrogen Atom with Benzene. Kinetics and Mechanism. *J. Phys. Chem.* **1984,** *88*, 2534-2541.

(239) Lankamp, H.; Nauta, W. T.; MacLean, C. A New Interpretation of the Monomer-Dimer Equilibrium of Triphenylmethyl- and Alkylsubstituted-Diphenyl Methyl-Radicals in Solution. *Tetrahedron Lett.* **1968,** *9*, 249-254.

(240) Zhang, G.; Vasudevan, K. V.; Scott, B. L.; Hanson, S. K. Understanding the Mechanisms of Cobalt-Catalyzed Hydrogenation and Dehydrogenation Reactions. *J. Am. Chem. Soc.* **2013,** *135*, 8668-8681.

(241) Hayashi, Y.; Yamamoto, T.; Yamamoto, A.; Komiya, S.; Kushi, Y. Carbon-Oxygen Bond Cleavage of Esters Promoted by Hydrido- and Alkylcobalt(I) Complexes Having Triphenylphosphine Ligands. Isolation of an Insertion Intermediate and Molecular Structure of Phenoxotris(triphenylphosphine)cobalt(I). *J. Am. Chem. Soc.* **1986,** *108*, 385-391.

(242) Gomes, P.; Gosmini, C.; Périchon, J. New Chemical Cross-Coupling between Aryl Halides and Allylic Acetates Using a Cobalt Catalyst. *Org. Lett.* **2003,** *5*, 1043-1045.

(243) Amatore, M.; Gosmini, C.; Périchon, J. Cobalt-Catalyzed Vinylation of Functionalized Aryl Halides with Vinyl Acetates. *Eur. J. Org. Chem.* **2005,** *2005*, 989-992.

(244) Gomes, P.; Gosmini, C.; Périchon, J. Allylation of Carbonyl Compounds by Allylic Acetates Using a Cobalt Halide as Catalyst. *Synthesis* **2003,** *12*, 1909-1915.

(245) Gomes, P.; Gosmini, C.; Périchon, J. Cobalt-catalyzed electrochemical vinylation of aryl halides using vinylic acetates. *Tetrahedron* **2003,** *59*, 2999-3002.

(246) Townsend, T. M.; Bernskoetter, W. H.; Brudvig, G. W.; Hazari, N.; Lant, H. M. C.; Mercado, B. Q. Synthesis of Organometallic Pincer-Supported Cobalt(II) Complexes. *Polyhedron* **2020,** *177*, 114308.

(247) a) Klán, P.; Šolomek, T.; Bochet, C. G.; Blanc, A.; Givens, R.; Rubina, M.; Popik, V.; Kostikov, A.; Wirz, J. Photoremovable Protecting Groups in Chemistry and Biology: Reaction Mechanisms and Efficacy. *Chem. Rev.* **2013,** *113*, 119-191. b) May, D. D.; Skell, P. S. Pivaloxy Decarboxylates Less Rapidly Than Propionoxy: Steric Retardation of the Decarboxylation of Aliphatic Carboxylate Radicals. *J. Am. Chem. Soc.* **1982,** *104*, 4500-4502.

(248) Noda, D.; Tahara, A.; Sunada, Y.; Nagashima, H. Non-Precious-Metal Catalytic Systems Involving Iron or Cobalt Carboxylates and Alkyl Isocyanides for Hydrosilylation of Alkenes with Hydrosiloxanes. *J. Am. Chem. Soc.* **2016,** *138*, 2480-2483.

APPENDIX A

RANDOM REACTIONS

Synthesis of (PNP)Co(Cl)$_2$. In an Ar-filled glove box, a 20 mL scintillation vial was charged with **603** (116 mg, 0.22 mmol) and 10 mL of diethyl ether. To this solution, trityl chloride (64 mg, 0.23 mmol) was added in one portion. The solution immediately turned purple and was stirred overnight. The stirring was stopped, and the solids were allowed to settle. The yellow supernatant was removed. The solids were washed with diethyl ether again in this manner (5 x 5mL). The metal complex was then dissolved in dichloromethane and layered with pentane prior to placing in a -35 °C freezer. Dark crystals were obtained. Yield: 99 mg (80%). ^{1}H NMR (C_6D_6, 500 MHz): δ 88.65, 48.65, 29.79, 27.83, 11.37, -7.00, -26.29, -63.94, -152.01.

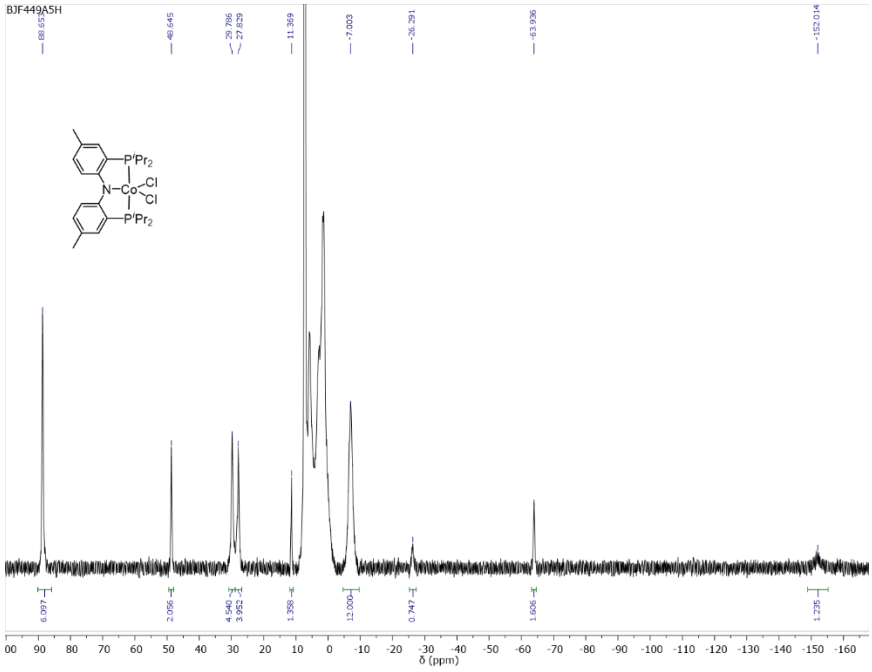

Figure X-1. ^{1}H NMR (500 MHz, C_6D_6) spectrum of (PNP)Co(Cl)$_2$

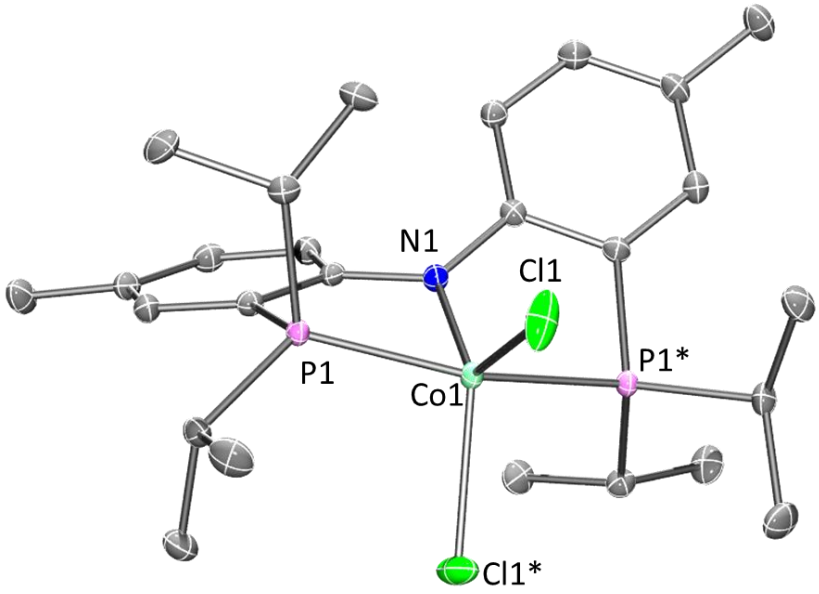

Figure X-2. POV-Ray renditions of ORTEP plots (50% probability ellipsoids) of $(PNP)Co(Cl)_2$ showing selected atom labeling. Hydrogen atoms are omitted. Selected bond distances (Å) and angles (deg) for $(PNP)Co(Cl)_2$ follow: N1-Co1, 1.8986(19); P1-Co1, 2.2760(6); Cl1-Co1, 2.2684(6); P1-Co1-P1*, 163.68(3); N1-Co1-Cl1, 126.329(17); Cl1-Co1-Cl1*, 107.34(3).

Synthesis of (SiNN)Ir(PMe$_3$)$_2$(Bpin). In an Ar-filled glovebox, a J. Young NMR tube was charged with $(SiNN)IrH(Bpin)_2$ (20 mg, 0.025 mmol) and trimethylphosphine (3 µL, 0.028 mmol) then diluted with 600 µL C_6D_6. ^{1}H NMR spectroscopy revealed the liberation of free HBpin and virtual *trans*-phosphine coupling in the phosphine methyl groups. ^{1}H NMR (C_6D_6, 500 MHz): δ 9.13 (1H), 8.45 (1H), 7.99 (1H), 7.42 (1H), 7.09 (1H), 6.63 (1H), 6.29 (1H), 2.45 (3H, tolyl CH_3), 2.30 (3H, tolyl CH_3), 1.83 (6H,

CH(C*H*$_3$)$_2$), 1.74 (6H, CH(C*H*$_3$)$_2$), 1.41 (2H, C*H*(Me)$_2$), 1.20 (12H, Bpin methyls), 0.93 (18H, P(C*H*$_3$)$_3$). ^{31}P{^{1}H} NMR (C_6D_6, 202 MHz): 37.32.

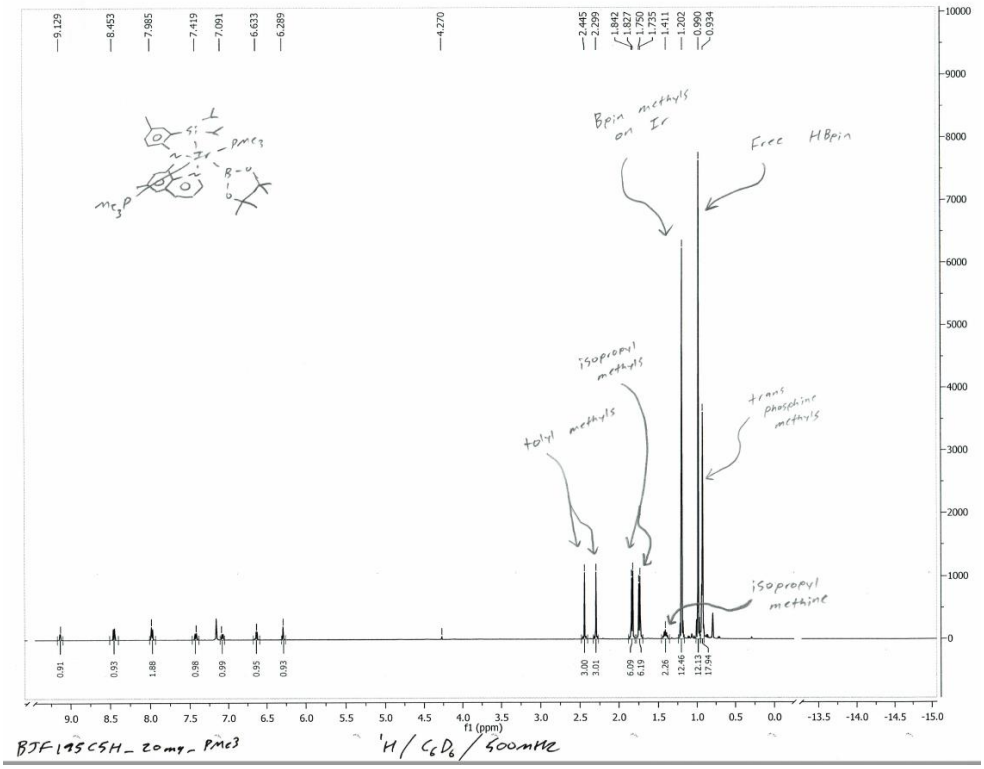

Figure X-3. ^{1}H NMR (500 MHz, C_6D_6) spectrum of (SiNN)Ir(PMe$_3$)$_2$Bpin. Sample contains 1eq. of free HBpin.

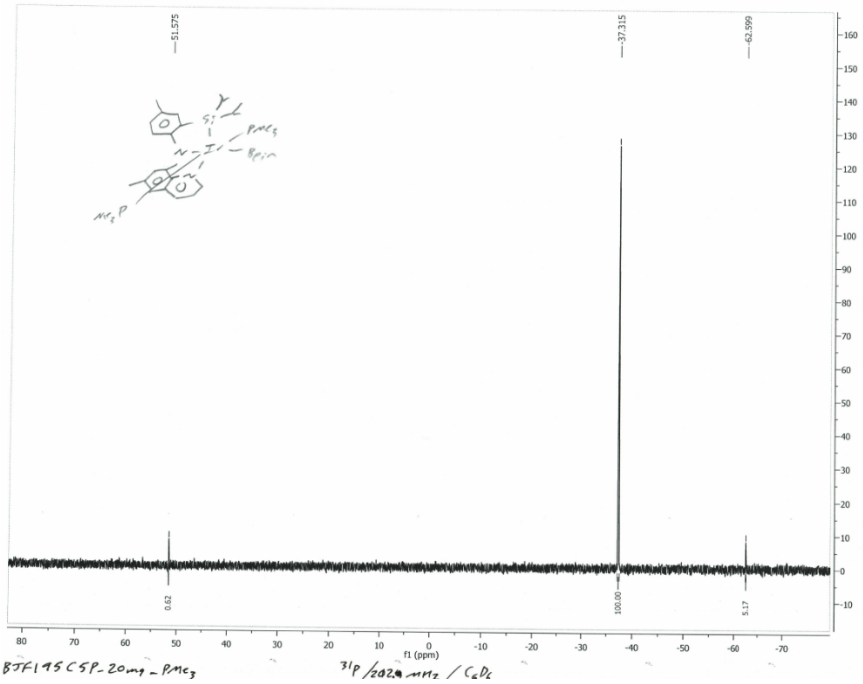

Figure X-4. $^{31}P\{^{1}H\}$ NMR (202 MHz, C_6D_6) spectrum of (SiNN)Ir(PMe_3)$_2$Bpin. Sample contains residual PMe_3.

APPENDIX B

LIST OF PUBLICATIONS RESULTING FROM PH.D. WORK

1. Foley, B. J.; Palit, C. M.; Timpa, S. D.; Ozerov, O. V. Synthesis of (POCOP)Co(Ph)(X) Pincer Complexes and Observation of Aryl-Aryl Reductive Elimination Involving the Pincer Aryl. *Organometallics* **2018**, *37*, 3803-3812.
2. Zhang, J.; Foley, B. J.; Bhuvanesh, N.; Zhou, J.; Janzen, D. E.; Whited, M. T.; Ozerov, O. V. Synthesis and Reactivity of Pincer-Type Cobalt Silyl and Silylene Complexes. *Organometallics* **2018**, *37*, 3956-3962.
3. Foley, B. J.; Ozerov, O. V. Air- and Water-Tolerant (PNP)Ir Precatalyst for the Dehydrogenative Borylation of Terminal Alkynes (DHBTA). *ACS Catal.* **2020**, *In Review*.
4. Foley, B. J.; Palit, C. M.; Bhuvanesh, N.; Zhou, J.; Ozerov, O. V. Concerted Aryl-Sulfur Reductive Elimination from PNP Pincer-Supported Co(III) and Subsequent Co(I)/Co(III) Comproportionation. *Chem. Sci.* **2020**, *In Review*.
5. Foley, B. J.; Bhuvanesh, N.; Zhou, J.; Ozerov, O. V. Combined Experimental and Computational Studies of the Mechanism of Dehydrogenative Borylation of Terminal Alkynes (DHBTA) Catalyzed by PNP Complexes of Iridium. *J. Am. Chem. Soc.* **2020**, *Submitted*.